VEGFR1 and VEGFR2 in dementia

Rachel Elizabeth Harris

A dissertation submitted to the University of Bristol in accordance with the requirements for award of the degree of Doctor of Philosophy in the Faculty of Health Sciences – Bristol Medical School

March 2018

Word count: 48,115

Abstract

Brain ischaemia is the defining pathological process in vascular dementia (VaD); however, cerebral blood flow is also reduced in Alzheimer's disease (AD) and there is evidence that hypoperfusion contributes to tissue damage. Vascular endothelial growth factor-A (VEGF) is a pro-angiogenic factor expressed in response to tissue hypoxia. VEGF receptor 2 (VEGFR2) mediates the actions of VEGF on endothelial cells leading to angiogenesis. VEGF receptor 1 (VEGFR1) has limited kinase activity and its soluble form (sVEGFR1) acts as a negative regulator of VEGF. VEGF protein is increased in AD, but without a corresponding increase in microvessel density. $A\beta_{1\text{-}42}$ was shown to bind to VEGFR2 and block signalling *in vitro* providing a possible mechanism for impaired angiogenesis; however, there are no studies of VEGFR1 or VEGFR2 in AD or VaD.

This thesis investigates whether altered expression of VEGF receptors might account for the lack of angiogenic response to VEGF in AD. Medial parietal cortex and white matter were dissected from AD, VaD and control brains. VEGFR1 and VEGFR2 mRNA and protein levels were measured and related to VEGF and microvessel density. sVEGFR1 isoforms were identified and measured. Human brain microvascular endothelial cells and pericytes were used to investigate VEGFR in response to hypoxia, $A\beta_{1\text{-}40}$ and $A\beta_{1\text{-}42}$.

VEGFR1 was expressed predominantly neuronally and was significantly reduced in AD, though blot analysis on a subset of brains showed an increase in the proportion of sVEGFR1 in AD. VEGFR2 was expressed by neurons, astrocytes and endothelial cells. VEGFR2 level was similar in AD, VaD and control. The finding that elevated VEGF fails to increase microvessel density in AD despite normal VEGFR2 level raises the possibility that VEGFR2 signalling is defective in AD. The increased proportion of sVEGFR1, supported by *in vitro* findings, may also contribute to reduced angiogenesis observed in advanced AD.

Acknowledgements

I would like to thank my supervisors, Dr Shelley Allen, Dr Scott Miners and Professor Seth Love, for providing me with advice and direction throughout my PhD. I would also like to express my gratitude to the University of Bristol Scholarship for bringing me to this glorious city.

This thesis is dedicated to the following:

- Mum and Dad for their continued support, food packages and red wine filled weekends
- My lab mates and Bristol buddies who have been a constant source of motivation and inspiration
- Andy for surviving a year of PhD related madness
- Long suffering friends from a time before the PhD for sticking with me, I will visit you all soon I promise!
- Tea and coffee for always being there

Declaration

I declare that the work in this dissertation was carried out in accordance with the requirements of the University's *Regulations and Code of Practice for Research Degree Programmes* and that it has not been submitted for any other academic award. Except where indicated by specific reference in the text, the work is the candidate's own work. Work done in collaboration with, or with the assistance of, others, is indicated as such. Any views expressed in the dissertation are those of the author.

SIGNED: ..... DATE:.....

Contents

List of tables

List of figures

List of equations

List of abbreviations

ACE	Angiotensin converting enzyme
AChE	Acetylcholinesterase
ACT-B	β-Actin
AD	Alzheimer's disease
AICD	APP intracellular domains
ALDH1L1	Aldehyde dehydrogenase 1 family member L1
ALS	Amyotrophic lateral sclerosis
AngII	Angiotensin II
APOE	Apolipoprotein E
APP	Amyloid precursor protein
APS	Ammonium persulphate
Aβ	Amyloid beta
BBB	Blood brain barrier
BBN	Brain bank network
BDNF	Brain derived neurotrophic factor
BSA	Bovine serum albumin
CAA	Cerebral amyloid angiopathy
CADASIL	Cerebral autosomal dominant arteriopathy with subcortical infarcts and leukoencephalopathy
CBF	Cerebral blood flow
CD31	Cluster of differentiation 31
CNS	Central nervous system
CoV	Coefficient of variation
DAB	3,3′-Diaminobenzidine
DAPI	4',6-diamidino-2-phenylindole
DLB	Dementia with Lewy bodies
DMSO	Dimethyl sulphoxide
dNTP	Deoxynucleotide triphosphate
DPX	Disterene–plasticizer–xylene
ECE	Endothelin converting enzyme
ECL	Enhanced chemiluminescence
EDNI	Endothelin I
EDTA	Ethylenediaminetetraacetic acid
ELISA	Enzyme-linked immunosorbent assay
FAD	Familial Alzheimer's disease
FBS	Fetal bovine serum
FDG	Fluorodeoxyglucose
FFPE	Formalin fixed parafin embedded
FLK1	Fetal liver kinase 1
FLT1	Fms-Related Tyrosine Kinase 1
FSP	Fibroblast surface protein
FTD	Frontotemporal dementia
GAPDH	Glyceraldehyde 3-phosphate dehydrogenase
GFAP	Glial fibrillary acidic protein

GWAS	Genome wide association studies
H&E	Haemotoxylin and eosin
HBMEC	Human brain vascular endothelial cells
HBVP	Human brain vascular pericytes
HCL	Hydrochloric
HIF	Hypoxia inducible factors
HRE	Hypoxia response element
HRP	Horseradish peroxidase
HSPG	Heparan sulphate proteoglycans
HUVEC	Human umbilical vein endothelial cells
Ig	Immunoglobulin
IHC	Immunohistochemistry
IQR	Interquartile range
ISF	Interstitial fluid
iVEGFR1	Intracellular VEGFR1
KDR	Kinase domain receptor
LDL	Low density lipoprotein
LRP1	Lipoprotein receptor related protein-1
LTP	Long term potentiation
M	Median
MAG	Myelin-associated glycoprotein
MAPT	Microtubule binding protein tau
mbVEGFR1	Membrane bound VEGFR1
MMP	Matrix metalloproteinases
MMSE	Mini mental state examination
MRC	Medical research council
MRI	Magnetic resonance imaging
mRNA	Messenger RNA
NCBI	National Centre for Biotechnology Information
NeuN	Neuronal nuclei
NFT	Neurofibrillary tangles
NICE	National Institute for Health and Care Excellence
NRP1	Neuropilin 1
NRP2	Neuropilin 2
OPC	Oligodendrocyte precursor cells
PDGF	Platelet derived growth factor
PDGFR	Platelet derived growth factor receptor
PECAM1	Platelet endothelial cell adhesion molecule 1
PET	Positron emission tomography
PlGF	Placental growth factor
PLP	Proteolipid protein
PMSF	Phenylmethanesulfonyl fluoride
PSEN1	Presenilin 1
PSEN2	Presenilin 2
PTP	Protein tyrosine phosphatases
PVDF	Polyvinylidene fluoride

p-VEGFR2	Phosphorylated VEGFR2
qPCR	Quantitative polymerase chain reaction
RAGE	Receptor for advanced glycation end products
RBFOX3	RNA binding protein, fox-1 homolog 3
ROS	Reactive oxygen species
RT-PCR	Reverse transcriptase polymerase chain reaction
SD	Standard deviation
SDS	Sodium dodecyl sulphate
SMA	Smooth muslce actin
sNRP1	Soluble NRP1
SVD	Small vessel disease
sVEGFR1	Soluble VEGFR1
sVEGFR2	Soluble VEGFR2
SVZ	Subventricular zone
SWDBB	South West Dementia Brain Bank
TBS	Tris-buffered saline
TBST	Tris-buffered saline and Tween 20
TE	Tris and EDTA
TEMED	Tetramethsylethylenediamine
Tyr	Tyrosine
UTR	Untranslated region
VaD	Vascular dementia
VCI	Vascular cognitive impairment
VCIND	Vascular cognitive impairment no dementia
VE-cadherin	Vascular endothelial cadherin
VEGF	Vascular endothelial growth factor
VEGF-Ax	VEGF-A extension
VEGFR1	Vascular endothelial growth factor receptor 1
VEGFR2	Vascular endothelial growth factor receptor 2
VIP	Very intense purple
vWF	Von Willebrand factor

Chapter 1 General introduction

1.1 Dementia

Dementia is a term that encompasses symptoms that occur when the brain is affected by certain diseases that affect cognitive function. These symptoms may include memory loss, and impairment of problem solving, language and communication [1].

It is estimated that dementia affects 46.8 million people worldwide, with that number predicted almost to double every 20 years [2]. Within the UK there are an estimated 850,000 people living with dementia and over one third of the population have a close friend or family member who has dementia [3] . There is no cure and there are no disease-modifying treatments available for any form of dementia. Though dementia does shorten the lives of those affected, its greatest impact is on quality of life, both for individuals living with dementia, and for their families and carers.

Alzheimer's disease (AD) and vascular dementia (VaD) are the two most common types of dementia.

1.1.1 Alzheimer's disease

AD is the most common neurodegenerative disease and cause of dementia.

AD patients experience a steady decline in the ability to form new memories. Early symptoms include forgetting names, events and faces, misplacing items or becoming disorientated. As AD progresses, memory declines as does the ability to make decisions and communicate. Patients may become unsteady on their feet and require help with daily activities. Significant problems with long and short-term memory, loss of speech, difficulties eating, and weight loss occur in the later stages of disease.

To reach a clinical diagnosis of possible AD a history of symptoms is taken from the patient and their carer. The mini mental state examination (MMSE) is one of a battery of tests commonly used to assess cognition [4] together with a physical assessment and psychiatric evaluation. The advent of positron emission tomography (PET) scans for markers of glucose uptake, amyloid and phosphorylated tau can lead provide a near definitive diagnosis during life, however these scans are expensive and not commonly available. A definitive diagnosis of AD can only be given post mortem following histological assessment as detailed in Chapter 2.

There are no disease-modifying treatments currently available for AD. The National Institute for Health and Care Excellence (NICE) has licensed 4 drugs for the symptomatic treatment

of AD in the UK: donepezil, galantamine and rivastigmine and memantine [5]. Acetylcholinesterase (AChE) inhibitors (donepezil, galantamine and rivastigmine) are recommended for managing mild and moderate AD. Memantine, an NMDA receptor antagonist, is recommended as an option for managing moderate and severe Alzheimer's disease or for those unable to take cholinesterase inhibitors [5]. Blocking the effects of high levels of glutamate on the NMDA receptor is thought to prevent excitotoxicity and resulting neuronal death. Controlling additional cardiovascular contributors to dementia, such as high blood pressure, high cholesterol and diabetes, may be of benefit in treating patients with AD [6] (1.1.3).

There is a loss of cholinergic neurons in the AD brain compared to controls [7]. This leads to a reduction in neurotransmitter acetylcholine [8], a finding that prompted the use of AChE drugs in AD. These drugs prevent the breakdown of the neurotransmitter acetylcholine to extend its actions at the synapse. AChE inhibitors make up 3 of the 4 approved treatments for AD in the UK [5]. AChE inhibitors offer symptomatic relief to some patients but have no impact on disease progression as cholinergic neuronal loss is a consequence of the underlying disease [9].

1.1.1.1 Neuropathology

AD is characterised by two defining pathologies: extracellular amyloid-β (Aβ) plaques and intracellular neurofibrillary tangles (NFT) [10].

1.1.1.1.1 Aβ production, aggregation and clearance

Aβ fragments are cleaved by β and γ secretases from amyloid precursor protein (APP) [11]. APP has several defined functions in synaptic maintenance, cholesterol homeostasis, cell growth and proliferation but other functions are still being elucidated [12]. APP is highly expressed in neurons [11]. APP processing occurs at cell membrane and Golgi body and it can either be processed via an amyloidogenic pathway or non-amyloidogenic pathway as detailed in Figure 1-1[13]. In the non-amyloidogenic pathway, APP is cleaved by α secretase then γ secretase. In the amyloidogenic pathway APP is cleaved by β secretase (β-secretase 1, BACE1) and then γ secretase. γ secretase is a multimeric protein in which presenilin 1 (PSEN1) or presenilin 2 (PSEN2) form the catalytic domain [14]. γ secretase cleaves the c-terminus of the potential Aβ site at between 40-44 amino acids to produce Aβ fragments. $Aβ_{1-40}$ and $Aβ_{1-42}$ are the most common peptides produced by this process [13].

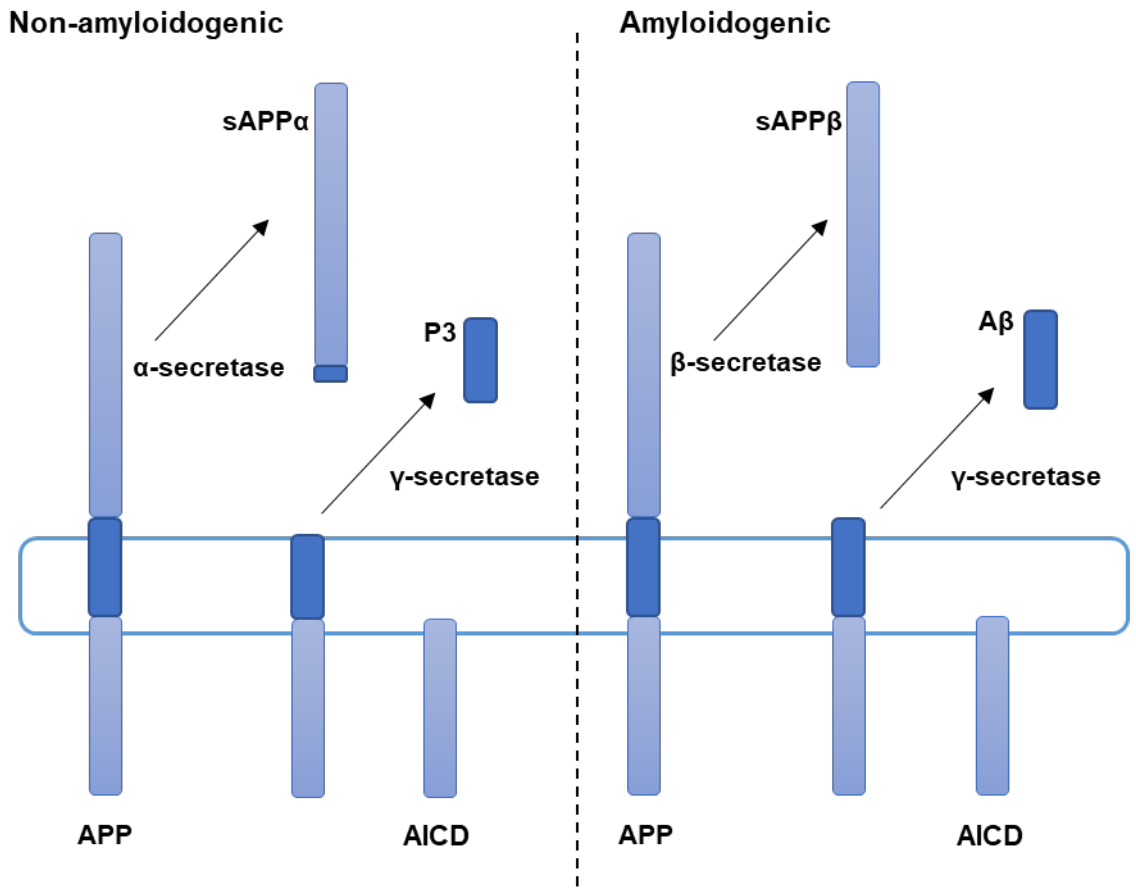

Figure 1-1 APP processing. Non-amyloidogenic pathway – α-secretase first cleaves APP to generate sAPPα followed by γ-secretase to generate. Amyloidogenic pathway: β-secretase first cleaves APP to form sAPPβ then γ-secretase cleaves to generate an Aβ fragment. Both pathways yield intracellular c-terminal fragments APP intracellular domains (AICD).

Aβ fragments are formed as monomers but readily aggregate into oligomers. $Aβ_{1-42}$ forms oligomers, fibrils and insoluble β sheet structure known as amyloid plaques which are observed in the AD brain (Figure 1-2A) [15]. $Aβ_{1-40}$ tends to aggregate in the walls of blood vessels to cause cerebral amyloid angiopathy (CAA) as seen in Figure 1-2C and discussed further in 1.1.1.1.2.

The specific role of amyloid plaques in the progression of AD is debated. Plaque load does not correlate well with memory impairment or reduced brain volume [16]. Oligomers on the other hand are known to be toxic to neurons [17, 18]. It is now thought that oligomers of $Aβ_{1-42}$ are the most damaging Aβ species in AD, while insoluble amyloid plaques may even have a protective role [19].

$Aβ_{1-40}$ is normally produced at higher concentrations than $Aβ_{1-42.}$ Certain conditions are known to increase the formation of $Aβ_{1-42}$ leading to increased concentration of toxic oligomers and aggregation. This shift in $Aβ_{1-42}$: $Aβ_{1-40}$ ratio is thought to be key to AD

pathogenesis. Certain conditions can lead to this shift, including *PSEN* mutations (1.1.1.2) and neuronal hypoxia (1.1.3).

As noted above, $A\beta_{1-42}$ accumulation may result from increased production. However, there must be a balance between Aβ production and clearance to maintain a healthy Aβ concentration. Reduced Aβ clearance or degradation can also increase the concentration of Aβ.

Aβ can be cleared or degraded in the brain via several mechanisms. Receptor-mediated transport across the blood brain barrier (BBB) is thought to be the primary method of Aβ clearance from the brain. The BBB has a key role in controlling the composition of interstitial fluid (ISF) and is described in further detail in 1.1.3.4. The lipoprotein receptor related proteins, such as LRP1, and ATP-binding cassette transporters, such as ABCB1, mediate the transcytosis of Aβ across the BBB [20]. Both LRP1 and ABCB1 have been shown to be reduced in AD [21] contributing to the accumulation of Aβ in the brain. Additional receptors, including ABCA1, can facilitate Aβ efflux in a APOE dependent manner with with ApoE2 and E3 forming complexes with Aβ more efficiently than E4 https://alzres.biomedcentral.com/articles/10.1186/alzrt187. Soluble transports, such as sLRP, bind to Aβ in the plasma preventing it from entering the ISF [21]. Bulk flow transport of ISF to the CSF and through the arachnoid villi into the blood stream provides another route of Aβ clearance.

The proteasome and lysosome are known to mediate proteolysis. The proteasome is a protease complex that degrades proteins that have been tagged with ubiquitin polymers [22]. In AD, ubiquitin tags are known to accumulate in both Aβ plaques and NFT. Proteasome activity is known to be reduced in the hippocampus in AD brain compared to control and Aβ has been shown to inhibit proteasome function [23]. Lysosomal degradation commonly degrades extracellular and cell surface proteins. Proteins are internalised by endocytosis and degraded within the lysosome, a double membrane vesicle containing proteases and acid hydrolyses (such as phosphatases) [22]. Dysfunction in lysosome autophagy has been reported in numerous studies and includes the presence of endosomes with undigested contents in AD [24].

In addition to the above processes, specific enzymes may degrade Aβ. However, the exact contribution of these enzymes and their effect on Aβ level in the human brain are yet to be established. These include endothelin-converting enzyme (ECE) and angiotensin converting enzyme (ACE) [22].

Increased permeability of the BBB can lead to infiltration of Aβ and other molecules from the blood as discussed further in section 1.1.3.4 [25]. In addition, transporters on the BBB can be

involved in uptake of Aβ into the brain. The receptor for advanced glycation end products (RAGE) transports Aβ from the blood across the BBB into the brain [26]. The level of RAGE is determined by the level of its ligands and RAGE levels on blood vessels and have been shown to be elevated in AD[27]. Consequently, RAGE has become a therapeutic target [20, 27].

1.1.1.1.2 Tau

In addition to Aβ plaques, intraneuronal NFTs are a second pathological hallmark of AD (Figure 1-2B). These are made up of paired helical filaments composed of hyperphosphorylated microtubule associated binding protein tau (MAPT) [28 29]. NFT pathology spreads through the brain in a predictable manner, as documented by Braak and Braak [30], leading to the use of 'Braak staging' to indicate disease progression. NFTs are present in the entorhinal region and subiculum in stages I-II, also involve the limbic region and adjacent inferior temporal neocortex in stages III-IV, and the neocortex in stages V-VI. Braak stages correlate well with the progression of AD symptoms, which indicates the importance of NTF in AD pathogenesis. In stages I-II, there is no clinical manifestation of disease. In stages III-IV symptoms include short term memory loss, lack of spatial awareness,

When NFT have progressed to the neocortex in stages V-VI the symptoms include a decline in the ability to communicate and changes in mood and behaviour [31].

The presence of tau pathology alone can cause other neurodegenerative disorders emphasising the involvement of tau in neurodegeneration. Together with AD these are collectively known as tauopathies. Tauopathies include several forms of frontotemporal lobe degeneration (FTD-tau), corticobasal degeneration and progressive supranuclear palsy [32].

1.1.1.1.3 Cerebrovascular pathology

The deposition of Aβ in blood vessel walls is known as CAA (Figure 1-2C). CAA is present in over 90% of patients with AD [33] and approximately 33% of elderly people who do not have AD [33]. CAA is often asymptomatic, though can present as intracranial haemorrhage and dementia [34]. The severity of CAA varies considerably, with advanced CAA being present in approximately 25% of AD patients [35]. Most of the Aβ deposited in the vasculature is $A\beta_{1\text{-}40}$ rather than $A\beta_{1\text{-}42}$. There are rare forms of heritable CAA in which mutations in the APP gene cause preferential build-up of Aβ in blood vessels leading to cerebral haemorrhage. In one study, Dutch type hereditary CAA dementia was predicted by the amount of severely amyloid laden vessels as opposed to severity of other AD pathologies [35].

Cerebral microbleeds are a hallmark of CAA and are present in higher numbers in AD when compared to the general population and other forms of dementia [35]. Moderate to severe CAA is associated with impaired cognition in the elderly even with controlling for other pathologies [36]. CAA is frequently present in AD with PSEN1 and Arctic APP mutations [37] and there is evidence that CAA in AD is correlated with more severe cognitive impairment than those with AD but no CAA [38] [39] [40]. In patients with CAA the vascular smooth muscle layer of arteries and arterioles tends to degenerate which probably contributes to the risk of rupture of the vessel wall and intracerebral bleeding. It is also increasingly recognised that ischaemic regions are common in CAA [41]. In AD microbleeds are associated with increased severity of dementia but it is not clear whether this is because they contribute directly or are simply a marker of severe CAA. There is evidence that Aβ contributes to the production of reactive oxygen species (ROS) in the vasculature, which can interfere with vascular signalling and damage proteins, lipids and DNA [42]. The extent of CAA has been reported to predict longitudinal episodic memory decline in presymptomatic autosomal dominant AD and global cognitive decline in symptomatic AD [43].

1.1.1.2 Genetics

Familial AD (FAD) is directly caused by heterozygous dominant mutations and makes up

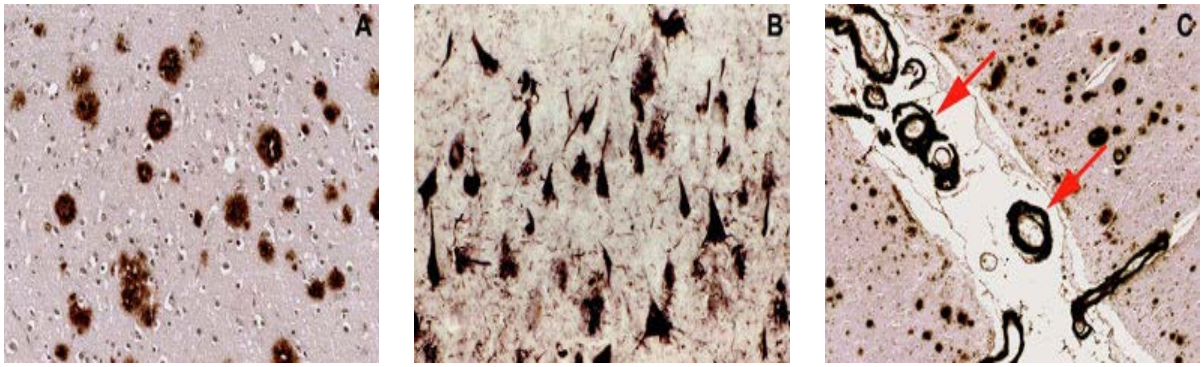

Figure 1-2 AD pathology. [A] Extracellular Aβ plaques immunolabelled for Aβ. [B] Intraneuronal neurofibrillary tangles immunolabelled for tau. [C] Deposition of Aβ in the walls of cerebrocortical and leptomeningeal blood vessels as indicated by the red arrows. Figure courtesy of the South West Dementia Brain Bank (SWDBB).

fewer than 5% of all AD cases [44]. FAD-causing mutations have been identified in the genes encoding APP (*APP*), presenilin 1 (*PSEN1*) and presenilin 2 (*PSEN2*). Although these full-penetrance disease causing mutations are rare, they provide insight into the mechanisms of sporadic AD.

Mutations in the gene encoding APP lead to the deposition of Aβ by favouring the processing of APP by β and γ secretase rather than α secretase. This results in the

formation of more $A\beta_{1-40}$ and $A\beta_{1-42}$ or a shift in the proportion of $A\beta_{1-42}$ production compared $A\beta_{1-40}$ [17, 45]. To date, over 40 pathogenic mutations of APP have been identified [46 47]. Mutations in PSEN1 and PSEN2 account for up to 80% of FAD [44]. Presenilin genes 1 and 2 code for the catalytic component of the γ-secretase complex [48] discussed in 1.1.1.1.1. The majority of mutations are found within the *PSEN1* gene with 205 pathogenic mutations identified to date. 13 pathogenic mutations have been identified within the *PSEN2* gene [46]. Mutations in *PSEN1* and *PSEN2* alter γ-secretase cleavage of APP, resulting in overproduction of $A\beta_{1-42}$ which forms plaques more readily than $A\beta_{1-40}$ [45 49].

Numerous other genetic risk factors have been identified by genome-wide association studies (GWAS). Genetic risk factors are variants in genes common in the population that can increase or decrease an individual's risk of developing a disease. GWAS studies are conducted using data form tens of thousands of individuals [50]. The AlzGene database is an open access resource that collates potential AD susceptibility genes and performs systematic meta-analysis with available data [51].

The gene encoding apolipoprotein E (apoE) is the highest ranked in the database with numerous case-controlled studies conducted across ethnic groups. ApoE is produced in the brain by neurons and astrocytes. It has roles in mobilisation of cholesterol during neuronal growth and after injury [44]. There are three main isoforms of apoE: apoE2, apoE3, and apoE4 encoded by three alleles of the *APOE* gene: *APOE*ε2, *APOE*ε3 and *APOE*ε4. Many studies have shown an association between the ε4 allele and an increased risk of developing late onset AD. The presence of an apoE4 allele is thought to accelerate disease development for a number of reasons, one of which may be causing increased deposition of Aβ by modulating its protein metabolism, aggregation, and deposition [52]. *APOE*ε4 increases the risk of AD in a gene-dose dependent manner: 20% of non-carriers have AD, ~45% of heterozygotes develop AD and over 90% of those homozygous for *APOE*ε4 develop AD[52, 53].

Since the discovery of APOE, further risk genes have been identified including those involved with inflammation (e.g. CLU, ABCA7) and synaptic functioning (e.g. PICALM, CD33) [50]. Next generation sequencing can sequence whole genomes at high throughput leading to the discovery of rare genetic variants [50]. *TREM2* has been identified with an effect size similar to that of APOE ε4 in association with late-onset Alzheimer's disease. *TREM2* is expressed on microglia and is thought to have a role in immune response [54]. GWAS and next generation sequencing are powerful tools for identifying risk genes, though the challenge of locating the variants directly involved in AD pathogenesis remains.

1.1.1.3 Amyloid cascade hypothesis

The amyloid cascade hypothesis was first proposed in 1992 [16], and updated in 2002 [17] and 2016 [55]. This is the leading hypothesis for the development of and, as a result, has become the focus of much AD research. The hypothesis states that the deposition of Aβ peptide is the cause of AD. It is then hypothesised that NFTs, cell loss, vascular damage and dementia following as a direct result of Aβ deposition. A driver behind the amyloid hypothesis is that mutations in the *APP* and *PSEN* genes cause AD, present with amyloid plaques and intraneuronal NFTs [56]. In contrast, mutations in *MAPT* cause a tauopathy but no amyloid plaques. This indicates that APP, and therefore Aβ, is further upstream in disease pathogenesis [32].

1.1.2 Vascular dementia

VaD is dementia that results from damage caused by reduced oxygenation of the brain as a consequence of systemic or cerebral vascular disease. VaD encompasses a group of conditions that together make up the 2nd largest cause of dementia [57]. The term vascular cognitive impairment (VCI) has more recently been used to describe a broader range of cognitive impairment associated with cerebrovascular disease, ranging from vascular cognitive impairment, no dementia (VCIND)/mild VCI to VaD as the most severe form.

There are several subtypes of VCI that each possess distinct clinical and pathological features. Subtypes of VaD include: cortical VaD (multi-infarct dementia, post-stroke VaD), subcortical VaD (small-vessel dementia, Binswanger's disease, subcortical ischaemic vessel disease) and strategic infarct dementia [58].

Reduction in blood flow leads to reduced oxygenation of the brain. The combination of reduced oxygen levels and impaired clearance of H^+ ions causes neurons and glial cells to degenerate, leading to the onset of symptoms. Clinical signs of VaD vary according to the subtype of VCI responsible, though symptoms can include memory impairment, dysexecutive syndrome, communication difficulties and a range of psychological symptoms. VaD is commonly diagnosed according to the NINDS-AIREN criteria [59]. The clinical history and examination, including assessment of cardiac risk factors, measurement of blood pressure and other aspects of cardiovascular function, are combined with results from cognitive testing to reach a diagnosis.

There are currently no drug treatments licenced for use specifically in VaD. Typically, treatment plans focus on controlling cardiovascular risk factors, such as diabetes, cigarette smoking and high blood pressure [6]. Treating VaD with AChE inhibitors and memantine has shown limited benefit [60].

1.1.2.1 Genetics

There are a limited number of autosomal dominant gene mutations that can cause VaD. Cerebral autosomal dominant arteriopathy with subcortical infarcts and leukoencephalopathy (CADASIL) is the most common form of inherited stroke and VaD. Patients with CADASIL exhibit similar symptoms and neuropathology to those with SVD but have an earlier age of onset. The mutation for CADASIL occurs in the gene encoding the Notch3 receptor on the smooth muscle of blood vessels[61]. These mutations alter the extracellular domain of the Notch3 receptor which causes accumulation of the Notch3 cleavage product in small arteries. Mice engineered to express CADASIL mutations have been used as a model of VaD [62].

1.1.2.2 Neuropathology

Atherosclerosis, small vessel disease (SVD) and CAA are the three main pathologies the contribute to VCI and VaD (hereafter the abbreviation VaD is used to encompass both VCI and VaD). Atherosclerosis effects large to medium blood vessels that supply blood to the brain, such as those of the circle of Willis. Atherosclerotic plaques form in blood vessels due to the deposition of cholesterol, and can thombose, fibrose, calcify or expand by inflammation and/or haemorrhage to narrow the vessel lumen. This directly reduces blood flow [63] and can also lead to embolism or dissection.

SVD is the most common cause of pathology underlying VaD [64]. SVD encompasses degenerative changes in the vessel wall of arterioles, capillaries and venuoles [65]. Arterioles are affected by arteriolosclerosis where deposition of cholesterol can lead to narrowing of vessel lumen and hardening of vessel walls. In addition, capillary damage is probably an under-recognised contributor to SVD in dementia [66]. SVD manifests in the subcortical white matter, leaving cortical vessels unaffected [63]. CAA has been described above (1.1.1.1.2) and presents in approximately 10% of VaD cases [64].

Atherosclerosis, SVD and CAA can all lead to destructive lesions within the brain, including infarcts, white matter lesions and haemorrhages. Atherosclerosis is commonly associated with large infarcts. SVD can produce multiple pathologies including white matter infarcts (typically lacunar infarcts) and intracerebral haemorrhages, often deep within the basal ganglia. CAA predominantly causes more superficial lobar haemorrhages [63].

Diagnosis of VaD is challenging due to the diverse cerebrovascular pathologies that can be associated with the disease and the absence of specific neuropathological findings [64]. The diagnosis of ‘pure’ VaD is made when a spectrum of vascular abnormalities are present without significant coexistent neurodegenerative pathologies in a person with dementia. However, this diagnosis of VaD by exclusion captures only a minority of people whose

dementia is associated with vascular brain damage [64], the contribution of which is probably markedly under-recognised.

1.1.3 Cerebrovascular aspects of AD

Atherosclerosis was observed in Alois Alzheimer's first report of AD and vascular abnormalities are once again a focus of attention in AD research [67]. There is growing evidence that vascular dysfunction has a role to play in the pathogenesis of AD.

1.1.3.1 Risk factors

Numerous epidemiological studies have highlighted links between cardiovascular factors and the development of dementia. Risk factors for cardiac disease are also risk factors for dementia, these include hypertension, tobacco smoking, type 2 diabetes and stroke [68]. Extra weight midlife has been correlated with earlier onset of dementia independent of other cardiovascular risk factors such as diabetes, hypotension and stroke [69]. Those with cardiac risk factors also exhibited more severe tau pathology and CAA accumulation [70]. Together with epidemiological studies, combined GWAS and pathway analysis has identified genetic links between cardiovascular disease pathways and AD [71].

1.1.3.2 Cerebral blood flow

Reduction in cerebral blood flow (CBF) is a defining pathological process in VaD and is thought to contribute to the pathology and exacerbate clinical manifestations of AD [72]. CBF is regulated by local neuronal activity and metabolism through a process known as neurovascular coupling. The pial and intracerebral arteries and probably also the capillaries control the local increase in CBF that occurs during brain activation – known as functional hyperaemia.

Reduced CBF results in a decrease in oxygen concentration in the brain and a chronic reduction in perfusion can result in cell death. Mild hypoperfusion negatively affects protein synthesis, required for long-term potentiation (LTP) and therefore alters synaptic plasticity and memory formation [42]. More severe CBF reduction can affect adenosine triphosphate (ATP) synthesis reducing the ability of neurons to form action potentials [73].

Blood flow and oxygenation are reduced in the cerebral cortex and underlying white matter in AD [74]. This has been shown through imaging studies using arterial spin labelling [75, 76] and via measuring fluorodeoxyglucose (FDG) uptake in the brain as a measure of blood flow (FDG is taken up by neurons in amounts directly proportion to their blood supply, but not then metabolised by glycolysis) [77]. Hypoperfusion has also been shown in post-mortem brain tissue, using molecular markers, including VEGF [78, 79]. CBF is reduced before cognitive

decline or brain atrophy [74, 80] and is associated with biochemical and MRI evidence of tissue damage [81, 82].

Reduced CBF and cerebrovascular dysfunction can increase the accumulation of toxic brain metabolites including Aβ [83 84]. This has been attributed to reduced clearance combined with increased APP production [85] via the γ secretase pathway [42 86] and HIF1α-mediated transcriptional increase in β-secretase expression [87].

1.1.3.3 Vasoconstriction

Together with CAA and SVD, the narrowing of blood vessels in AD appears to be compounded by an increase in molecular factors that cause vasoconstriction. Aβ itself, in addition to its role in causing CAA, can lead to vasoconstriction. This finding has been replicated in murine models overexpressing APP [88, 89]. Endothelin 1 (EDNI) is a potent vasoconstrictor; in post-mortem human brain the levels of EDNI was found to be elevated in AD compared to controls [79, 90]. Angiotensin II (AngII) is another vasoconstrictor whose levels are significantly elevated in the post-mortem AD brain [91]. Nitric oxide produced by endothelial cells can signal smooth muscle to relax, therefore mediating vasodilation of blood vessels. In AD, nitric oxide signalling is impaired by Aβ, this has been shown *in vitro* [92] and *in vivo* [93]. Finally, there is a reduction in cholinergic innervation of cerebral vessels which is likely to cause vasoconstriction. ACh is a potent vasodilator, so a reduction in the availability of this ligand would result in vasoconstriction and reduced CBF. The use of AChE inhibitors to treat AD by prolonging the action of ACh may indeed provide therapeutic benefit by its action on the cerebral vasculature [94, 95].

1.1.3.4 Blood-brain barrier

The BBB is a formed by specialised endothelial cells that line the blood vessels at the interface of the circulatory system and the CNS. The cells are joined by tight junctions to form an interface that limits the entry of red blood cells, leukocytes and components of plasma to the brain and regulates the entry of nutrients and metabolites. Pericytes, astrocytes and neurons, together with endothelial cells work to control blood flow, maintain the integrity of the BBB and regulate the clearance of metabolites, including potentially toxic molecules such as Aβ [73]. The maintenance of an intact BBB is essential for healthy neuronal function. The BBB can be disrupted by a number of pathological conditions including stroke, certain pathogens and AD as well as an increase in angiogenic factors such as VEGF. The dysfunction and breakdown of the BBB allows infiltration of immune cells, large molecules such as fibrinogen and ions, and affects clearance from the brain [96]. The results can include neuroinflammation, neuronal dysfunction, and eventually, neurodegeneration.

BBB breakdown has been demonstrated in several post mortem studies of AD [37]. Magnetic resonance imaging (MRI) studies have demonstrated BBB permeability in cognitively normal individuals at risk of AD [97], AD patients [98, 99] and carriers of APOEe4 [98, 100]. The levels of tight junction and adherens proteins are known to decrease in AD and the age-dependent loss of pericytes in mice has been shown to lead to BBB dysfunction, neurodegeneration and cognitive decline [73]. AD patients and animal models have also shown reduced Aβ clearance from the brain [73, 101].

1.1.3.5 Blood vessel density and angiogenesis

There is strong evidence that capillary density decreases with age in animal and human brain [102]. Studies have also reported a decrease in capillary density in AD. This includes decreases of up to 16% with age matched controls [102].

It has been hypothesised that AD is caused by an increase in blood vessel density at least in the early stage of disease. In one study the length of blood vessels was measured in the hippocampal regions of control, AD, VaD and post-stroke post mortem tissue [103]. The length density of vessels in the CA1 region of the hippocampus was found increased in AD compared to control whereas the vessel diameter was reduced in AD and VaD samples [103]. This implies that there may be increased angiogenesis in response to reduced CBF in AD though this increase could be a result of tissue atrophy in the hippocampus in AD. The decrease vessel diameter is likely to be due to increased vasoconstriction in AD and VaD as described in 1.1.3.3. Despite a possible increase in vessel density, blood vessels in AD and VaD appear less effective at perfusing brain tissue.

Another study of post-mortem tissue showed that though overall brain mass was reduced capillary density was not reduced in AD compared to control [104]. However, there was an increase in string capillaries, in AD compared to control groups indicating that cerebrovascular may be dysfunctional in AD. String capillaries are caused by a collapse of functional capillaries following reduced CBF and are not able to carry blood flow [105].

1.2 VEGF

The VEGF superfamily consists of 7 members with structural and functional similarities but different physiological functions. In mammals, the VEGF family comprises four homologues (VEGF-A, -B, -C and -D) and placental growth factor (PlGF)[106]. Structurally similar VEGF-E is found in parapoxvirus and VEGF-F exists in snake venom [107]. VEGF-A, -B and –C and PlGF have been described in the human nervous system. Each form of VEGF can bind to and activate tyrosine kinase receptors (VEGFR1, VEGFR2 and VEGFR3) and numerous co-receptors. This thesis focuses on VEGF-A and two of its tyrosine kinase receptors, VEGFR1

and VEGFR2. The interactions between the VEGF-A, -B and -C and their tyrosine kinase receptors summarised in Figure 1-3.

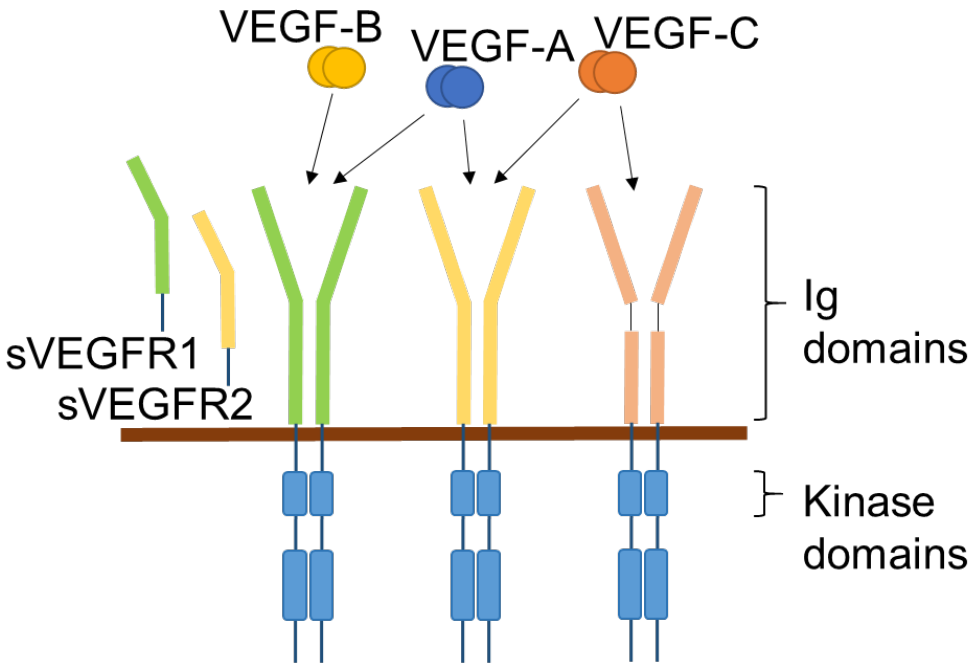

Figure 1-3 The interaction between VEGF-A, -B and C and their tyrosine kinase receptors in the nervous system. VEGF-A binds to VEGFR1 and VEGFR2, as well as the soluble form of VEGFR1, sVEGFR1. VEGF-A weakly binds to sVEGFR2. VEGF-B binds only to VEGFR1 and sVEGFR1. VEGF-C binds to VEGFR2, sVEGFR2 and VEGFR3.

1.2.1 VEGF-A

VEGF-A, hereafter referred to as VEGF, is a homodimeric glycoprotein comprised of two subunits to form a protein of approximately 40 kDa [107]. VEGF expression is induced by hypoxia. Hypoxia allows stabilisation of hypoxia inducible factors (HIFs) which bind to the hypoxia response element on the *VEGF-A* promotor resulting in VEGF transcription [107].

Transcription of the human *VEGF-A* gene results in the production of 9 mRNA isoforms: 111, 121, 145, 148, 162, 165, 183, 189 and 206 [108]. These are formed by the alternate splicing of exons 6 and 7 with the numbers representing the number of amino acids in the resulting protein [109]. Isoform 121 is freely diffusible while 186 and 206 are nearly completely sequestered in the extracellular matrix. $VEGF_{165}$ has intermediate properties with 50% freely diffusible and 50% in the extracellular matrix [109]. The most commonly expressed isoforms are 121, 165, 189 with $VEGF_{165}$ being the most well studied [110] [111]. There are two families of VEGF-A isoforms: $VEGF_{xxx}a$ and $VEGF_{xxx}b$. $VEGF_{xxx}b$ is formed by the alternate splicing of terminal exon 8 of *VEGF-A* and is described in more detail in 1.2.1.2 [112, 113].

VEGF acts through its receptors on the cell surface and soluble receptors in the cytoplasm as well as via co-receptors. These include tyrosine kinase receptors VEGFR1 and VEGFR2 (shown in Figure 1-3) and co-receptors, such as neuropilin 1 (NRP1) and 2 (NRP2). In all VEGF-A variants exons 2–5 determine the specificity for VEGFRs while exons 6 and/or 7 and 8 determine co-receptor binding. VEGFs can simultaneously bind two distinct receptors such as VEGFR2 and co-receptors, such as neuropilins, even when those receptors are expressed separately on adjacent cells [114].

VEGF-A is by far the most thoroughly investigated subtype of VEGF in health and disease. First discovered as a lymphatic factor [115], VEGF is most well known in relation to angiogenesis. Expressed in development, it is vital for the correct formation of the vascular system as illustrated by the finding that heterozygous VEGF knock-outs die *in utero* [116, 117]. VEGF and its receptors have also been heavily studied in pathological angiogenesis, particularly in relation to tumour development [118-120]. More recently new roles for VEGF within the nervous system have emerged. VEGF is involved in neuroprotection and neurogenesis in the hippocampus. VEGF is also a modulator of inflammation and astrocyte proliferation [121].

1.2.1.1 Other VEGFxxx isoforms

1.2.1.2 VEGFxxxb

This VEGF subtype is formed from a splice variant that causes a change in the 6 terminal amino acids of the protein. As a result, the $VEGF_{xxx}b$ family has the same number of amino acids as $VEGF_{xxx}a$ but has a different biological role. Due to the difference of only the 6 terminal amino acids, detection can prove difficult [112], leading to debate over the existence of $VEGF_{xxx}b$ isoforms [111]. To date three members of the $VEGF_{xxx}b$ family have been identified: $VEGF_{165}b$, $VEGF_{121}b$ and $VEGF_{186}b$ [122-124].

$VEGF_{165}b$ isoforms have anti-angiogenic actions, opposing the actions of $VEGF_{165}a$ [112, 113] and investigation has revealed $VEGF_{165}b$ phosphorylates VEGFR2 in a different way to $VEGF_{165}a$ [109]. The ratio of these subtypes may prove important in disease as indicated by one study that measured $VEGF_{165}a$ and $VEGF_{165}b$ expression level in human lung biopsies and found significant changes in subtypes between control and disease tissue [109]. There has been one published investigation of the $VEGF_{xxx}a$ and $VEGF_{xxx}b$ subtype levels and distribution in the CNS [125]. $VEGFR_{165}b$ was identified by immunohistochemistry and strongly expressed by neurons in the hippocampus and expressed in a small number of neurons throughout the cortex [125]. $VEGFR_{165}b$ was estimated to make up to 45% of total VEGF in the hippocampus and cortex [125].

1.2.1.3 VEGF-Ax

To complicate the VEGF story further, another variant was identified by Eswarappa et al (2014) [126]. VEGF-Ax was first identified in mammalian endothelial cells, including human umbilical vein endothelial cells (HUVECs), and immunofluorescence confirmed VEGF-Ax present in human brain [75]. VEGF-Ax has also been shown to be altered in disease states [75].

The VEGF-Ax ('x' standing for extension) variant has a unique 22 amino acid C-terminus extension in comparison to $VEGF_{165}$. VEGF-Ax is formed by programmed translational read-through of *VEGFA* mRNA. In normal translation, the stop codon prevents translation of any sequence following it. In programmed translational read-though, a cis-acting sequence lies downstream of the stop codon and 'programmes' read-through, distinguishing the process from translational error. In the case of VEGF-Ax, an RNA segment following the stop codon encodes the peptide extension of VEGF-A and acts as a cis-acting regulatory element driving the post-translational read-through [126].

VEGF-Ax was initially reported to have an anti-angiogenic effect [126], though a recent report from Xin et al (2016) contradicted this finding [127]. In work conducted on endothelial cells, VEGF-Ax administration was reported to reduce migration, proliferation and tube formation. This was reported to be due to VEGF-Ax binding to VEGFR2 at a similar affinity to VEGF but not to the co-receptor NRP1. It was also found to activate the non-canonical pathway of VEGFR2 signalling, a finding leading to the hypothesis that it acts as a decoy ligand [126, 128]. In the later study, VEGF-Ax was found to stimulate endothelial cell migration, angiogenesis and permeability and induce VEGFR2 receptor phosphorylation [128]. In agreement with Eswarappa et al. (2014), VEGF-Ax was found to be less potent than VEGF, consistent with its inability to bind to NRP1[126]. Further work is needed to establish the function of this isoform in the brain.

1.2.1.4 VEGF-B

VEGF-B binds only to VEGFR1 and NRP1 [106]. Two isoforms of VEGF-B have been described in humans, $VEGF\text{-}B^{167}$ and $VEGF\text{-}B^{186}$, formed by alternative splicing of the gene, *VEGFB,* [129]*.* Unlike VEGF, *VEGFB* knock-out mice are born healthy, indicating that VEGF-B is not essential for development under normal conditions [129]. VEGF-B does not optimally rotate VEGFR1, like PlGF, so is a weaker activator of signalling [130]. VEGF-B may be more relevant to angiogenesis under pathological conditions [106]. VEGF-B was found to have a detrimental effect in a mouse model of stroke. VEGF-B expression increased infarct volume by up to 40% when the middle cerebral artery was ligated in mice [131].

Although it probably only has a minor role in angiogenesis, it is thought that VEGF-B may have a more important role in the nervous system function. VEGF-B is highly expressed in murine CNS development, where VEGF-B mRNA levels were higher than *VEGF*-A [132]. VEGF-B has been identified in cortical neurons, spinal motor neurons and retinal ganglion cells [129]. VEGF-B has a role in adult neurogenesis. VEGF-B deficient mice were given VEGF-B and neurogenesis returned to wild type levels [133]. VEGF-B is also neurotrophic, promoting the survival of neurons by acting on VEGFR1. ALS mutant mice lacking VEGF-B experience more severe motor neuron neurodegeneration [134].

1.2.1.5 VEGF-C

VEGF-C has a major role in lymphogenesis [135] but also has roles in the nervous system including angiogenesis, neuronal and oligodendrocyte development [136, 137]. VEGF-C acts via VEGFR2, VEGFR3 [135] and coreceptor, NRP2 [106]. The sVEGFR2 isoform is an endogenous antagonist for VEGF-C actions, binding and limiting the bioavailability of the ligand [106].

VEGF-C, acting through VEGFR3, is essential for lymphogenesis but is also required for coordinating tip cell sprouting in new blood vessels. VEGF-C is produced by macrophages and promotes vessel sprouting via VEGFR3 [138].

In the nervous system VEGF-C regulates neural cell development via VEGFR3 [138]. VEGF-C also regulates expansion of oligodendrocyte precursor cells (OPCs) and neural progenitors [136]. Mice deficient in VEGF-C have selective loss of OPCs from optic nerve [136].

1.2.2 VEGF receptors

1.2.2.1 VEGFR1

VEGFR1 is able to bind VEGF-A, VEGF-B (Figure 1-3) and PlGF [139]. Membrane-bound VEGFR1 (mbVEGFR1) has an extracellular domain with 7-immunoglobulin like loops, a short transmembrane domain and an intracellular tyrosine kinase domain. VEGFR1 is mostly present as a homodimer. VEGFR heterodimers have been discovered, though their physiological function remains unknown [129]. VEGFR1 shares 40.3% total sequence homology with VEGFR2. Despite the kinase domain being the most highly conserved between receptors, the VEGFR1 kinase is impaired [125140126]. The level of phosphorylation catalysed by VEGFR1 tyrosine kinase is low and only detectable in models that overexpress the receptor [107]. VEGFR1 is expressed in response to hypoxia as the promotor region contains a 40bp hypoxia response element, including the HIF binding site.

VEGFR1 was initially thought to be expressed only on vascular endothelium but has now been identified throughout the body [109]. In the vascular system VEGFR1 has a direct role in endothelial cell migration [106]. In the brain VEGFR1 expression has been observed in cultured

microglia [141], by immunohistochemistry in microglia in human brain [142] and in developing and adult neurons [110]. There is debate over the expression of VEGFR1 by astrocytes (Chapter 3).

VEGFR1 was hypothesised to act as a decoy receptor to prevent the over activation of VEGFR2. This was based on evidence that VEGFR1 lacking a tyrosine kinase domain is sufficient for normal development and angiogenesis [143] and VEGFR1 possesses a higher binding affinity for VEGF than VEGFR2 [129]. This view has been challenged as VEGFR1 appears important in postnatal angiogenesis, neuroprotection and immune cell migration. It has been demonstrated that VEGFR1 and VEGFR2 both play distinct roles in signal transduction in endothelial cell models [144]. VEGFR1 is upregulated in certain pathological conditions such as hypoxia and malignancy, so much so that it may become the dominant signal transducer [145].

The VEGFR1 gene, *FLT1*, produces at least 9 splice isoforms that transcribe proteins with different cellular localisations and properties. VEGFR1 splice isoforms can be membrane bound (mbVEGFR1), soluble (sVEGFR1) and intracellular (iVEGFR1), as summarised in

Table 1-1 and Figure 1-4. sVEGFR1 is described in detail below (1.2.2.1.1). Four isoforms of iVEGFR1 have been identified. iVEGFR1 isoforms possess the intracellular domains including one or two kinase regions and the c terminal tail. They were first identified in cancer cell lines and can activate Src signalling pathways [146]. There have been no investigations into iVEGFR1 in the nervous system to date.

1.2.2.1.1 sVEGFR1

sVEGFR1 receptor negatively regulates VEGF binding [147]. sVEGFR1 has the highest binding affinity for VEGF of any of its receptors and accounts for more than half of vascular endothelial bound VEGF receptor sites [148]. It should be noted that many studies focus on VEGF-A as the only ligand for sVEGFR1 but sVEGFR1 is also able to bind VEGF-B and PlGF which are also present in the nervous system [149].

sVEGFR1 isoforms exist in monomeric (110) and dimeric forms (220 kDa)[149] both of which are also detectable when bound to VEGF resulting in a band at higher molecular weights (~140 and ~240 kDa respectively) [147, 150, 151]. To date four soluble isoforms of VEGFR1 have been reported. sVEGFR1 isoforms have Ig-like domains but do not possess any transmembrane and cytoplasmic regions (Figure 1-4). Changes in nomenclature have made identification of isoforms in the literature challenging. The sVEGFR1 isoforms described are summarised in Figure 1-4 and

Table 1-1. sFlt_v1 was discovered first by Kendall et al (1993)[147] and is commonly referred to as sVEGFR1. sFlt_v2, otherwise known as sFlt-14 or sFlt1_e15a, was discovered by Thomas et al. (2007) [152]. sFlt_v2 has a predicted molecular weight of 82 kDa and is observed around 135 kDa but has been reported at other molecular weights from 95-135 kDa due to varying glycosylation states [153-155]. sFlt1_v2 has been found expressed up to 600x more than other sVEGFR1 subtypes in placenta [156]. sFlt_v3 differs from sFlt_v2 by alternate splicing of exon 15 leading to its alternative name, sFlt_e15b [153, 157, 158]. sFlt_v4 was first discovered by Jin et al. (2008) [159] and then confirmed by Thomas et al. (2009)[160]. sFlt_v4 possesses a distinct c-terminal sequence[159]. Overall the regulation of sVEGFR1 isoforms appears to be tissue and disease specific with the molecular details still being uncovered [151, 161].

In addition to alternative splicing there is increasing evidence of sVEGFR1 production via proteolytic cleavage. First reported by Cai et al. (2006) in endothelial cells [162] cleavage of mbVEGFR1 released an 80 kDa c-terminal fragment intracellularly, the cleavage was found to be dependent on γ-secretase [163, 164]. Cleavage is dependent on the VEGFR1 c-terminal remaining intact and VEGFR1 being present as a homodimer rather than a heterodimer with VEGFR2 [165]. This cleaved version was found in the conditioned media of cells at 130 kDa [164, 165]. The cleaved sVEGFR1 was shown to have the same antagonist action as the splice variant of VEGFR1 [164]. The cleavage and intracellular trafficking of receptor tyrosine kinases via proteolytic cleavage has now been reported in at least 10 receptor tyrosine kinase subfamilies and has been reviewed in further detail [166].

When measuring the level of sVEGFR1, the relative abundance of sVEGFR1 appears to be tissue- and condition-specific. In HUVECs, sVEGFR1 transcripts have been reported to be 1.5–2.5-fold more abundant than VEGFR1. In cytotrophoblasts, a cell type specific to the placenta, sVEGFR1 transcripts are 250-fold more abundant than VEGFR1 [160]. Lack of consistency in reporting sVEGFR1 protein level has been documented by Wu et al. (2010) [149]. The variability in reported sVEGFR1 levels may be due to differing protocols and sample processing as well as tissue heterogeneity [149]. Relative abundance of sVEGFR1 in the nervous system has not been reported.

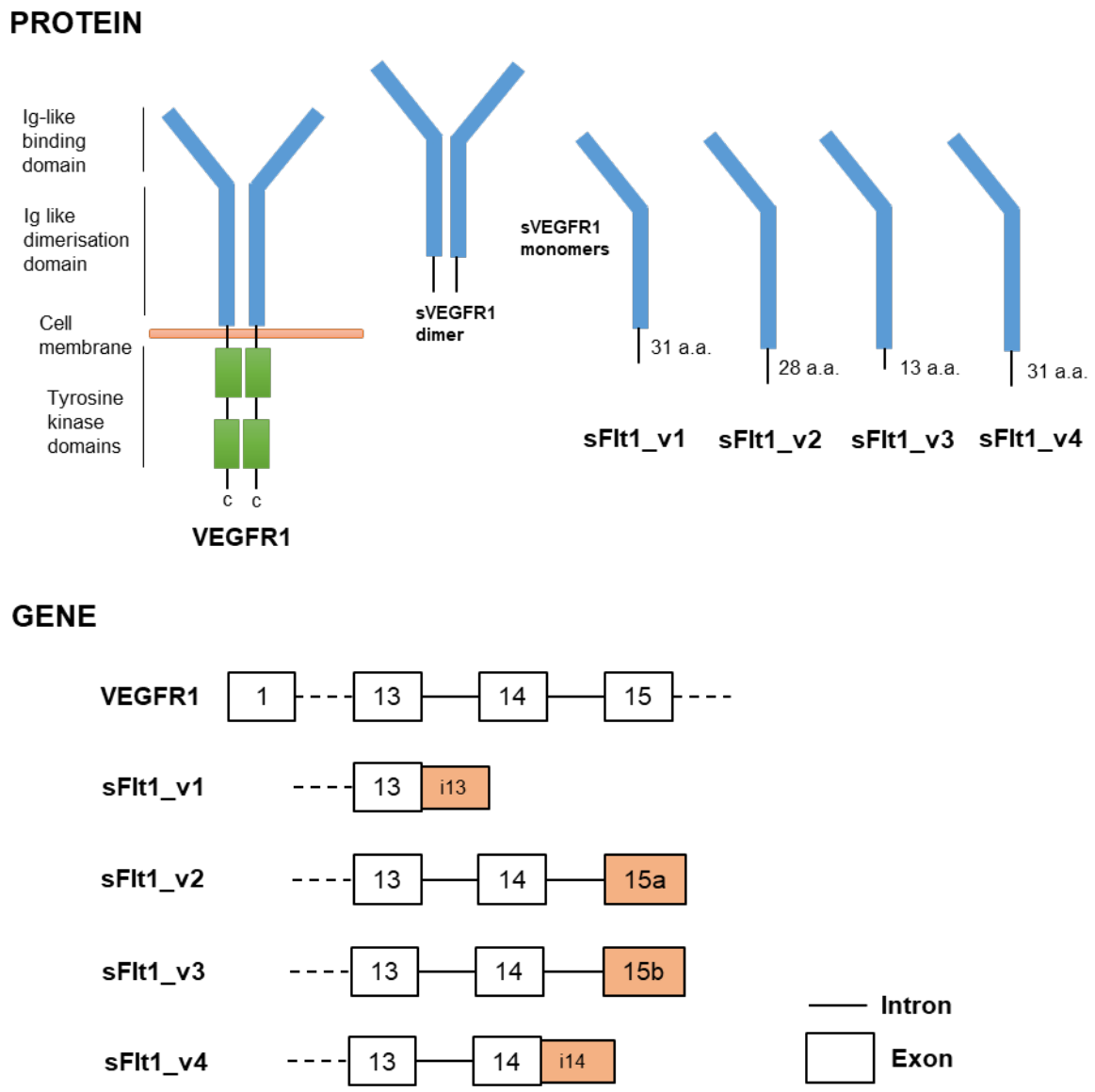

Figure 1-4 VEGFR1 and sVEGFR1 protein and splice variants. mbVEGFR1 is a dimer with extracellular immunoglobulin (Ig)-like domains and intracellular tyrosine kinase domains. sVEGFR1 can be found as a dimer or a monomer. There are 4 splice variants that result in the production of four protein products with different c-terminal lengths and sequences. All sVEGFR1 isoforms contain exons 1-13. sFlt1_v1 consists of additional intron 13. sFlt1_v2 consists of addition sequence in exon 14 and 15. sFlt1_v3 consists of additional sequence from exon 14 and 15. sFlt1_v4 consists of additional sequence from intron 14. Figure adapted from [149, 157, 158].

VEGFR1 isoforms	Alias	Location	Nucleotide RefSeq NCBI	Protein RefSeq NCIB	qPCR Primer ID	Primary Antibody	Predicted kDa	Observed kDa	Notes
1	VEGFR1 Flt1	Cell membrane Endosome	NM_002019.4	NP_002010.2	Hs01052961_m1	Abcam Ab32152 (Y103)	151	180	Longest form. Transmembrane receptor including kinase region.
2	sVEGFR1 sFlt1 sFlt_v1[158] sFlt_i13[152]	Secreted	NM_001159920.1	NP_001153392.1	Hs01052961_m1	Abcam Ab32152 (Y103)	77	100	Short distinct c terminus, lacks transmembrane and cytoplasmic regions of isoform 1. Truncation of intron 13 [167].
3	sFlt1-14[153] sFlt1_v2[158] sFlt1_e15a[152]	Secreted	NM_001160030.1	NP_001153502.1	Hs01052961_m1	Abcam Ab32152 (Y103)	82	135	Short distinct c terminus, lacks transmembrane and cytoplasmic regions of isoform 1. Alternative splicing - exon 15a[152]. Highly expressed in placenta [156, 157].
4	sFlt1_v3 sFlt1_e15b[158]	Secreted	-	-	-	Abcam Ab32152 (Y103)	82	135	Differs in exon 15 – alternative splicing of exon 15b creates a unique 13 a.a. tail [158].
5	sFlt1_v4 Isoform 4	Secreted	NM_001160031.1	NP_001153503.1	Hs01052961_m1	Abcam Ab32152 (Y103)	61	100	Short distinct c terminus, lacks transmembrane and cytoplasmic regions of isoform 1[159].
6	i15VEGFR1[146] i15[146] [i15asVEGFR1]	Intracellular	-	-	-	N/A	63	-	i15VEGFR1 and i15asVEGFR1 differ by alternative splicing of intron 15[146].
7	i18VEGFR1[146] I18[146]	Intracellular	-	-	-	N/A	53	-	Part of the ATP-binding domain (without ATP-binding sequences), the kinase insert, the phosphotransferase domain, and the C-terminal tail[146].
8	i21VEGFR1[146] I21[146]	Intracellular	-	-	-	N/A	39	-	Truncated kinase domain (163 of 332aa). No kinase insert domain. [146] Phosphotransferase domain and c terminal[146].
9	I21asVEGFR1[146]	Intracellular	-	-	-	N/A	41	-	Alternative 7 a.a. initial sequence [146]. Truncated kinase domain (174 of 332aa). 11aa of kinase insert.

Table 1-1 VEGFR1 isoforms. The VEGFR1 gene produces at least 9 splice isoforms that transcribe proteins with different cellular localisations and properties. The table presents the membrane bound isoform, 5 soluble isoforms and 4 intracellular isoforms. Aliases for each isoform are presented. NCBI nucleotide and protein reference sequence numbers are provided where available. Primers used for qPCR and antibody used in this work are provided. Predicted and observed molecular weights are provided. NCBI: National centre for biotechnology information.

1.2.2.2 VEGFR2

VEGFR2 is also known as kinase domain receptor (KDR) and previously as fetal liver kinase 1 (Flk1). Both VEGF and VEGF-C act on VEGFR2 (Table 1-2) but it is the effects of VEGF-A that are the most thoroughly studied in the nervous system. Like VEGFR1, VEGFR2 is formed of a 7-immunoglobulin extracellular domain and predominantly forms homodimers [129]. VEGF binds to the extracellular domain of VEGFR2 with an affinity approximately 10-fold lower than that of VEGFR1. Ligand binding results in receptor dimerization and phosphorylation. VEGFR2 has a highly active kinase region VEGFR2 able to activate numerous downstream pathways, described in more detail in section 1.2.2.3 [168] [107]. The VEGFR2 promotor is not directly regulated by hypoxia but by VEGF binding.

VEGFR2 is known to form heterodimers with VEGFR1 and VEGFR3 [130, 169]. Signalling of heterodimers is still being elucidated and the extent of heterodimerisation in the nervous system is not known [130].

VEGFR2 was first identified as a major regulator of angiogenesis [170] and is now known to stimulate migration, proliferation and survival of various neural cell types as well as mediating vascular permeability [129, 168]. Disruption of the VEGFR2 gene in development does not impair nervous system development or viability, suggesting that it is not essential for neuronal or glial development [110].

1.2.2.2.1 sVEGFR2

A soluble form of VEGFR2, sVEGFR2, has been discovered in humans. sVEGFR2 has a poor affinity for VEGF-A, although it binds with a higher affinity to VEGF-C. Unlike the complex splice variants of sVEGFR1, only two isoforms of sVEGFR2 have been identified and are detailed in Table 1-2. sVEGF2 is thought trap VEGF-C in the cytoplasm acting as a negative regulator for lymphogenesis [106]. This mechanism could also regulate VEGF-C activity in the CNS. sVEGFR2 has been reported as being present on astrocytes [171], though this has been debated [172].

VEGFR2 isoforms	Alias	Location	Nucleotide RefSeq NCBI	Protein RefSeq NCIB	qPCR Primer ID	Primary Antibody	kDa	Notes
1	VEGFR2 KDR FLK1 mbVEGR2 CD309	Cell membrane Cytoplasm Nucleus Cytoplasmic vesicle Early endosome	NP_002010.2	NM_002019.4	Hs00911700_m1	Cell Signalling #2479	151 (observed at 210 and 230 due to N-glycosylation)	Longest form - transmembrane
2	sVEGFR2[173]	Secreted					76	Splice variant Inhibits lymphogenesis via inhibition of VEGF-C[173]
3	VEGFR2-712[159]	Secreted					80	

Table 1-2 VEGFR2 isoforms. The VEGFR2 gene produces at least 3 splice isoforms. The table presents the membrane bound isoform and 2 soluble isoforms. Aliases for each isoform are presented. NCBI nucleotide and protein reference sequence numbers are provided where available. Primers used for qPCR and antibody used in this work are provided. Predicted and observed molecular weights are provided.

1.2.2.3 Downstream signalling

The binding of VEGF to VEGFR2 results in the activation of intracellular signalling pathways. Numerous phosphorylation sites have been identified on VEGFR2 kinase domains, though only 6 have been fully validated in the full-length receptor [174]. Phosphorylation at these sites triggers pathways that control endothelial survival, permeability, migration, and proliferation. Downstream pathways are summarised in Figure 1-5.

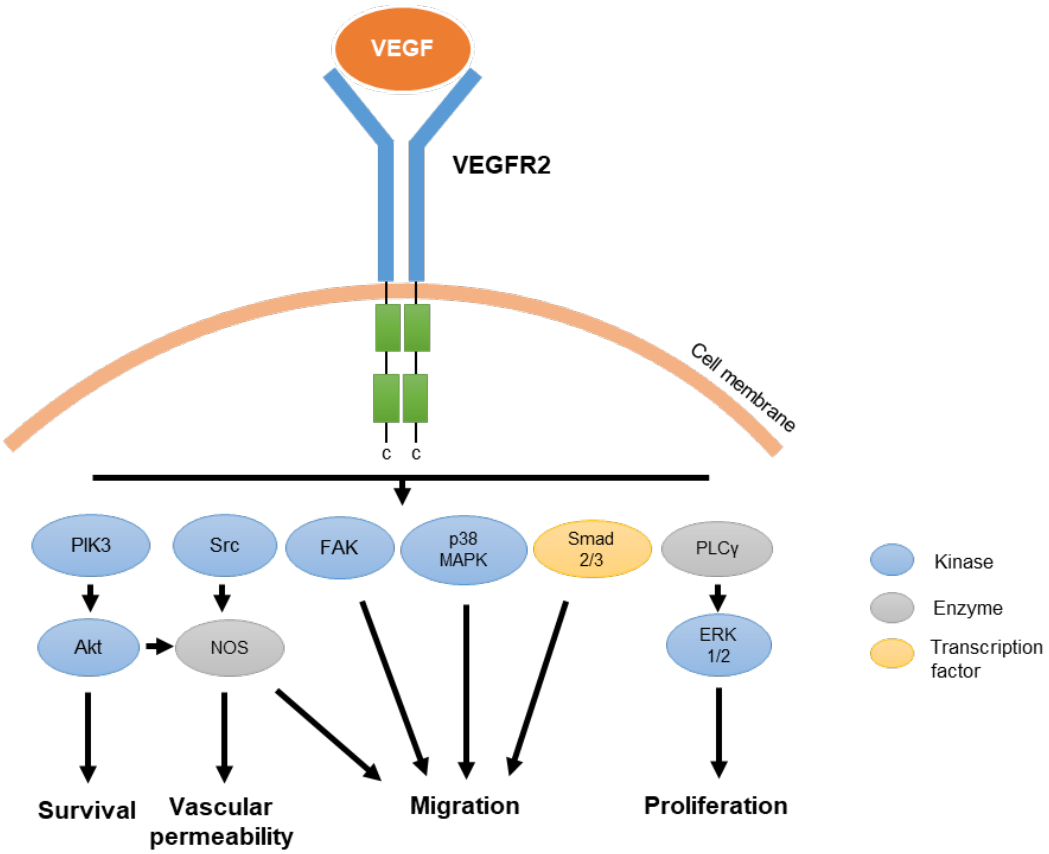

Figure 1-5 VEGFR2 signalling. VEGFR2 receptor phosphorylation activates numerous downstream targets, including kinases, enzymes and transcription factors, that mediate cell survival, permeability, migration and proliferation.

Non-VEGF ligands and mechanical forces such a shear stress can activate VEGFR2. These form the non-canonical pathway of VEGFR2 activation. These ligands activate the cytoplasmic tyrosine kinase Src which phosphorylates downstream VEGFR2 and initiates downstream signalling [130]. As discussed in 1.2.2.1, iVEGFR1 can also activate Src signalling.

1.2.2.4 VEGFR3

VEGFR3 is also known as Fms-related tyrosine kinase 4 (FLT4). In contrast to VEGFR1 and VEGFR2, VEGF is not a ligand for VEGFR3. VEGF-C and VEGF-D bind to VEGFR3, the main role of which is to moderate lymphogenesis. VEGFR3 is expressed by blood and

lymphatic endothelial cells in development. VEGFR3 knock-out mice display defective blood vessel formation leading to embryonic lethality before the formation of the lymphatic system [175]. In adults VEGFR3 expression is usually confined to lymphatic endothelial cells, [176] though the receptor can be re-expressed on vascular endothelium in certain situations. VEGFR3 has been found in vascular endothelium in tumour formation in human tissue [177] and wound healing [178]. VEGFR3 upregulation has also been shown to mediate angiogenesis in the absence of VEGF-VEGFR2 signalling in the retina via a notch-dependent mechanism [179].

VEGFR3 has been reported in cerebral vascular cells, neurons and astrocytes. The deletion of VEGFR3 from endothelial cells in the cerebral vasculature resulted in excessive sprouting and angiogenesis in the mouse hindbrain, indicating a role in angiogenesis, at least in development. VEGFR3 was found expressed in neurons and astrocytes via *in situ* hybridisation and double immunohistochemistry [180, 181] as well as by neuronal progenitors [136] and oligodendrocyte precursors [181]. In the developing nervous system VEGFR3 is reported to be present in the subventricular zone (SVZ), hippocampal gyrus, olfactory bulbs and cortex. Further investigation of VEGFR3 in the SVZ resulted in discovery of its role in neurogenesis on neural stem cells and astrocytes mediated by VEGF-C in mice [137].

In contrast to the study of VEGFR2, much of VEGFR3 signalling is still being elucidated [130, 176]. NRP1 and NRP2 are both involved with VEGFR3 signalling at least in the lymphatic system [176]. $VEGF_{189}$a, VEGF-C and VEGF-D have been shown to modulate signalling of VEGFR3 positive receptors, which are thought to be VEGFR2-VEGFR3 heterodimers [130]. VEGFR3 has also been reported to bind with VEGFR2 and vascular endothelial cadherin (VE-cadherin) to make a mechanosensory complex that responds to shear stress on endothelial cells [182, 183].

1.2.2.5 Co-receptors

1.2.2.5.1 Neuropilins

NRP1 and NRP2 were originally discovered as receptors for semaphorins. They were later found to be co-receptors for VEGF-A, -B, -C, -D and PlGF [184]. The receptors are single membrane-spanning glycoproteins with 3 extracellular domains: A, B and C. On NRP1, semaphorins bind to both domains A and B; members of the VEGF family only bind to B. Extracellular domain C is required for oligomerisation with VEGFR2. NRP1 and NRP2 bind $VEGF_{165}$a, possibly $VEGF_{189}$a but not $VEGF_{121}$a [110]. NRP1 has a high affinity for VEGFR1 and binds to VEGF-B and PlGF. NRP2 can bind to VEGF-C and PlGF [106, 130].

Neuropilins enhance VEGF signalling by acting as co-receptors with VEGFRs. NRP1 and VEGFR2 co-localise in the presence of VEGF to enhance VEGFR2 phosphorylation and

signalling [129]. Motifs on *VEGFA* exon 7 and 8 bind to NRP1 and NRP2, although with a 50 fold stronger affinity to NRP1 [130]. Enhanced $VEGF_{165}$a-mediated proliferation and migration was noted when NRP1 and VEGFR2 were co-expressed in the same cells [109].

NRP1 is expressed on the endothelium of arteries. The deletion of NRP1 in development causes various vascular defects including impaired formation of the cerebral vasculature [110] [110]. NRP2 is expressed on the endothelium of venous and lymphatic vessels. Following the deletion of NRP2 in development, embryos are viable [129].

NRP1 can bind to VEGF without VEGFR2 and sequester it. In retinal neurons VEGF binds to VEGFR2 and NRP1 but in hindbrain neurons VEGFRs are not expressed and VEGF is sequestered by NRP1 [130]. VEGF can also signal directly through NRP1 without VEGFR2 [138]. The branchiomotor neuron cell bodies in the mouse brainstem are the only known neuronal cell type where NRP1 has been identified as the main receptor for VEGF [110] [138]. In addition to the membrane-bound NRP receptors, a soluble form of NRP1 (sNRP1) that binds VEGF has been identified in vivo [185] but there has been no investigation of this subtype in the CNS.

Both NRP1 and NRP2 have been detected on adult neurons. NRP1 was co-expressed with VEGF on motor neurons and in axons of peripheral cells [186]. NRP1 is upregulated on neurons and endothelial cells after CNS ischaemia [110]. It has been difficult to determine the importance of NRP1 and 2 in VEGF signalling in the adult nervous system as they also act as receptors for the semaphorins.

In a transgenic mouse model of AD, *in situ* hybridisation showed moderate intensity of NRP1 expression in subcortical regions such as entorhinal, somatosensory and frontal cortices as well as hippocampal of transgenic mice and controls [187]. As the mice aged, NRP1 was reported to be upregulated in the entorhinal cortex. Double immunofluorescence on VEGF and NRP1 protein showed them colocalised in endothelial cells and microglia in transgenic mice. NRP1 reported upregulated following middle cerebral artery occlusion and acute optic nerve injury [187].

1.2.2.5.2 Heparan sulphate proteoglycans

The heparan sulphate proteoglycans (HSPGs) are another group of proteins that act as co-receptors for VEGF. HSPGs bind to heparin growth factors on the plasma membrane or in extracellular matrix. HSPGs, such as perlecan, can prolong the action of VEGFR2 signalling [130]. Other HSPGs, such as glypican, may have dual roles, both controlling VEGF localisation vascular system and influencing VEGFR signalling [114].

1.2.3 Angiogenesis

Angiogenesis is the process by which new blood vessels are formed from existing vessels. Adult vessels rarely form new branches but can respond to environmental cues such as hypoxia. Angiogenesis is highly regulated and controlled by several growth factors, of which VEGF is of major importance. VEGF is a major mediator of angiogenesis in the adult central nervous system. Sprouting angiogenesis is the predominant form of angiogenesis in adults and is described below [188].

A hypoxic environment leads to the stabilisation of hypoxia inducible factors (HIFs). HIFs are regulated by oxygen-sensing domains. HIFs are regulators of angiogenesis due to their ability to activate multiple genes that mediate short and long-term adaptation to hypoxia [189]. HIF consists of an α subunit and a β subunit. The α subunit can be one of three subtypes; HIF1α, HIF2α or HIF3α, any of which can combine with a constant HIF1β subunit. HIF1 activates the transcription of VEGF [190] and PDGF [189]. HIF-1α and HIF-2α are both able to induce VEGF expression by binding to the hypoxia response element (HRE) preceding the VEGF coding region. HIF2α stabilisation upregulates VEGFR1 [188].

Angiogenesis in response to hypoxia is presented in Figure 1-6. Upon VEGF stimulation, endothelial cells degrade the basement membrane and pericytes detach. This allows endothelial cells to migrate. VEGF/Notch signalling selects tip and stalk cells, and filopodia guide tip cells by sensing cues in the local environment [188]. Tip cells fuse (not shown in Figure 1-6) and notch signalling leads to tip cell stabilisation. This is followed by lumen formation and the cells remodel in response to blood flow. Pericyte recruitment is stimulated by PDGF release and leads to vessel stabilisation and maturation. Successful angiogenesis restores blood flow and tissue perfusion to the hypoxic area.

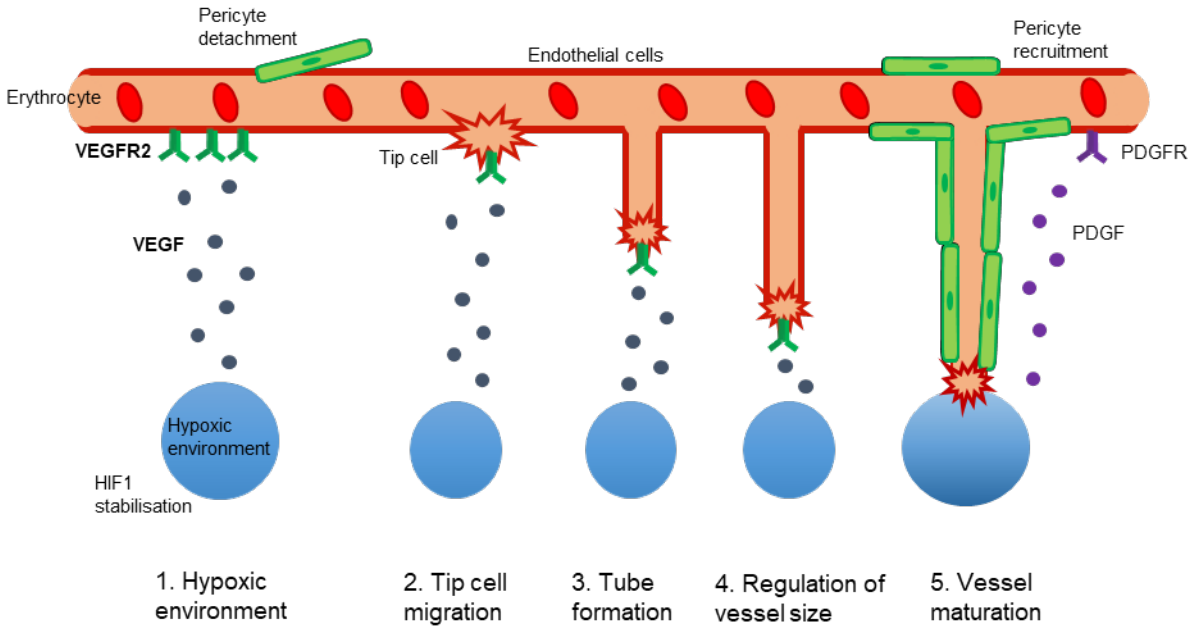

Figure 1-6 Angiogenesis in response to hypoxia. 1. A hypoxic environment leads to the stabilisation of HIF1 and the transcription of numerous proteins, including VEGF. VEGF stimulates endothelial cells to degrade the basement membrane and cause pericytes to detach. 2. VEGF acts via VEGFR2 to stimulate tip cell growth. 3. Tube formation occurs. 4. Vessel size is regulated by cross talk between VEGFR2 and Notch signalling. 5. PDGF stimulates pericyte attachment via its receptor PDGFR. Once the tissue is reperfused and adequately oxygenated, HIF is no longer stabilised and VEGF levels decrease.

1.2.4 VEGF in disease

Disruption to angiogenesis can lead to disease. Aberrant angiogenesis has been heavily investigated in tumour formation and diabetic retinopathy, while reduced angiogenesis has a role in preeclampsia, diabetic neuropathy, stroke and amyloid lateral sclerosis (ALS) [191].

Focusing on the nervous system, ALS is the first neurodegenerative disease to show clear involvement of VEGF and insufficient angiogenesis in disease pathogenesis. ALS is caused by the degeneration of motor neurons in the spinal cord, brainstem, and motor cortex [192]. Oosthuyse et al (2001), showed that the deletion of the hypoxia response element in the *VEGF-A* promotor region led to motor neuron degeneration in mice [186]. 60% of mice homozygous for the mutation died before birth and the remaining 40% displayed physiological and neuropathological signs of motor neuron degeneration [186]. In humans, polymorphisms in the promoter region of the VEGF gene cause reduced VEGF expression which results in increased risk of developing ALS [193]. Two main hypothesis were put forward to explain the role of VEGF in motor neuron degeneration: either there is reduced neurotrophic support from VEGF, or there is reduced vascular support due to a lack of VEGF which makes motor neurons more vulnerable to ischaemic insult [121].

Supporting the theory that the neurodegeneration is due to chronic hypoxia, mutant mice experienced lower baseline neural blood flow and had decreased capillary lumen size in skeletal muscle [186]. Overexpression of VEGFR2 on motor neurons protected cells from SOD1 mutant protein (implicated in familial ALS) *in vivo*, although it is not clear if the effect was due to neuronal or glial actions [194]. VEGF was regarded as a promising therapeutic target, and intracerebroventricularly delivered recombinant human $VEGF_{165}$ reached a phase II clinical trial in ALS patients [195].

1.3 VEGF in dementia

1.3.1 VEGF as a biomarker

VEGF has previously been identified as a potential AD biomarker. Higher VEGF levels were found in the plasma of AD patients when compared to control [196], while lower levels were observed in AD patient serum [197]. VEGF levels in cerebrospinal fluid (CSF) have been reported increased [198] and unchanged [199] [200] compared to control. VEGF was suggested as a prospective AD biomarker as levels of VEGF correlated with the MMSE scores in AD, but not with MMSE scores in other neurodegenerative diseases [199]. VEGF levels were measured for the first time in VaD where they were found unchanged compared to control and AD CSF[200]. The levels of other members of the VEGF family and VEGF receptors have not been investigated in cognitively impaired subjects [37].

1.3.2 *VEGFA* polymorphisms

Due to the detrimental effect of VEGF disruption in ALS, polymorphisms in the promotor regions of *VEGFA* have been investigated in several types of dementia. A polymorphism is a variant in the gene which is common in the population. Variants in the gene can increase or decrease the risk of disease.

VEGF promotor polymorphisms were identified as risk factors for VaD in one study [201]. The study identified three variants after comparing *VEGFA* in 207 VaD and 207 controls. One polymorphism, -7C/T, in the 5- prime untranslated region (5'UTR) was associated with increased VaD risk. This polymorphism also interacted with two other variants in the promoter region and the three-prime untranslated region (3'UTR) to increase VaD risk [201]. This study needs validating in other populations but suggests that VEGF could influence dementia risk. A VEGF promotor polymorphism was also identified as a risk factor in another form of dementia, frontotemporal dementia (FTD) [129].

In AD, there has been a debate in the literature over two VEGF promotor polymorphisms and relation to risk. Of the several polymorphisms described, -2578C/A and -1154G/A were

most commonly identified in studies on AD. Polymorphisms were previously reported to affect the activity and responsiveness of the promoter region and consequent expression of VEGF [202].

Several studies have found evidence both for [196, 203, 204] and against [204 205 206] the association of these polymorphisms with disease. Two meta-analysis concluded that there was no overall link between the identified polymorphisms and AD [207, 208] though the polymorphisms may be associated with AD risk in an ApoE-dependent manner. There was a link identified between ApoE status and a risk variant for AD (-2578C/A polymorphism) and also a protective variant (-1154G/A). Caveats to the meta-analysis results, detailed in Liu et al. 2013 [208], include small sample sizes and the heterogeneous methods used between studies which may be masking effects. Overall it is hypothesised that any changes in the VEGF promoter activity will be minor [186].

1.3.3 VEGF and BBB dysfunction

VEGF is a known permeability factor. As BBB increased permeability has a probable detrimental effect in AD (1.1.3.4), the interaction between VEGF and this structure is an important consideration in the disease. VEGF derived from astrocytes was shown to increase BBB permeability in mice [29]. In the same study, VEGF induced VEGFR2 signalling on endothelial cells resulting in disrupted expression of junction-forming proteins and BBB breakdown [29]. Thus, increased VEGF in the brain may have detrimental effects on the BBB in AD.

The recognition of VEGF as a potent angiogenic factor has led to investigations into its possible therapeutic applications. However, the permeability effects of VEGF on the BBB may offset any potential benefit of VEGF treatment in the nervous system [209].

1.3.4 VEGF in neurons and glia

As has been noted, VEGF is expressed not just by endothelial cells but also by neuronal populations and glia.

Most VEGF research in the nervous system has been conducted on neuronal populations. VEGF is expressed by neurons and has been specifically identified in CA1 pyramidal neurons in the hippocampus, in the olfactory bulb in pyramidal cells of the cortex and Purkinje cells of the cerebellum. VEGF is a neurogenic factor, though its exact role in the sub-processes of neurogenesis are yet to be elucidated. VEGF maintains the stem cell niche in the dentate gyrus and SVZ through its role in angiogenesis and glial cell proliferation. VEGF stimulates the migration of neuroblasts from their niche to a remote site. From the SVZ, neuroblasts travel along a vascular scaffold produced by VEGF-secreting astrocytes

which enhances migration. VEGF also has a role in neuroblast differentiation. The inhibition of VEGF signalling impairs maturation of olfactory bulb neurons derived from the SVZ [210] and application of VEGF enhanced neurite growth and survival in explanted neuronal cultures [194].

There is evidence that VEGF can modulate LTP, independent of its role in angiogenesis and neurogenesis. LTP describes the increase in synaptic strength that occurs after repeated stimulation of a synapse and is thought to be the mechanism behind learning and memory. VEGF upregulation increased neurogenesis, angiogenesis and LTP in the dentate gyrus of the adult mouse hippocampus [211]. Blocking VEGF prevented LTP and impaired memory whilst there was no reduction in perfusion or neurogenesis in the mouse [211]. This could be attributed to stimulatory and inhibitory effects of VEGF on ion channels surrounding the synapse, possibly due to the differing signal pathways of VEGFR1 and VEGFR2 [210].

Despite the abundance of work on the neuronal population, it is astrocytes that are the biggest producers of VEGF in the brain [212]. Astrocytes are known to regulate angiogenesis in the CNS [213] [119]. VEGF-A induces astrocyte proliferation [121] [194]. In microglia, VEGF induces proliferation and increases chemotaxis [141] [142].

Pericytes are glial cells found surrounding capillaries in the brain, they have a key role in capillary blood flow and a key role in BBB maintenance. VEGF is known to be expressed in pericytes and they are reported to express both VEGFR1 and VEGFR2[214, 215]. VEGFR2 has also been shown to form heterodimers with platelet-derived growth factor receptor (PDGFR), in immature vasculature [216].

VEGFR1 has a direct role in endothelial cell migration [106]. VEGFR1 expression has been observed on cultured microglia [141], and by immunohistochemistry, on microglia in human brain [142] and on developing and adult neurons [194]. There is debate over the expression of VEGFR1 on astrocytes (Chapter 3).

1.3.5 VEGF in post-mortem human brain

Examination of post-mortem AD brain has identified increased VEGF levels compared to age matched controls [212]. More recently VEGF level was reported to be significantly increased in the parahippocampus in AD brain tissue compared to controls [78]. In the same study an increase in VEGF was observed in regions of VaD brains but this was not significant. As there is known to be a reduction in blood flow in the AD brain it was hypothesised that VEGF is increased in response to chronically reduce tissue oxygenation. Thomas et al. (2015) used von Willebrand factor (vWF) as a surrogate measure of microvessel density and reported that levels of this factor were decreased in the

parahippocampal and frontal lobes despite increased levels of VEGF [78]. This indicates that despite high levels of VEGF, angiogenesis in the AD brain is not increased, potentially interfering with the ability of the brain to compensate for cerebral hypoperfusion.

There is substantial literature to support VEGF upregulation in conditions of acute ischemia in the brain - both in animal models and in human stroke. VEGF levels remain upregulated for up to 7 days after an ischaemic incident in the human brain [217] and in AD upregulation may be a permanent state. The effect of acute hypoxia on VEGFRs have also been studied, using animal models and explants, but little is known of the changes in VEGFRs in AD.

One study does highlight increased microvessel density in transgenic AD mice and a small cohort of AD brains (n=4) when compared to control [218]. The study measured the level of CD105, also known as endolin, by western blot and by IHC and found it increased in AD [218]. However, the study was in a small cohort and endolin is induced by hypoxia so may not be a marker of new blood vessel formation[219] and has been shown as a marker of microglia activity. The group also measured laminin by IHC which has in turn been shown to increase in AD [220] and may be subject to morphological changes that are known to occur to capillaries in AD [221].

1.3.6 VEGF and AD pathology

It has been proposed that Aβ acts as a 'molecular sink' for VEGF. VEGF was found to bind to Aβ with the same affinity as it binds to its own receptors and has been found sequestered in Aβ plaques [222]. There is also evidence that Aβ induces expression of VEGF *in vitro* [223]: Normal adult human astrocytes showed increased production of VEGF when exposed to Aβ in normoxic conditions. This provides evidence that increased VEGF concentration in AD brain may not be due to hypoxia only but may also be elevated as a direct effect of Aβ. There is also evidence that Aβ can directly activate HIF1α *in vitro* [224] though this has been disputed [225]. The ability of Aβ to activate HIF1α, a transcription factor able to upregulate multiple genes including VEGF, would lead to a further increase in VEGF levels in the brain. Though increases in VEGF are beneficial for the formation of new blood vessels, chronic VEGF increases may lead to undesirable effects such as an increase in BBB permeability as described above. The effect of Aβ on VEGF and VEGFRs is summarised in Figure 1-7.

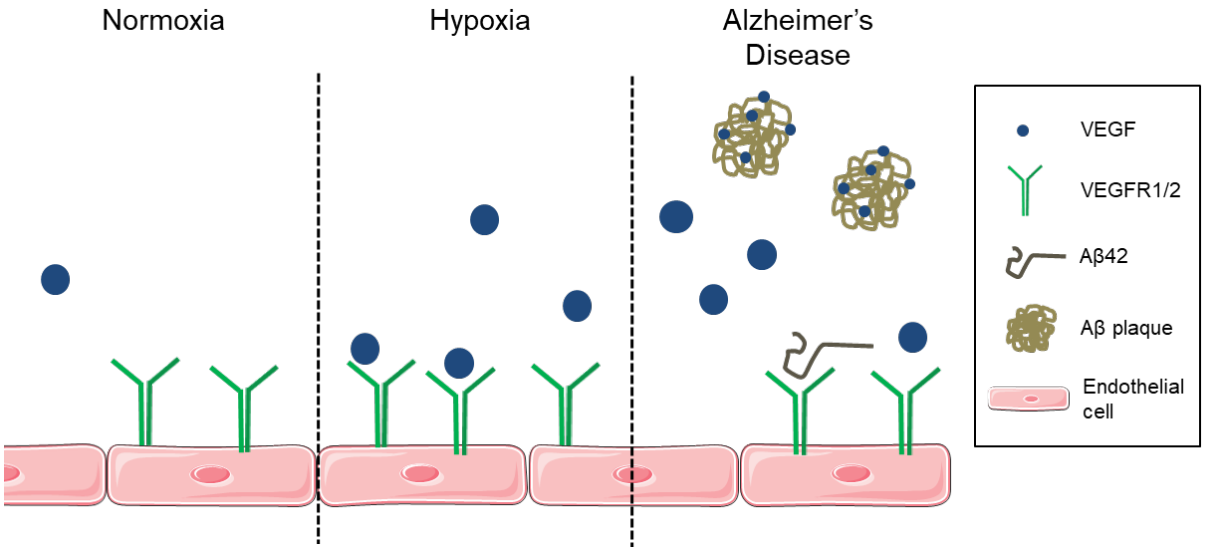

Figure 1-7 Hypothesised effect of Aβ on VEGFR1 and VEGFR2 on endothelial cells in AD. In hypoxia increases in the number of VEGFR1 receptors and presence of VEGFR2 enable angiogenesis. In AD, with the presence of $A\beta_{1\text{-}42,}$ VEGF is bound to Aβ plaques reducing bioavailability of the ligand. $A\beta_{1\text{-}42}$ may also bind to VEGFR2, which will prevent receptor activation by VEGF.

1.4 Hypothesis and aims

1.4.1 Hypothesis

There is disruption of VEGF receptor expression or function in AD.

This follows on from previous findings from our research group showing that brain tissue is hypoperfused in AD using molecular markers. Levels of vasoconstrictors such as endothelin 1 (EDN1) [90, 226], ACE and AngII are elevated in the AD brain compared to control [91, 227]. Increases in these molecules can cause vasoconstriction and therefore contribute to cerebral hypoperfusion. VEGF, a marker for hypoxia, was found upregulated in AD, and VaD brain, by our group[61, 67]. Following investigation in relation to microvessel density, it was found that although microvessel density increased with increasing VEGF in VaD, this was not the case in AD[78].

Despite high levels of VEGF microvessel density in the AD brain is not increased and the brain is unable to compensate for cerebral hypoperfusion. Disruption to the VEGF receptor system via alteration in receptor level, direct interaction with AD pathology or disruption of downstream signalling may explain the lack of VEGF induced angiogenesis.

1.4.2 Aims

[1] To examine the cellular localisation of VEGFRs in post-mortem parietal lobe tissue.

[2] To measure the levels of VEGFR1 and VEGFR2 mRNA in the post mortem control and AD parietal lobe.

[3] To measure the levels of VEGFR1 and VEGFR2 protein in the post mortem control, AD and VaD parietal lobe.

[4] To investigate VEGFR1 and VEGFR2 in relation to hypoxia and Aβ pathology *in vitro*.

Chapter 2 Materials and Methods

2.1 Materials

The details of chemical, equipment, software, common solutions, commercial kits and antibodies used can be found in Appendix 1-8.

2.2 Human brain tissue

2.2.1 Tissue acquisition

Tissue was obtained from the Human Tissue Authority-licensed South West Dementia Brain Bank (SWDBB), University of Bristol, Southmead Hospital, UK. All work was conducted with local research ethics committee approval.

Brains were removed within 72 hours of death. Brains were cut midsagittally and the left hemisphere sliced coronally and frozen at -80°C. The right hemisphere was placed in 10% buffered formalin for a minimum of 3 weeks. Blocks of frontal, mid-temporal, mid-parietal and occipital regions, midbrain, pons, cerebellum, vermis, medulla, basal ganglia and any macroscopically visible lesions were then cut and processed in a tissue processor before being embedded in paraffin wax. All brains had undergone routine histological assessment. Sections of tissue from each of the brain regions detailed above were stained with haemotoxylin and eosin (H&E) and immunolabelled with Aβ, tau and α-synuclein antibodies to allow the cellular morphology, Aβ plaques, neurofibrillary tangles, and Lewy body pathology to be examined by a neuropathologist.

AD was diagnosed post-mortem by assessment of Aβ plaque and neurofibrillary tangle density in combination with information from clinical records indicating presence or absence of dementia, according to the CERAD criteria[228] and also by the neurofibrillary tangle Braak stage method. As described in Chapter 1, it is rare to have a definitive diagnosis of AD prior to death due to the heterogeneity of dementia symptoms and the expense of neuroimaging. The CERAD criteria are a standardised, validated measures for the assessment of Alzheimer's disease (AD) [229]. This l assessment includes reviewing of clinical documentation and neuropathological examination of NFT density. Braak stages provide a purely neuropathological assessment of NFT progression. Briefly, NFTs begin in the transentorhinal region in stage I and are present in the entorhinal region and subiculum in stage II. NFTs then involve the limbic region and adjacent inferior temporal neocortex in stages III-IV. Finally NFTs are present all layers of the occipital and frontal neocortex in stages V-VI [30]. All AD brains studied had a CERAD diagnosis of probable or definite AD with a Braak stage of III to VI. Control brains from the SWDBB were all from donors with no clinical history of

dementia and at post-mortem diagnosis there was no evidence of neuropathological abnormalities, limited or no plaques, and a Braak stage of III or less.

Sections of cortical tissue were also examined to determine the severity of cerebral amyloid angiopathy (CAA) and graded using a method based on that of Olichney et al [230] and Ellis [231]. A score of 0 corresponded to vessels devoid of amyloid, a score of 1 to scattered deposition of amyloid in a few leptomeningeal or cortical blood vessels, a score of 2 to more widespread deposition of amyloid in vessels, and a score of 3 to severe and widespread amyloid deposition.

The severity of small vessel disease (SVD) was scored in frontal, temporal, parietal and more recently the occipital regions of the brain. Paraffin embedded tissue was used to assess SVD on a 4-point semi-quantitative scale. SVD severity was rated on the following scale: 0 = normal vessel wall thickness, 1 = slightly increased thickness, 2 = moderately increased thickness, 3 = markedly increased thickness such that for many arterioles the diameter of the lumen was <50% of the outer diameter of the blood vessel [230, 231]. CAA score was provided for the parietal cortex and white matter of control, AD and VaD cases.

Frozen brain tissue was use for RNA extraction and protein studies. Formalin fixed paraffin embedded tissue (FFPE) tissue was used for immunohistochemistry and immunofluorescence.

2.2.2 Cohort selection

Control, AD and VaD cohorts were used. Tissue was taken from the parietal cortex and white matter case summarise in Table 2-1.

Parietal cortex and white matter		**Control**	**AD**	**VaD**
N		36	50	19
Age (years)	Range	58 - 95	57 - 93	67 - 97
	Mean ± SD	80.1 ± 8.7	77.5 ± 8.1	82.9 ± 7.3
Gender	Female	11	26	9
	Male	25	24	10
Post-mortem delay (hours)	Range	3 - 67	4 - 85	20 - 85
	Mean ± SD	32.5 ± 16.3	31.6 ± 19.0	47.6 ± 19.0

Table 2-1 Summary of the neuropathological and demographic features of control, AD and VaD. Details of cases are listed in Appendix 9

FFPE sections of control and AD frontal lobe were used for VEGFR1 and VEGFR2 immunohistochemistry. Details of cases can be found in the Appendix 10.

2.2.3 Brain tissue homogenisation

One hundred mg of tissue was dissected from the desired region into a 2ml screw top tube with 5 x 2.3 mm ceramic beads (Stratech Scientific) and 1ml of desired lysis buffer. The tissue was homogenised at 6000rpm using the automated homogeniser (Precellys 24) for 2 x 15 seconds. Samples were placed in the 4°C centrifuge for 15 minutes at 17000 g. Supernatant was removed and transferred to a new 1.5 ml tube and stored at -80˚C.

2.3 Protein quantification

Total protein concentrations of cell or tissue homogenates were determined using the Total protein kit (Sigma) according to the manufacturer's instructions. Samples were thawed and diluted in 0.85% NaCl. Human brain homogenates were diluted 1:20 and cell lysate was diluted 1:5. Brilliant blue dye was diluted 1:5 in distilled water and 250 µl dye solution was then added to wells of a clear 96-well microplate for each reaction. 5 µl of diluted sample was added to the dye solution in duplicate followed by duplicates of blanks (5 µl of 0.85% NaCl) and protein standards (5 µl of 0.3 mg/ml; supplied). The samples were incubated for 2 minutes before absorbance readings were taken. The results were blank corrected, and the protein concentration of samples was calculated, adjusting for the dilution factor.

2.4 Western Blot

2.4.1 Gel electrophoresis and transfer

	12% Resolving gel (ml)	**Stacking gel (ml)**
Milli-Q water	3.3	6.8
30% Acrylamide	4.0	1.7
1.5M Tris pH 8.8	2.5	-
1.0M Tris pH 6.8	-	1.25
10% SDS	0.1	0.1
10% APS	0.1	0.1
TEMED	0.004	0.01
Total	10	10

Table 2-2 Composition of 12% resolving gel and stacking gels used for western blotting.

Precast 7.5% and graduated 4-20% gels (Bio-Rad Laboratories) were used and 12% SDS gels were prepared as described in Table 2-2. Gels were positioned within the gasket and placed in the module tank (Mini-PROTEAN 3; Bio-Rad Laboratories) with 1x SDS running buffer. Cell lysate or tissue homogenate samples (30 µg), recombinant standard (1 ng) and ladder (5 µl) were loaded into the wells of the gel and the module was attached to the power supply. Separation of the denatured proteins by electrophoresis took place at 150V for 60 minutes. The proteins were transferred to nitrocellulose membrane using an electrophoretic transfer cell (Mini Trans-Blot; Bio-Rad Laboratories). The gel, with the sheet of nitrocellulose (ThermoFisher Scientific) positioned on top, was arranged between two sheets of blotting paper and two fibre pads within the gel holder cassette. The cassette was positioned into the

transfer cell tank on ice with 1 L of pre-cooled 1x blotting buffer and an ice pack to keep the system cool during the protein transfer. The gels were blotted at 100V for 1 hour at room temperature.

2.4.2 Protein detection

All incubations took place at room temperature on a shaking platform unless otherwise stated. The transfer cell was dismantled and the membrane briefly washed with TBS-T. The membrane was incubated in blocking buffer for at least 1 hour or overnight at 4˚C. The membrane was washed in TBS-T (3 x 10 minutes) then incubated with primary antibody at an assay-dependent dilution/incubation time in appropriate antibody buffer solution. The membrane was washed again in TBS-T (3 x 10 minutes) and incubated with peroxidase-labelled secondary antibody for 1 hour, then washed in TBS-T (3 x 10 minutes). ECL western blotting substrate (ThermoFisher Scientific) were added to the membrane according to the manufacturer's instructions; a 1:1 dilution of reagents 1 and 2, for 3-5 minutes. Membranes were imaged using a chemiluminescent imager (Bio-Rad Laboratories) with ImageLab software (BioRad Laboratories).

To re-probe the membrane antibodies were 'stripped' from the membrane after imaging. Membranes were washed with TBS-T then incubated with stripping buffer (ThermoFisher Scientific) for 10 minutes. The membranes were then washed with TBS-T (3 x 10 minutes) before proceeding to the blocking stage of the protein detection protocol.

2.5 Dot Blot

All incubations were at room temperature unless otherwise stated.

Sample homogenates and homogenate standards were diluted to the desired concentration in TBS. The dot blot manifold (BioRad Laboratories) containing nitrocellulose membrane was assembled according to manufacturer's instructions and vacuum tightened. With vacuum switched off and manifold exposed to air 100 µl of sample was added in triplicate to wells and left to filter through membrane for 1 hour. Serial dilutions of a homogenate standard were used to create a 7-point standard curve for each dot blot. 100 µl of TBS was added to blanks and unused wells. The manifold was disassembled and membrane briefly washed in TBS-T and placed in desired blocking solution for 1 hour. Primary antibodies were incubated overnight at 4˚C. Peroxidase-labelled secondary antibody was applied for 1 hour. Dot blots were developed with HRP substrate as for western blotting (2.4). The background adjusted volume was calculated using ImageLab software and relative values were each sample were calculated by interpolating from the standard curve.

2.6 Sandwich enzyme-linked immunosorbant assay

Enzyme-linked immunosorbant assays (ELISA) were completed as per manufacturer's instructions (R&D Systems, Abcam). All incubations were at room temperature unless otherwise stated.

Clear 96 well plates (R&D Systems) were coated with capture antibody and left overnight. Wells were drained and tapped dry then filled with wash buffer, this was repeated 5 times. Wells were incubated with 200 µl of blocking buffer for 1 hour. Blocking buffer was drained and wells washed as previously. Recombinant standard and samples were diluted in PBS and 50 µl added to each well in duplicate. Blanks were filled with PBS. Samples were incubated for 2 hours then wells drained and washed. 100 µl of detection antibody was added to each well and incubated for 2 hours. After draining and washing, 100 µl of streptavidin-HRP was added to each well and incubated away from direct light for 20 minutes. Following washing, 100 µl substrate solution added to each well and incubated away from direct light for 20 minutes. 50 µl of 2N sulphuric acid (stop solution) was added and the optical density determined immediately using a 450 nm filter on the plate reader. Readings were blank corrected and standard curve constructed and the protein concentration for each sample interpolated from the standard curve.

2.7 Direct enzyme-linked immunosorbant assay

Fifty µl of standard and sample were added to each well of a clear 96 well plate (R&D Systems) and incubated for two hours. The plate was washed 5 times with 0.05% PBS-T and tapped dry after the final wash. Each well was incubated with 100 µl of detection antibody for 2 hours. The plate was washed as previously described, and incubated with 100 µl of biotinylated antibody in PBS, for 20 minutes and protected from light. After further washing, 100 µl of HRP-labelled streptavidin diluted in PBS was loaded to each well and incubated for another 20 minutes and protected from light. A final wash stage was performed and each well was incubated with 100 µl substrate (C2 kits) in the absence of light to visualise the captured antigen. The reaction was stopped using 50 µl of 2N sulphuric acid and the optical density was measured using a plate reader at 450 nm. Readings were blank corrected and a 7-point curve was constructed. Sample values were determined by interpolated. Samples were measured in duplicate on each plate and corrected for the total protein concentration of each sample.

2.8 Adjustment for total protein concentration

Protein levels for each sample were adjusted for the total protein concentration of the sample. Total protein concentration was measured as described in 2.3. Adjustment for protein level was calculated using Equation 2-1.

$$\frac{\boldsymbol{Sample\ total\ protein\ concentration}}{\boldsymbol{Mean\ total\ protein\ concentration}} \times \boldsymbol{Sample\ target\ protein} = \boldsymbol{Adjusted\ value}$$

Equation 2-1 Adjustment for total protein concentration.

2.9 Immunohistochemistry

2.9.1 Immunoperoxidase staining of paraffin embedded tissue

Sections 7 µm in thickness were cut from paraffin blocks containing desired brain regions using a microtome and mounted on to charged microscope slides prior to the start of this study.

Slides were incubated overnight in a 60°C oven dewaxed in clearene (2 x 5 minutes) and dehydrated in 100% ethanol (2 x 3 minutes). Endogenous peroxidase was blocked by incubation with 3% hydrogen peroxide in methanol for 30 minutes, followed by a 10 minute wash under running water. Sections underwent the antigen retrieval pre-treatment required for the primary antibody before being washed under running water for 10 minutes, equilibrated in PBS and circled with a wax pen. Sections were blocked with 20% normal horse serum for 20 minutes and slides drained before application of primary antibody in 5% BSA, which was left to incubate overnight at 4°C. Sections were washed in two changes of PBS (2 x 3 minutes) and biotinylated universal antibody (Vector Laboratories) applied and left to incubate for 20 minutes. Sections were washed in two changes of PBS (2 x 3 minutes), VectaElite ABC complex (Vector Laboratories) was prepared 30 minutes prior and applied and sections left to incubate for 20 minutes. Sections were then washed in two changes of PBS (2 x 3 minutes), DAB (Vector Laboratories) applied and left to incubate for 7-10 minutes, and subsequently washed under running water for 10 minutes. Sections were immersed in copper sulphate DAB enhancer for 4 minutes, washed under running water for 5 minutes, counterstained in Gills haematoxylin (Leica) for 5-30 seconds for nuclei staining, and washed under running water for at least 10 minutes. Finally, sections were dehydrated in 100% ethanol (2 x 3 minutes), cleared in clearene (2 x 5 minutes) and mounted in DPX (Sigma).

2.9.2 Double immunoperoxidase staining of paraffin embedded tissue

Sections were immunolabelled for the first antigen with DAB as described in section x. After sections had been immersed in copper sulphate and washed in water, they were incubated in 20% normal horse serum for 20 minutes. Sections were then incubated overnight with antibody against the second antigen. Sections were washed in two changes of PBS and biotinylated universal antibody was applied for 20 minutes. Sections were washed in two changes of PBS, then VectaElite ABC complex, which had been prepared and left to sit for 30 minutes, was applied for 20 minutes. Sections were washed in two changes of PBS, incubated for 5-10 minutes in VIP substrate kit and washed in running water for 10 minutes. Sections were counterstained with Gills haematoxylin, and washed under running water for at least 10 minutes, before being dehydrated, cleared and mounted as for single staining as above (2.9.1).

2.9.3 Antigen retrieval pre-treatments

2.9.3.1 Citrate buffer treatment

Sections were immersed in citrate buffer and microwaved for 5 minutes until boiling. Sections were left to stand at room temperature for 5 minutes then returned to the microwave for a further 5 minutes. Sections were cooled in running water for 10 minutes.

2.9.3.2 EDTA buffer treatment

Sections were immersed in EDTA buffer and microwaved for 10 minutes until boiling. Sections were cooled in running water for 10 minutes.

2.10 Double immunofluorescence staining of paraffin embedded tissue

Sections 7 µm in thickness were cut from paraffin blocks containing desired brain regions using a rotary microtome and mounted on to charged microscope slides.

Slides were incubated overnight in a 60°C oven dewaxed in clearene (2 x 5 minutes) and dehydrated in 100% ethanol (2 x 3 minutes). Sections were washed 3x in PBS. Autofluorescence blocking pre-treatment was applied if necessary. Sections underwent the antigen retrieval pre-treatment required for the primary antibody before being equilibrated in PBS and circled with a PAP pen. Sections were blocked with 10% normal goat serum (NGS) for 30 minutes and slides drained before application of primary antibody in 10% NGS, which was left to incubate overnight at room temperature. Sections were washed in three changes of PBS (3 x 3 minutes) and a direct secondary fluorophore applied and left to incubate for 30 minutes. Sections were washed in three changes of PBS (3 x 3 minutes) and treatment to quench autofluorescence was applied if necessary. Sections were washed in three changes

of PBS (3 x 3 minutes) and mounted in Vectorstain medium with DAPI and sealed with nail varnish. Sections were viewed and imaged on a fluorescent microscope.

2.10.1 Autofluorescence quenching

2.10.1.1 Copper sulphate pre-treatment

Copper sulphate was used to reduce lipofuscin-like fluorescence [232]. Copper sulphate was applied after the first wash step for 1 hour at room temperature.

2.10.1.2 Sudan black post-treatment

Sudan black was used as a post-treatment to reduce auto fluorescence [232-234]. Sudan black solution was applied following secondary antibody incubation and left for 15 minutes at room temperature.

2.11 RNA Extraction

2.11.1 Frozen human brain tissue

Certified RNAse free pipette tips and Eppendorf tubes were used. 2ml screw top homogenisation tubes were autoclaved to minimise contamination.

One hundred mg of tissue was dissected from the desired region and put in a 2ml screw top tube with 5 x 2.3 mm ceramic beads and 750 µl TRIzol reagent (ThermoFisher Scientific). The tissue was homogenised at 6000 rpm using the Precellys 24 automated homogeniser (Bertin Technologies) for 2 x 15 seconds and left to settle on ice. In a fume hood, 160 µl chloroform was added and the sample vortexed for 15 seconds. Samples were then incubated for 3 minutes and then centrifuged at 17,000 g for 15 minutes at 4°C for phase separation. The aqueous phase was transferred to a 1.5 ml tube to which 500 µl of isopropanol was added. The preparation was mixed by inversion and incubated for 10 minutes to precipitate the RNA. The sample was then centrifuged at 17,000 g for 10 minutes at 4°C, the supernatant removed, and the resulting RNA pellet washed by inversion with 800 µl 70% ethanol. The pellet was re-formed by centrifugation at 9000 rpm for 5 minutes at 4°C, supernatant removed and left to air-dry. The pellet was then re-suspended in 30 µl RNase-free distilled water and aliquoted into 2 15 µl samples. Samples were stored at -80°C for future use.

2.11.2 DNase-1 treatment

To eliminate any genomic DNA, 0.6 µl $MgCl_2$ (ThermoFisher Scientific) and 2 µl DNase-I (Roche) were added to a 15 µl aliquot of RNA. This was incubated for 1 hour at 37°C followed by inactivation at 90°C for 5 minutes. The samples were spun down by short centrifugation then incubated on ice or transferred to the -80°C freezer for future use.

2.11.3 Quantification of RNA

RNA concentration was determined using a RiboGreen RNA quantitation kit (Invitrogen). A standard curve was generated in the range of 1-1000 ng/ml, diluting the working standard in TE buffer to a final volume of 100 µl in the plate Nunc black 96-well untreated plate, and a blank of 100 µl TE buffer. RNA stock was diluted 1 in 20,000 in TE buffer to a concentration within the standard range to a final volume of 100 µl. RiboGreen fluorescent dye was diluted 1 in 200 in TE buffer, and 100 µl added to each well. The plate reader was programmed to shake the plate for 30 seconds to aid mixing before taking fluorescence readings with filters set to excite at 485 nm and read emission at 520 nm.

2.11.4 Generation of cDNA

For each sample, 10 µg of RNA diluted in 50 µl of RNase-free distilled water. This was added to 50 µl of the high capacity cDNA reverse transcription kit (ThermoFisher Scientific). The adapted protocol is detailed in Table 2-3. The samples were then incubated 25°C for 10 minutes, followed by 37°C for 2 hours and inactivation at 85°C for 5 seconds in a thermal cycler. cDNA was stored at -80°C until use.

Component	Vol per reaction tube (µl)
10x RT buffer	10
10x Random primers	10
Reverse Transcriptase	5
25x dNTP mixture	4
H_2O	21
Final volume	50

Table 2-3 High capacity cDNA kit with adapted protocol. Up to 10 ug of RNA combined with RNase free H_2O and added to the Master Mix.

2.11.5 Quantification of cDNA

cDNA concentration was determined by using a PicoGreen DNA quantitation kit (Invitrogen). A standard curve was generated in the range of 1-1000 ng/ml, diluting the working standard in TE buffer to a final volume of 100 µl in the black 96-well untreated plate, and a blank of 100 µl TE buffer. cDNA stock was diluted 1 in 100 with TE buffer to a concentration within the standard range to a final volume of 100 µl. PicoGreen fluorescent dye was diluted 1 in 200 in TE buffer, and 100 µl added to each well. The plate reader was programmed to shake the plate for 30 seconds to aid mixing before taking readings with correct filters set to excite at 485 nm and read emission at 520 nm.

Subsequently the use of Picogreen dye was found to be an ineffectual measure of ssDNA levels. Despite the used of cDNA quantification to load PCR reactions this will not adversely affect interpreted results. Measurement of RNA ensured a set quantity was converted to cDNA. Volumes loaded from cDNA varied between samples. Despite variation the PCR

reaction was not overloaded as detailed by cycle threshold (C_T) values which fell between the range of 20 and 39 across all targets and there was no correlation between cDNA volume added to reaction and resulting C_T (Appendix 11). In addition, the $2^{-\Delta\Delta Ct}$ method for relative quantification of gene expression was used to calculate fold change in gene expression. The C_T of the endogenous control is subtracted the gene of interest for each sample to normalises the samples for the volume of cDNA or RNA added[235].

2.12 Quantitative PCR

Samples were plated on 0.1 ml Fast plates (Thermofisher Scientific) with each well containing, 10 µl of fast advanced master mix (Thermofisher Scientific), 1 µl of primer (Table 2-4) and 10 ng of cDNA made up to a total volume of 20 µl with RNase free water. Samples were run in triplicate for each gene probed. Each plate contained non-template controls for genes probed. Samples were incubated according to Taqman fast conditions set out in Figure 2-1.

Name	Alias	Gene symbol	Primer ID*	Amplicon length	NCBI chromosomal location**
ALDH1L1	10-FTHFDH, 10-fTHF, FDH, FTHFD	ALDH1L1	Hs00201836_m1	94	Chr.3: 125822408 - 125899485
β-Actin	BRWS1, PS1TP5BP1	ACTB	Hs01060665_g1	115	Chr.7: 5566779 - 5570232
PECAM1	CD31, GPIIA', PECA1, PECAM-1, endoCAM	PECAM1	Hs00169777_m1	65	Chr.17: 62396775 - 62404856
NeuN	FOX-3, FOX3, HRNBP3, NEUN	RBFOX3	Hs01370653_m1	58	Chr.17: 77085427 - 77478563
VEGFR1	FLT, FLT-1, VEGFR-1,	FLT1	Hs01052961_m1	72	Chr.13: 28874483 - 29069265
VEGFR2	CD309, FLK1, KDR VEGFR-2,	KDR	Hs00911700_m1	83	Chr.4: 55944426 - 55991762

Table 2-4 Details of qPCR primers used (ThermoFisher Scientific). Primer maps are displayed in Appendix 13

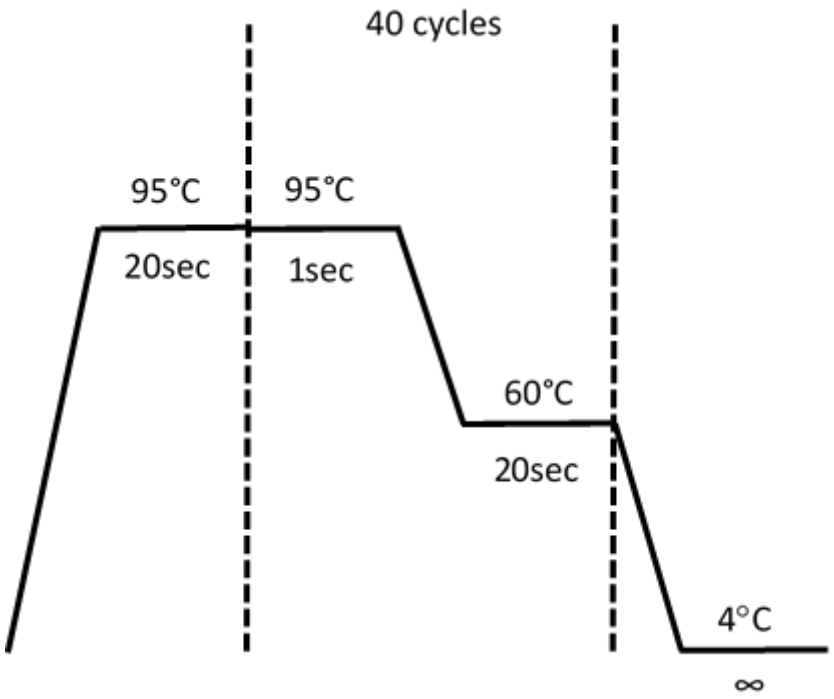

Figure 2-1 Plot of qPCR cycle conditions for all primers.

Gene expression for each sample was calculated compared to control using the $2^{-\Delta\Delta Ct}$ method for relative quantification of gene expression developed by Livak et al [235]. In this study one disease group (AD) was compared to one control group (C). The cycle threshold (C_T) of the gene of interest for each sample was first normalised to an endogenous control in the same sample (ΔCt). The genes of interest in this study were FLT1 (VEGFR1) and KDR (VEGFR2). The ACTB gene for β-actin was chosen as a reference gene expressed in all cell types. Three reference genes were chosen to account for expression of the genes of interest on multiple cell types in brain tissue. These were ALDH1L1 (expressed on astrocytes), PECAM1 (expressed on endothelium) and RBFOX3 (expressed on neurons). The difference in gene expression between control and disease groups was then calculated via the $2^{-\Delta\Delta Ct}$ method detailed in Equation 2-2.

$$Fold\ change = 2^{-\Delta\Delta Ct}$$

$$C_T\ target\ gene - C_T\ reference\ gene = \Delta Ct$$

$$\Delta C_T\ disease\ case - mean\ value\ of\ control\ \Delta C_T = \Delta\Delta Ct$$

Equation 2-2 The $2^{-\Delta\Delta Ct}$ method for calculating relative gene expression.

The geometric mean of control and disease group $2^{-\Delta\Delta Ct}$ values was subsequently established to allow comparison between the cohorts. Relative change in gene expression in each disease case is compared to the average of control values.

2.13 Primary cell culture

All cell culture experiments were conducted in a class II biological safety cabinet (MDH InterMed) at room temperature and the cultures were maintained in a 5 % CO_2 humidified incubator at 37 ºC (Sanyo Electric co.). Cells were cultured in tissue culture treated plasticware (Greiner). 70% isopropanol was used to clean out safety hood before and after each use to prevent infection of cultures. The dH_2O and PBS was autoclaved prior to used. Cell medium was stored at 4 ºC and were pre-warmed to room temperature prior to use.

2.13.1 Initiating primary cell culture

Complete cell medium was prepared. Cells we removed from liquid nitrogen or -150 °C and thawed in a 37 ºC water bath. The ampule was removed and contents were transferred to a T75 containing culture medium. The flask was placed in the incubator overnight and media changed the next day to remove any residual DMSO.

2.13.2 Subculture of primary cells

The media was changed every 3 days until 70% confluent then every day until the culture was 90% confluent when cultures were passaged. The existing media was removed and remaining cells were washed with PBS and 2 ml of trypsin-EDTA solution (Sigma) was applied. The flask was placed in in the 37 ºC incubator for 3 minutes. The flasks were gently agitated to detach the cells, they were harvested and added to a 15 ml falcon tube containing fresh media. 50 µl was removed for cell quantification (2.13.3). Cells were then pelleted with centrifugation at 200 g for 4 minutes at room temperature in a bench top centrifuge (ThermoFisher Scientific). The media was aspirated, cell pellet re-suspended in fresh media and plated as required. Cells were seeded at a density of 6000 cells/cm^2.

2.13.3 Cell counting

To determine the number of living cells present in a sample, trypan blue exclusion was performed with a level of less than 10% cell death considered acceptable. A 50µl aliquot of the cell suspension was taken and mixed with an equal volume of trypan blue dye. 50µl of the 1:1 mixture was added into both grids of a haemocytometer (Hawksley). Dead cells appear blue as the die permeates the cell membrane while live cells remain.

Cell viability was calculated by counting live cells and total cells (live and dead) in grids of the haemocytometer using an inverted phase contrast microscope (Nikon). Equation

2-3 was used to establish % viability. A % viability of 80% or over was considered acceptable.

$$\frac{\boldsymbol{Number\ of\ viable\ cells}}{\boldsymbol{Total\ number\ of\ cells}\ (\boldsymbol{live\ and\ dead})} \times \mathbf{100} = \%\,\boldsymbol{Viability}$$

Equation 2-3 Cell viability

Cell number was established by counting the live cells (>100 cells to increase accuracy) in grids of the haemocytometer. Equation 2-4 was used to calculate the viable cells/ml.

$$\frac{\boldsymbol{Number\ of\ viable\ cells}}{\boldsymbol{Number\ of\ squares\ counted}} \times \mathbf{2}\ (\boldsymbol{Dilution\ factor}) \times \mathbf{10^4} = \boldsymbol{cells/ml}$$

Equation 2-4 Cell number

2.13.4 Human umbilical vein endothelial cells

Human umbilical vein endothelial cells (HUVEC) primary cell were grown by the Lung Research Group, Southmead Hospital, University of Bristol, UK. Lysates were provided for use as positive control for antibody characterisation.

2.13.5 Human brain microvascular endothelial cells

Human brain microvascular endothelial cells (HBMEC) were obtained from ScienCell (#1000) and maintained using endothelial cell growth media (ScienCell, #1001). Cells were maintained in accordance with ScienCell guidelines. Serum-free medium was prepared by adding endothelial cell growth supplement and penicillin/streptomycin solution. Flasks were coated in fibronectin (ScienCell) at a concentration of 2 µg/cm^2 in Ca^{2+} and Mg^{2+}-free PBS (Sigma) and placed in the 37 ºC incubator overnight. Fibronectin solution was removed and flasks washed twice with dH_2O prior to use.

2.13.6 Human brain vascular pericytes

Human brain microvascular endothelial cells (HBVP) were obtained from ScienCell (#1200) and maintained using pericyte medium (ScienCell, #1201). Complete medium was prepared by adding all supplements and refrigerated until use. Serum-free medium was prepared by adding pericyte growth supplement and penicillin/streptomycin solution. Flasks were coated in poly-l-lysine (ScienCell) at a concentration of 2 µg/cm^2 in dH_2O and placed in the 37 ºC incubator overnight. Poly-L-lysine solution was removed and flasks washed twice with dH_2O prior to use.

2.13.7 Long-term storage of cells

Cell lines and primary cells were stored in the presence of the cryoprotector DMSO. Cells were grown in T75 tissue culture flasks until 90 % confluent and processed as described for routine maintenance. In the last step, instead of re-suspending the pellets in fresh media, the cells were re-suspended in a mixture of 10 % DMSO and 90 % FBS and allowed to freeze at a controlled rate alcohol-free cell freezing container (Biocision) at -80 °C. After 24 hours cryovials were transferred into liquid nitrogen or -150 °C storage for future use.

2.13.8 Aβ preparation

$A\beta_{1-40}$ (Anaspec, AS-24236) and $A\beta_{1-42}$ (Anaspec, AS-24224) were lyophilised in 35% acetonitrile-H_2O.

2.13.9 Hypoxic chamber

The hypoxic chamber (SCI-tive, Baker Ruskinn) was set to 2% O_2 and 5% CO_2 and a temperature of 37°C. O_2, and CO_2 levels were maintained with compressed O_2, air and nitrogen. The station was humified with dH_2O.

2.14 Statistical approaches

The statistical analyses were performed using GraphPad Prism (GraphPad Software). The D'Agostino-Pearson omnibus K2 normality test [236] was used to indicate if data sets were of normal distribution. A null hypothesis is that all the values were sampled from a Gaussian distribution. *A p* value of < 0.05 indicates the data is not normally distributed, > 0.05 indicates the data set is normally distributed. Normality tests were not used to determine sample distribution in isolation as they are susceptible to outliers and small sample sizes. The data was plotted to observe the distribution and the presence of outliers and lognormal distributions was considered before choosing an appropriate statistical test.

Normally distributed data sets were compared using the unpaired, two tailed t-test. The null hypothesis for this test is that there is no difference in the means of the groups being compared. For a *p*-value of <0.05, the null hypothesis is rejected and the difference between the means of the two data sets being compared was deemed significantly different.

One-way ANOVA was used to compare three or more unmatched groups with normal distributions. The null hypothesis for this test is that the means of all groups are same. If the *p*-value was <0.05 the null hypothesis was rejected and groups were deemed to have different means. This does not mean all groups had different means but at least one group differed from the others. If the one-way ANOVA reported a significant difference either the Dunnett test or the Tukey-Kramer multiple comparisons test were used as post-hoc tests, depending on experimental setup. The Dunnett test was used to compare every group to a

mean, usually control, value. The null hypothesis is that test is that the means of both groups are same. The Dunnett test does not report an exact *p* value but provides a list of significant or not significant decisions for each pair analysed (>0.05, <0.05, <0.01, or <0.001). If a *p*-value was <0.05 the null hypothesis was rejected and the mean of two data groups was deemed significantly different. The Tukey-Kramer test compares the mean of one group with every other group and allows for unequal sample sizes and has the same null hypothesis and assumptions at the Dunnett test.

Pearson's correlation was used to assess linear correlation in normally distributed data sets. The correlation coefficient, r, reports the direction and magnitude of the correlation with 1 a perfect positive correlation, -1 a perfect negative correlation and 0 denoting no correlation. The null hypothesis is that the data were sampled from a population where there is no correlation between the two variables. If a *p*-value was <0.05 the null hypothesis was rejected and the two data sets was deemed significantly correlated.

Non-normally distributed data sets were compared using non-parametric tests. The Mann-Whitney test was used to establish the difference between two groups. Values are ranked from low to high regardless of group. The null hypothesis is that the distributions of both groups are identical. If a *p*-value was <0.05 the null hypothesis was rejected and the distribution of the two data sets was deemed significantly different.

The Kruskal-Wallis test was used to establish the difference between three or more unmatched groups. Values are ranked from low to high regardless of group. The null hypothesis is the distributions of all groups are identical. If a *p*-value was <0.05 the null hypothesis was rejected and the distribution of the data sets was deemed significantly different. Dunn's multiple comparisons test was used if Kruskal-Wallis reported a significant difference. The Dunn's test compares the sum of ranks in two groups with the expected average, dependent on number of samples and groups. The null hypothesis is that distributions are identical for each pair. The Dunn's test does not report an exact *p* value.

Spearman's correlation was used to assess rank order correlation in non-normally distributed data sets. The null hypothesis is that the data were sampled from a population where there is no correlation between the two variables. If a *p*-value was <0.05 the null hypothesis was rejected and the two data sets was deemed significantly correlated and the r value reports the direction of the correlation.

Chapter 3 VEGFR1

3.1 Introduction

VEGF is a pro-angiogenic factor [117, 237] upregulated in response to hypoxia [238, 239] (1.2.1). VEGF primarily acts on two tyrosine kinase receptors in the nervous system, VEGFR1 and VEGFR2. VEGF is vital for angiogenesis and mediates its effects via receptors expressed on the endothelial cell surface. VEGFR2 mediates most of the actions of VEGF and is a major regulator of angiogenesis [170]. VEGFR2 to mediates endothelial cell proliferation, migration, permeability and survival [107, 129, 168] resulting in the formation and maintenance of blood vessels. This results in increased blood flow and reduction in hypoxia. The role of VEGFR2 in the nervous system and AD will be covered in more detail in Chapter 4.

VEGFR1 has broadly been viewed as a negative regulator of VEGF, however important roles for the receptor are being elucidated in the adult CNS. sVEGFR1 isoforms are produced by alternate splicing and possess no kinase region (1.2.2.1.1). sVEGFR1 isoforms act as negative regulators of VEGF action by sequestering VEGF in the extracellular matrix [143, 148]. The membrane bound VEGFR1 (mbVEGFR1) has a high affinity for VEGF [148] but limited kinase activity [240]. mbVEGFR1 transduces signals for endothelial cell proliferation and permeability and is important in the regulation of postnatal angiogenesis [120, 241, 242]. VEGFR1 has been reported as being expressed on neurons and has a role in neuroprotection [243, 244] and neurogenesis [245] in the adult brain. VEGFR1 expression is upregulated in hypoxic conditions [145, 246-249]. CBF is reduced in AD resulting in cerebral hypoperfusion and hypoxia.

There have been conflicting reports of VEGFR1 localisation on astrocytes and microglia. VEGFR1 has been identified on microglia in ischaemic rat brain [250] and in control and AD post mortem study [142]. There is also evidence for a role of VEGFR1 in microglial migration [141, 142]. However, in other rat and porcine models of hypoxia, VEGFR1 expression was not seen on microglia [251-253]. VEGFR1 has also been reported on rat astrocytes in hypoxic models [142, 172, 251, 254-256] though was not observed in all animal models [252, 253, 257] or in human brain [142]. The level of VEGFR1 in tissue of critical importance as a negative regulator of VEGF function. In animal models of hypoxia elevated levels of VEGFR1 mRNA [142, 252-254, 256, 258] and protein [250, 253, 257] have been reported in the brain.

Despite increases in VEGF [72, 198, 212] it has previously been reported that there is no increase in microvessel density in the AD brain [78]. There are several possible explanations for this disparity including alteration in VEGFR location, level and downstream activation. VEGFR1 has a prominent anti-angiogenic role and is of importance in the understanding of dysregulated angiogenesis in AD. There have been few studies addressing VEGFR1

distribution in human brain. An increase in VEGFR1 due to hypoxia or in combination with other changes, may result in reduced angiogenesis in AD.

Frontal lobe was used as it provides a large area of tissue for examination of grey and white matter. Parietal lobe was used for all investigation on non-fixed tissue due to its relative abundance in post-mortem brains.

Results presented in this chapter on the cellular localisation of VEGFR1 and the level of VEGFR1 in human brain tissue were recently published [259].

3.1.1 Hypothesis

[1] VEGFR1 will be located on endothelial cells, microglia and neurons and not astrocytes in the frontal lobe. VEGFR1 has not been identified on astrocytes in human studies and several animal models, and physiological function for VEGFR1 on astrocytes is yet to be identified.

[2] Hypoxia directly regulates the transcription of VEGFR1, therefore the level of VEGFR1 mRNA will be increased in the AD brain compared to age matched control in the parietal cortex.

[3] Hypoxia directly regulates the transcription of VEGFR1, which can to regulate the protein level. The level of VEGFR1 protein will be increased in the AD brain compared to age matched control in the parietal cortex.

3.1.2 Aims

[1] Examine the cellular localisation and cerebral distribution of VEGFR1 in AD and control post-mortem frontal lobe using immunostaining.

[2] Measure the level of VEGFR1 mRNA in parietal cortex from AD compared with controls by qPCR.

[3] Measure the VEGFR1 protein level in parietal cortex from AD compared with controls by ELISA and western blot.

3.2 VEGFR1 localisation

Due to debate in the literature over the localisation of VEGFR1 in the glial population (3.1) it was important to establish the cellular location of the receptor in the AD brain.

3.2.1 Methods

3.2.1.1 Study cohort

Control and AD cases were neuropathologically confirmed as described in Chapter 2 and detailed in Table 3-1. The neuropathological and demographic features of control and AD

cases used for immunostaining are summarised in Table 3-2 and detailed here. Details of individual cases can be found in the Appendix 9. FFPE frontal lobe was used to investigate VEGFR1 localisation and was sectioned as described in Chapter 2 prior to the start of this study.

Parietal cortex and white matter		Control	AD
N		36	50
Age (years)	Range	58 - 95	57 - 93
	Mean ± SD	80.1 ± 8.7	77.5 ± 8.1
Gender	Female	11	26
	Male	25	24
Post-mortem delay (hours)	Range	3 – 67	4 - 85
	Mean ± SD	32.5 ± 16.3	31.6 ± 19.0

Table 3-1 Summary of the neuropathological and demographic features of control and AD cohorts used in mRNA and protein analysis

Frontal cortex		Control	AD
N		4	5
Age (years)	Range	75-85	60-97
	Mean ± SD	79.0 ± 4.5	80.2 ± 15.0
Gender	Female	1	2
	Male	3	3
Post-mortem delay (hours)	Range	23-92	24-65
	Mean ± SD	48.4 ± 30.9	37.3 ± 16.5

Table 3-2 Summary of the neuropathological and demographic features of control and AD cohorts used in immunolabelling studies. See Appendix 10 for individual case details.

Parietal cortex from control cases was used to perform western blotting and the cohort used is detailed in 3.4.1.1.

3.2.1.2 Western blot

Total protein concentration for tissue homogenates was calculated as described in 2.2.3. Western blotting was carried out as described in 2.4. Samples were run on 4-20% precast gels. The membrane was blocked with 3% BSA-TBST for 1 hour and incubated overnight at 4°C with anti-VEGFR1 antibody at a concentration of 1:2000 in 3% BSA-TBST. β-Actin was used as a loading control at 1:5000 in 5% milk-TBST. Human umbilical vein endothelial cell (HUVEC) lysates express both VEGFR1 and VEGFR2 and were used as a positive control. Recombinant VEGFR1 and VEGFR2 (R&D) were used to confirm the specificity of the antibody.

3.2.1.3 Immunohistochemistry

Immunohistochemistry was performed as described in 2.9.1. The antibody was titred to determine the optimal concentration and tested with both EDTA and citrate buffer pre-

treatment to enhance straining as described in 2.9.3. Sections were pre-treated with citrate buffer prior to immunolabelling with anti-VEGFR1 Ab32152 at 1:200. A no-primary control was included to account for any non-specific binding of the secondary antibody. Antibody diluent was applied, followed by secondary antibody incubation and detection as described. An immunoglobulin control was performed to ensure staining was not caused by non-specific interactions of immunoglobulin in the tissue. Sections were incubated with an immunoglobulin of the same isoform, species and concentration as the primary antibody. Secondary antibody incubation and detection were carried out as described in section 2.9.1. In this case rabbit IgG was used at a concentration of 2 µg/ml and incubated for 1 hour at RT.

3.2.1.4 Double immunofluorescence and immunohistochemistry

VEGFR1 co-localisation in glial cells was investigated by double immunohistochemistry (2.9.2) and double immunofluorescence (2.10).

Distribution of VEGFR1 was investigated using anti-VEGFR1 Ab32152 at 1:200. Antibodies against glial fibrillary acidic protein (GFAP), an astrocyte marker, and HLA-RD, a class II major histocompatibility antigen known to be a marker of microglia and macrophages, were both used at a concentration of 1:200. Sections were pre-treated with citrate buffer prior to immunolabelling with the first antibody. VEGF receptors were labelled first and bound antibody visualised with DAB (brown) and glial cells were labelled second and visualised using VIP (purple). AD tissue was used as it contains an increased number of GFAP positive astrocytes and areas of immune cell activation in comparison to control brain tissue.

3.2.2 Results

3.2.2.1 Validation of VEGFR1 antibody specificity

The antibody used was raised to the N terminus of VEGFR1 detecting only membrane bound and soluble forms. Western blot confirmed the presence of mbVEGFR1 in parietal cortex at 180 kDa (Figure 3-1). This molecular weight corresponded to the 180 kDa observed in the HUVEC lysate used as a positive control. sVEGFR1 isoforms were observed between 90 kDa and 135 kDa in parietal cortex homogenate. The antibody was shown to be specific to VEGFR1 recombinant protein at 220 kDa corresponding to the predicted weight of a sVEGFR1 homodimer [147, 150, 151]. No cross-reactivity was observed with VEGFR2 (210 kDa and 230 kDa).

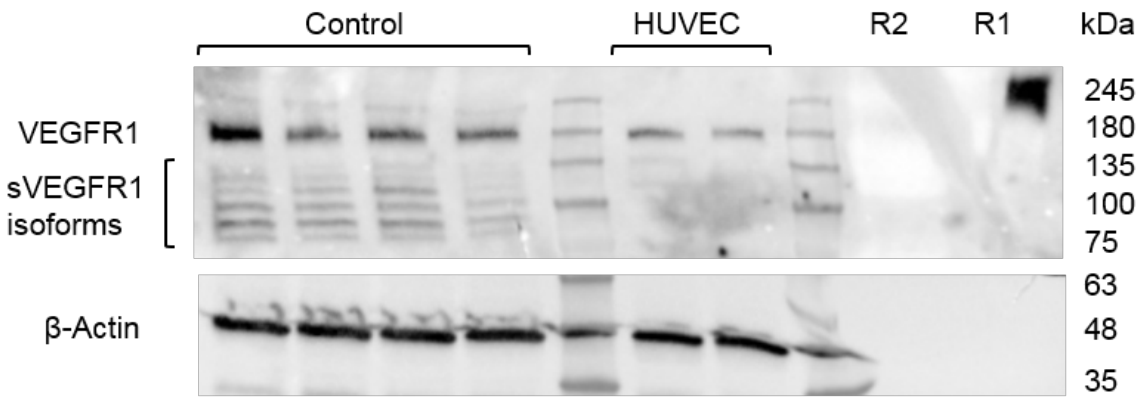

Figure 3-1 Western blot validation of VEGFR1 antibody in parietal cortex homogenate. HUVEC lysate was used as a positive control as HUVECs express both VEGFR1 (R1) and VEGFR2 (R2). VEGFR1 was observed at 180 kDa corresponding to HUVEC lysate. sVEGFR1 isoforms are also observed from 80 - 135 kDa in brain homogenate. The antibody was shown to be specific to VEGFR1 recombinant protein at 220 kDa corresponding to the predicted weight of the sVEGFR1 homodimer.

3.2.2.2 Localisation of VEGFR1 in control and AD brain

Immunohistochemistry was performed to elucidate the cellular localisation of VEGFR1 in AD and control frontal cortex. No labelling was observed on negative (no primary antibody) or IgG controls (Figure 3-2).

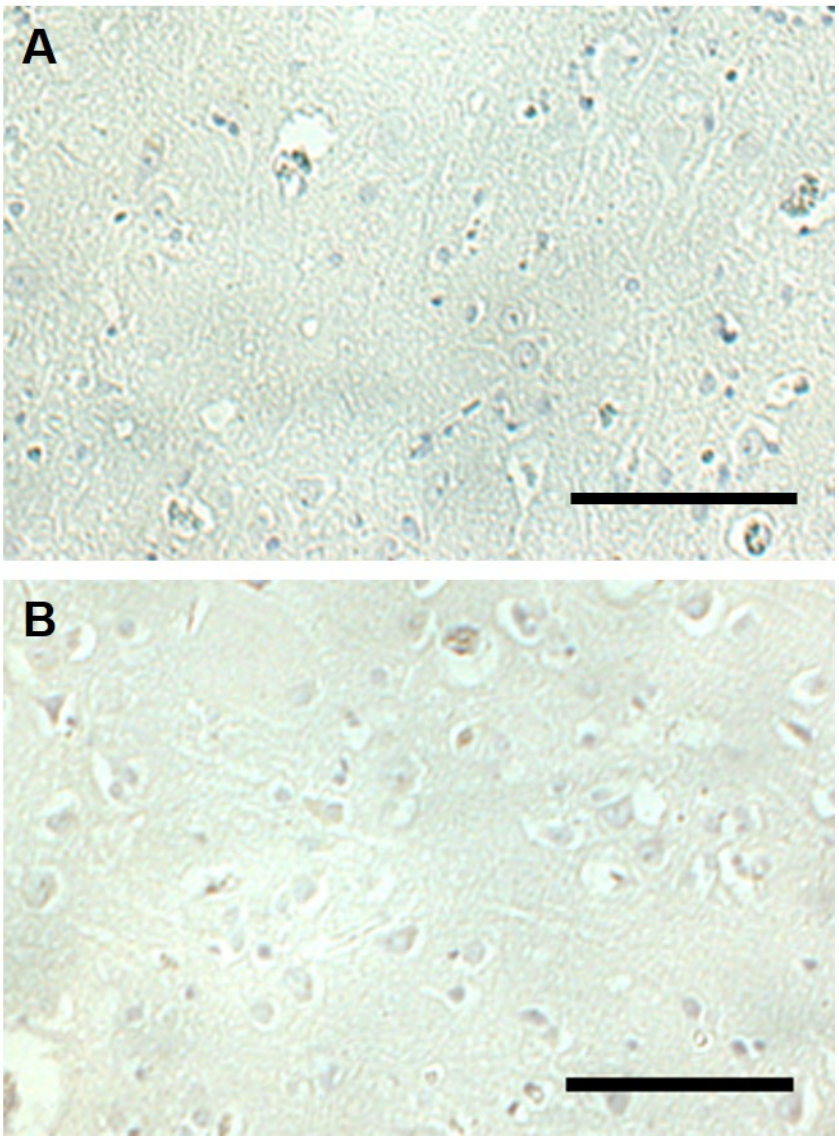

Figure 3-2 Negative control signal in sections of human frontal lobe. [A] No-VEGFR1-primary-antibody control. [B] IgG control for VEGFR1. Scale bars = 100 µm

Intense immunolabelling of VEGFR1 can be seen in the grey matter of the frontal cortex with white matter labelled much less intensely (Figure 3-3). VEGFR1 was clearly identified within the neuropil and neurons of the grey matter with some neuronal populations showing particularly intense staining (Figure 3-4A, B). VEGFR1 labelling was also observed in the endothelium of capillaries and arterioles (Figure 3-4C, D).

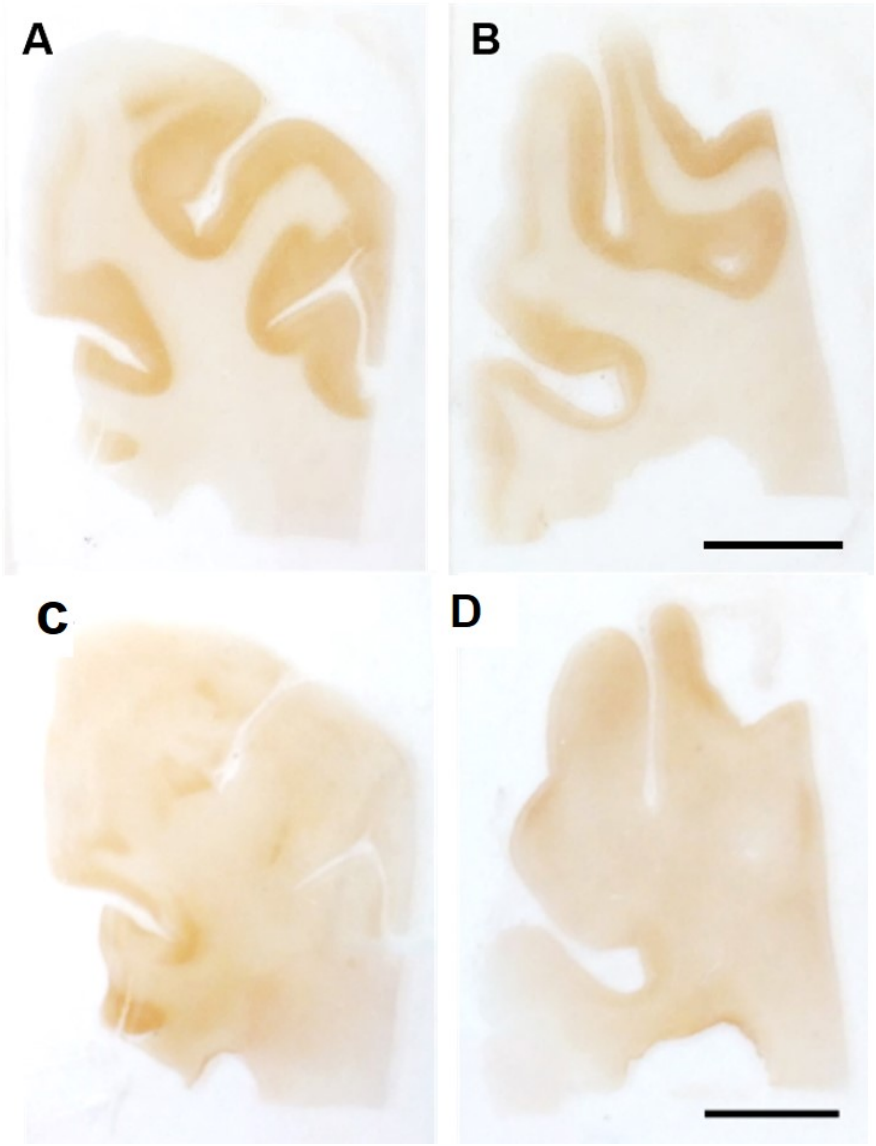

Figure 3-3 VEGFR1 IHC of control [A] and AD [B] frontal lobe. Strong immunopositivity is observed in the cortex compared to the white matter in control [A] and AD [B]. VEGFR2 IHC of control [C] and AD [D] frontal lobe is shown for comparison. In [C] there is some artefactual signal but that in general the labelling is weaker and not specific to the cerebral cortex. A more uniform level of immunopositivity is observed with VEGFR2. bar = 1 cm

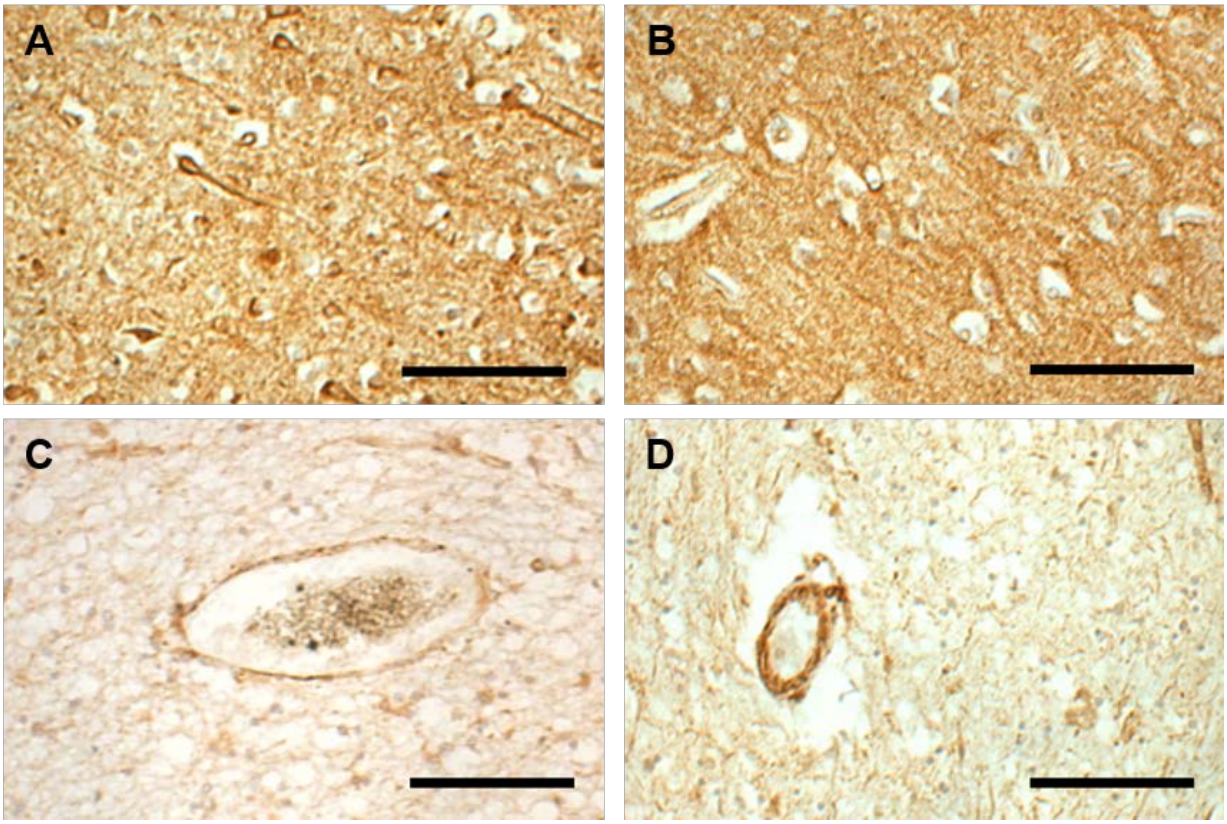

Figure 3-4 VEGFR1 labelling of control and AD frontal lobe. VEGFR1 antibody labelled the neuropil and neurons in the grey matter in control [A] and AD [B]. Approximately 100% of the neuropil was immunopositive for VEGFR1, with the pyramidal neurons displaying intense immunopositivity. VEGFR1 labelling was seen in capillaries and arterioles in control [C] and AD [D]. This was seen on 100% of capillaries and arterioles in C and AD. Scale bars = 100 µm.

3.2.2.3 Glial localisation of VEGFR1 in AD brain

To look for possible cellular localisation of VEGFR1 on glial cells double immunolabelling was performed. Double immunofluorescence using two fluorophores stimulated at different wavelengths was attempted. High levels of background fluorescence were observed and persisted despite the adjustment of primary antibody concentration and the use of pre- and post-treatments to reduce autofluorescence (Appendix 12). Double immunoperoxidase labelling was therefore used as an alternative.

Double immunolabelling of VEGFR1 (brown) with GFAP, an astrocyte marker, and HLA-DR, a microglial marker, (purple) is shown in Figure 3-5. VEGFR1 was again readily detectable, by immunohistochemistry, in the neuropil of the parietal cortex in AD (Figure 3-5A) and control brains, with most intense immunolabelling of neuronal cell bodies (Figure 3-5B, C). There was minimal co-localisation with GFAP-positive astrocytes (Figure 3-5B) or HLA-DR-positive microglia (Figure 3-5C).

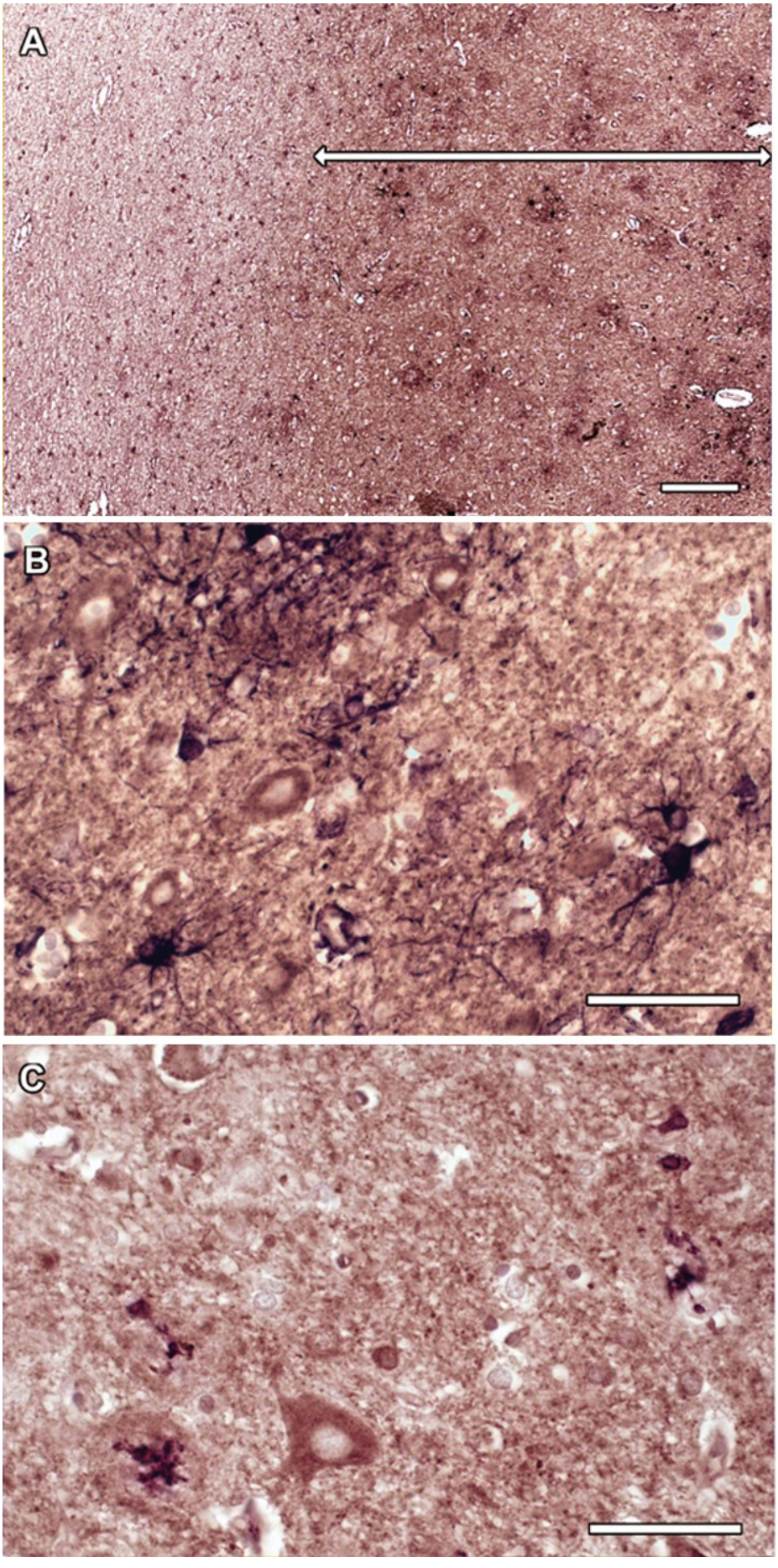
A
B
C

Figure 3-5 Cellular localisation of VEGFR1 in human parietal cortex. The examples shown are from an AD brain. [A] Double-labelling of VEGFR1 (brown) and GFAP (purple) shows VEGFR1 to be present in the cerebral cortex (double-headed arrow) but not the underlying white matter. Scale bar = 2 mm. [B] At higher magnification VEGFR1 is detectable within neurons and neuropil, with minimal labelling of GFAP-positive astrocytes. Scale bar = 50 µm. [C] Double-labelling of VEGFR1 (brown) and HLA-DR (purple) shows minimal VEGFR1 immunopositivity in HLA-DR-positive microglia. Scale bar = 50 µm.

3.3 VEGFR1 mRNA level in control and Alzheimer's disease

The aim of this work was to measure the VEGFR1 mRNA level in the parietal cortex of control and AD.

3.3.1 Methods

3.3.1.1 qPCR study cohort

Parietal cortex from control and AD patients was used to investigate VEGFR1 mRNA expression. Control and AD cases were neuropathologically confirmed as described in 2.2. Control and disease subjects were age-matched and, where possible, matched for gender. All subjects had a post-mortem delay of less than 90 hours. The neuropathological and demographic features of control and AD cohorts are described in Table 3-3.

Parietal cortex		**Control**	**AD**
N		36	50
Age (years)	Range	58 - 95	57 - 93
	Mean ± SD	80.1 ± 8.7	77.5 ± 8.1
Gender	Female	11	26
	Male	25	24
Post-mortem delay (hours)	Range	3 - 67	4 - 85
	Mean ± SD	32.5 ± 16.3	31.6 ± 19.0

Table 3-3 Summary of the neuropathological and demographic features of control and AD cohorts used for VEGFR1 mRNA analysis and protein analysis. Details of individual cases are listed in the Appendix 9.

3.3.1.2 Selection of primers for VEGFR1

Several sVEGFR1 isoforms can be produced by alternative splicing of the *FLT1* gene as described in 1.2.2.1.1, and several were found to be present in human brain tissue (see 3.2.1.2). The primer set was selected to measure mbVEGFR1 and sVEGFR1 mRNAs. The genomic map containing primer location can be found in Appendix 13.

3.3.1.3 Selection of reference genes for relative quantification

The use of appropriate reference genes is essential for the proper interpretation of qPCR results. The ideal reference gene should be expressed in the same cell types as the gene of

interest so that expression is not affected by changes in cellular composition of the tissue with disease. Reference gene selection in tissue can be confounded by the heterogeneity of cell type, and different cell types may be affected differently by disease, therefore selection of appropriate reference genes is extremely important. Multiple reference genes were used to help to distinguish between changes in the cellular expression of the gene of interest, and changes in mRNA levels caused by changes in cellular composition in AD. Reference genes were needed to account for total cell content and for the relative number of neurons and endothelial cells on which VEGFR1 is present.

The gene encoding β-actin, *ACTB,* was used to adjust for total cell content. *ACTB* is a commonly used reference gene with stable expression across all cell types. It has been identified as an intermediately stable reference gene in hypoxic conditions [260] [261] and stable in control and AD post-mortem human brain tissue [262].

To establish whether changes in VEGFR1 expression might reflect loss of neurons in AD (3.2.2.2), a specific neuronal gene was used as one calibrator. In AD there is a decrease in the number of neurons in the brain. If the level of VEGFR1 mRNA was reduced in AD when calibrated to *ACTB* this could either be a result of the loss of neurons on which VEGFR1 is expressed or due an overall reduction in VEGFR1 mRNA expression. Calibration with reference to a neuronal marker helps to interpret any changes in VEGFR1 mRNA. Neuronal nuclei protein (NeuN), also known as neuronal specific splicing regulator, Fox-3 [263], was selected as an established neuronal mRNA [264].

Given the presence of VEGFR1 on endothelial cells in the brain (3.2.2.2), a specific endothelial cell gene transcript as a calibrator. The endothelial marker, platelet endothelial cell adhesion molecule (PECAM1), also known as cluster of differentiation 31 (CD31) [265, 266] was used to investigate whether changes in VEGFR1 mRNA could be explained by altered endothelial cell content.

3.3.1.4 qPCR

RNA was extracted from fresh frozen parietal cortex as detailed in 2.11.1. cDNA was generated as described in 2.11.4, added to primers and master mix and made up to total volume with RNase free water. Samples were analysed in triplicate with non-template controls on each plate using the protocol detailed in 2.12.

3.3.1.5 Statistical analysis

The $2^{-\Delta\Delta Ct}$ method was used to determine the fold difference between VEGFR1 and reference gene (*ACTB*, *RBFOX3* and *PECAM1*) mRNA levels, as described in 2.12. Groups were tested for normality and were found to have a non-normal distribution, as expected from exponential values. The geometric mean and 95% confidence interval were calculated

for each group. Mann Whitney test was used for comparisons between individual sample $2^{-\Delta\Delta Ct}$ values in control and AD groups.

3.3.2 Results

3.3.2.1 Expression of reference genes in control and AD

Reference genes were validated prior to investigating genes of interest. There was no significant difference in the C_T values of *ACTB*, encoding β-actin, between control and AD samples (Figure 3-6).

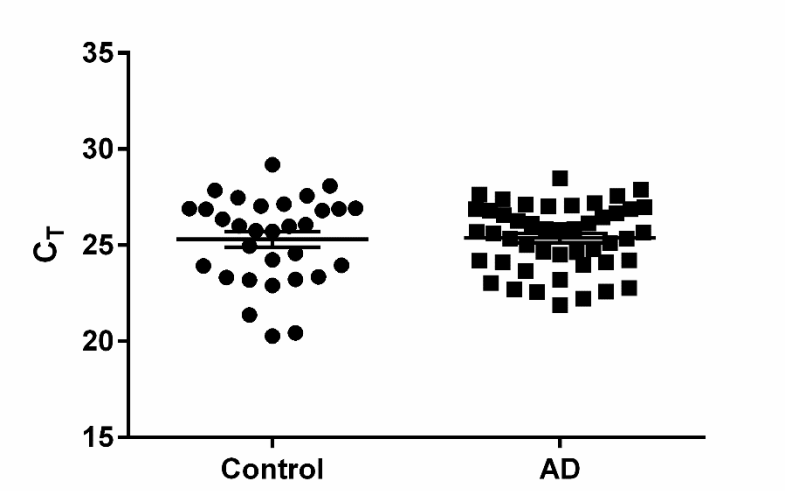

Figure 3-6 *ACTB* C_T values were measured by qPCR in human parietal cortex. There was no significant difference in mean C_T value when control and AD samples were compared. The mean and standard error of the mean are displayed. C: n= 31, AD: n= 47.

ACTB was shown to be stable in control and AD samples and is expressed at similar levels in all cell types. *RBFOX3* is expressed in neuronal cells and *PECAM1* in endothelial cells. The fold change of *RBFOX3* and *PECAM1* in AD was calculated relative to the mean level in control tissue using *ACTB* as the calibrator and results shown in Figure 3-7. There was no significant difference in the fold change of *RBFOX3* between control and AD (~1.1-fold higher, p= 0.436). There was a significant ~1.6-fold increase in *PECAM1* in AD samples compared to control (p= 0.021). A significant fold increase in *PECAM1* could indicate an increase cell type expressing PECAM1 in the AD brain compared to control.

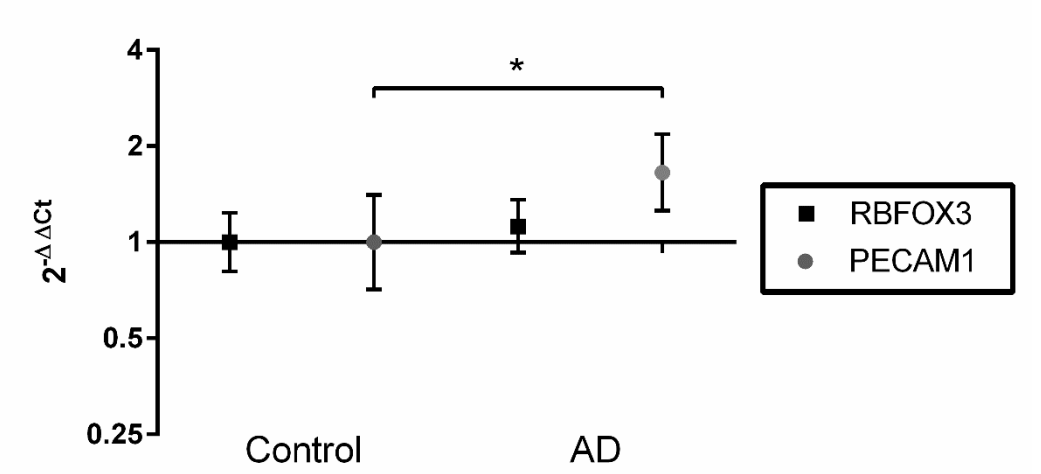

Figure 3-7 *RBFOX3* and *PECAM1* mRNA levels were measured by qPCR in parietal cortex. Fold difference in RBFOX3 and PECAM1 mRNA was calculated via the $2^{-\Delta\Delta Ct}$ method using *ACTB* as a calibrator gene and compared to mean levels in control tissue. There was no significant difference between the fold change of *RBFOX3* between control and AD (*p*= 0.439). There was a significant increase in the fold change of *PECAM1* in AD samples compared to control (*p*= 0.021). This indicates an increase in the number of cells expressing PECAM1. The geometric mean and 95% confidence intervals of the $2^{-\Delta\Delta Ct}$ values are shown for each group on a $\log_2$ scale. Horizontal line indicates $2^{-\Delta\Delta Ct}$ fold change of 1 assigned to control samples, increases or decreases from this line in disease subjects indicate corresponding fold changes in gene expression in disease. C: n= 31, AD: n= 47. * p<0.05.

3.3.2.2 VEGFR1 mRNA levels in AD and control brain

In relation to expression of *ACTB*, that of VEGFR1 was significantly increased in AD compared to controls of 2.4-fold (*p*= 0.014). As would be expected from the previous results (see 3.3.2.1), VEGFR1 was also significantly increased in relation to *RBFOX3*, by ~2.2-fold in AD compared to controls (*p*= 0.014). The level of VEGFR1 relative to *PECAM1* was not significantly increased in AD compared with controls (*p*= 0.114). It should be noted, however, that my immunohistochemical findings indicated that most of VEGFR1 in the brain tissue was neuronal rather than endothelial.

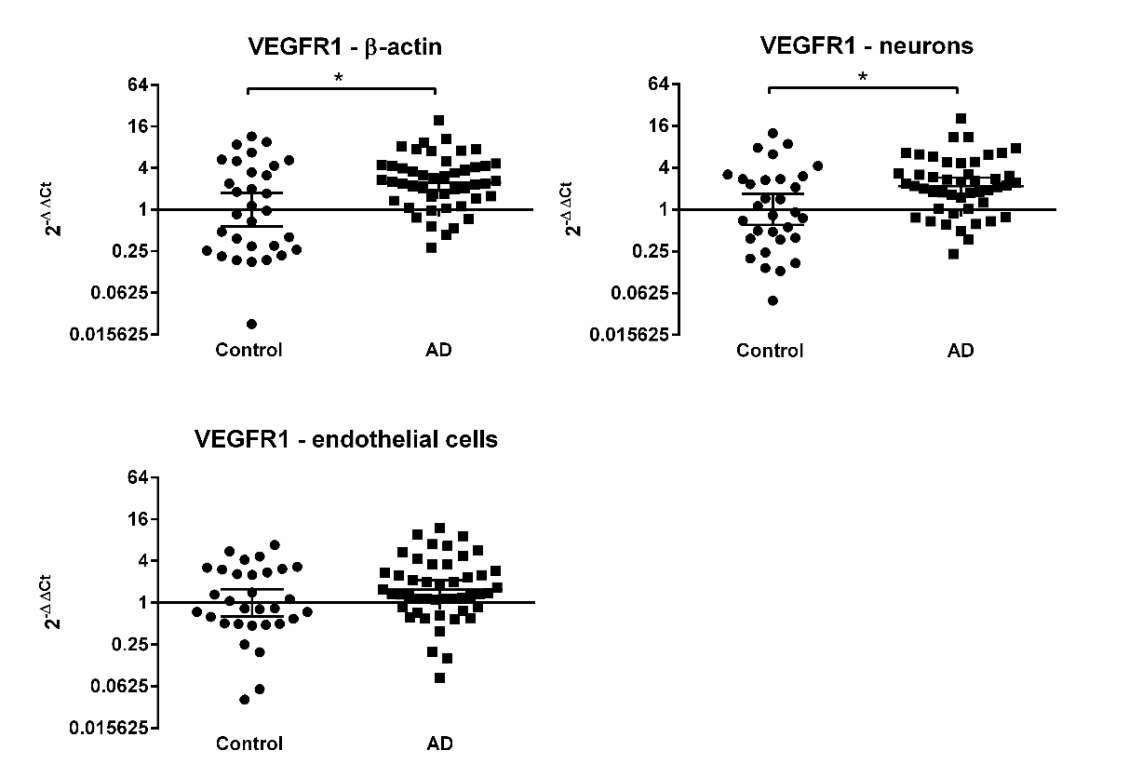

Figure 3-8 VEGFR1 mRNA levels measured by qPCR in homogenates of parietal cortex. The fold difference relative to the mean in control tissue was calculated for each sample by the $2^{-\Delta\Delta Ct}$ method. Significant increases were observed with *ACTB* (β-actin) (*p*= 0.014) and *RBFOX3* (neuronal marker) (*p*= 0.014) as calibrators, but not when VEGFR1 mRNA was calibrated to *PECAM1* (endothelial cell marker) (*p= 0.114)*. The geometric mean and 95% confidence intervals of the $2^{-\Delta\Delta Ct}$ values are shown for each group on a $\log_2$ scale. C: n= 30, AD: n= 48. * p< 0.05.

3.4 VEGFR1 protein level in control and Alzheimer's disease

The aim of this work was to measure VEGFR1 protein level in control and AD parietal cortex.

3.4.1 Methods

3.4.1.1 Protein level study cohort

Fresh frozen parietal cortex and white matter from control and AD patients was used to investigate VEGFR1 protein expression. Control and disease subjects were age-matched and, where possible, matched for gender. All subjects had a post-mortem delay of less than 90 hours. The demographic features of the control and AD cohort are summarised in Table 3-3.

3.4.1.2 VEGFR1 sandwich enzyme-linked immunosorbent assay

Human total VEGFR1 (FLT1) duoset IC ELISA kit was used to measure VEGFR1 protein level in human brain homogenate. Frozen brain samples were homogenised as detailed in 2.2.3 using the manufacturers recommended NP-40 based lysis buffer with phosphatase and protease inhibitors (Lysis buffer #9). The assay was carried out according to manufacturer's instructions summarised in 2.6. Readings were blank corrected and a 7-point curve was constructed using VEGFR1 recombinant standards. A 4-parameter logistic curve fit was applied and sample values interpolated. 50 µl of standard and sample were added to each well. Samples were measured in duplicate on each plate.

3.4.1.3 Spike, recovery and linearity testing

The ELISA kit had been validated for use on cell culture supernatant, serum and plasma samples by the supplier. To validate the ELISA kit for use on human brain tissue, homogenates were spiked with recombinant protein, and recovery and linearity testing was performed. 2000 pg/ml of VEGFR1 recombinant protein was used to 'spike' neat brain tissue homogenate, to make the spiked sample, and control diluent (PBS), to make the control spike. The spiked sample, unspiked sample and control spike were mixed thoroughly and serial dilutions performed. Percentage recovery and linearity were calculated using Equation 3-1 and Equation 3-2. Spiked values should return an increase in signal compared with the unspiked sample dependent on the amount of recombinant protein added. Values outside the accepted range indicate interference by one or more substances in the sample matrix. Samples homogenised in different buffers were tested (SDS and Triton X-100) and spike testing was repeated once. Percentage recovery and linearity did not fall within the acceptable range of 80-120% as stated by the manufacturer (Table 3-4).

$$\% \, Recovery = \frac{Observed - Unspiked}{Expected} \times 100$$

Equation 3-1 Percentage recovery for spiked sample

$$\% \, Recovery \, (1{:}\, x) = \frac{Observed \; value \; of \; 1 \; in \; x \; dilution}{Expected \; value \div x} \times 100$$

Equation 3-2 Percentage recovery for linearity

Observed: Spiked sample value
Unspiked: Unspiked sample value
Expected: Amount spiked into sample
x: dilution factor

	% Recovery		
	Spiked	Unspiked	Control
Neat	6.2	-	-
1:2	137.8	132.1	91.5
1:4	135.6	155.2	125.8

Table 3-4 Percentage recovery and linearity of brain tissue homogenate on VEGFR1 ELISA. Spiked samples were treated with 2000 pg/mL of VEGFR1 recombinant protein and diluted. Unspiked samples contained brain homogenate only. Percentage recovery and linearity of brain homogenates did not fall within the manufacturer's acceptable range of 80-120%. Control samples contain PBS diluent spiked with 2000 pg/mL of VEGFR1 and remained within the accepted range.

3.4.1.4 VEGFR1 dot blot

Dot blots were performed on cortex samples from control and AD cortex detailed in 3.4.1.1. Western blot displayed low levels of VEGFR1 in white matter which was confirmed by minimal immunolabelling of the white matter observed by IHC (3.2.1.3).

Dot blotting for VEGFR1 was carried out as described in 2.5. Serial dilutions of homogenate standard were prepared using a 1:100 starting dilution in TBS. Homogenate samples were diluted at a concentration of 1:1000 in TBS. Following sample incubation for 1 hour the membrane was blocked with 5% BSA-TBST. VEGFR1 Ab32152 was used at a concentration of 1:2000 in 5% BSA-TBST and applied overnight at 4˚C. Secondary antibody was applied and membranes were developed and analysed using BioRad ImageLab software. A representative dot blot is shown in Figure 3-9 which shows the standard curve used to calculate relative units and the samples in triplicate. The background adjusted volume was calculated for each dot and relative values for each sample were calculated by interpolating from the 4-parameter logistic curve fit standard curve. A 7-point standard curve was created for each blot. Coefficient of variation (CoV) was performed between samples on each blot to calculate intra-assay reliability. Each sample was measured on two membranes and inter-assay reliability calculated by CoV. Any samples outside of the acceptable range were repeated. Values were corrected for the total protein concentration of the sample.

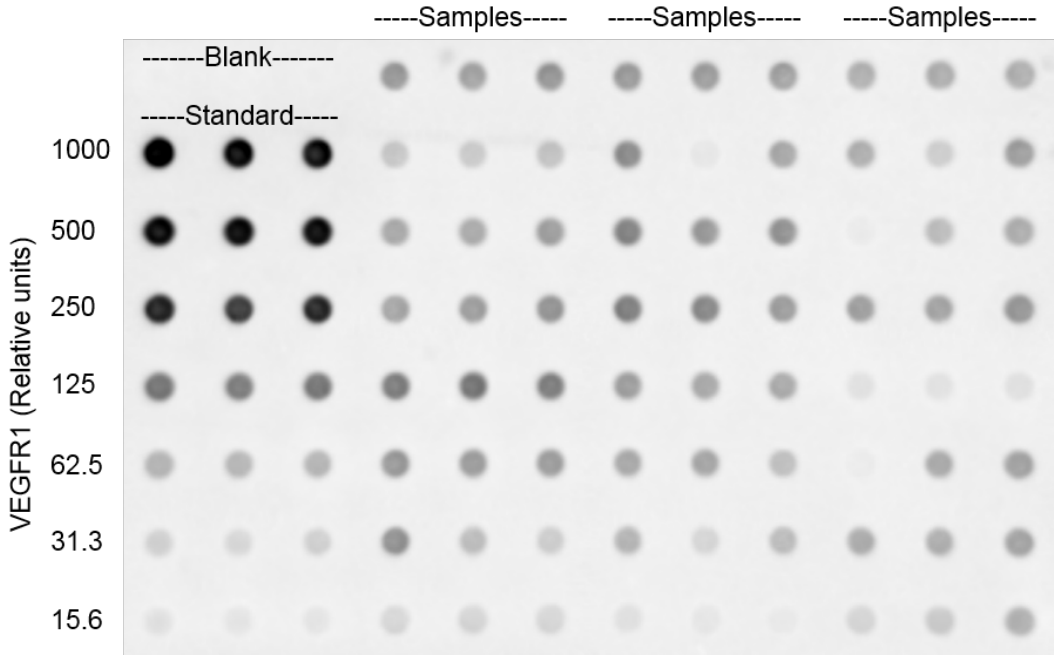

Figure 3-9 Representative VEGFR1 dot blot. Blank and 7-point homogenate standard were run in triplicate. High standard was a 1:100 concentration of homogenate. The corresponding relative units for the homogenate standard are listed. Homogenates were diluted at a concentration of 1:1000 and assayed in triplicate. Coefficient of variation (CoV) was calculated for each sample for intra-assay and inter-assay reliability.

3.4.2 Results

3.4.2.1 VEGFR1 protein level in control and AD cortex

An ELISA provides an accurate way to measure VEGFR1 protein levels in tissue homogenate. A commercially available Human VEGFR1 ELISA kit (R&D Systems) was used to develop an ELISA on brain tissue. Spike and recovery experiments demonstrated poor percentage recovery and linearity in human brain samples suggesting that a factor in the brain homogenate was interfering with the measurement. As a result, dot blotting with a validated antibody was used to assess VEGFR1 protein level in control and AD tissue samples.

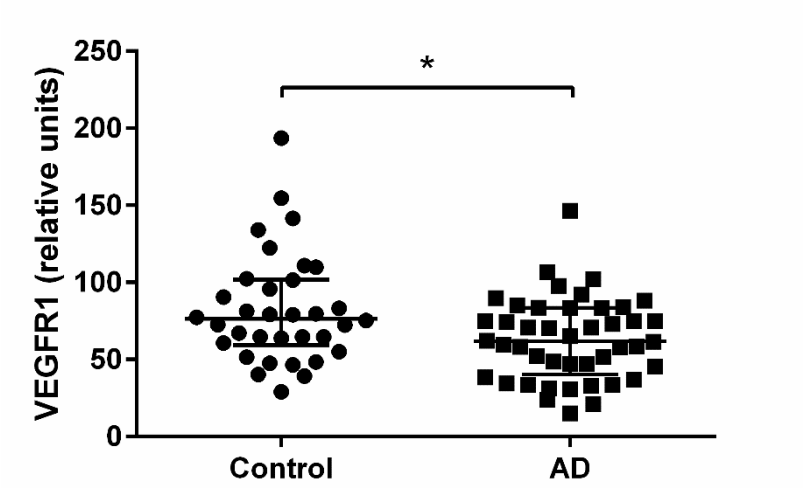

Figure 3-10. VEGFR1 protein level was significantly lower in AD than control brains (*p*= 0.02). Median ± interquartile range is displayed. C: n= 34, AD: n= 44. * p< 0.05.

The level of VEGFR1 was measured in the parietal cortex of AD and control brains. The median level of VEGFR1 was significantly lower in AD than control brains (*p*= 0.02) although there was substantial overlap between the two groups (Figure 3-10).

3.5 Proportion of VEGFR1 and sVEGFR1 in control and Alzheimer's disease

To follow the measurement of total VEGFR1 in the cortex, the level of sVEGFR1 in relation to membrane bound VEGFR1 was investigated. The aim of this work was to measure the proportion of sVEGFR1 in control and AD parietal cortex.

3.5.1 Methods

3.5.1.1 Western blot

The western blotting for VEGFR1 as described in 3.2.1.2. Control samples and disease samples were selected at random from the parietal cortex cohort described in 3.4.1.1. The cases used were not age-matched and are detailed in Appendix 14.

3.5.1.2 Calculation of mbVEGFR1:sVEGFR1 ratio

sVEGFR1 isoforms have been identified and described in 3.2.2.1. Membranes were developed and analysed using BioRad ImageLab software. Western blot lanes and samples bands were selected. Molecular weights of sample bands were calculated with the 'MW Analysis Tool' using protein ladder(s) as a reference. Analysis table reports the volume of the intensities within band boundaries. These volumes were used to calculate the ratio of mbVEGFR1 to the sum of its soluble forms.

$$\boldsymbol{mbVEGFR1}:\boldsymbol{sVEGFR1} = \frac{\boldsymbol{mbVEGFR1}}{\boldsymbol{SUM}(\boldsymbol{sVEGFR1\ isoforms})}$$

Equation 3-3 mbVEGFR1: sVEGFR1 ratio

mbVEGFR1: membrane bound VEGFR1 (reported intensity)
sVEGFR1: soluble VEGFR1 (reported intensity)

3.5.1.3 Calculation of normalised densitometry of mbVEGFR1 and sVEGFR1

The densitometry of mbVEGFR1 and the sum of sVEGFR1 isoforms was normalised to β-actin. Membranes were analysed using BioRad ImageLab software as described in 3.5.1.2. The reported intensities for mbVEGFR1 and sVEGFR1 isoforms in were divided by the reported intensity of the β-actin band.

3.5.2 Results

3.5.2.1 mbVEGFR1:sVEGFR1 in control and AD parietal cortex

Western blots with antibody to the N terminus of VEGFR1 were used to quantify membrane bound and soluble forms of VEGFR1 (Figure 3-11). mbVEGFR1 migrates at 180 kDa and sVEGFR1 isoforms range from 90-135 kDa. mbVEGFR1:sVEGFR1 was significantly lower in AD than controls (p= 0.046, Figure 3-12A). There was a significant decrease in mbVEGFR1 in AD compared to control when normalised to β-actin (p= 0.0057, Figure 3-12B). No difference was observed in sVEGFR1 between control and AD when normalised to β-actin (Figure 3-12C). Uncropped blots are displayed in Appendix 15.

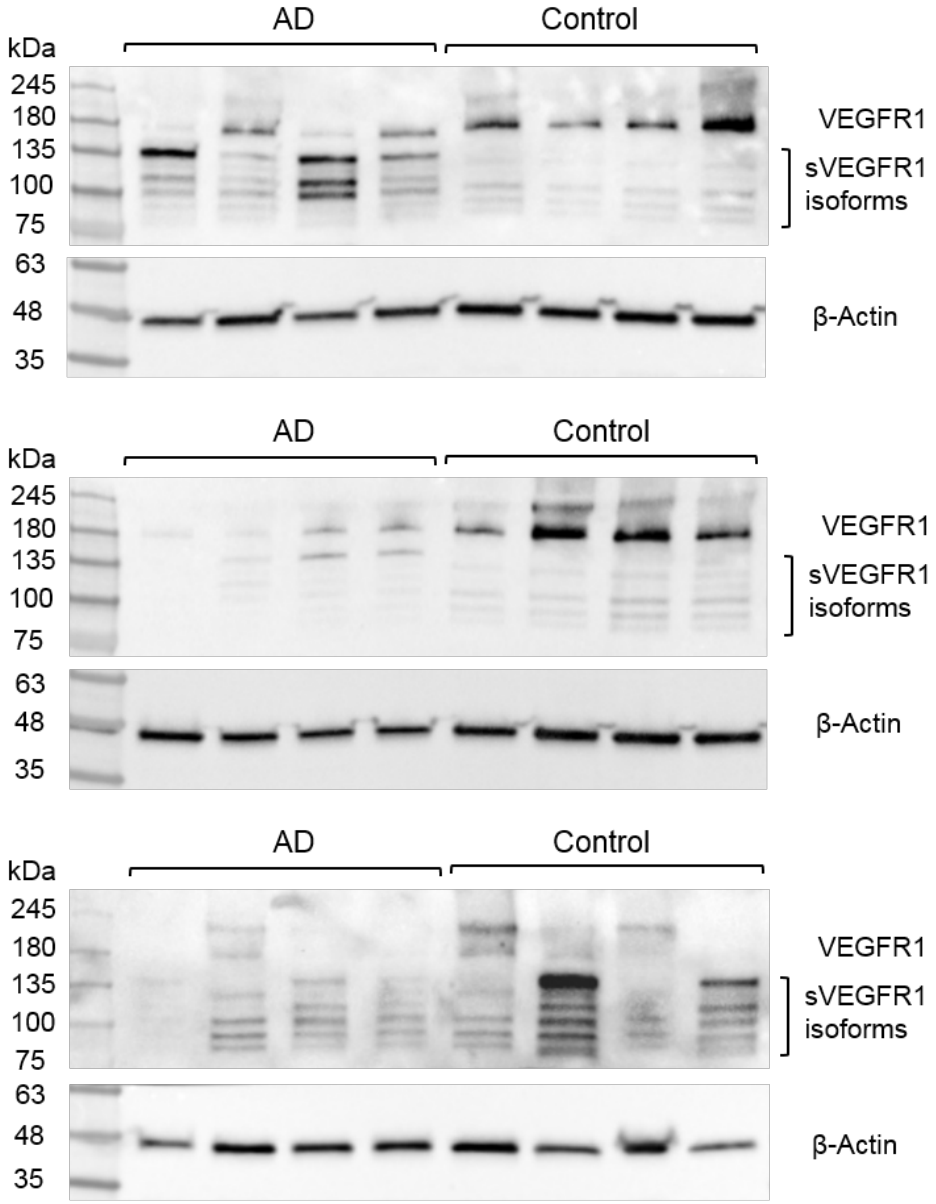

Figure 3-11 VEGFR1 western blots on control and AD parietal cortex homogenates. mbVEGFR1 was observed at 180 kDa. sVEGFR1 isoforms were observed between 80-135 kDa. β-actin was used as a loading control.

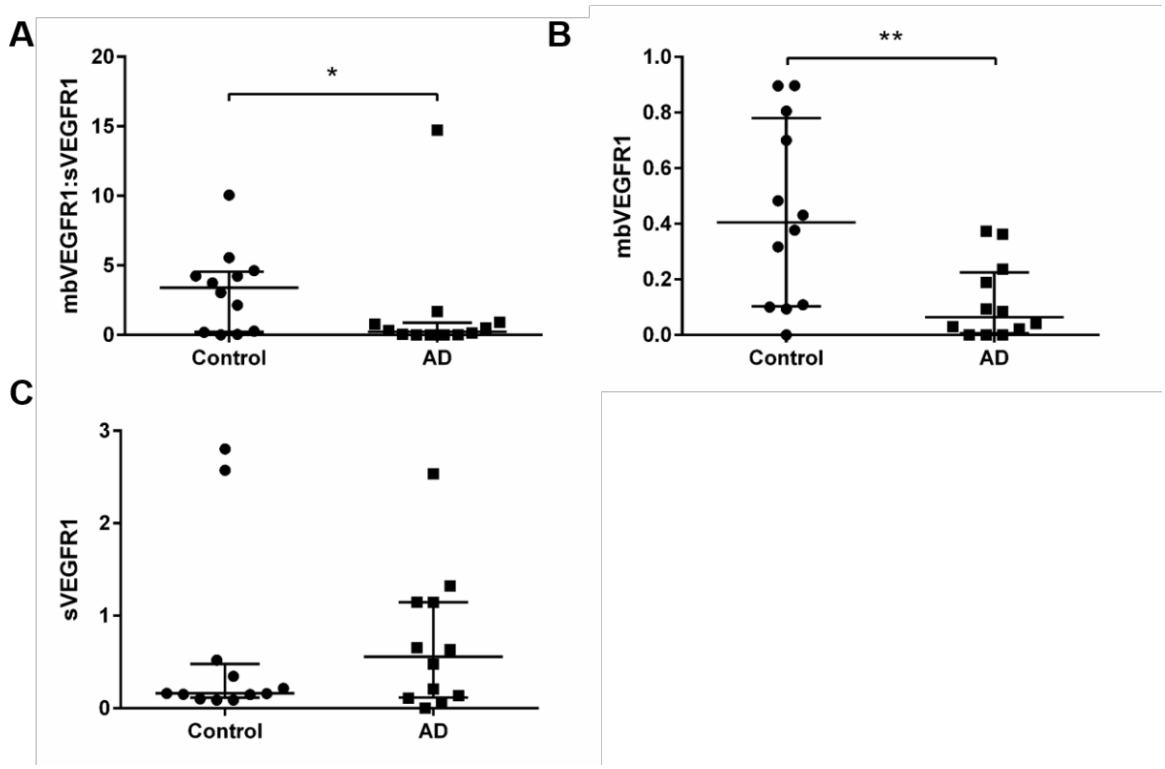

Figure 3-12 Densitometry of VEGFR1 western blots. [A] Scatterplot showing mbVEGFR1:sVEGFR1 in control and AD parietal cortex, as determined from integrated area-density measurement of the western blot bands. The ratio was significantly lower in the AD brains (*p*= 0.046). [B] mbVEGFR1 normalised to β-actin. There was a significant reduction in mbVEGFR1 in AD compared to control. [C] The sum densities of sVEGFR1 isoforms normalised to β-actin. Median ± interquartile range is displayed. C: n= 12, AD: n= 12. ** *p* < 0.01.

3.6 Discussion

The aim of this work was to determine the cellular distribution and levels of VEGFR1 mRNA and protein in human post-mortem cerebral cortex in AD and controls.

The localisation of VEGFR1 was investigated by IHC in control and AD brain. The expression of VEGFR1 by neurons is in keeping with previous evidence of its involvement in neuroprotection [243, 244] and neurogenesis [245]. It is also in accord with the roles of VEGF in neurogenesis, neuronal migration and synaptic plasticity [121, 210, 211, 267, 268]. VEGFR1 was previously reported to be present on primary rat cultured microglia [141], in rat brain following middle cerebral artery occlusion [250] and in human control and AD brain [142]. In contrast, VEGFR1 was not seen on microglia in other rat and porcine models of hypoxia [251-253]. VEGFR1 immunopositivity within microglia was not seen in either AD or control brains in this study, contrary to the findings of Ryu et al (2009) who identified VEGFR1 in microglia in

control and AD brain tissue [142]. The cohort used in this study was of modest and would benefit from expansion to confirm VEGFR1 localisation on microglia. Other reasons for the disparity could include their use of a different VEGFR1 antibody whose specificity was not confirmed, and a different fixation protocol. The same study identified VEGFR1 on microglia and a subset of astrocytes in a mouse model of AD [142]. In the present study VEGFR1 was not observed on astrocytes in human frontal lobe. VEGFR1 was previously reported on astrocytes in fetal and early postnatal cortical rat explants [172], on a subset of reactive astrocytes in a rat model of CNS trauma [256] and in a rat model of hypoxia [255]. Expression of VEGFR1 mRNA was also reported in rat astrocytes after addition of VEGF [254] but not in animal models of trauma and hypoxia [252, 253, 257] or transgenic AD mice [142]. Animal models of hypoxia use differing experimental designs, making comparison difficult. It is also possible that there may be species or developmental differences in VEGFR1 expression. As there is evidence that VEGFR1 is expressed at low levels in astrocytes in normal CNS [250], it would be of benefit to conduct further studies on unfixed frozen tissue to assess VEGFR1 co-localisation both in the healthy adult brain and in AD.

The level of VEGFR1 mRNA was measured by qPCR in human parietal cortex. It was hypothesised that there would be an increase in VEGFR1 mRNA expression in AD. A reduction in CBF leads to reduced tissue oxygenation in AD and might be expected to upregulate VEGFR1 transcription [145, 246, 247] via hypoxia-inducible factor 1 (HIF1α) [269].

In this study, there was a significant increase in VEGFR1 mRNA level in AD parietal cortex when calibrated against a control mRNA expressed in all cell types. VEGFR1 mRNA was also increased in relation to a neuronal transcript not affected by AD, in keeping with an increase in neuronal expression of VEGFR1 in AD. This finding is consistent with previous studies which have identified significant upregulation of VEGFR1 in neuronal populations in animal models and cell models of acute cerebral hypoxia [252, 254, 256]. AD is a neurodegenerative disease and it might be expected that there would be neuronal loss in disease compared to controls [270]. However, the level of the calibrator neuronal transcript was unchanged within the samples analysed. It would be useful to run a panel of neuronal markers in post mortem human tissue to assess stability with in control and disease.

VEGFR1 was also increased but not significantly in relation to an endothelial calibrator mRNA, the level of which was itself elevated in AD. The elevation of VEGFR1 mRNA in endothelial cells was expected, due to its increased expression in hypoxic conditions and important role as a regulator of angiogenesis [144, 271]. Since this study, the endothelial marker, *PECAM1*, has been found to be expressed by monocytes and neutrophil populations, and to be elevated in response to blood brain barrier disruption which may lead to its increased

expression in AD [272]. In future studies, it would be worth using the gene encoding von Willebrand factor (*vWF)* as a more specific endothelial cell reference gene.

In future qPCR studies it would be useful to use multiple reference genes for each cell type. In particular it would be beneficial to include an additional reference gene that would control for all cell types to accompany ACTB, for example, 18S rRNA or 28S rRNA shown to be stable under hypoxic conditions [260] [261] and CYC1 found to be stable in post mortem brain tissue [262]. This would ensure that changes in the gene of interest were attributed to disease state and not due to changes in the reference gene.

Quantification of mRNA provided an indicator of VEGFR1 gene expression in the brain but proteins are subject to regulation at the translational and posttranslational level. To assess VEGFR1 protein level, VEGFR1 protein was measured by dot blot in the same samples. It was hypothesised that VEGFR1 protein would be increased in AD compared to controls in consequence of the elevation of VEGFR1 mRNA, as established by qPCR. Contrary to this, a reduction was seen in total VEGFR1 level in AD. This may reflect post-translational modifications or possible increased protein degradation in disease. There has been little investigation into VEGFR1 internalisation and degradation though VEGFR2 expression has been shown to be tightly regulated [130].

Ikeda et al (2011) previously demonstrated downregulation of VEGFR1 in human microvascular endothelial cells, cultured under hypoxic conditions for 48 hours [273]. The reduction in total VEGFR1 was attributed to a reduction in sVEGFR1 mRNA and protein, while the level of membrane bound VEGFR1 remained unchanged [273]. Under conditions of chronic hypoxia the downregulation of sVEGFR1 may be physiologically beneficial, as sVEGFR1 isoforms are negative regulators of angiogenesis. Increased sVEGFR1 in AD could inhibit angiogenesis and reductions in sVEGFR1 isoforms could result in increased vessel formation to combat reduced oxygenation. To investigate this possibility western blots were used to assess the proportion of mbVEGFR1 and sVEGFR1 in control and disease parietal cortex. In contrast to the hypothesis, the ratio of mbVEGFR1 to sVEGFR1 was decreased in AD compared to control. When further investigated, the level of mbVEGFR1 was found to be reduced in AD compared to control and there was no difference in sVEGFR1 level. This indicates an increase in the proportion of sVEGFR1 isoforms which may contribute to impaired angiogenesis despite the chronic hypoperfusion. There is evidence that VEGF can induce the expression of sVEGFR1 expression without effecting mbVEGFR1 transcription via a VEGF-A responsive element in intron 13 [274]. This direct regulation of sVEGFR1 splicing may explain the pattern of VEGFR1 expression in AD.

Soluble forms of VEGFR1 are yet to be investigated in the nervous system but have been found to be biologically important in cancer research and preeclampsia [275-277]. To expand on the present work, future studies could include the measurement of mRNA level of soluble isoforms via qPCR and development of a sVEGFR1 specific ELISA in the control and AD brain to analyse changes in sVEGFR1 levels in a larger cohort.

In future, it would be beneficial to conduct the mRNA and protein analysis on VaD samples to gain insight into possible changes in VEGFR1 expression in disease. This would provide further insight into the VEGF system in hypoxic disease and allow comparison with AD.

Angiogenesis may be active in very early AD although structural abnormalities have been reported in several studies [278-281] and there is no reported increase in microvessel density in AD [78]. Reduction in total VEGFR1 and mbVEGFR1 despite transcriptional upregulation may indicate a physiological adjustment to chronic hypoperfusion but an increase in the proportion of sVEGFR1 isoforms may contribute to impaired angiogenesis in AD.

Chapter 4 VEGFR2

4.1 Introduction

VEGFR2 (KDR, Flk-1) is a major regulator of angiogenesis in health and disease and is the main signal transducer for VEGF [107, 129, 168, 170]. In the adult nervous system VEGFR2 also mediates neurogenesis [267], LTP [211], neuronal survival [268], astrocyte migration [282] and proliferation [283, 284] (1.2.2.2). VEGFR2 level is regulated by VEGF binding [285, 286] and by HIF-2α [287]. VEGFR2 activation can occur by the binding of its canonical ligands VEGF, VEGF-C, VEGF-D and by non-canonical activation via shear stress, gremlins, galectins, lactate and low density lipoproteins (LDLs) [130]. Co-receptors, NRP1 and NRP2 and HSPGs, can also mediate the activation of VEGFR2. Receptor activation is regulated by internalisation and degradation, and the activity of protein tyrosine phosphatases (PTPs) [130, 288]. PTPs are enzymes that remove phosphate groups from phosphorylated tyrosine kinase residues and therefore regulate receptor function via altering the duration and extent of phosphorylation. Several PTPs act on VEGFR2 and there is evidence that some PTPs act on specific VEGFR phosphotyrosines [130, 174].

CBF is reduced in AD more than can be accounted for by a reduction in metabolic demand, and this results in cerebral hypoxia. Few studies have addressed VEGFR2 localisation in the human brain although there have been several published studies considering its distribution in models of brain ischaemia. VEGFR2 has been shown to be present on endothelial cells and neurons [129, 134]; however, there is debate in the literature as to whether the receptor is localised on glial cells.

In human post-mortem studies VEGFR2 has been observed on astrocytes in the developing brain [289, 290]. In contrast, VEGFR2 was not observed on astrocytes in a large cohort, human post-mortem study of white matter lesions [291]. Looking to animal literature for clarification, models of trauma and hypoxia in the nervous system are similarly contradictory. VEGFR2 has been identified on primary rat astrocytes [284], in a subset of GFAP-positive astrocytes in the normal and aged rat brain [292] and on astrocytes in mouse hippocampus [293]. Astrocytes immunopositive for VEGFR2 were reported in rats treated with an endothelin receptor type B receptor agonist [294]. VEGFR2 immunoreactivity was also reported on glial cells and endothelial cells in a rat study of transient and permanent brain ischaemia. However, double immunolabelling to confirm cellular localisation was not carried out [250]. In contrast, VEGFR2 was not identified on astrocytes in the rat brain after direct VEGF infusion [254] or brain trauma [255], nor was it identified on astrocytes in pigs after hypoxia preconditioning or transient ischaemia[253]. There have been conflicting reports of the presence of VEGFR2 on microglia

in animal studies [141, 251, 295]. Human post-mortem studies also provide conflicting evidence as VEGFR2 has previously been reported on activated microglia in a study of white matter lesions in normal aged brains [291] but was not identified in a study of temporal cortex and white matter in control or epilepsy cases [296]. *In vivo* models of acute ischaemia have identified VEGFR2 mRNA in microglia by qPCR [251] but not *in vitro* by examination of mRNA or protein in murine microglia [141]. There have been no studies that have shown that VEGFR2 modulates microglial function, although there is evidence in favour of VEGFR1 as a mediator of microglial migration and proliferation [141]. From the evidence so far, it was not entirely clear whether microglia would express VEGFR2 in the human brain tissue in this study.

Since cerebral hypoperfusion and hypoxia are part of AD pathology, and as VEGF signalling, via VEGFR2, controls vascular sufficiency by angiogenesis, it is important to look not only at the level of VEGF in AD brain but also to correlate this with expression of the receptor. VEGFR2 expression is regulated by VEGF [285, 286] and there is evidence that VEGFR2 is directly upregulated by HIF-2α [287]. VEGFR2 mRNA has been shown to be upregulated by hypoxia in human lung [248] and injured rat brain [254]. VEGFR2 mRNA was shown to be stable or downregulated in human umbilical vein endothelial cells (HUVECs) [297] and in other *in vitro* primary endothelial cell models of hypoxia [298], and no change was seen in VEGFR2 mRNA, measured by northern blot, in mouse brain after exposure to hypoxic conditions for 6 hours [258]. I hypothesised that VEGFR2 would be increased in AD, compared to controls, due to the relative cerebral hypoxia in AD and elevated VEGF level.

Studies of VEGFR2 protein expression in animal models of brain ischemia and *in vitro* models of nervous system hypoxia have yielded conflicting results. In some, VEGFR2 protein has been reported as upregulated in response to hypoxia *in vitro* [299, 300], rat [301], porcine [253] and primate [302] models. In other studies, VEGFR2 was reported unchanged in a mouse model [258] or reduced by 70% in primary endothelial cells exposed to hypoxia [298]. It is hypothesised that VEGFR2 will increase in AD, compared to control, in accordance with a mRNA increase and evidence of VEGFR2 elevation in animal models.

In addition, the level of VEGFR2 activation is also of interest in both AD and VaD. The binding of VEGF results in receptor dimerization and autophosphorylation of the highly active VEGFR2 receptor kinase region [174] to give phosphorylated VEGFR2 (p-VEGFR2). At least 19 phosphorylation sites have been characterised on VEGFR2 [303]. Of the tyrosine residues present in the VEGFR2 intracellular domain, those known to play a major role are Tyr (tyrosine, Y) 951/996 [303], Tyr1054/9 [107] and Tyr1175 [130, 303]. Tyr1054/9 are required for maximum kinase activity [107] and mutation analysis has shown Tyr996 is essential for receptor activation [304, 305]. Mutagenesis of Tyr1175 has the same phenotypic effect as

VEGFR2 knock out and is crucial for PLCγ activation [130]. The level of VEGF induced p-VEGFR2 at Tyr996 and Tyr1175 were reported to be reduced in human coronary artery primary endothelial cells when exposed to hypoxia in correlation with a reduction in VEGFR2 expression [298].

Disruption of VEGFR2 location, level or downstream signalling could contribute to reduced angiogenesis in AD despite elevated VEGF level [78]. The presence of Aβ in AD brain may also have an impact on VEGFR2 bioavailability and signalling. $A\beta_{1-42}$ has been reported to be anti-angiogenic [306, 307] and is able to bind to VEGFR2 and block receptor phosphorylation at Tyr996 *in vitro* [308]. To assess the impact of Aβ on VEGFR1 and VEGFR2 protein, white matter was used as an internal control and VaD used as a disease control in which there is hypoperfusion but Aβ pathology is absent. There have been no studies assessing VEGFR2 localisation in AD and the level of VEGFR2 in post-mortem human brain is yet to be investigated by qPCR or protein measurement.

Results presented in this chapter on the cellular localisation of VEGFR2 and the level of VEGFR2 in human brain tissue were recently published [259].

4.1.1 Hypotheses

[1] VEGFR2 will be located on endothelial cells, astrocytes and neurons. VEGFR2 has been identified on astrocytes in human studies and several animal models,

[2] VEGF directly regulates the transcription of VEGFR2, therefore the level of VEGFR2 mRNA will be increased in the AD parietal cortex compared to control.

[3] Hypoxia directly regulates the transcription of VEGFR1, which can regulate the protein level. Therefore the level of VEGFR2 protein will be increased in AD and VaD parietal cortex and white matter compared to control.

[4] Following that VEGFR2 protein level and VEGF protein level are elevated in the AD and VaD brain. As hypothesised in [3] above, if the level of the VEGFR2 is increased, it is hypothesised that the level of phosphorylation of VEGFR2 will be increased in VaD and AD compared to control.

4.1.2 Aims

[1] To examine the cellular localisation and distribution of VEGFR2 protein in control and AD post-mortem frontal lobe tissue by immunohistochemistry.

[2] To measure the level of VEGFR2 mRNA in parietal cortex from AD compared with brain tissue from controls by qPCR.

[3] To measure the level of VEGFR2 protein level in parietal cortex and white matter from control, AD and VaD by ELISA.

[4] To measure VEGFR2 phosphorylation in control, AD and VaD parietal cortex and white matter by ELISA.

4.2 VEGFR2 localisation

The aim of this work was to examine the localisation of VEGFR2 in human brain. There have been conflicting reports of VEGFR2 localisation on glial cells in the literature and identifying the location of VEGFR2 will help to further understand its role in disease.

4.2.1 Methods

4.2.1.1 Study cohort

Control and AD cases were neuropathologically confirmed as described in 2.2. The neuropathological and demographic features of control and AD cases used for immunostaining are summarised in 3.2.1.1 and details of individual cases can be found in the Appendix 10. FFPE frontal lobe, sectioned prior to the start of this study, was used to investigate VEGFR2 localisation. Frozen parietal cortex from control cases was used to perform western blotting and the cohort used is detailed in 4.3.1.1

4.2.1.2 Western blot

Total protein concentration for tissue homogenates was calculated as described in 2.3. Western blotting was carried out as described in 2.4. Samples were run on 7.5% precast gels. The membrane was blocked with 5% BSA-TBST for 1 hour and incubated overnight at 4°C with anti-VEGFR2 antibody at a concentration of 1:1000 in 3% BSA-TBST. β-Actin was used as a loading control at 1:5000 in 5% milk-TBST. HUVEC lysates express both VEGFR1 and VEGFR2 and were used as a positive control.

4.2.1.3 Immunohistochemistry

Immunohistochemistry was performed as described in 2.9.1. The antibody was titred to determine the optimal concentration and tested with both EDTA and citrate buffer pre-treatment to enhance straining as described in 2.9.3. Sections were pre-treated with citrate buffer prior to immunolabelling with anti-VEGFR2 antibody at 1:200. A no primary control was carried out to account for any non-specific binding of the secondary antibody. Antibody diluent was applied, followed by secondary antibody incubation and detection. An immunoglobulin control was performed to ensure staining was not caused by non-specific interactions of immunoglobulin in the tissue. Sections were incubated with an immunoglobulin of the same isoform, species and concentration as the primary antibody

then secondary antibody incubation and detection was carried out. In this case anti-rabbit IgG was used at a concentration of 260 ng/ml and incubated or 1 hour at RT.

4.2.1.4 Double immunofluorescence and immunohistochemistry

VEGFR2 co-localisation in glial cells was investigated by double immunohistochemistry (2.9.2) and double immunofluorescence (2.10).

Distribution of VEGFR2 was investigated using anti-VEGFR2 antibody at 1:200. Antibodies against GFAP, an astrocyte marker, and HLA-RD, a microglia and macrophage marker, were both used at a concentration of 1:200. Sections were pre-treated with citrate buffer prior to immunolabelling with the first antibody. VEGF receptors were labelled first and visualised with DAB (brown). Glial cells were labelled second and visualised with VIP (purple). AD tissue was used to provide areas of immune cell activation, often not present in control brain tissue.

4.2.2 Results

4.2.2.1 Validation of VEGFR2 antibody specificity

Western blot confirmed the presence of VEGFR2 in human brain homogenate. Bands in human brain homogenate were present at the predicted molecular weight of VEGFR2 (210 and 230 kDa) corresponding to the bands in HUVEC lysate used as a positive control. The 230 kDa band is the glycosylated mature form of the receptor and the 210 kDa band corresponds to the non-glycosylated mature form of the receptor [309, 310]. There was no cross-reactivity with VEGFR1 as no bands were seen at the predicted molecular weight of mbVEGFR1 (180 kDa) or sVEGFR1 (80-130 kDa) in human brain homogenate or in HUVEC lysate.

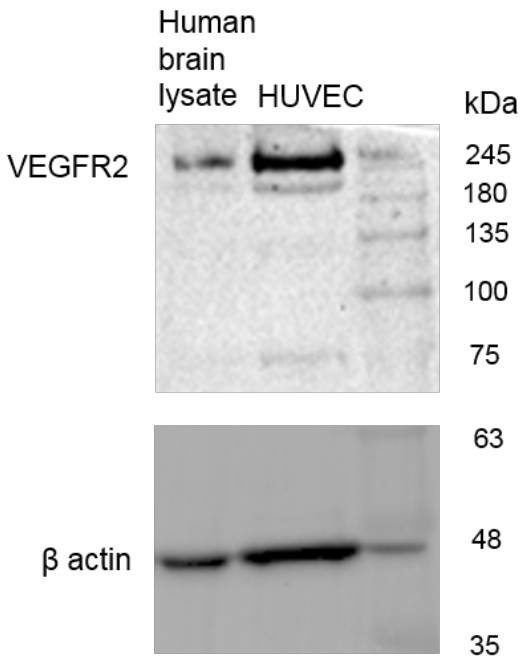

Figure 4-1 Western blot validation of specificity of VEGFR2 antibody in parietal cortex. HUVEC lysate was used as a positive control, as the cells express both VEGFR1 and VEGFR2. Bands in human brain homogenate were labelled at the predicted molecular weight of VEGFR2 (210 kDa and 230 kDa), corresponding to the bands in HUVEC lysate.

4.2.2.2 Localisation of VEGFR2 in control brain and AD brain

Immunohistochemistry was performed to elucidate the cellular localisation of each of VEGFR2 in AD and control cortex. No labelling was observed on negative (no primary antibody) or IgG controls (Figure 4-2).

Macroscopically VEGFR2 appeared uniform in intensity across grey and white matter and no difference was observed between control and AD cases (Figure 4-3). VEGFR2 antibody labelled some but not all neurons in the grey matter (Figure 4-4A, B). VEGFR2 immunopositivity was identified on glial cells in the white matter of both control and AD cases (Figure 4-4C, D). VEGFR2 labelled the endothelium of capillaries and tunica media of arterioles on control and AD cases (Figure 4-4E and F).

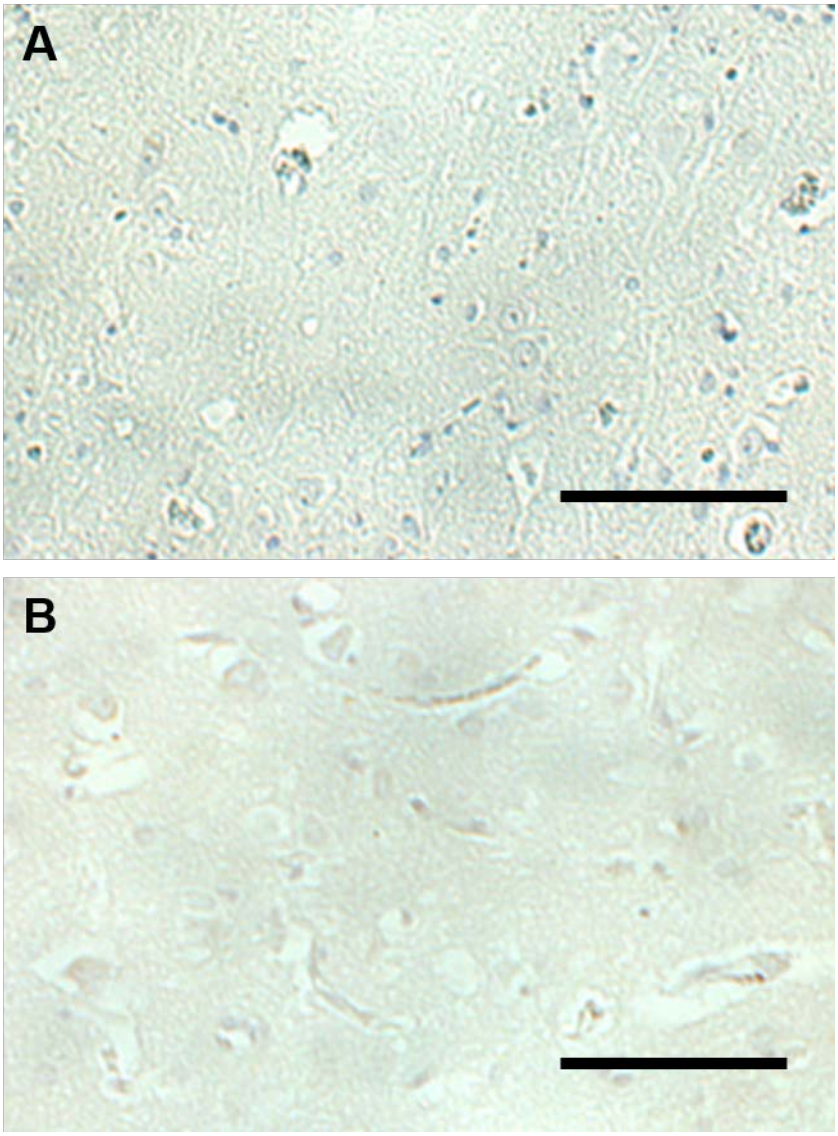

Figure 4-2 Negative controls on human frontal lobe. [A] No-VEGFR2-primary antibody control. [B] IgG control for VEGFR2. Scale bars = 100µm

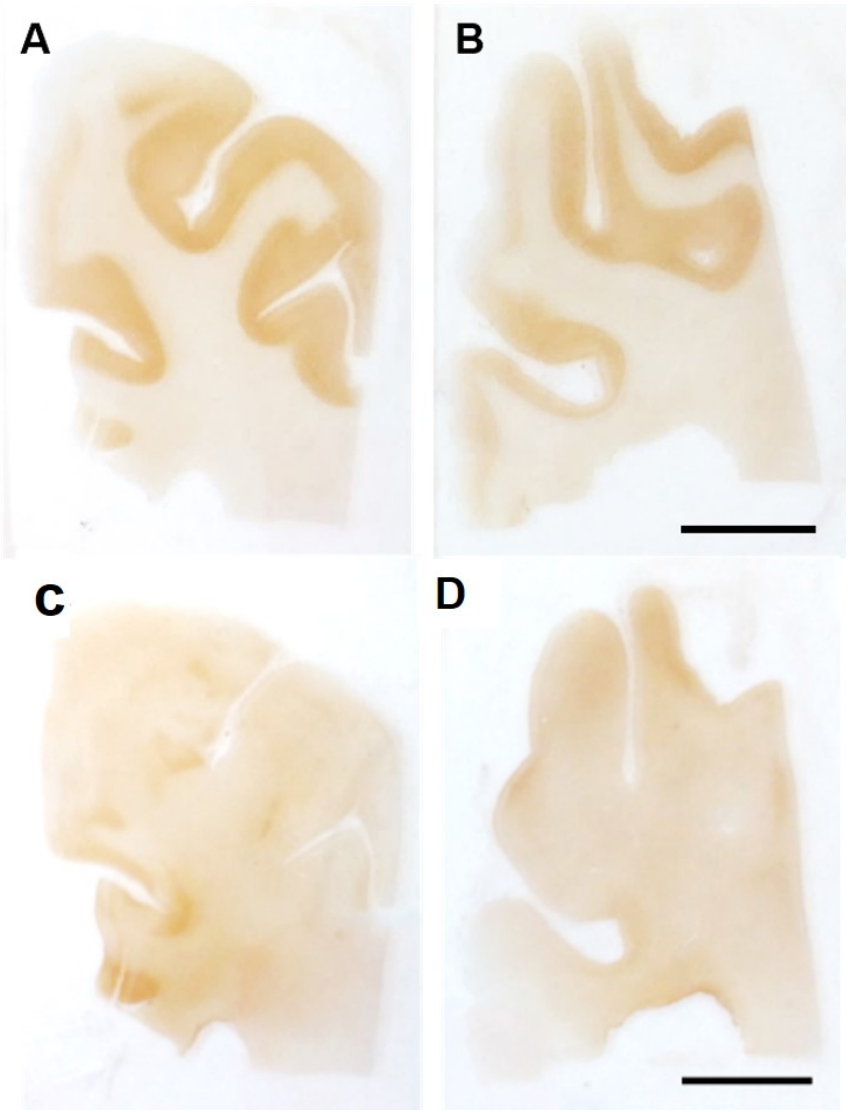

Figure 4-3 VEGFR2 IHC of control and AD frontal lobe. A uniform pattern of labelling was seen across grey and white matter. No difference was observed between control [C] and AD [D]. In [C] there is some artefactual signal but that in general the labelling is weaker and not specific to the cerebral cortex. VEGFR1 IHC of control [A] and AD [B] frontal lobe is shown for comparison. Strong immunopositivity is observed in the cortex compared to the white matter in control and AD. Scale bar = 1 cm

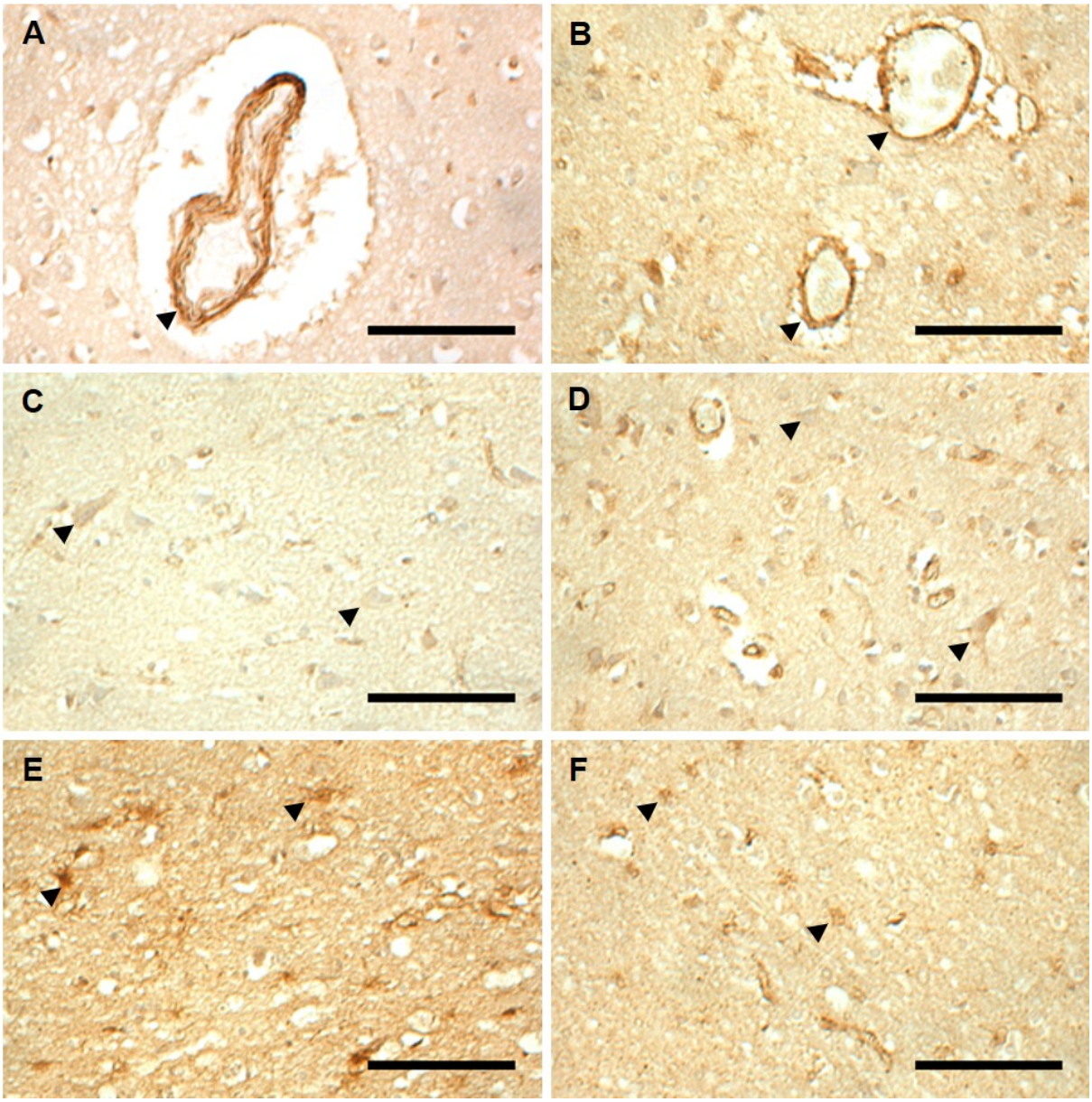

Figure 4-4 VEGFR2 antibody labelling of control and AD frontal lobe. VEGFR2 labelling was seen in the endothelium of capillaries and venules (arrowhead) in control [A] and AD [B]. Approximately 100% the capillaries and arterioles were immunopositively for VEGFR2 in C and AD. VEGFR2 antibody weakly labelled scattered neurons (arrowheads) in the grey matter in control [C] and AD [D]. Approximately 10% of neurones in the cortex could be visualised with VEGFR2 immunopositivity. VEGFR2 immunopositivity was identified on glial cells (arrows) in the white matter of control [E] and AD [F]. Approximately 70% of astrocytes were positively identified by VEGFR2 immunopositivity. Scale bars = 100µm.

4.2.2.3 Glial localisation of VEGFR2 in AD brain

To assess cellular localisation of VEGFR2 on glial cells double immunolabelling was performed. Double immunofluorescence was first attempted. High levels of background fluorescence were observed and persisted despite the adjustment of primary antibody

concentration and the use of pre- and post-treatments to reduce autofluorescence (Appendix 16). Double immunoperoxidase labelling was used as an alternative.

Double-labelling of VEGFR2 (brown) and either GFAP, an astrocyte marker, or HLA-DR, a microglial marker, (purple) in AD and control brains (Figure 4-5). VEGFR2 immunolabelling was present select neuronal cell bodies but not the surrounding neuropil (Figure 4-5A). In endothelial cells, VEGFR2 labelled the cytoplasmic membranes (Figure 4-5A, C) and tunica media of larger blood vessels (Figure 4-5A). VEGFR2 was colocalised with GFAP-positive astrocytes in the white matter and deep cortex (Figure 4-5A, B). VEGFR2 was not detected convincingly within HLA-DR-positive microglia (Figure 4-5C).

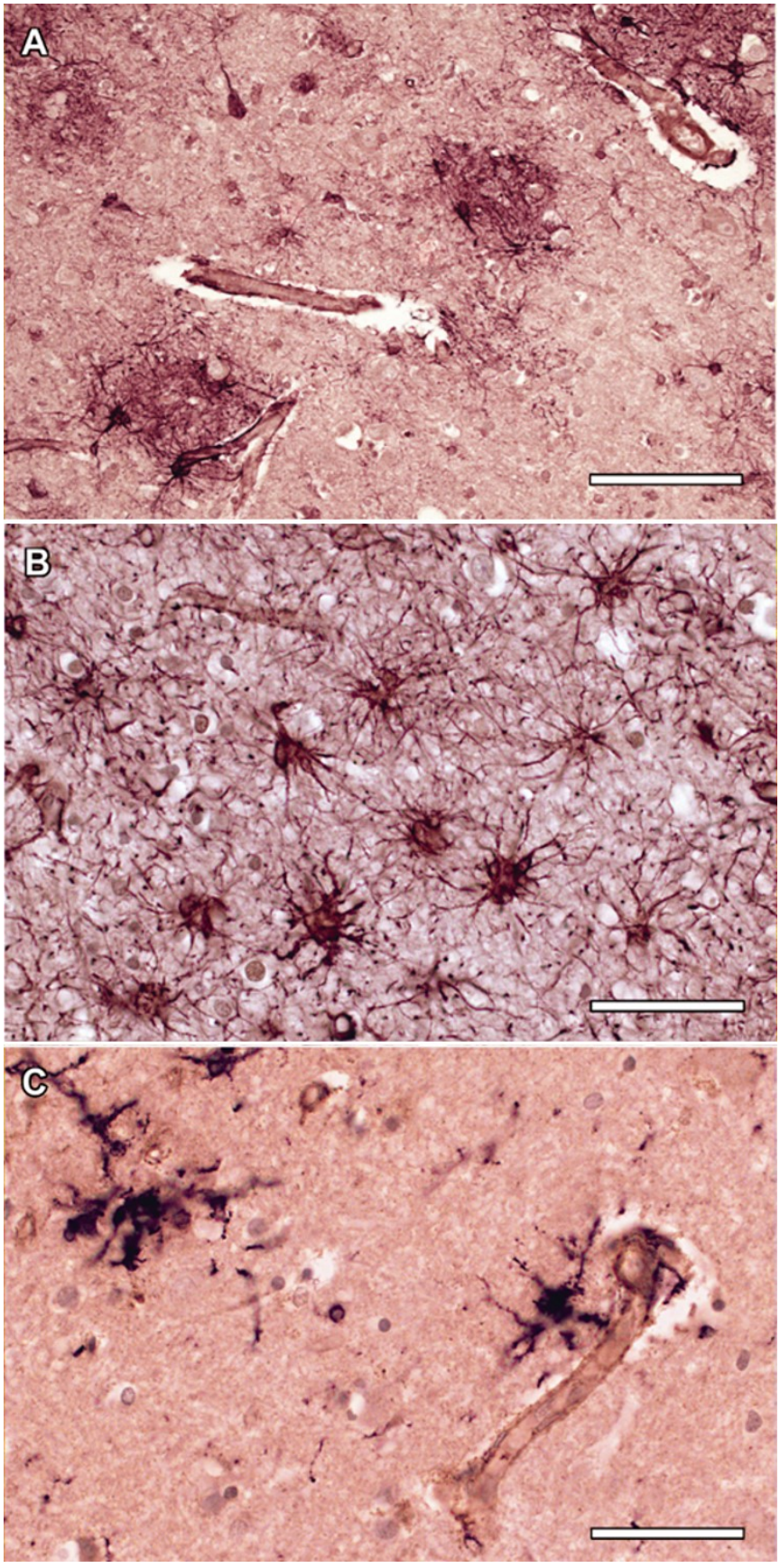
A
B
C

Figure 4-5 Cellular localisation of VEGFR2 in human parietal cortex. [A] Double-labelling of VEGFR2 (brown) and GFAP (purple) reveals VEGFR2 within endothelial cells, the tunica media of larger vessels, in neurons and GFAP-positive astrocytes. Bar = 100 µm. [B] This image shows more clearly the co-localisation of VEGFR2 with GFAP within astrocytes. Bar = 50 µm. [C] Double-labelling of VEGFR2 (brown) and HLA-DR (purple) does not show convincing co-localisation of these antigens within microglia. A capillary shows a membranous pattern of VEGFR2 immunolabelling. Bar = 50 µm

4.3 VEGFR2 mRNA level in control and Alzheimer's disease

The aim of this work was to measure the VEGFR2 mRNA level in the parietal cortex of control and AD.

4.3.1 Methods

4.3.1.1 qPCR study cohort

Fresh frozen parietal cortex from control and AD patients was used to investigate VEGFR2 mRNA expression. Control and disease subjects were age-matched and, where possible, matched for gender. All subjects had a post-mortem delay of less than 90 hours. The neuropathological and demographic features of control and AD cohorts are described in Table 3-3.

4.3.1.2 Selection of primers for VEGFR2

Alternate splicing of the kinase insert domain receptor (KDR) gene can produce membrane bound VEGFR2 and a soluble isoform known as sVEGFR2 (1.2.2.2.1). This study focuses on membrane bound VEGFR2 as the main mediator of VEGF action and the primer set was selected to measure membrane bound VEGFR2 only. The genomic map containing primer location can be found in Appendix 13.

4.3.1.3 Selection of reference genes for relative quantification

In this study VEGFR2 was expressed on neurons, endothelial cells and astrocytes in the control and AD brain (4.2.1.4). *ACTB*, encoding β-actin, was used to normalise for total cell content. *RBFOX3*, encoding NeuN, was used to normalise to the neuronal population and *PECAM1*, encoding platelet endothelial cell adhesion molecule (CD31) was used to normalise to the endothelial cell population. The rationale behind the selection of these reference genes is presented in 3.3.1.3.

To normalise for the expression of VEGFR2 on astrocytes the astrocyte specific reference gene aldehyde dehydrogenase 1 family member L1 (ALDH1L1) was selected. In contrast to the traditional astrocytic marker, *GFAP*, *ALDH1L1* has a wider pattern of astrocytic expression and is not preferentially expressed on reactive astrocytes [311, 312].

4.3.1.4 qPCR

RNA was extracted from fresh frozen parietal cortex as detailed in 2.11.1. cDNA was generated as described in 2.11.4, added to primers and master mix and made up to total volume with RNase free water. Samples were analysed in triplicate with non-template controls on each plate using the protocol detailed in 2.11.5.

4.3.1.5 Statistical analysis

The $2^{-\Delta\Delta Ct}$ method was used to determine the fold difference between VEGFR2 and reference genes (*ACTB*, *RBFOX3*, *PECAM1* and *ALDH1L1*) as described in (2.12). Groups were tested for normality and were found to have a non-normal distribution, as expected with exponential values. The geometric mean was calculated for each group and has been displayed with a 95% confidence interval. Individual sample $2^{-\Delta\Delta Ct}$ values were used to perform the Mann Whitney test for difference in distribution between control and AD groups.

4.3.2 Results

4.3.2.1 Expression of the reference genes in control and AD

Reference genes were validated prior to investigating genes of interest. *ACTB* acted as a reference gene expressed at similar levels in all cell types. The stability of *ACTB* in control and AD brain is displayed in 3.3.2.1. *RBFOX3* is expressed in neuronal cells, *ALDH1L1* is expressed in astrocytes and *PECAM1* in endothelial cells. The fold change in mRNA levels of *RBFOX3*, *PECAM1 and ALDH1L1* was calculated relative to the mean level in control tissue using *ACTB* as the calibrator. There was no significant difference in the fold change of *RBFOX3* between control and AD (~1.12-fold increase, $p = 0.436$) and there was a significant ~1.6-fold increase in *PECAM1* ($p = 0.021$) as reported in 3.3.2.1. There was a ~1.8-fold increase in *ALDH1L1* ($p < 0.0001$) and in AD samples compared to control.

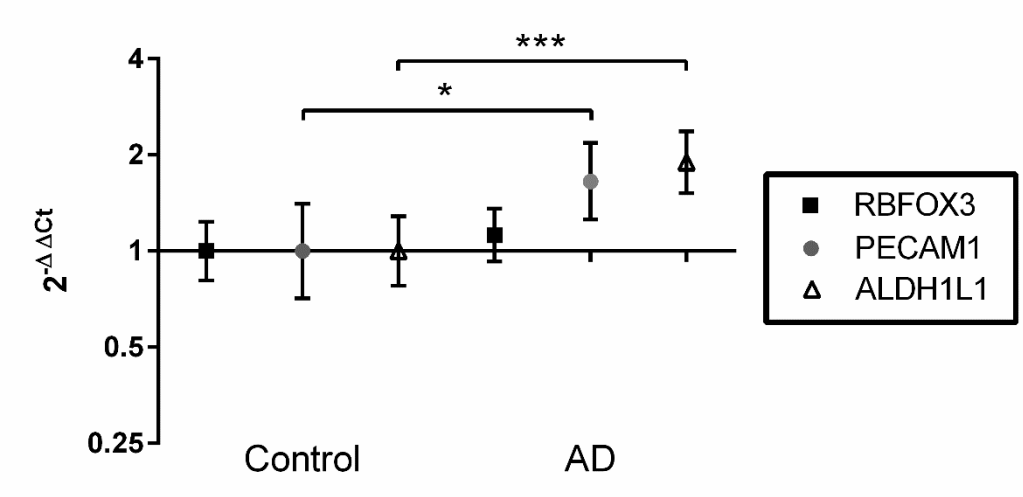

Figure 4-6 RBFOX3, PECAM1 and ALDH1L1 mRNA levels were measured by qPCR in parietal cortex. Fold difference in RBFOX3, PECAM1 and ALDH1L1 mRNA was calculated via the $2^{-\Delta\Delta Ct}$ method using ACTB as a calibrator gene and compared to mean levels in control tissue. There was a significant increase in the fold change of PECAM1 (p = 0.021) and ALDH1L1 (p< 0.0001) in AD samples compared to control. There was no significant difference between the fold change of RBFOX3 between control and AD. The geometric mean and 95% confidence intervals of the $2^{-\Delta\Delta Ct}$ values are shown for each group on a $\log_2$ scale. Horizontal line indicates $2^{-\Delta\Delta Ct}$ fold change of 1 assigned to control samples, increases or decreases from this line in disease subjects indicate corresponding fold changes in gene expression in disease. C: n = 31, AD: n = 47. * p < 0.05 *** p < 0.001

4.3.2.2 VEGFR2 mRNA levels in control and AD brain

VEGFR2 mRNA levels were calibrated against four reference genes displayed in Figure 4-7. Assessment of VEGFR2 mRNA with reference to *ACTB* showed a significant increase in AD compared to control (3.4-fold respectively, p= 0.0002). VEGFR2 mRNA with reference to *RBFOX3* showed in a significant increase in AD compared to controls (~2.9-fold increase, p= 0.0003). VEGFR2 calibrated against *PECAM1* also displayed a significant increase in AD compared to control (~2.1-fold increase, p= 0.008). VEGFR2 mRNA with reference to *ALDH1L1* showed a significant fold-increase in AD compared to controls (~1.8-fold increase, p= 0.019).

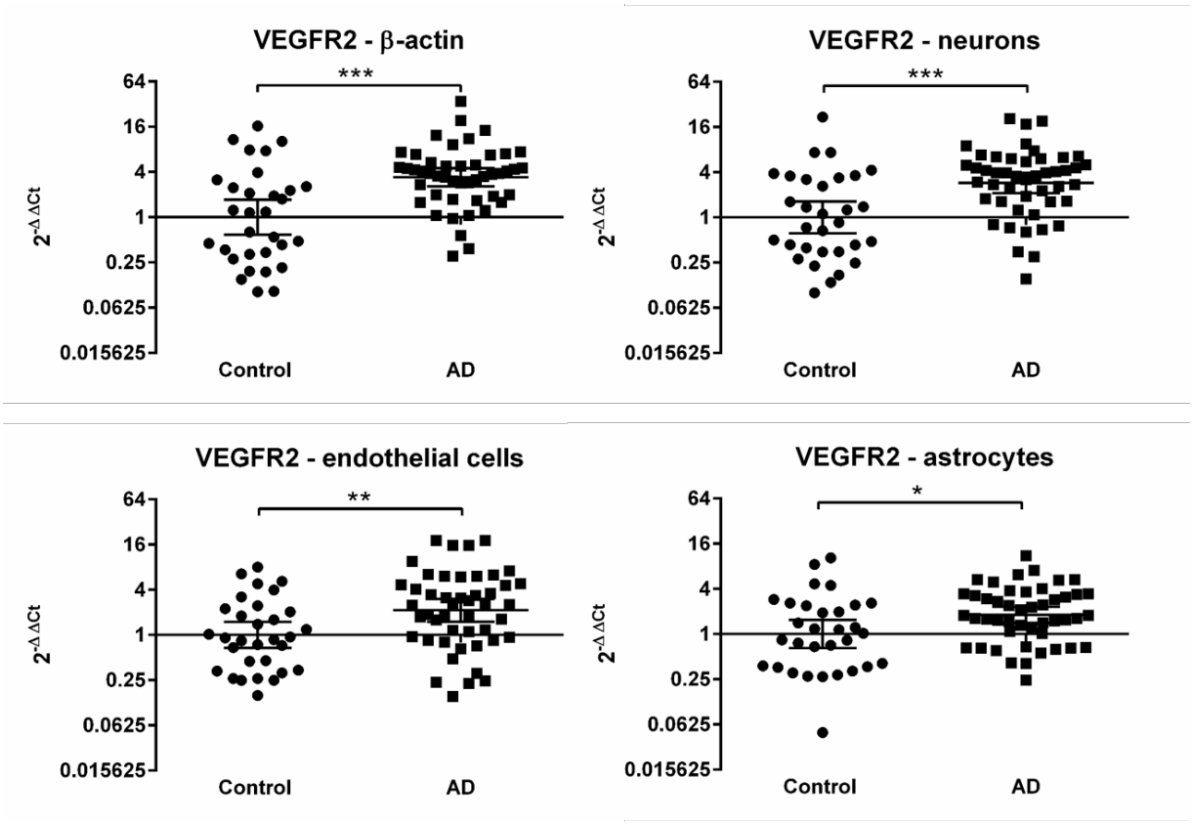

Figure 4-7 VEGFR2 mRNA levels measured by qPCR in homogenates of parietal cortex. The fold difference relative to the mean in control tissue was calculated for each sample by the $2^{-\Delta\Delta Ct}$ method, with *ACTB* (β-actin), *RBFOX3* (neuronal), *ALDH1L1* (astrocytic) and *PECAM1* (endothelial) as calibrators. The geometric mean and 95% confidence intervals of the $2^{-\Delta\Delta Ct}$ values are shown for each group on a $\log_2$ scale. C: n = 32, AD: n = 46. * $p<0.05$ ** $p<0.01$ *** $p < 0.001$

4.4 VEGFR2 protein level in control, Alzheimer's disease and vascular dementia

The aim of this work was to measure total VEGFR2 and p-VEGFR2 protein level in control, AD and VaD parietal lobe.

4.4.1 Methods

4.4.1.1 VEGFR2 protein cohort selection

VEGFR2 level was measured in the parietal cortex and white matter of control, AD and VaD cases. In addition to the parietal cortex, white matter of the same brains was used as an internal control. White matter in the AD brain is hypoperfused but contains little or no Aβ [72]. VaD was used as a disease control. VaD is defined by hypoperfusion but with the absence of the Aβ and tau pathology present in AD (1.1.2). AD and VaD can display mixed pathology, VaD cases in this study were selected to have little or no AD pathology.

Parietal cortex and white matter		Control	AD	VaD
N		36	50	19
Age (years)	Range	58 - 95	57 - 93	67 - 97
	Mean ± SD	80.1 ± 8.7	77.5 ± 8.1	82.9 ± 7.3
Gender	Female	11	26	9
	Male	25	24	10
Post-mortem delay (hours)	Range	3 - 67	4 - 85	20 - 85
	Mean ± SD	32.5 ± 16.3	31.6 ± 19.0	47.6 ± 19.0

Table 4-1 Summary of the neuropathological and demographic features of the control, AD and VaD cohorts used for VEGFR2 protein analysis. Demographic and neuropathological features of individual cases are listed in the Appendix 9.

4.4.1.2 VEGFR2 sandwich enzyme-linked immunosorbent assay

Human total VEGFR2 (KDR) duoset IC ELISA kit was used to measure VEGFR2 protein level in human brain tissue. Frozen brain samples were homogenised as detailed in 2.2.3 using the manufacturers recommended NP-40 based lysis buffer with phosphatase and protease inhibitors (Lysis buffer #9). The assay was carried out according to manufacturer's instructions summarised in 2.6. Readings were blank corrected and a 7-point curve was constructed from VEGFR2 recombinant standards. A 4-parameter logistic curve fit was applied, and sample values were interpolated.

Fifty µl of standard and sample was added to each well. Samples were measured in duplicate on each plate and selected samples were measured on two plates to test interassay reliability. Additional controls were performed to ensure that no other factors were interfering with the accuracy of the assay. Capture antibody was replaced with PBS to test for VEGFR2 binding to the plate. Lysis buffer was used in place of sample to account for the interference of buffer components with measurement. Detection antibody and streptavidin HRP solution were each replaced with IC diluent #14 to account for any non-specific binding. All controls returned the same reading as blank values. The detection antibody was tested for specificity on human brain lysate by western blot and displayed bands at the predicted molecular weight for VEGFR2 (Appendix 17).

4.4.1.2.1 Spike, recovery and linearity testing

The ELISA kit had been validated for use on cell culture supernatant, serum and plasma samples by the supplier. To validate the ELISA kit for use on human brain tissue, homogenates were spiked with recombinant protein, and recovery and linearity testing was performed. 1000 pg/ml of VEGFR2 recombinant protein was added to 'spike' neat brain tissue homogenate and to control diluent (IC diluent 14) to make the control spike. The spiked sample, unspiked homogenate and control spike were mixed thoroughly and serial dilutions performed. Percentage recovery and linearity were calculated as described in

3.4.1.3. Percentage recovery and linearity with recombinant protein added were within the manufacturer's acceptable range of 80-120% (Table 4-2).

	% Recovery		
	Spiked	Unspiked	Control
Neat	87.3	-	-
1:2	96.9	108.6	118.9
1:4	93.6	115.7	113.9

Table 4-2 Percentage recovery and linearity of brain tissue homogenate on VEGFR2 ELISA. Spiked samples were treated with 1000 pg/mL of VEGFR2 recombinant protein and diluted. Unspiked samples contained brain homogenate only. Percentage linearity was within the manufacturer's acceptable range of 80-120%. Control samples contain IC diluent #14 spiked with 1000 pg/mL of VEGFR1 and remained within the accepted range.

4.4.1.2.2 Interassay reliability

The interassay reliability of the VEGFR2 ELISA was tested by measuring the same sample on two different plates. The coefficient of variation (CoV) was used to compare the mean values of the first plate to the second. The CoV was less than 5% for each of the samples tested showing that the assay is reliable (Table 4-3).

MRC Identifier	**VEGFR2 (pg/ml)**		**CoV (%)**
	Plate 1	Plate 2	
BBN_9106	867.2	865.8	3.1
BBN_9112	611	605.2	4.2
BBN_4205	231.7	242.9	4.1
BBN_9354	248.5	255.4	1.9

Table 4-3 VEGFR2 ELISA interassay reliability. Homogenates from the same samples were measured on two different plates. CoV was performed to assess the relative variability of sample readings. CoV: coefficient of variation.

4.4.1.3 p-VEGFR2 sandwich ELISA

To measure the level of VEGFR2 phosphorylation in human brain tissue a p-VEGFR2 ELISA kit was tested. The ELISA was carried out in accordance with manufacturer's instructions and as described in 2.6. The assay was not specific to one phosphorylation site but used a capture antibody specific to VEGFR2 and an anti-phosphor-tyrosine-HRP specific to phosphorylated tyrosine residues. Spike, recovery and linearity testing revealed recovery and linearity were outside the manufacture's accepted range so the assay was not used (Appendix 18).

4.4.1.4 p-VEGFR2 western blot

Samples were run on a 4-20% precast gel. The membrane was blocked with 3% BSA-TBST for 1 hour and incubated overnight at 4°C with anti-p-VEGFR2 (Tyr 996) antibody at a

concentration of 1:200 in 3% BSA-TBST. β-Actin was used as a loading control at 1:5000 in 5% milk-TBST. HUVEC lysates express both VEGFR1 and VEGFR2 and were used as a positive control. Western blots did not show a band at the predicted molecular weight for p-VEGFR2 (150 kDa) in human brain tissue or cell lysate so the antibody was not used (Appendix 19).

4.4.2 Results

4.4.2.1 VEGFR2 protein level in control, AD and VaD cortex

The level of VEGFR2 in the cortex and white matter of control, AD and VaD cases was measured by ELISA. There was no significant difference in the level of VEGFR2 between control, AD and VaD cases in the parietal cortex (Figure 4-8).

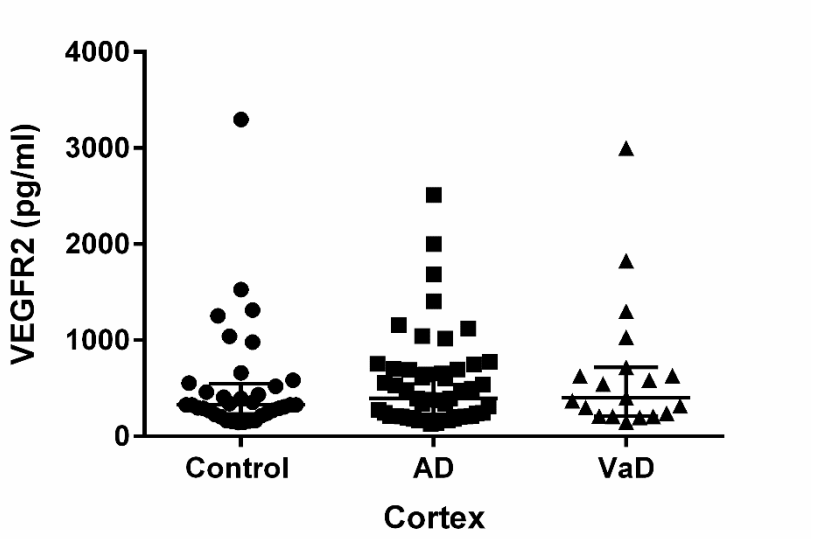

Figure 4-8 VEGFR2 protein levels in parietal cortex measured by sandwich ELISA. No significant difference was observed between control and disease groups. Median ± interquartile range for each group are displayed. C: median = 328.8, interquartile range = 314.1, n= 36, AD: median 394.6, interquartile range: 491.1, n= 48, VaD: median = 400, interquartile range = 506.6, n= 19

4.4.2.2 VEGFR2 protein level in control, AD and VaD white matter

A significant difference in median values was reported between groups (p= 0.037) (Control: Median = 151.7, Interquartile range = 127.4, AD: Median = 174.1, Interquartile range = 113.5, VaD: Median = 131.0, Interquartile range = 102.6) and pairwise analysis revealed a significantly lower value for the VEGFR2 level in VaD compared to AD (p< 0.05, Figure 4-9).

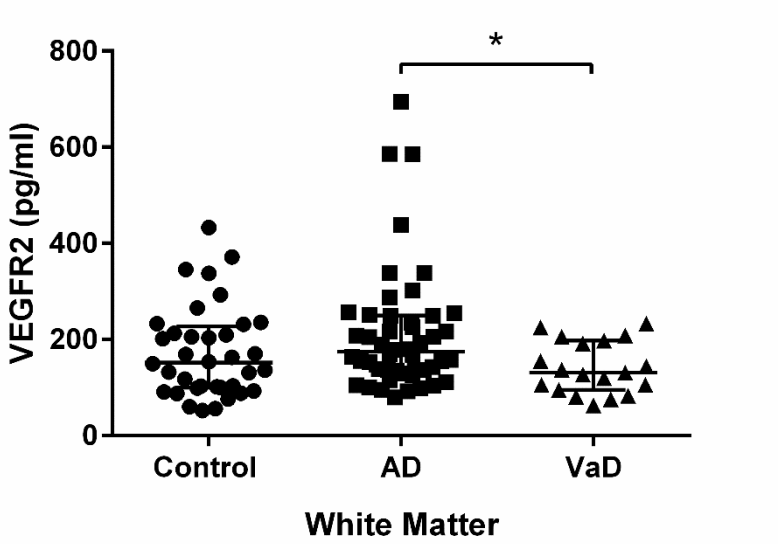

Figure 4-9 VEGFR2 protein levels in parietal white matter measured by sandwich ELISA. No difference was reported in VEGFR2 level between control and disease groups. A significantly lower value was observed for VaD compared with AD (p< 0.05). Median ± interquartile range for each group are displayed. C: median = 151.7, interquartile range: 127.4, n= 36, AD: median: 174.1, interquartile range: 113.5, n= 50, VaD: median 131.0, interquartile range: 102.6, n= 19

4.5 Discussion

The aim of this work was to determine the cellular distribution and level of VEGFR2 mRNA in human post-mortem cerebral cortex in AD and controls. The cohort was expanded to include measurement of VEGFR2 protein level in the cortex and white matter of control, AD and VaD brains.

The cellular localisation of VEGFR2 is clearly critical to its function in the brain but the literature includes conflicting accounts of VEGFR2 location, particularly on glia. The first aim of this study was to investigate this by visualisation of VEGFR2 by IHC in control and AD brain. VEGFR2 was not detectable on all neurons, an observation that has been noted in the literature [313]. This labelling of some but not other neurons suggests possible neuronal subtype specificity, or the influence of localised microenvironmental factors. For example, VEGFR2 was identified on pyramidal neurons by Boer et al (2008) [296] and VEGFR2-positive neurons were increased in acute hypoxic conditions compared to control [302]. VEGFR2 localisation correlates with VEGF expression in the human brain [72, 212] and supports the role

of VEGFR2 as the mediator of VEGF in neurogenesis, neuronal migration and synaptic plasticity [121, 210, 211, 245, 267, 268, 293].

In this study VEGFR2 was identified on astrocytes in control and AD brain. VEGFR2 was not identified on astrocytes in control subjects in a study on post mortem spinal cord, and was identified on GFAP-positive-astrocytes in only 2 out of 15 cases of ALS [313]. This raises the possibility that the activation state of astrocytes may affect their expression of VEGFR2. No VEGFR2 immunopositivity was identified on microglia in control or AD brains in this study. This supports work by Boer et al [296] and provides further evidence that VEGFR1 rather than VEGFR2 is the main mediator of VEGF action on microglia.

Following the completion of this work, a study of VEGFR2 immunohistochemical labelling was published, using the same anti-VEGFR2 antibody as used here, in human brain [171]. The group looked at sections from the caudate and putamen of controls, those with a range of SVD severity, and CADASIL patients with a genetically determined form of SVD (1.1.2.1). The group identified sparse labelling of neurons in agreement with results reported here. VEGFR2 labelling was found on some but not all capillaries, and in vascular smooth muscle cells. In agreement with the results presented here, the group reported labelling of a subset of astrocytes and no labelling of microglia [171].

The second aim of the present study was to measure the level of VEGFR2 mRNA in control and AD by qPCR. There was a significant increase in VEGFR2 mRNA in relation to β-actin mRNA in AD compared to control brains. To ensure that this was not simply due to an increase in the proportion of astrocytes or other VEGFR2-expressing cells within the tissue, I also assessed VEGFR2 mRNA level in relation to that of astrocyte-, endothelium- and neuron-specific mRNAs. This revealed an increase in VEGFR2 mRNA in relation to all of these cell type-specific mRNAs, indicating that the upregulation of VEGFR2 mRNA that I detected in AD is not an artefact of altered cellular composition of the tissue. It may be relevant that there is also significant upregulation of neuronal VEGFR2 mRNA in animal models of CNS trauma [256], in which, as in AD, there is also upregulation of VEGF, reactive astrocytosis and, at least temporarily, a potential disparity between metabolic demand and cerebral oxygenation. VEGFR2 was measured by qPCR *in vitro* and *in vivo* in mice and found to increase with hypoxia [283].

Measuring mRNA levels is a useful indicator of VEGFR2 expression but proteins are also subject to translational and post-translational modification. The third aim of this study was to measure VEGFR2 total protein level in the same samples of parietal cortex, as well as white matter from the same AD cases, and cortex and white matter from the parietal lobe of VaD cases.

The level of VEGFR2 protein was not changed in AD or VaD compared to control cortex or white matter. In the white matter however, there was a 25% lower level of VEGFR2 in VaD than AD. I had expected that VEGFR2 would be increased in AD, in keeping with mRNA results, due to the relative hypoxia and associated increase in VEGF. Studies of VEGFR2 expression in animal models of brain ischaemia and *in vitro* models of nervous system hypoxia have yielded conflicting results. An *in vitro* study by Waltenberger et al. (1996) on two endothelial cell types found that exposure to hypoxia initially upregulated VEGFR2 protein, reaching a peak at 24 hours, but VEGFR2 expression then declined, becoming undetectable after 48 hours [297]. In the same study, VEGFR2 mRNA level remained stable during hypoxic conditions. This indicates post-translational regulation of VEGFR2 in hypoxic conditions and suggests a possible explanation for the disparity between expression of the mRNA and protein in the present study.

As expected, the level of VEGFR2 was lower in white matter than in cortex in control, AD and VaD brains. A reduction in VEGFR2 level in VaD in comparison to AD could be secondary to more pronounced hypoxic damage to astrocytes and/or endothelial cells in the white matter in VaD than in AD [102, 105] but further studies are needed to clarify the specific mechanisms underlying the differences.

The fourth aim of this work was to measure the level of p-VEGFR2 in human brain tissue, but an effective method of measurement could not be optimised. The report of $A\beta_{1-42}$ acting directly on VEGFR2 to block receptor phosphorylation at Tyr996 [308] suggested that the presence of Aβ could have a direct effect on angiogenesis in AD. Future work to elucidate phosphorylation levels in human tissue would provide insight into receptor activation and the possible impact of Aβ on VEGFR2 function.

The lack of difference in VEGFR2 level between control and AD brains is in keeping with the absence of any increase in microvessel density in AD, as previously reported [78]. There was no difference in receptor localisation was between control and disease. Elevated VEGF [72, 78, 198, 212, 314] seems unable to increase microvessel density in AD despite normal VEGFR2 level, suggesting that VEGFR2 signalling is defective in AD. Disruption of VEGFR2 ligand binding or alteration in downstream signalling could be responsible. Further work is needed to elucidate the underlying mechanisms.

Chapter 5 VEGFR1 and VEGFR2 correlations with blood vessel density, hypoperfusion and Aβ

5.1 Introduction

The observation that prompted this work is that CBF is reduced in AD and associated with elevation of VEGF but without a corresponding increase in microvessel density. The aim was to investigate whether abnormalities in the VEGF-VEGFR system might be responsible for disrupted angiogenesis in AD. As part of this investigation, the levels of VEGFR1 and VEGFR2 were measured in the parietal lobe. This chapter covers further studies aimed at understanding the relevance of the differences observed in VEGFR1 and VEGFR2 between control and dementia brains, and describes the analysis of the relationship between these receptors and markers of cerebral hypoperfusion and AD pathology in controls, AD and VaD.

vWF has previously been used as a surrogate measure of microvessel density in human post-mortem samples [72, 315, 316]. Previously, this marker of microvessel density has been shown not to be changed in AD despite the increased VEGF [78]. VEGF is a key regulator of angiogenesis and the main ligand for VEGFR1 and VEGFR2. Measurement of VEGF and vWF should provide information about responsiveness to angiogenic stimulation in the parietal lobe. I hypothesised that in AD there would be a negative relationship between VEGF and VWF as a consequence of abnormal expression of VEGFR1 and VEGFR2. I have also assessed whether the expression of VEGFR1 and VEGFR2 is altered by cerebrovascular pathology in AD and VaD.

Cerebrovascular abnormalities are the defining pathological hallmarks of VaD and are observed in 90% of AD cases. The underlying pathologies include cerebral amyloid angiopathy (CAA) and small vessel disease (SVD). CAA is the deposition of Aβ in the cerebral blood vessels (1.1.1.1.3). CAA is present in up to 98% AD cases [317, 318] and can contribute to hypoperfusion and ischaemia in AD [230, 314, 319].

CAA severity in the brain was measured [231] and compared with the levels of soluble and insoluble $A\beta_{1\text{-}40}$, measured previously in the parietal cortex and white matter of the same cases. This allows the investigation of the relationship between VEGFR1 and VEGFR2 levels with CAA scores and $A\beta_{1\text{-}40}$. In contrast to the cerebral cortex, in which $A\beta_{1\text{-}42}$ is deposited, $A\beta_{1\text{-}40}$ makes up the most of Aβ deposited in blood vessels. $A\beta_{1\text{-}40}$ is more soluble than $A\beta_{1\text{-}42}$ and when it is secreted from cells it travels via perivascular drainage and can become deposited in blood vessel walls [320, 321]. CAA severity in the brain had previously been assessed using a semi-quantitative scale [231] and the levels of soluble and insoluble

$A\beta_{1\text{-}40}$ had been measured in the parietal cortex and white matter. This facilitated the investigation of the relationship between VEGFR1 and VEGFR2 levels with CAA scores and $A\beta_{1\text{-}40.}$ SVD encompasses degenerative changes in the vessel wall of small arteries and arterioles, including arteriolosclerosis [65] (1.1.2.2). SVD has been correlated with reduced CBF [322, 323] and increasing SVD severity correlated with biochemical evidence of reduced white matter perfusion, in a post-mortem study [314]. Increasing SVD severity has also been linked to a decline in cognitive function [324-326]. SVD severity had been measured on a semi-quantitative scale [230, 231] allowing receptor levels to be related to pathology. Both CAA and SVD are prevalent in AD and can disrupt endothelial cell function so I hypothesised that with increasing severity of SVD and/or CAA, endothelial VEGF receptor levels would decrease [327-329].

Aβ may also have a direct effect on the VEGF-VEGFR2 system in AD. Aβ has been found to impair capillary formation in human brain endothelial cells in culture [306] and in a transgenic mouse model of CAA [306]. There is also evidence that Aβ inhibits angiogenesis by blocking VEGF-induced mitogenesis via the Akt1 pathway [308, 330], and $A\beta_{1\text{-}42}$ has been implicated as an antagonist of VEGFR2 [307, 308]. The group also showed a peptide fragment common to both $A\beta_{1\text{-}40}$ and $A\beta_{1\text{-}42}$ able to exhibit the same anti-angiogenic effects [308]. There have been no studies into the effect of Aβ on VEGFR1 level. Soluble and insoluble levels of $A\beta_{1\text{-}40}$ and $A\beta_{1\text{-}42}$ had previously been measured in the parietal cortex and white matter in my cohorts. This provided the opportunity to investigate the effect of Aβ concentration on the levels of VEGFR1 and VEGFR2. Understanding the relationship between VEGFR1 and VEGFR2 with Aβ species could provide insight into the effect Aβ pathology might have on blood vessel formation in AD, though there has been little work in this area, the effect of Aβ, if any, on receptor is difficult to predict.

5.1.1 Hypotheses

[1] The level of VEGF will be elevated in AD and VaD compared to control in cortex and white matter.

[2] The level of vWF will be elevated in VaD and remain unchanged in AD compared to control in cortex and white matter.

[3] VWF will not correlate positively in AD but are correlated in control and VaD. vWF will not correlate positively with VEGF in AD, but will correlate in control and VaD. Since VEGFR1 protein was shown to be decreased in AD compared to control (Chapter 3) and VEGF level has been shown to be elevated in AD compared control, therefore it is hypothesised that VEGFR1 will negatively correlate with VEGF in parietal cortex. VEGFR2 protein level was

unchanged in AD and VaD compared to control (Chapter 4). Therefore it is hypothesised that VEGFR2 will display no correlation with VEGF in control, AD and VaD.

[4] As a result of deteriorating blood vessel structure and endothelial cells, it is hypothesised that VEGFR1 and VEGFR2 decrease with increasing CAA and SVD severity.

[5] VEGFR1 protein was shown to be decreased in AD compared to control (Chapter 3), it is hypothesised that VEGFR1 level will decrease with increasing Braak score. VEGFR2 protein level was unchanged in AD and VaD compared to control (Chapter 4), it is hypothesised that VEGFR2 will decrease with increasing Braak scores.

5.1.2 Aims

[1] To determine the level of VEGF in control, AD and VaD parietal white matter by ELISA.

[2] To determine the level of VWF in control, AD and VaD parietal cortex and white matter by ELISA.

[3] To assess the relationship between VEGF, VEGF receptor levels and vWF.

[4] To determine whether VEGFR1 and VEGFR2 levels are related to with CAA and SVD scores.

[5] To examine the relationship of VEGFR1 and VEGFR2 levels to Braak stage and the levels of $A\beta_{1\text{-}40}$, $A\beta_{1\text{-}42}$ and $A\beta_{42:40}$ in the parietal cortex.

5.2 Methods

5.2.1 VEGFR1 dot blot

The method and results of VEGFR1 dot blot to measure protein level in control and AD cortex is detailed in Chapter 3.

5.2.2 VEGFR2 ELISA

The method and results of VEGFR2 ELISA to measure protein levels in control, AD and VaD cortex and white matter is detailed in Chapter 4.

5.2.3 VEGF sandwich ELISA

VEGF levels were measured by the VEGF duoset ELISA kit specific for $VEGF_{121}$ and $VEGF_{165}$. This kit has previously been optimised for brain tissue [78]. Frozen brain samples were homogenised as detailed in 2.2.3 using an SDS lysis buffer. The assay was carried out according to manufacturer's instructions summarised in 2.6. Readings were blank corrected and a 7-point curve was constructed using VEGF recombinant standards. A 4-parameter logistic curve fit was applied and sample values interpolated. 50 µl each of standard and

sample were added to each well. Samples were measured in duplicate on each plate. Spike and recovery testing was not performed as this assay has been validated on human tissue.

The VEGF level had previously been measured in control and AD cortex from the parietal cortex by the Dementia Research Group, University of Bristol, UK. VEGF levels were measured in VaD cases and white matter of control and AD cases in this study. VEGF measurement in parietal cortex could not be repeated on the same samples as there was not enough remaining dissected tissue for homogenisation.

5.2.4 Von Willebrand factor dot blot

VWF is a multimeric glycoprotein and endothelial cell marker [331]. VWF, measured by dot blot, has previously been established as an accurate measure of vessel density in human brain [68, 72, 315].

Dot blotting was carried out as described in 2.5. Briefly, samples were spun at 16,200 g for 10 minutes. Samples were kept at 4°C to reduce interference of sample matrix with the assay. Serial dilutions of homogenate standard were prepared using a 1:100 starting dilution in TBS. Homogenate samples were diluted at a concentration of 1:1000 in TBS. The nitrocellulose membrane was blocked with 5% milk/TBS-T; anti-human-vWF antibody, at a concentration of 1:3000 in 5% milk/TBS-T, was applied overnight at 4˚C. After washing, a peroxidase conjugated rabbit secondary antibody was applied for 1 hour. The background-adjusted volume was calculated for each dot and a 7-point standard curve was created for each blot. Relative values for each sample were calculated by interpolating from the standard curve. The coefficient of variation (CoV) between samples on each blot was calculated to assess intra-assay reliability. Each sample was measured on two membranes and inter-assay reliability also assessed by calculation of the CoV.

5.2.5 Von Willebrand factor sandwich ELISA

VWF level was determined using human vWF ELISA kit () according to the manufacturer's guidelines. The ELISA was validated using spike, recovery and linearity testing as described in 3.4.1.3. The ELISA used a vWF antibody as a capture antibody and a biotinylated vWF detection antibody. Briefly, samples were diluted 1:10 with supplied sample diluent and 50 µl of samples were added in duplicate and incubated for 2 h at room temperature. Absorbance was measured at 450 nm and vWF concentration was interpolated from a standard curve generated by serial dilution of human recombinant vWF (2.5–80 mU/ml).

5.2.5.1 Spike, recovery and linearity testing

The vWF ELISA kit had been validated for use on cell culture supernatant, serum and plasma samples by the supplier. To validate the ELISA kit for use on human brain tissue,

homogenates were spiked with recombinant protein, and recovery and linearity testing was performed. 16 mU/ml of vWF recombinant protein was used to 'spike' brain tissue homogenate (diluted 1:10) to make the spiked sample, and added to control diluent (PBS) to make the control spike. Recovery and linearity values were within the acceptable range of 80-120% shown in Table 5-1.

	% Recovery		
	Spiked	Unspiked	Control
1:10	98.2	-	-
1:20	116.3	120.4	111.4

Table 5-1 Percentage recovery and linearity of brain tissue homogenate on vWF ELISA. Spiked samples were treated with 16 mU/ml of vWF recombinant protein and diluted. Unspiked samples contained brain homogenate only. Percentage recovery and linearity of brain homogenates were within the manufacturer's acceptable range of 80-120%. Control samples contained PBS diluent spiked with 16 mU/ml of vWF and remained within the accepted range.

5.2.5.2 Interassay reliability

The interassay reliability of the vWF ELISA was tested by measuring the same sample on two different plates. The CoV was used to compare the mean values of the first plate to the second. The CoV was less than 10% for each of the samples tested showing the assay is reliable.

MRC Identifier	**VWF (mU/ml)**		**CoV (%)**
	Plate 1	Plate 2	
BBN_9026	15.0	17.1	9.3
BBN_9162	12.3	11.3	6.0
BBN_9173	15.5	17.6	9.0
BBN_9275	57.4	53.1	5.5

Table 5-2 VWF ELISA interassay reliability. Homogenates from the same samples were measured on two different plates. CoV was performed to assess the relative variability of sample readings. The CoV was less than 10% for each of the samples tested. CoV: coefficient of variation.

5.2.6 MAG:PLP ratio as a measure of cerebral hypoperfusion

Oligodendrocytes are specialist glia that provide the myelin sheath that surrounds the axons of neurons in the central nervous system. The myelin sheath acts to insulate the axon and allow increases speed of action potential transmission from the neuronal cell body, down the axon to the synapse. Loss or damage of myelin can disrupt transmission of the action potential. Our group has previously shown the ratio of myelin-associated glycoprotein (MAG) and myelin proteolipid protein (PLP) to be a biochemical measure of cerebral hypoperfusion [72, 78, 314]. MAG is located predominantly in the periaxonal membrane of CNS myelin

internodes in the myelin sheath [332, 333] making it more vulnerable to injury than PLP which is expressed at higher levels due to its distribution throughout the myelin sheath [334]: the periaxonal membrane is furthest from the oligodendrocyte cell body and therefore it requires more energy to transport MAG for insertions into the sheath in comparison to other proteins, such as PLP, inserted at shorter distances from the cell body [335]. It is probably this that makes MAG more susceptible to reduction in energy supply. The disproportionate reduction in MAG has been reported in stroke and ischaemic-type plaques in multiple sclerosis [336, 337]. MAG loss in white matter lesions is associated with nuclear expression of HIF-1α [336] a marker of reduced oxygenation (1.2.3). MAG loss has also been previously described in AD and VaD [314, 338]. MAG level was found to decrease in AD and VaD whereas PLP expression remained stable. Additionally, an increased MAG:PLP ratio declined with increasing CAA and SVD severity [314].

5.2.6.1 MAG direct ELISA

A MAG ELISA was developed and previously validated by the Dementia Research Group, University of Bristol, UK and used to establish MAG level in human brain samples [314]. Frozen brain samples were homogenised using an SDS lysis buffer. Briefly, samples were spun at 16,200 g for 10 minutes at 4°C to reduce interference of sample matrix with the assay and were diluted 1:10 in PBS. Recombinant MAG was used to create a 7-point standard curve (400, 200, 100, 50, 25, 12.5 and 6.25 ng/mL). 50 µl of standard and sample were added to each well of a clear 96 well plate and incubated for two hours. The plate was washed 5 times with 0.05% PBS-T and tapped dry after the final wash. Each well was incubated with 100 µl of mouse-anti-human MAG antibody for 2 hours. The plate was washed as previously described, and incubated with 100 µl of biotinylated anti-mouse antibody 1:500 in PBS, for 20 minutes and protected from light. After further washing, 100 µl of HRP-labelled streptavidin diluted 1:500 in PBS was loaded to each well and incubated for another 20 minutes and protected from light. A final wash stage was performed and each well was incubated with 100 µl substrate in the absence of light to visualise the captured antigen. The reaction was stopped using 50 µl of 2N sulphuric acid and the optical density was measured using a plate reader at 450 nm. Readings were blank corrected and a 7-point curve was constructed using MAG recombinant standards. Sample values were determined by interpolated. Samples were measured in duplicate on each plate and corrected for the total protein concentration of each sample.

5.2.7 Aβ measurement

The following data on Aβ concentration was previously collected by members of the Dementia Research Group, University of Bristol, UK. All protein data were adjusted for total protein concentration. Soluble and insoluble homogenates were prepared from frozen tissue

from the parietal cortex and white matter were prepared as described in [72, 79, 339]. 200 mg of tissue was homogenised in 1 ml of TBS extraction buffer for 30 seconds in a homogeniser. Homogenates were spun at 20,817g for 15 minutes at 4°C and the supernatant (soluble fraction, containing soluble Aβ) was stored at -80°C until used. The pellet was homogenised in 6.25 M guanidine HCL in 50 mM Tris (pH 8.0), incubated for 4 hours at 25°C and spun at 20,817g for 20 minutes at 4°C. The supernatant was saved as the guanidine-HCL-soluble fraction (containing insoluble Aβ) and stored at -80°C until use.

5.2.7.1 $A\beta_{1-40}$ levels

A 96-well clear plate was coated with a mouse monoclonal anti-human $A\beta_{1-16}$ (Covance) at a concentration of 2 µg/ml in PBS and incubated overnight at room temperature. The plate was washed and non-specific binding blocked with 300 µl protein-free PBS blocking buffer (Thermo scientific) for 2 hours, followed by further washing. The test samples were diluted (1:49 for guanidine extracts and 1:3 for soluble extracts) in PBS containing 1% 1,10-phenanthroline and added, in duplicate, to the plate along with duplicates of the human $A\beta_{1-40}$ recombinant standards, for 2 hours. The plates were again washed and incubated with the detection mouse monoclonal anti-human $A\beta_{1-40}$ antibody (Covance) at a concentration of 1 µg/ml, which had been biotinylated using the biotin conjugation kit (Lightning-Link Innova Bioscience) and left to incubate for 2 hours, before being washed off. A streptavidin-peroxidase antibody diluted 1:200 in 0.05% Tween-20/PBS was applied for 1 hour at room temperature. The plate was washed and the substrate was added in the absence of light to visualise the amount of antigen captured. The luminescence was measured using the plate reader at 450 nm and $A\beta_{1-40}$ levels were interpolated from a standard curve generated from serial dilutions of recombinant human $A\beta_{1-40}$. Each measurement was repeated on two separate occasions and the average calculated.

5.2.7.2 $A\beta_{1-42}$ level

A 96-well clear plate was coated with a mouse monoclonal anti-human $A\beta_{1-16}$ at a concentration of 2 µg/ml in PBS and incubated overnight at room temperature. The plate was washed and non-specific binding blocked with 300 µl protein-free PBS blocking buffer (Thermo scientific) for 3 hours, followed by further washing. The test samples diluted (1:49 for guanidine extracts and 1:3 for soluble extracts) in PBS containing 1% 1,10-phenanthroline were added, in duplicate, to the plate along with duplicates of the human $A\beta_{1-42}$ recombinant standards for 5 hours. The plates were again washed and incubated with the detection mouse monoclonal anti-human $A\beta_{1-42}$ antibody (Covance) at a concentration of 1 µg/ml, which had been biotinylated using the biotin conjugation kit and left to incubate for 2 hours, before being washed off. This was followed by a streptavidin-peroxidase antibody (diluted 1:200) in 0.05% Tween-20/PBS, which was applied for 30 minutes at room

temperature. The plate was washed and the substrate was added in the absence of light to visualise the amount of antigen captured. Sample luminescence was measured using the plate reader at 450 nm and levels of $A\beta_{1-42}$ were interpolated from a standard curve generated from serial dilutions of recombinant human $A\beta_{1-42}$. Each measurement was repeated on two separate occasions and the average calculated.

5.2.8 Neuropathology

For each case in the cohort the Braak stage was established. In addition, parietal cortex and white matter were scored for CAA severity and SVD severity by a neuropathologist as detailed in Chapter 2.

5.2.8.1 Braak stage

Braak stage was semi-quantitatively assessed in the mid-parietal lobe and 4 other cortical areas as part of the routine neuropathological assessment as described in 2.2.1. Braak stage is determine by the localisation of NFT in the brain: Stages I and II: NFT in transentorhinal region of the brain; Stages III and IV = NFT present in limbic regions; Stages V and VI: NFT in the neocortex.

5.2.8.2 CAA scoring

CAA was semi-quantitatively assessed in the parenchymal and meningeal vessels in five cerebral regions, including the parietal cortex. CAA severity was rated on the following scale: 0 = none; 1 = sparse or mild; 2 = moderate; 3 = frequent or severe [231]. CAA score was provided for the parietal cortex and white matter of control, AD and VaD cases.

5.2.8.3 SVD scoring

SVD was semi-quantitatively assessed in the parenchymal and meningeal vessels in four cerebral regions, including the parietal lobe. SVD severity was rated on the following scale: 0 = normal vessel wall thickness, 1 = slightly increased thickness, 2 = moderately increased thickness, 3 = markedly increased thickness such that for many arterioles the diameter of the lumen was <50% of the outer diameter of the blood vessel [230, 231]. CAA score was provided for the parietal cortex and white matter of control, AD and VaD cases.

5.2.9 Statistics

Data sets were tested for normality and returned non-normal distributions as is common in for human data. Spearman's rank correlation coefficient was used to assess correlation between two variables. The Mann-Whitney test was used to establish the difference between two groups. The Kruskal-Wallis test was used to establish the difference between three or more groups. If the Kruskal-Wallis test reported a significant difference in median values, the Dunn's post-hoc test was used to assess pairwise significance between all groups. Median

(M) and interquartile range (IQR) are displayed as horizontal bars in the scatterplots. Spearman r and *p* values are displayed on scatter plots.

5.3 Results

5.3.1 Von Willebrand factor levels in human parietal cortex and white matter

VWF has previously been assessed by dot blot [72, 315, 316]. Samples were assessed fo intra and interassay reliability. Dot blots for vWF were not found to be reproducible as assessed by interassay reliability (Appendix 20). This was attributed to the use of a NP-40 based lysis buffer as opposed to an SDS buffer with which the assay was previously optimised [68, 72, 315]. As a result, and in order to make use of samples already homogenised in NP-40, a sandwich ELISA kit was used to determine the concentration of vWF. Spike, recover and linearity testing was performed and confirmed the suitability of the assay for use with human brain tissue.

To ensure that changes in receptor level were not due to a reduction in blood vessel density in AD or VaD, vWF was measured in both the parietal cortex and white matter homogenates from each individual. In the cortex there was a significant difference between the groups ($p = 0.007$) and pairwise analysis reported a significant reduction in VaD compared to AD ($p < 0.01$, Figure 5-1A). There was no difference in vWF level between any of the groups in the white matter (Figure 5-1B). There was no significant difference in VWF between Braak stages in control and AD (Figure 5-1C, D)

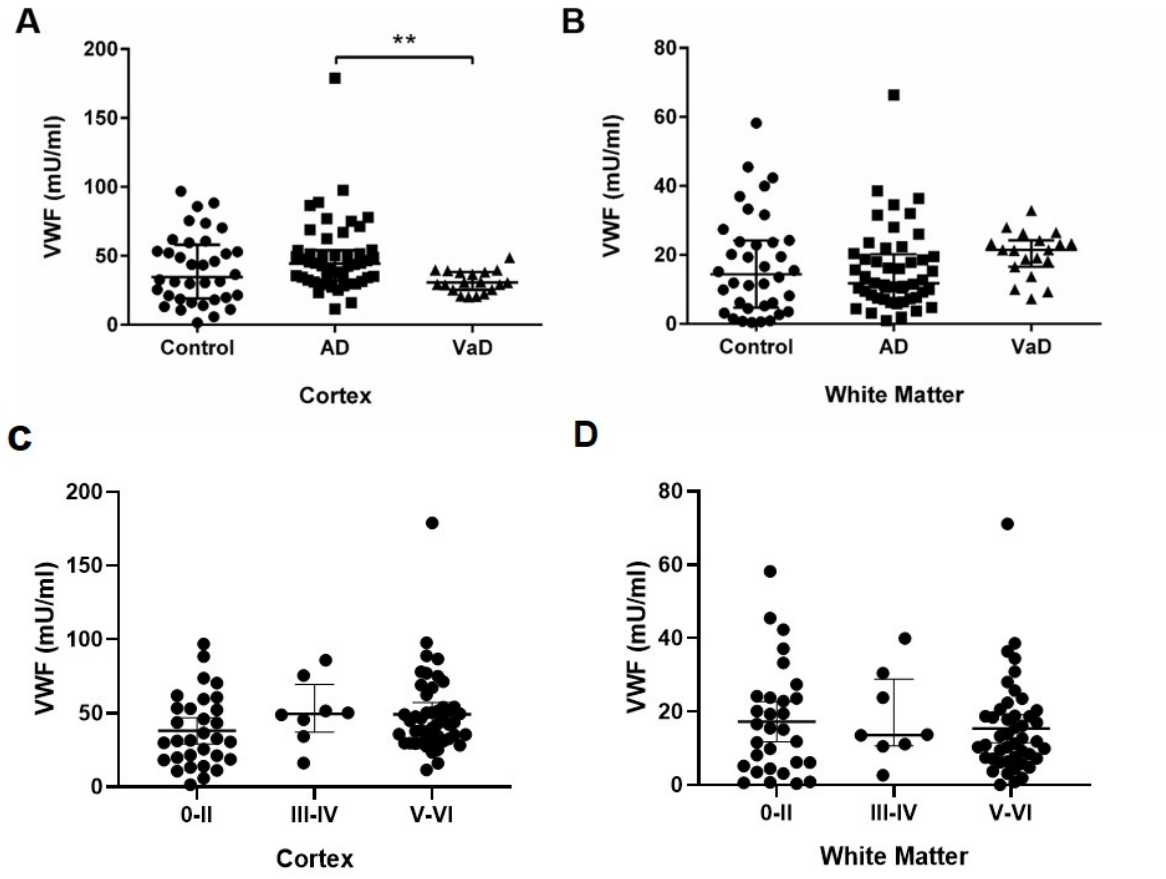

Figure 5-1 VWF level in parietal cortex and white matter of control, AD and VaD samples. [A] There was a significant difference between medians of three white matter groups (*p*= 0.007, C: M= 34.65, IQR= 39, n= 36; AD: M= 44.35, IQR= 21.77 n= 50, VaD: M= 30.72, IQR= 17.94, n= 19). Pairwise analysis revealed the vWF level was significantly lower in VaD cortex when compared to AD (*p*< 0.01). [B] The level of vWF did not differ significantly between the white matter of control, AD and VaD brains (*p*= 0.07, C: M= 14.37, IQR= 19.5 n = 36, AD: M= 11.77, IQR= 12.66, n = 50, M= 21.43, IQR= 7.72 VaD: n= 19). [C] The level of vWF did not differ significantly between the Braak stages in control and AD samples in the parietal cortex (I-II: M= 31.61, IQR= 34.67; III-IV: M= 49.57, IQR= 32.49; V-VI: M= 43.92, IQR= 22.66). [D] The level of vWF did not differ significantly between the Braak stages in control and AD samples in the parietal cortex (I-II: M= 15.34, IQR= 18.85; III-IV: M= 13.66, IQR= 18.12; V-VI: M= 11.93, IQR= 12.4). The median ± IQR is displayed. ** *p*< 0.01

5.3.2 VEGF levels in human parietal cortex and white matter

VEGF level was measured in homogenates, as an indicator of hypoxia. VEGF measurements had previously been conducted on control and AD cortex and new measures were performed for VaD parietal lobe and the control and AD white matter. There was a trend towards an increase in VEGF in the AD brains, although this did not reach significance (p = 0.069, Figure 5-2A). There was a significant difference between medians in the white matter (p = 0.019) and pairwise analysis reported a significant decrease in VEGF level in the white matter of VaD compared to control (p < 0.05, Figure 5-2B).

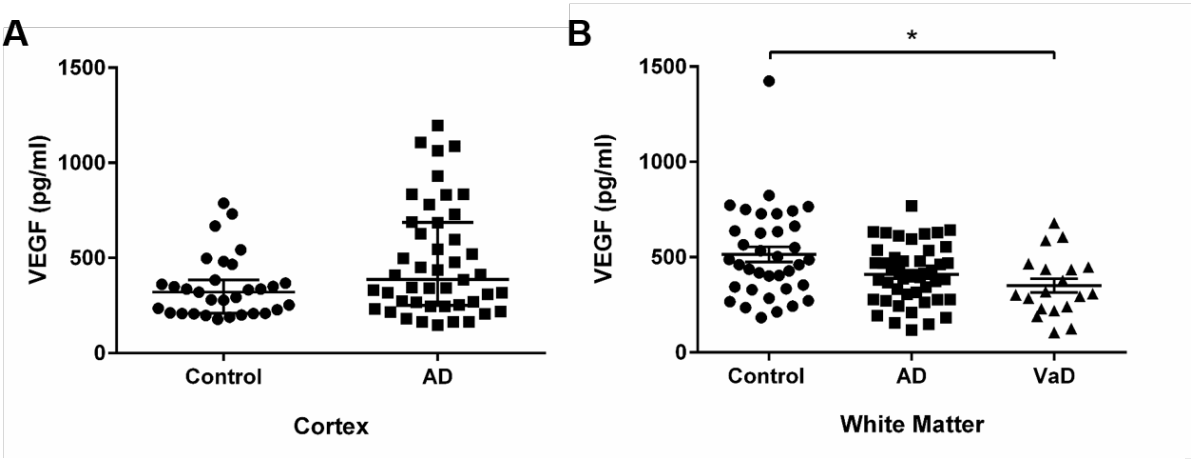

Figure 5-2 VEGF level in parietal cortex and white matter of control, AD and VaD samples. [A] VEGF level was higher in AD than control cortex although this did not reach significance (p= 0.069, C: M= 321, IQR= 174.5, n = 31, AD: M= 386.9, IQR= 436.3, n = 45) [B] There was a significant group difference between medians of three white matter groups (p= 0.019, C: M= 473.6, IQR= 319.5, n = 31, AD: M= 397, IQR= 227.8, n = 45, VaD: M= 308, IQR= 218.4, n= 19). Pairwise analysis revealed VEGF level was significantly lower in VaD when compared to control white matter (p< 0.05). * p< 0.05.

5.3.3 MAG level in control and VaD white matter

In order to further investigate hypoperfusion the relative level of myelin protein, MAG, was used as a biochemical measure of cerebral hypoperfusion. A decrease in VEGF level in VaD compared to control was reported in Figure 5-2, so the state of perfusion in these cases was investigated. There was a significant decrease in the MAG concentration in the white matter of VaD cases compared to control (p= 0.0058) (Figure 5-3).

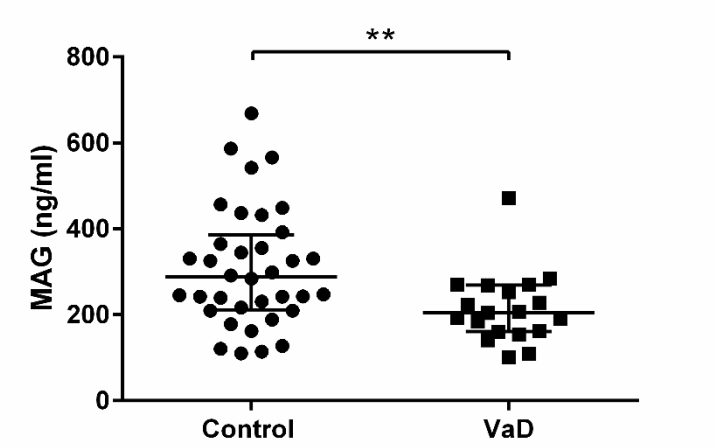

Figure 5-3 MAG level in control and VaD white matter. There was a significant decrease in the MAG level in VaD (M= 287.9, IQR= 173.8, n= 36) compared to control (p= 0.0058, M= 204.5, IQR= 108.2, n= 19). ** p< 0.01.

5.3.4 Relationship between VEGF and vWF in parietal cortex and white matter

No correlation was seen between VEGF and vWF in control (p= 0.525, r= 0.119) or AD (p= 0.437, r= −0.119) parietal cortex (Figure 5-4A). There was no correlation between VEGF and vWF in the white matter of control (p= 0.956, r= -0.01) or AD subjects (p= 0.132, r= 0.226) (Figure 5-4B). A significant positive correlation was seen in the white matter of VaD cases (p= 0.037, r= 0.481, Figure 5-4B). Details of correlations are provided in Appendix 21.

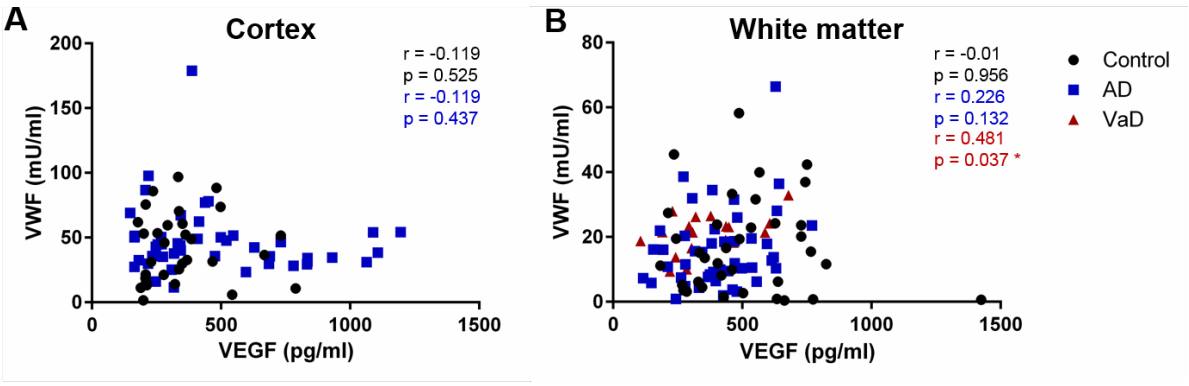

Figure 5-4 Relationship between VEGF and vWF in parietal cortex and white matter. [A] No correlation was observed between VEGF and vWF in control (p= 0.525, r= 0.119, n= 31) or AD (p= 0.437, r= −0.119, n= 45) parietal cortex. [B] No correlation was observed between VEGF and

vWF in control white matter (*p*= 0.956, r = -0.01, n= 36) or AD white matter (*p*= 0.132, r= 0.226, n= 48). A significant positive correlation was observed between VEGF and vWF in VaD white matter (*p*= 0.037, r= 0.481, n= 19).

5.3.5 Relationship between VEGF receptors and VEGF and vWF in parietal cortex and white matter

The correlation between VEGFR1 level and VEGF or vWF was examined in control and AD cortex. VEGFR1 correlated positively with vWF in AD cortex (*p*= 0.003, r= 0.438) (Figure 5-5A). There was no correlation between VEGFR1 and VEGF in control (*p*= 0.192, r= 0.229, Figure 5-5B) or AD cortex (*p*= 0.413, r= −0.133).

Next VEGFR2 was correlated with VEGF and vWF in control, AD and VaD cortex and white matter. A significant positive correlation was found between vWF and VEGFR2 in AD cortex (*p*= 0.048, r= 0.287, Figure 5-5C) but no correlation was found in control (*p*= 0.135, r= 0.254) or VaD cortex (*p*= 0.764, r= 0.074). There was no correlation reported between VEGF and VEGFR2 in control or AD cortex (*p*= 0.013, r= 0.366, Figure 5-5D) and no correlation between VEGFR2 and VEGF in control cortex (*p*= 0.071, r= 0.328). No correlation was found between VEGFR2 and vWF (Figure 5-5E) or VEGF (Figure 5-5F) and VEGFR2 in the white matter or control, AD or VaD cases. Summary tables of VEGFR1 and VEGFR2 correlations are provided in Appendix 22-24.

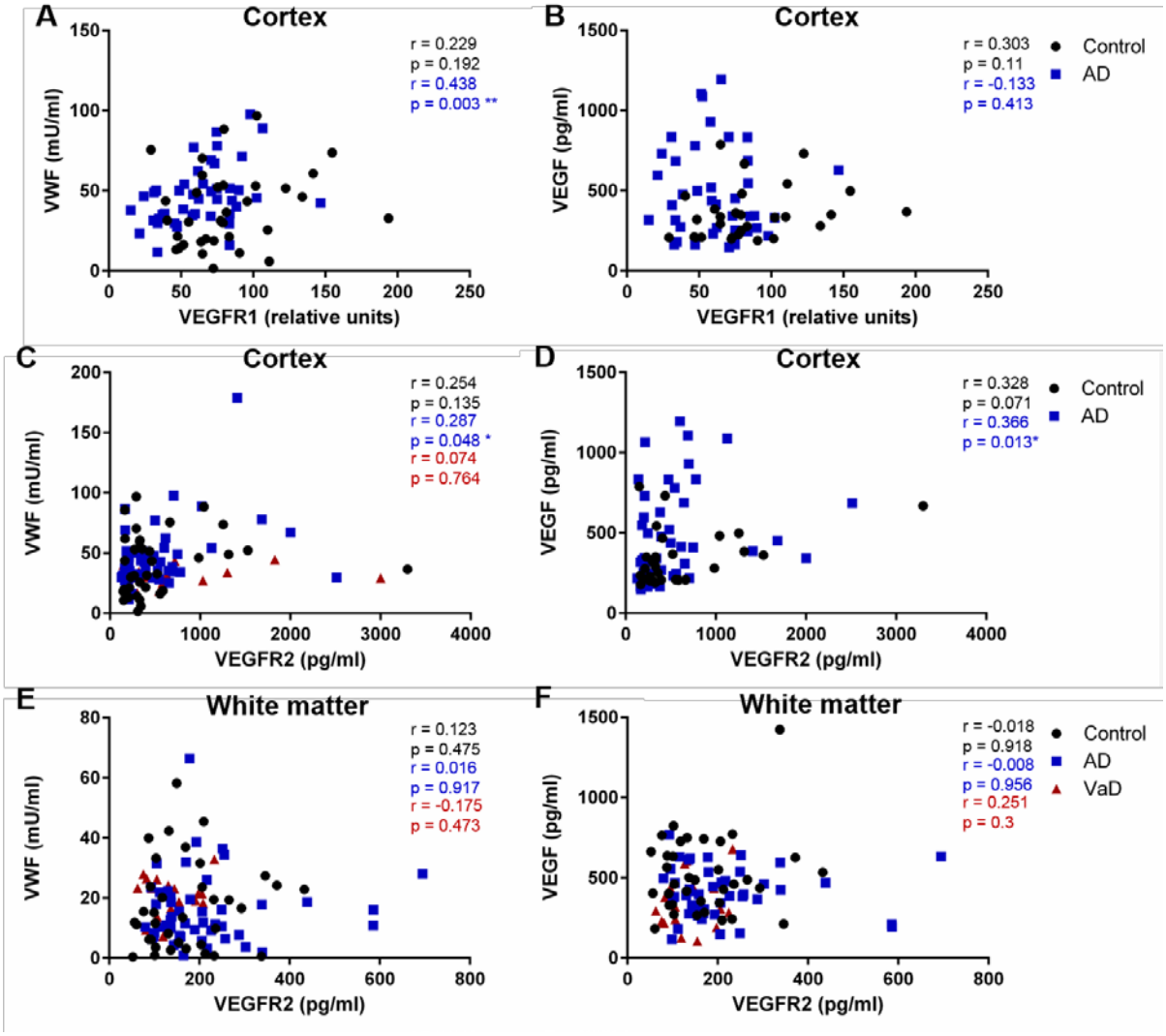

Figure 5-5 Relationship between VEGF receptors and VEGF and vWF. [A] A significant positive correlation was observed between vWF and VEGFR1 in AD cortex (*p*= 0.003, r= 0.438, n= 34). No correlation was observed in control cortex (*p*= 0.192, r= 0.229, n= 44). [B] No correlation between VEGF and VEGFR1 in control (*p*= 0.192, r= 0.229, n= 29) or AD cortex (*p*= 0.413, r = −0.133, n= 45) [C] A significant correlation between vWF and VEGFR2 in AD cortex (*p*= 0.048, r = 0.287, n= 48). No correlation between vWF and VEGFR2 in control cortex (*p*= 0.135, r= 0.254, n= 36) or VaD cortex (*p*= 0.764, r= 0.074, n= 19). [D] A significant correlation between VEGF and VEGFR2 in AD cortex (*p*= 0.013, r= 0.366, n= 45). No correlation between VEGF and VEGFR2 in control (*p*= 0.071, r= 0.328, n= 31). [E] No correlation between vWF and VEGFR2 in control white matter (*p*= 0.475, r= 0.123, n= 36), AD white matter (*p*= 0.917, r= 0.016, n= 48) and VaD white matter (*p*= 0.473, r= −0.175, n= 19). [F] No correlation between VEGF and VEGFR2 in control white matter (*p*= 0.918, r= -0.018, n= 36), AD white matter (*p*= 0.956, r= −0.008, n= 48) and VaD white matter (*p*= 0.3, r= 0.251, n= 19).

5.3.6 Relationship between VEGF receptors and CAA

The relationship between VEGFR1 and VEGFR2 and CAA severity was examined. There was no difference in VEGFR1 between cases with no or sparse CAA and those with moderate to severe CAA in the parietal cortex (Figure 5-6A). Similarly, there was no change in VEGFR2 level with increasing CAA severity in cortex (Figure 5-6B) or white matter (Figure 5-6C). Summary statistics are provided in Appendix 25.

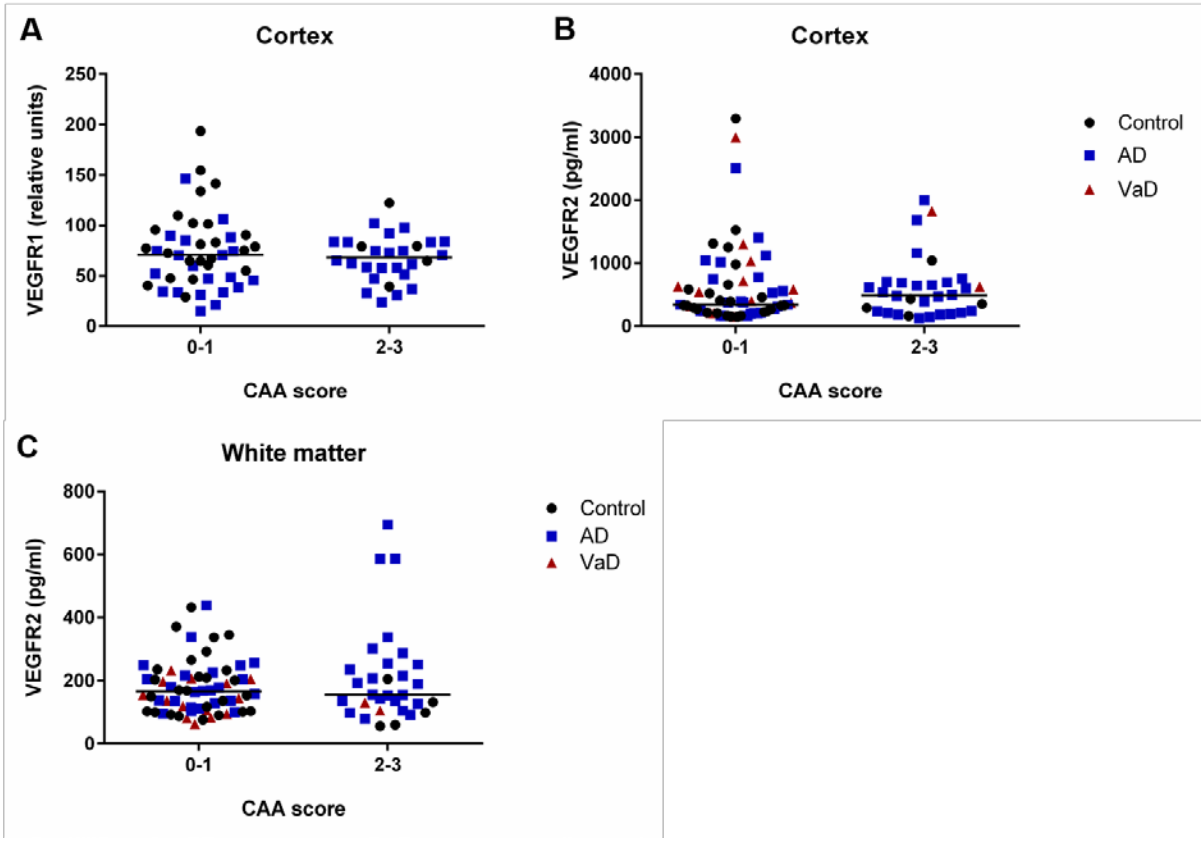

Figure 5-6 VEGFR1 and VEGFR2 level in relation to CAA score. [A] No significant difference between the cortex VEGFR1 cases with no or mild CAA, scored 0-1 (M= 70.6, IQR= 43.5, n= 46), and those with moderate to severe CAA, scored 2-3 (*p*= 0.82, M= 67.99, IQR= 30.39, n= 28). [B] No significant difference between the cortex of VEGFR2 cases with a CAA severity score of 0-1 (M= 340, IQR= 476.9, n= 65) and those with scores of 2-3 (*p*= 0.55, M= 490.9, IQR= 475.3, n= 32). [C] No significant difference between the white matter of VEGFR2 cases with a CAA severity score of 0-1 (M= 166.4, IQR= 108.5, n= 64) and those with scores of 2-3 (*p*= 0.834, M= 154.7, IQR= 145.9, n= 31). The horizontal lines indicate the grand median.

5.3.7 Relationship between VEGF receptor level and SVD

The relationship between SVD score and VEGFR1 and VEGFR2 level in cortex and white matter was investigated. No significant differences in the level of VEGFR1 were observed between control and AD cases with no or mild SVD and those with moderate to severe SVD in the cortex (Figure 5-7A). Similarly, VEGFR2 level in control, AD and VaD cases was unchanged with increasing SVD severity in the cortex and white matter (Figure 5-7B, C). Summary statistics are provided in Appendix 26.

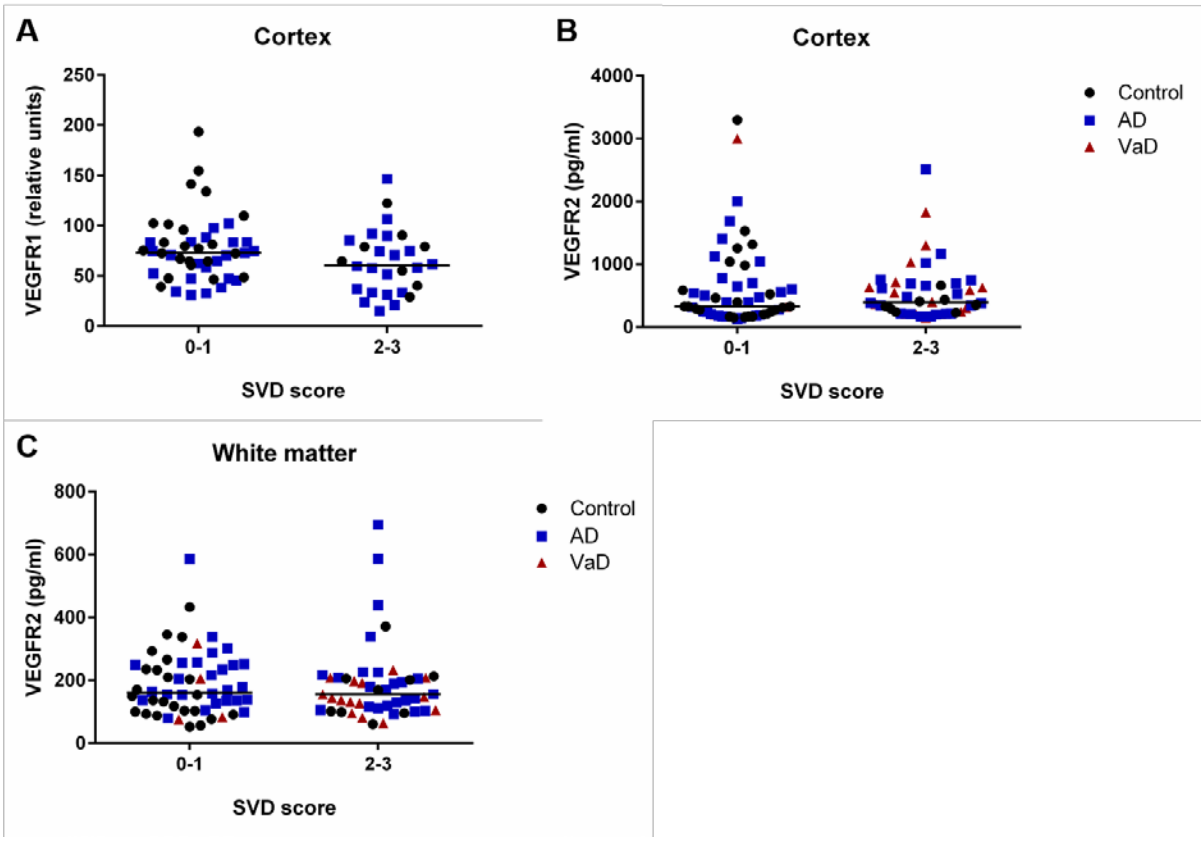

Figure 5-7 VEGFR1 and VEGFR2 level in relation to SVD score. [A] No significant difference between the cortex VEGFR1 cases with no or mild SVD, scored 0-1 (M= 72.87, IQR= 33.69, n= 46), and those with moderate to severe SVD, scored 2-3 (*p* = 0.105, M= 60.59, IQR= 49.26, n= 28). [B] No significant difference between the cortex of VEGFR2 cases with a SVD severity score of 0-1 (M= 328.9, IQR= 499.2, n= 55) and those with scores of 2-3 (*p*= 0.473, M= 391.1, IQR= 443, n= 46). [C] No significant difference in the white matter of VEGFR2 cases with a SVD severity score of 0-1 (M= 157.8, IQR= 144.8, n= 53) and those with scores of 2-3 (*p* = 0.637, M= 155.4, IQR= 102.3, n= 46). The horizontal lines indicate the grand median.

5.3.8 VEGFR1 and VEGFR2 level in relation to Braak stage in control and AD

VEGFR1 and VEGFR2 levels from control and AD cohorts were examined in relation to Braak stage as a measure of AD progression. Controls are defined here as Braak stage 0-II. There was a significant difference between the median VEGFR1 levels in different Braak

stage (p= 0.02) and pairwise analysis reported a significant decrease in the level of VEGFR1 between cases at 0-II and those at stages V-VI (p < 0.05, Figure 5-8A). There was no significant difference between VEGFR2 level and Braak stage in the cortex (p= 0.456, Figure 5-8B) or white matter (p= 0.223, Figure 5-8C). Summary statistics are provided in Appendix 27.

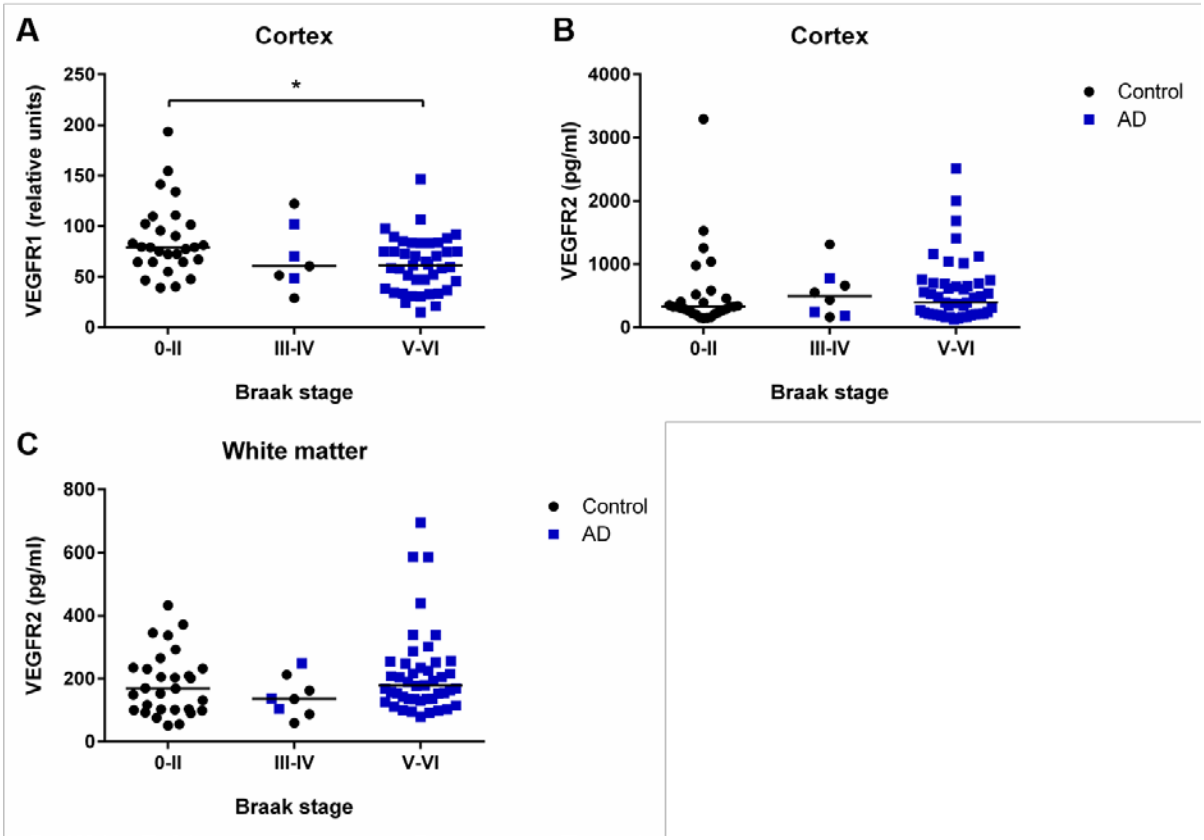

Figure 5-8 VEGFR1 and VEGFR2 level in relation to Braak stage. [A] There was a significant difference between the medians (p = 0.02) and pairwise analysis revealed a significant reduction in VEGFR1 between Braak stages 0-II and V-VI (p < 0.05) (0-II: M= 78.21, IQR= 37.36, n= 30; III-IV: M= 65.6, IQR= 46.82, n= 8; V-VI: M=59.59, IQR= 45.71, n= 41). [B] No significant difference in VEGFR2 level in the cortex when comparing Braak stage (p = 0.456) (0-II: M= 326.8, IQR= 232.9, n= 31; III-IV: M= 495.4, IQR= 551.2, n= 8; V-VI: M= 395.4, IQR= 489.1, n= 47).[C] No significant difference in VEGFR2 level in the cortex when comparing Braak stage (p = 0.223) (0-II: M= 169.1, IQR= 133.2, n= 29; III-IV: M= 137.2, IQR= 108.44, n= 8; V-VI: M= 178.2, IQR= 114.2, n= 45). The horizontal lines indicate the grand median. * p < 0.05

5.3.9 Relationship between VEGF receptors and Aβ in control and AD

To investigate any relationship between VEGF receptor expression and Aβ in AD, the levels of VEGFR1 and VEGFR2 were assessed in relation to the levels of soluble and insoluble $Aβ_{1-40}$, $Aβ_{1-42}$ and $Aβ_{42:40}$ previously measured in the parietal cortex and white matter of the same cases.

5.3.9.1 VEGFR1 in relation to Aβ in parietal cortex

VEGFR1 displayed no correlation with soluble or insoluble $A\beta_{1\text{-}40}$ or $A\beta_{1\text{-}42}$ in control or AD cortex (Figure 5-9A-F).

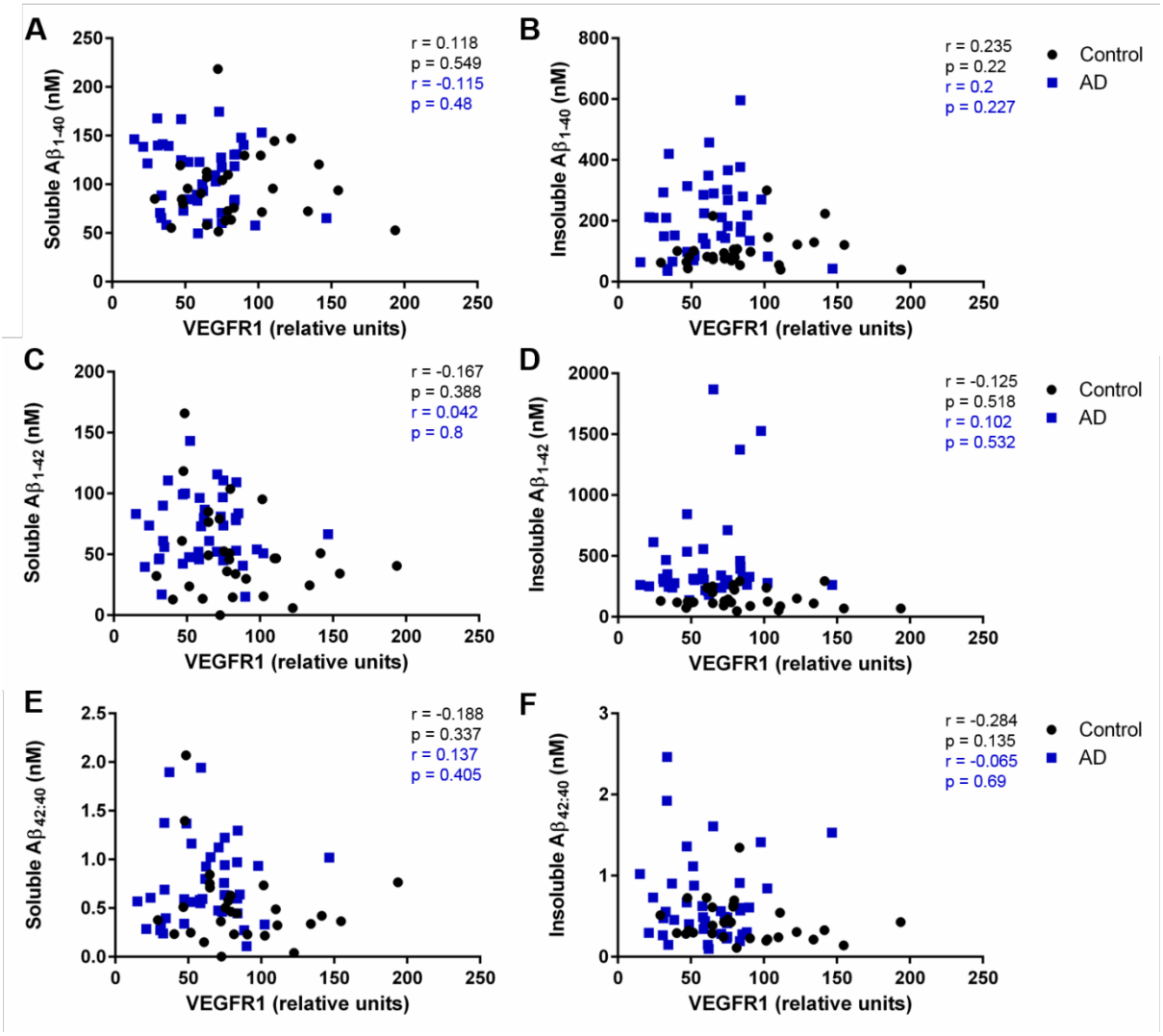

Figure 5-9 Relationship of VEGFR1 cortex level and Aβ. [A] No correlation between VEGFR1 and soluble $A\beta_{1\text{-}40}$ in control (p = 0.549, r = 0.118, n = 28) or AD cortex (p = 0.48, r = −0.115, n = 40). [B] No correlation between VEGFR1 and insoluble $A\beta_{1\text{-}40}$ in control (p = 0.22, r = 0.235, n = 29) or AD cortex (p = 0.227, r = 0.2, n = 40). [C] No correlation between VEGFR1 and soluble $A\beta_{1\text{-}42}$ in control (p = 0.388, r = −0.167, n = 29) or AD cortex (p = 0.8, r = 0.042, n = 39). [D] No correlation between VEGFR1 and insoluble $A\beta_{1\text{-}42}$ in control (p = 0.518, r = −0.125, n = 29) or AD cortex (p = 0.532, r = 0.102, n = 40). [E] No correlation between VEGFR1 and soluble $A\beta_{42:40}$ in control (p = 0.337, r = −0.188, n = 28) or AD cortex (p= 0.405, r = 0.137, n = 39). [F] No correlation between VEGFR1 and insoluble $A\beta_{42:40}$ in control (p= 0.135, r = −0.284, n = 29) or AD cortex (p = 0.69, r = −0.065, n = 40).

5.3.9.2 VEGFR2 in relation to Aβ in parietal cortex

No correlation was observed between VEGFR2 and soluble or insoluble $A\beta_{1\text{-}40}$ in control or AD cortex (Figure 5-10A, B). A significant negative correlation was identified between VEGFR2 and soluble $A\beta_{1\text{-}42}$ in controls (p = 0.011, r = −0.449, Figure 5-10C). There was no correlation between VEGFR2 and insoluble $A\beta_{1\text{-}42}$ in control or AD cortex (Figure 5-10 D). A significant negative correlation was seen between VEGFR2 and $A\beta_{42:40}$ in control cortex (p = 0.005, r = −0.503, Figure 5-10E). VEGFR2 correlated positively with the insoluble $A\beta_{42:40}$ in AD cases (p = 0.047, r = 0.298, Figure 5-10F).

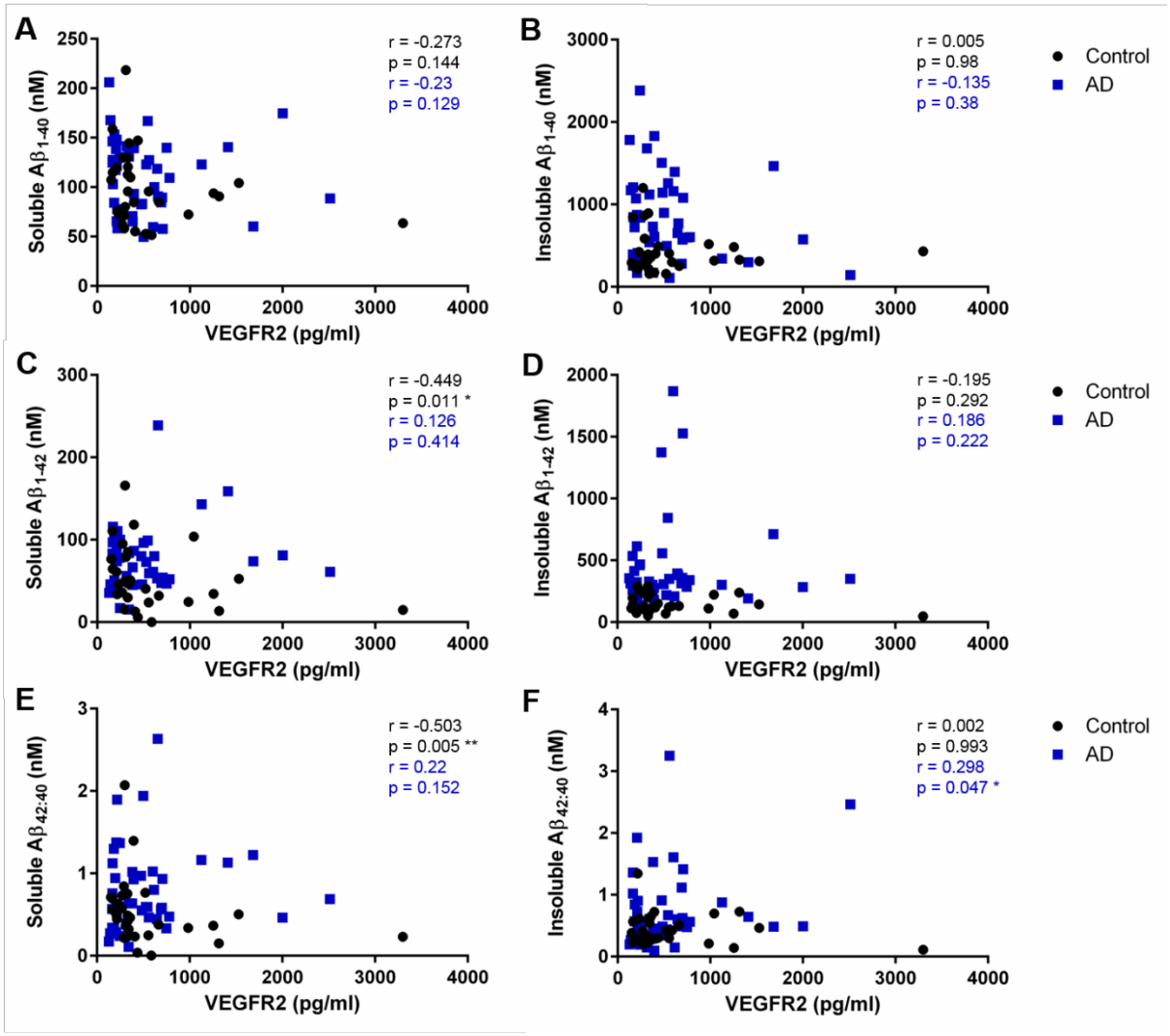

Figure 5-10 Relationship of VEGFR2 level and Aβ in cortex. [A] No correlation between VEGFR2 and soluble $A\beta_{1\text{-}40}$ in control (p= 0.144, r= −0.273, n = 30) or AD cortex (p= 0.129, r= −0.23, n= 45). [B] No correlation between VEGFR2 and insoluble $A\beta_{1\text{-}40}$ in control (p = 0.98, r= 0.005, n= 31) or AD cortex (p= 0.38, r= −0.135, n= 45). [C] No correlation between VEGFR2 and soluble $A\beta_{1\text{-}42}$ in control cortex (p = 0.011, r= −0.449, n= 31) or AD cortex (p= 0.414, r= 0.126, n= 44). [D] No correlation between VEGFR2 and insoluble $A\beta_{1\text{-}42}$ in control (p= 0.292, r= −0.195, n= 31) or AD cortex (p= 0.222, r= 0.186, n= 45). [E] A significant negative correlation was observed

between VEGFR2 and soluble $A\beta_{42:40}$ in control (p= 0.005, r= −0.503, n= 30). No correlation was observed in AD cortex (p= 0.152, r= 0.22, n = 44). [F] No correlation between VEGFR2 and insoluble $A\beta_{42:40}$ in control (p= 0.993, r= 0.002, n= 31). A significant positive correlation was found in AD cortex (p= 0.047, r= 0.298, n= 44). * p < 0.05, ** p < 0.05

5.3.9.3 VEGFR2 in relation to Aβ in parietal white matter

No correlation was observed between VEGFR1 or VEGFR2 level and $A\beta_{1-40}$ or $A\beta_{1-42}$ in the cortex or white matter of control and AD parietal lobe (Figure 5-11A-F).

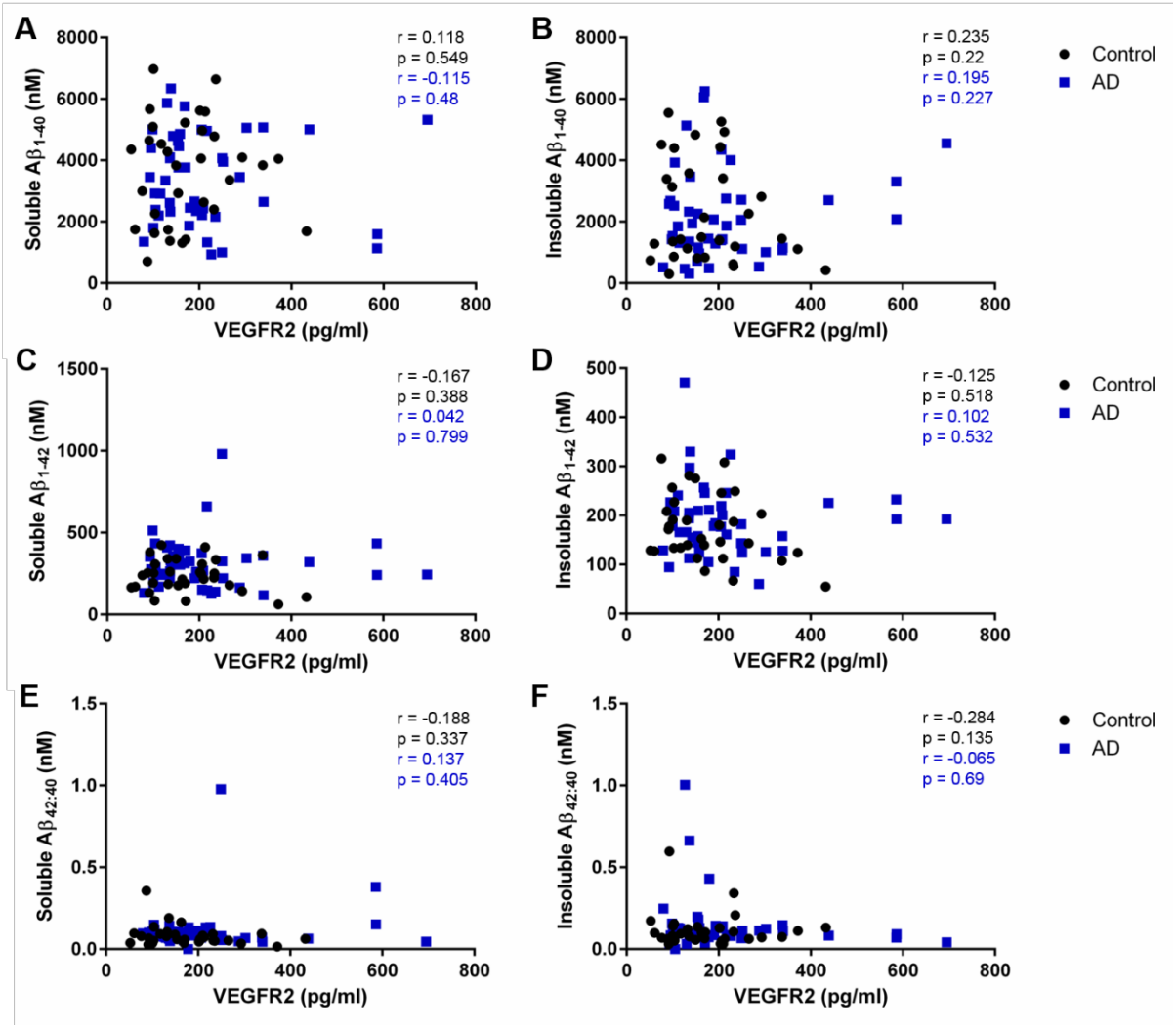

Figure 5-11 Relationship of VEGFR2 level and Aβ in white matter. [A] No correlation between VEGFR2 and soluble $A\beta_{1-40}$ in control (p= 0.549, r= 0.118, n= 32) or AD white matter (p= 0.22, r= 0.235, n= 45). [B] No correlation between VEGFR2 and insoluble $A\beta_{1-40}$ in control (p= 0.388, r= −0.167, n= 31) or AD white matter (p= 0.227, r= 0.195, n= 43). [C] No correlation between VEGFR2 and soluble $A\beta_{1-42}$ in control (p= 0.388, r= −0.167, n= 32) or AD white matter (p= 0.799, r= 0.042, n= 44). [D] No correlation between VEGFR2 and insoluble $A\beta_{1-42}$ in control (p= −0.125, r= 0.518, n= 32) or AD cortex (p= 0.532, r= 0.102, n= 44). [E] No correlation between VEGFR2 and soluble $A\beta_{42:40}$ in control (p= 0.337, r= −0.188, n= 32) or AD white matter (p= 0.405, r= 0.137, n= 45). [F] No correlation between VEGFR2 and insoluble $A\beta_{42:40}$ in control (p= 0.135, r= −0.284, n= 31) or AD white matter (p= 0.69, r= −0.065, n= 43).

5.3.10 VEGFR1 and VEGFR2 level in relation to age and post mortem delay

VEGFR1 or VEGFR2 were investigated in relation to age and post-mortem delay. No correlation was found between VEGFR1 and age or post-mortem delay in the cortex or white matter of control, AD or VaD (Figure 5-12A, B). No correlation was found between VEGFR2 and age or post-mortem delay in the cortex (Figure 5-12C, E) or white matter of control, AD or VaD (Figure 5-12D, F).

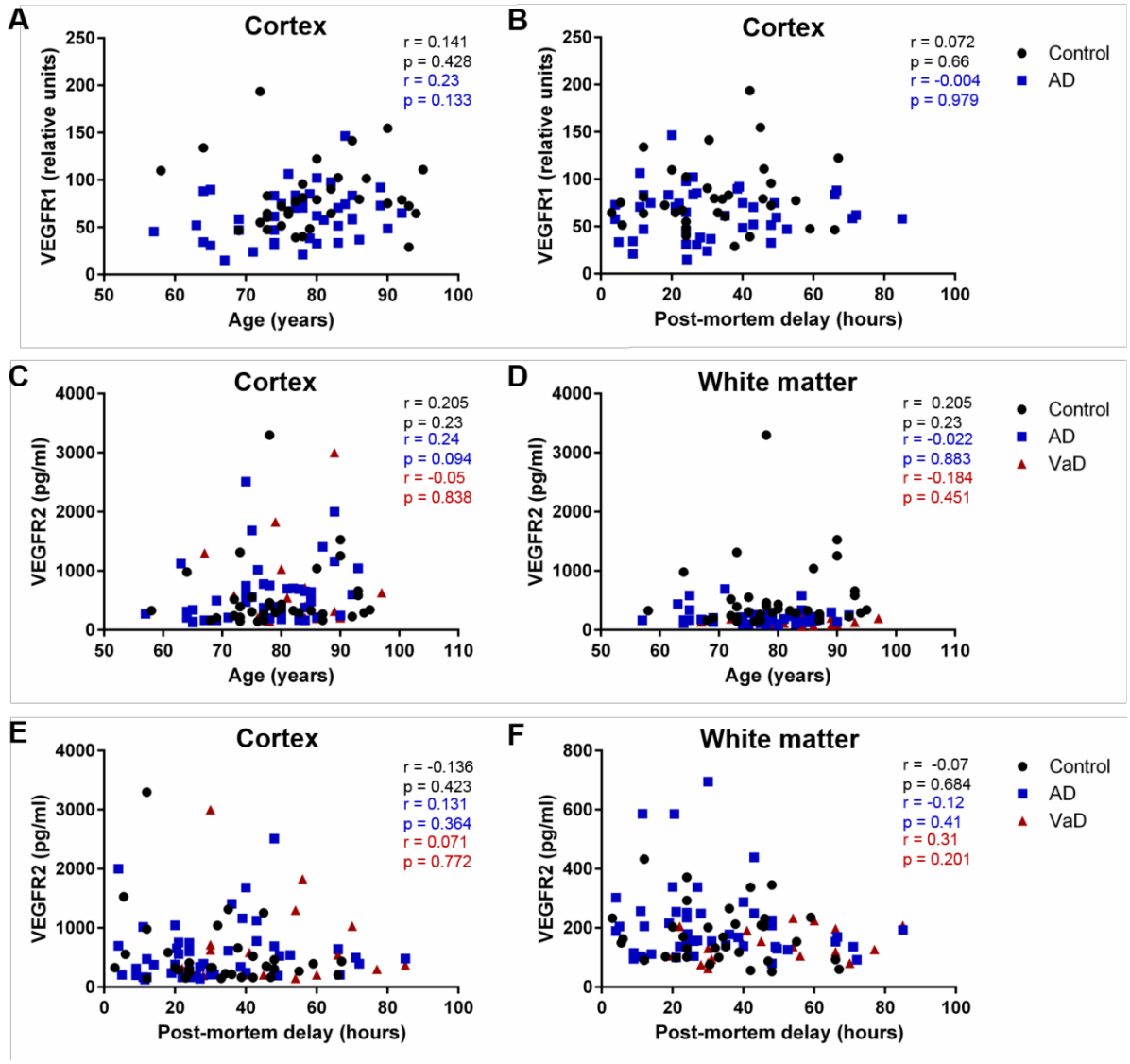

Figure 5-12 Relationship between VEGFR1 and VEGFR2 level to age and post-mortem delay. [A] No correlation between VEGFR1 and age in control (*p*= 0.428, r= 0.141, n= 34) or AD cases (*p*= 0.133, r= 0.23, n= 44). [B] No correlation between VEGFR1 and post-mortem delay in control (*p*= 0.66, r= 0.072, n= 34) or AD cases (*p*= 0.979, r= −0.004, n= 44). [C] No correlation between VEGFR2 level in cortex and age in control (*p*= 0.423, r= −0.136, n= 36), AD (*p*= 0.364, r= 0.131, n= 50) or VaD cases (*p*= 0.772, r= 0.071, n= 19). [D] No correlation between VEGFR2 level in white matter and age in control (*p*= 0.23, r= 0.205, n= 36), AD (*p*= 0.883, r= −0.022, n= 48) or VaD cases (*p*= 0.451, r= −0.184, n= 19) [E] No correlation between VEGFR2 level in

cortex and post-mortem delay in control (*p*= 0.423, r= −0.136, n= 36), AD (*p*= 0.364, r= 0.131, n= 50) and VaD cases (*p*= 0.772, r= 0.72, n= 19). [F] No correlation between VEGFR2 level in white matter and post-mortem delay in control (*p*= 0.684, r= −0.07, n= 36) AD (*p*= 0.41, r= −0.12, n= 48) or VaD cases (*p*= 0.201, r= 0.31, n= 19).

5.4 Discussion

VEGFR1 and VEGFR2 have been investigated in the brain to understand the VEGF-VEGFR system and to find out whether abnormalities in this system might contribute to disruption of angiogenesis in AD. To assess the extent of hypoperfusion and microvessel density, the levels of VEGF and vWF were determined and these were then examined in relation to VEGFR1 and VEGFR2. The possible impact of CAA and SVD on receptor levels was also investigated, as were the effect of AD progression/ severity (as indicated by Braak tangle stage) and the level of Aβ.

Firstly, VWF level was determined in the parietal cortex and white matter of control, AD and VaD cases. In agreement with Thomas et al (2015) [78], no change was observed in vWF level between control and AD cortex. There was a decrease in the vWF level in VaD cortex but this finding should be interpreted with caution in view of the smaller sample size in this subgroup. In white matter, vWF level was unchanged across control, AD and VaD groups, in agreement with previous with what was reported previously[72]. There was no significant difference in VWF level between Braak stages in control and AD. This supports previous work finding that though overall brain mass was reduced capillary density was not reduced in AD compared to control [104].

The VEGF level was measured and there was a trend (*p*= 0.069) towards an increase in VEGF in AD cortex, in keeping with previous observations [78]. In contrast to prior studies by my research group this result was not statistically significant. The current study continues to support an increase in VEGF concentration in AD compared to control in the largest cohort tested to date.

In agreement with Barker et al (2014), there was no change in VEGF level between the control and AD white matter [72]. Unexpectedly, there was a decrease in VEGF in the white matter of VaD cases. This was not expected as the group had previously measured VEGF in parietal white matter and found no change in VEGF level compared to control [72] and VEGF had been elevated in VaD cortex compared to control [78]. This was further investigated by establishing the level of MAG as a measure for hypoperfusion in the white matter of control and VaD cases. A PLP assay was not performed so the ratio of MAG:PLP was not calculated. In future it would be desirable to complete the PLP assay to compare to the MAG levels in the same samples. There was a significant reduction in MAG in VaD cases as

expected in the presence of hypoperfusion. The reason for the reported decrease in VEGF level in VaD white matter despite hypoperfusion may be due to the age of some of the post-mortem samples. In the VaD cohort, 17 of the 19 samples were donated over 15 years previously, the oldest donation being 32 years previous. Despite the aliquoting of my samples to prevent multiple freeze thaw, the likelihood of multiple freeze thaw cycles when brain slices were removed from storage over many years may have degraded the proteins of interest and make replicating results from earlier studies difficult. Comparison with a VaD cohort from another brain bank would provide a valuable control in future work. The present finding is in overall agreement with previously published work showing a trend to increase in VEGF in AD compared to control.

Assessment of VEGF in relation to vWF revealed no relationship between the two markers in the cortex of control or AD cases. In the white matter, however, there was a positive correlation between VEGF and vWF in VaD cases. The correlation might be expected, as in VaD white matter, VEGF level increases and so, therefore, should vessel density, though not sufficiently to correct cerebral hypoperfusion. In contrast, in the AD white matter, although VEGF level increases there is no corresponding increase in vessel density. Previously published work on the white matter in a pure VaD cohort and a mixed AD and VaD cohort which there was a positive correlation between VEGF and vWF [72]. In this study, AD and VaD data were correlated individually rather than being pooled together and analysed as in Barker et al. [72] highlighting the importance of examining cohorts separately. In agreement with Barker et al (2014), this work shows that ischaemic changes may be affecting the cortex and white matter differently and the importance of analysing both regions.

VEGFR1 and VEGFR2 correlated positively with vWF level in the AD cortex. VEGFR2 correlated with VEGF in the AD cortex whereas there was no correlation with VEGFR1 and VEGF. Prior to establishing that VEGFR1 level is decreased in AD (3.4.2.1) it might have been expected that VEGFR1 would correlate positively with VEGF level as both can be upregulated by hypoxia [145, 247]. Similarly, the unchanged level of VEGFR2 in control and disease (4.4.2.1) resulted in no correlation with VEGF.

To investigate the possibility of VEGFR1 and VEGFR2 alteration as a result of amyloid or non-amyloid small vessel disease, VEGF receptor levels were analysed with respect to the severity of CAA and SVD. CAA and SVD both effect blood vessel function could potentially interfere with vascular cells expressing VEGFR1 and VEGFR2 [327-329]. However, changes in VEGF receptor levels were found not to be related to CAA or SVD severity.

Lastly, the relationship between receptor level and severity of AD neuropathology was examined. As hypothesised, VEGFR1 level decreased with increasing Braak stage and

VEGFR2 remained unchanged in both cortex and white matter. VEGFR1 did not correlate with the level of soluble or insoluble $A\beta_{1-40}$ or $A\beta_{1-42}$ suggesting that VEGFR1 reduction in AD is not driven directly by Aβ level and may result from some other abnormality in AD, such as reduction in CBF and consequent tissue hypoxia. VEGFR2 was negatively correlated with soluble $A\beta_{1-42}$ and soluble $A\beta_{42:40}$ in control cortex. A reduction in the levels VEGFR2 with increasing soluble $A\beta_{1-42}$ may result from interaction between Aβ and VEGF. This could be due to sequestration of VEGF by $A\beta^{222}$ which would reduce the availability of VEGF to bind to VEGFR2 and regulate expression. In addition, Aβ interaction with VEGFR2 itself may decrease VEGFR2 expression again preventing the binding of its ligand VEGF which regulates receptor expression. In AD cortex however, there was no correlation of VEGFR2 level with soluble $A\beta_{1-42}$ and only a weak positive correlation with insoluble $A\beta_{1-40}$. This study found no relationship between VEGFR levels and age or post-mortem delay.

The present findings may be influenced by the number of late-stage AD cases in this study. Reduction in CBF is an early change in AD, and the disparity between metabolic demand and tissue oxygenation/blood supply becomes less pronounced in advanced disease [74]. Any changes in receptor levels may therefore be more prominent in the early stages of disease. In this study the majority of AD cases had Braak tangle stages of V or VI. In future studies the cohort should be expanded to include Braak stages III-IV.

In this chapter findings on examining the relationship between VEGF receptor levels and cerebrovasculature, and AD pathology were described. vWF level, a marker of microvessel density, is unchanged in the parietal lobe despite a trend towards elevated VEGF level and there is a negative relationship between VEGF and vWF level in AD white matter. VEGFR1 and VEGFR2 correlated with vWF in the AD cortex but were not associated with severity of CAA or SVD. Receptor levels were only weakly related to the levels of Aβ. Factors that may account for the reduced or unchanged microvessel density in hypoperfused cortex in AD [78] include sequestration of VEGF by $A\beta_{1-42}$ [222] or decreased VEGFR1:sVEGFR1 ratio (3.5.2.1), and binding of $A\beta_{1-42}$ to VEGFR2, shown by Patel et al [308] to block VEGF-mediated signalling.

Chapter 6 VEGFR1 and VEGFR2 in human brain microvascular endothelial cells and pericytes

6.1 Introduction

With evidence of elevated VEGF and unchanged levels of receptor VEGFR2 in response to brain hypoperfusion in AD, further questions are raised about the mechanism behind the unchanged microvessel density in AD. As previously discussed by Thomas et al.[78], since VEGFRs can be independently upregulated in response to hypoxia there may be reduced receptor activation due to VEGF sequestering by $A\beta$[222]. There is also evidence that $A\beta_{1-42}$ can interact and bind to the extracellular domain of VEGFR2 and block VEGF-induced tyrosine phosphorylation of VEGFR2 in human brain microvascular endothelial cells (HBMECs) and human brain vascular pericyte (HBVP) models [308].

Endothelial cells and pericytes are key members of the neurovascular unit and contribute to angiogenesis in the brain (1.2.3). Though endothelial cells have been the main focus of studies of angiogenesis, the importance of pericytes is increasingly being recognised not only in relation to vessel function but also for normal angiogenesis. Pericytes modulate BBB permeability, CBF, clearance of metabolites into the bloodstream, and neuroinflammation [340, 341]. The highest density of pericytes in the body is found in the brain, [342] where they cover an estimated 70%-80% of capillary tubes in the CNS [343].

Pericytes maintain integrity of the BBB by controlling the expression of BBB-specific proteins in endothelial cells and the polarisation of astrocyte end-feet [344, 345]. Pericytes can control blood flow at the capillary level within the brain. They do this by contracting and relaxing within capillary walls, altering vessel diameter. Pericytes respond to neuronal activity, neurotransmitter activity and depolarisation [341].

Pericytes also regulate angiogenesis and vessel stability and their absence in development leads to the formation of microaneurysms [346]. Pericytes have roles in multiple stages of angiogenesis. They secrete angiogenic factors, including VEGF, which stimulate sprouting formation and endothelial proliferation (1.2.3). They also secrete matrix metalloproteinases (MMPs) which degrade basement membrane proteins and facilitate endothelial cell migration. Pericytes help to conclude angiogenesis by preventing proliferation and by inhibition of MMP-mediated degradation of basement membrane proteins [343]. Pericytes are able to stabilise the vascular wall, promote endothelial cell maturation and contribute to basement membrane structure [343]. They can also phagocytose small molecules and may help to clear certain macromolecules such as $A\beta$ [340, 343, 347]. Pericytes probably have a role in

neuroinflammation, as they can phagocytose, present antigens, and release inflammatory mediators [340, 348].

The degeneration of pericytes has been implicated in neurovascular dysfunction and neurodegeneration in AD. Pericyte loss has been reported in the cortex and hippocampus in human AD post-mortem studies [349]. Pericyte loss, as indicated by loss of the pericyte marker PDGFRβ, was strongly linked to cerebral hypoperfusion in the AD precuneus [350]. A pericyte-deficient mouse model displayed vascular dysfunction including reduction in brain microcirculation resulting in a reduction in blood flow. This caused chronic hypoxia and BBB breakdown leading to secondary neurodegenerative changes [345]. Pericyte deficient mice have also shown reduced capillary blood flow resulting in reduced oxygen supply in the brain [351]. Some studies have suggested vascular factors, such as hypertension, contribute to pericyte loss [343]. The accumulation of Aβ has also been implicated in pericyte degeneration. Aβ is toxic to cultured brain pericytes [352] and amyloid deposits have been identified in pericytes in post-mortem human studies [353, 354]. A mouse model overexpressing mutant APP, when crossed with a pericyte deficient mouse, showed accelerated deposition of $A\beta_{1-40}$ and $A\beta_{1-42}$, due to reduced clearance. The loss of pericytes also resulted in tau deposition and early degeneration not usually seen in this mouse model [347]. ApoE4 carriers with AD have been shown to have increased pericyte degeneration, and ApoE4 was shown to be associated with BBB breakdown in both mouse models [355] and man, as evidenced by a rise in CSF albumin [356] and an increase in perivascular leakage of plasma proteins in human brain tissue [354, 357].

The VEGF system is important in the maintenance of pericytes and in cross-talk with endothelial cells. Pericytes secrete VEGF which acts through autocrine and paracrine signalling. VEGF induces proliferation and migration of pericytes via mbVEGFR1 as shown in primary bovine retinal pericytes in hypoxia [214]. VEGF derived from pericytes promotes endothelial cell survival, stability [358, 359], angiogenesis and vascular permeability [340, 360] via its activation of VEGFR2.

VEGF levels were upregulated in pericytes in a rat model of brain trauma [361]. VEGF was reported to promote pericyte coverage of brain capillaries and improve CBF in subsequent transient brain ischaemia in a mouse model of stroke [362]. Contrary to this, there are reports that pericytes also migrate from areas of ischaemia. Pericytes were shown to migrate away from endothelial cells in a study of acute ischaemia in the feline brain [363] and a rat model of head trauma, whilst pericytes which continued to abut the endothelial cells were positive for an apoptotic marker [361].

VEGFR1 is the dominant VEGF receptor on pericytes. The first study into VEGF receptors on primary bovine retinal pericytes identified only VEGFR1 by mRNA [215]. Yamagishi et al. (1999) later showed the expression of VEGFR1 and VEGFR2 on bovine retinal pericytes [214]. In that study, both VEGFR1 and VEGFR2 were detected by PCR, with VEGFR1 as the dominant receptor. The expression of VEGFR1 mRNA increased further with decreasing O_2 and was two to three times higher at 2.5% and 0% O_2 than at atmospheric levels. In contrast, VEGFR2 mRNA expression remained stable in pericytes and even tended to be reduced in hypoxia. Under normoxic conditions, VEGFR1 protein was clearly detectable in pericytes while VEGFR2 was almost undetectable by western blot. Elevated VEGF and VEGFR1 in hypoxia increase pericyte proliferation and migration [214]. This should promote angiogenesis, resulting in increased perfusion. The group did not measure the level of sVEGFR1 by mRNA or protein in conditioned media of the pericytes, but in this study it is hypothesised that sVEGFR1 are also increased in hypoxia to negatively regulate VEGF. Pericytes have recently been shown to regulate VEGF-induced endothelial cell sprouting via expression of sVEGFR1 in the mouse retina [364], highlighting the importance of crosstalk between pericytes and endothelial cells.

In AD, pericyte degeneration has been demonstrated but there has been little investigation of the VEGF-VEGFR system despite the importance of pericytes in maintaining capillaries and sustaining normal neurovascular function. HBMECs and HBVP cultures were used in this study to investigate the influence of hypoxia and Aβ on mbVEGFR1, sVEGFR1 and VEGFR2 receptor levels.

6.1.1 Hypothesis

[1] HBMECs and HBVPs will express VEGFR1 and VEGFR2.

[2] HBMEC will increase expression of VEGFR1 and VEGFR2 in hypoxia but this response will be impaired in the presence of $A\beta_{1\text{-}40}$ or $A\beta_{1\text{-}42}$.

[3] HBMEC will increase expression of sVEGFR1 in hypoxia but this response will be impaired in the presence of $A\beta_{1\text{-}40}$ or $A\beta_{1\text{-}42}$.

[4] HBVP will increase expression of VEGFR1 and VEGFR2 in hypoxia but this response will be impaired in the presence of $A\beta_{1\text{-}40}$ or $A\beta_{1\text{-}42}$.

[5] HBVP will increase expression of sVEGFR1 in hypoxia but this response will be impaired in the presence of $A\beta_{1\text{-}40}$ or $A\beta_{1\text{-}42}$.

6.1.2 Aims

[1] To characterise expression of VEGFR1 and VEGFR2 on HBMECs and HBVPs by immunofluorescence.

[2] To measure the level of VEGFR1 and VEGFR2 on HBMECs in normoxic and hypoxic conditions by ELISA, with and without exposure of the cells to $A\beta_{1-40}$ or $A\beta_{1-42}$.

[3] To measure the level of sVEGFR1 in the culture medium of HBMECs grown in normoxic and hypoxic conditions by ELISA, with or without exposure of the cells to $A\beta_{1-40}$ or $A\beta_{1-42}$.

[4] To measure the level of VEGFR1 and VEGFR2 in HBVPs in normoxic and hypoxic conditions by ELISA, with or without exposure of the cells to $A\beta_{1-40}$ or $A\beta_{1-42}$.

[5] To measure the level of sVEGFR1 in the culture medium of HBVPs grown in normoxic and hypoxic conditions by ELISA, with or without exposure of the cells to $A\beta_{1-40}$ or $A\beta_{1-42}$.

6.2 Methods

6.2.1 HBMEC culture

HBMECs were sourced from ScienCell and maintained in accordance with supplier's directions and as described in 2.13.5. Plates and coverslips were coated in fibronectin overnight at a concentration of 2 µg/cm^2 in Ca^{2+} and Mg^{2+}-free PBS and then washed twice in dH_2O. Cells were seeded at $1.5x10^4$ cells per well in a 24 well plate to prepare for immunofluorescence.

6.2.2 HBVP culture

HBVP were cultured and maintained by Scott Miners of the Dementia Research Group, University of Bristol, UK. HBVPs were sourced from ScienCell and maintained in accordance with supplier's directions and as described in 2.13.6. Plates and coverslips were coated and poly-L-lysine (ScienCell) at a concentration of 2 µg/cm^2 in dH_2O for 1 hour and then washed twice with dH_2O. Cells were seeded at $3x10^4$ cells per well in a 24-well plate to prepare for immunofluorescence.

6.2.3 Aβ preparation

$A\beta_{1-40}$ (Anaspec, AS-24236) and $A\beta_{1-42}$ (Anaspec, AS-24224) were lyophilised in 35% acetonitrile-H_2O and added to cells at a final concentration of 1 µM. This concentration was selected as it represents a physiologically relevant level of Aβ present in the brain. Levels of soluble $A\beta_{1-40}$ and $A\beta_{1-42}$ measured in human brain were shown in Chapter 5 and did not exceed 1 µM.

6.2.4 Hypoxic chamber

Hypoxia workstation (Ruskin SCI-tive) was set to 2% O_2 and 5% CO_2 and a temperature of 37°C.

6.2.5 Exposure of cells to $A\beta_{1-40}$, $A\beta_{1-42}$ and hypoxia

HBMEC and HVPCs were seeded in T75 flasks or on coverslips as described in 6.2.1 and 6.2.2. Once cells were 90% confluent, complete medium was exchanged for serum free medium prepared as detailed in (2.13.5 and 2.13.6). 6 flasks were prepared for each cell type according to the conditions outlined in Table 6-1. Following exposure, cells were processed as detailed in 6.2.6 and 6.2.7. Each experiment was repeated at least 3 times.

Normoxia 24 hours	**1.**	**Serum free medium**
	2.	**Serum free medium + 10 µg/ml $A\beta_{1-40}$**
	3.	**Serum free medium + 10 µg/ml $A\beta_{1-42}$**
Hypoxia (2%) 24 hours	1.	Serum free medium
	2.	Serum free medium + 10 µg/ml $A\beta_{1-40}$
	3.	Serum free medium + 10 µg/ml $A\beta_{1-42}$

Table 6-1 Experimental conditions for exposure of HBMECs and HBVPs to $A\beta_{1-40}$, $A\beta_{1-42}$ and hypoxia.

6.2.6 Cell lysis

Conditioned media was collected from cells and stored at −80°C until use. Cells were detached from the flask using accutase (Sigma) and incubated for 5 minutes at 37°C. PBS was added to the flask to make 10 ml in total and the tube centrifuged at 200 g to produce a pellet. The pellet was washed in 1 ml of PBS and transferred to a 1.5 ml tube and centrifuged again. Finally, PBS was removed, and the pellet was re-suspended in 90 µl of lysis buffer (CelLytic M Cell Lysis reagent, Sigma). Total protein level was measured as described in 2.3 and lysates stored at −80°C until required.

6.2.7 Immunofluorescence

Coverslips were washed in 100% ethanol and autoclaved prior to use. Coverslips were coated as required and washed in dH_2O. Cells were plated at the desired density and left to adhere overnight. Serum free media was removed, and cells gently washed in PBS. Cells were then fixed using 4% paraformaldehyde in PBS at room temperature for 10 minutes, permeabilised with methanol if required, and washed 3 times in PBS. Cells were incubated with 3% BSA-PBST or normal serum for 1 hour at room temperature to block non-specific binding. Desired concentration of primary antibody was prepared in 1% BSA-PBST and cells were incubated overnight at 4°C. Cells were washed 3 times in PBS and incubated with secondary antibody in 1% BSA-PBST for 1 hour in the dark at room temperature. Cells were washed 3 times with PBS and mounted using mounting medium containing DAPI to counterstain cell nuclei. Coverslips were sealed on slides using nail varnish to prevent

drying. Coverslips were imaged on a fluorescent microscope using 488 nm laser to visualise the protein of interest and 405 nm laser to visualise DAPI. Both images were then overlaid. No primary controls were performed for each of the immunoglobulins tested. HBMECs were imaged at passage 2 (p2) and pericytes were imaged at p6.

vWF was used as an endothelial marker. Fibroblast surface protein (FSP) was used a fibroblast marker. Fibroblast surface protein was chosen as it has been reported to be specific to fibroblasts unlike more traditional markers such as vimentin that may be able to recognise multiple cell types. Details of antibody conditions and concentrations are presented in Table 6-2. Initial pericyte characterisation of HBVPs was carried out by Scott Miners of the Dementia Research Group, University of Bristol, UK. Platelet derived growth factor receptor-β (PDGFRβ) was used as a pericyte marker. As pericytes express smooth muscle actin (SMA), although it is not specific for this cell type, antibody to SMA was also used for assessment.

Protein	Permeabilisation and block	Manufacturer, Catalogue number	Primary antibody concentration	Secondary antibody conditions
FSP	3% BSA-PBST	Abcam, Ab11333	1/100 1/200 1/500	1/500 Goat anti-mouse IgM Alexa Fluor 488
PDGFRβ	100% Methanol, 5% donkey serum:PBS 0.1% triton X-100	ThermoFisher, RB-1692	1/10 1/20 1/50	1/500 Donkey anti-rabbit IgG Alexa Fluor 488
SMA	100% methanol, 5% donkey serum:PBS 0.1% tritton X-100	Abcam, Ab5694	1/100 1/500 1/1000	1/500 Donkey anti-rabbit IgG Alexa Fluor 488
VEGFR1	3% BSA-PBST	Abcam, Ab32152	1/100 1/200 1/500	1/500 Donkey anti-rabbit IgG Alexa Fluor 488
VEGFR2	3% BSA-PBST	Cell signalling, #2472	1/100 1/200 1/500	1/500 Donkey anti-rabbit IgG Alexa Fluor 488
VWF	3% BSA-PBST	Dako, A0082	1/100 1/200 1/500	1/500 Donkey anti-rabbit IgG Alexa Fluor 488

Table 6-2 Antibodies used for immunofluorescence of HBMECs and HBVPs. FSP was used as a fibroblast marker. SMA and PDGFRβ were used as a pericyte markers. VWF was used as an endothelial marker.

6.2.8 VEGFR1 ELISA

A human total VEGFR1 (FLT1) duoset IC ELISA kit was used to measure VEGFR1 protein level in cell culture supernatant and conditioned media. The ELISA kit had been validated for use on cell culture supernatant, serum and plasma samples by the manufacturer. The ELISA was performed as detailed in 3.4.1.2. Briefly, cell culture supernatant was diluted 1:20 with 1% BSA-PBS and conditioned media was added neat. 50 µl of standard and diluted sample was added to each well. Samples were measured in triplicate on the plate. Readings were

blank corrected, and a 7-point curve was constructed from VEGFR1 recombinant standards and sample values were interpolated.

6.2.9 VEGFR2 ELISA

A human total VEGFR2 (KDR) duoset IC ELISA kit was used to measure VEGFR2 protein level in cell culture supernatant. The ELISA kit had been validated for use on cell culture supernatant, serum and plasma by the manufacturer. The ELISA was performed as detailed in 4.4.1.2. Briefly, cell culture supernatant was diluted 1:10 with reagent diluent #14. Fifty µl of standard and diluted sample was added to each well. Samples were measured in triplicate on the plate. Readings were blank corrected, and a 7-point curve was constructed from VEGFR2 recombinant standards and sample values were interpolated.

6.2.10 Statistics

The Kruskal-Wallis test was used to test for significant difference between three or more groups. If the Kruskal-Wallis test indicated a significant difference in median values, Dunn's post-hoc test was used to assess pairwise significance between the mean rank of the control group and all other groups. Median and interquartile range are displayed on scatter bars.

6.3 Results

Immunofluorescence was first performed to characterise HBMECs and HBVPs and to identify any visible changes in receptor labelling in the presence of $A\beta_{1\text{-}40}$ or $A\beta_{1\text{-}42}$, with and without hypoxia. This was followed by measuring the level of the receptor proteins by ELISA. Work in Chapter 3 identified changes in the sVEGFR1 level in the AD parietal cortex compared to control. ELISA of the culture medium of the cells allowed the quantification of sVEGFR1 production.

6.3.1 Characterisation of HBMECs

To establish the phenotype of HBMECs, immunofluorescence was used to identify endothelial cell markers and the presence of VEGFR1 and VEGFR2. Endothelial cells are known to differentiate into fibroblasts with increasing passage. An endothelial marker, vWF, and a fibroblast marker, FSP, were used to establish the phenotype of HBMECS. VEGFR2 itself is also used as a marker for endothelial cells and endothelial progenitors [365, 366]. HBMECs clearly expressed vWF in Figure 6-1. Some expression of fibroblast surface protein was also observed. VEGFR1 was clearly observed in all HBMECs and VEGFR2 was also detectable, though to a lesser extent. No primary controls are shown in the Appendix 28.

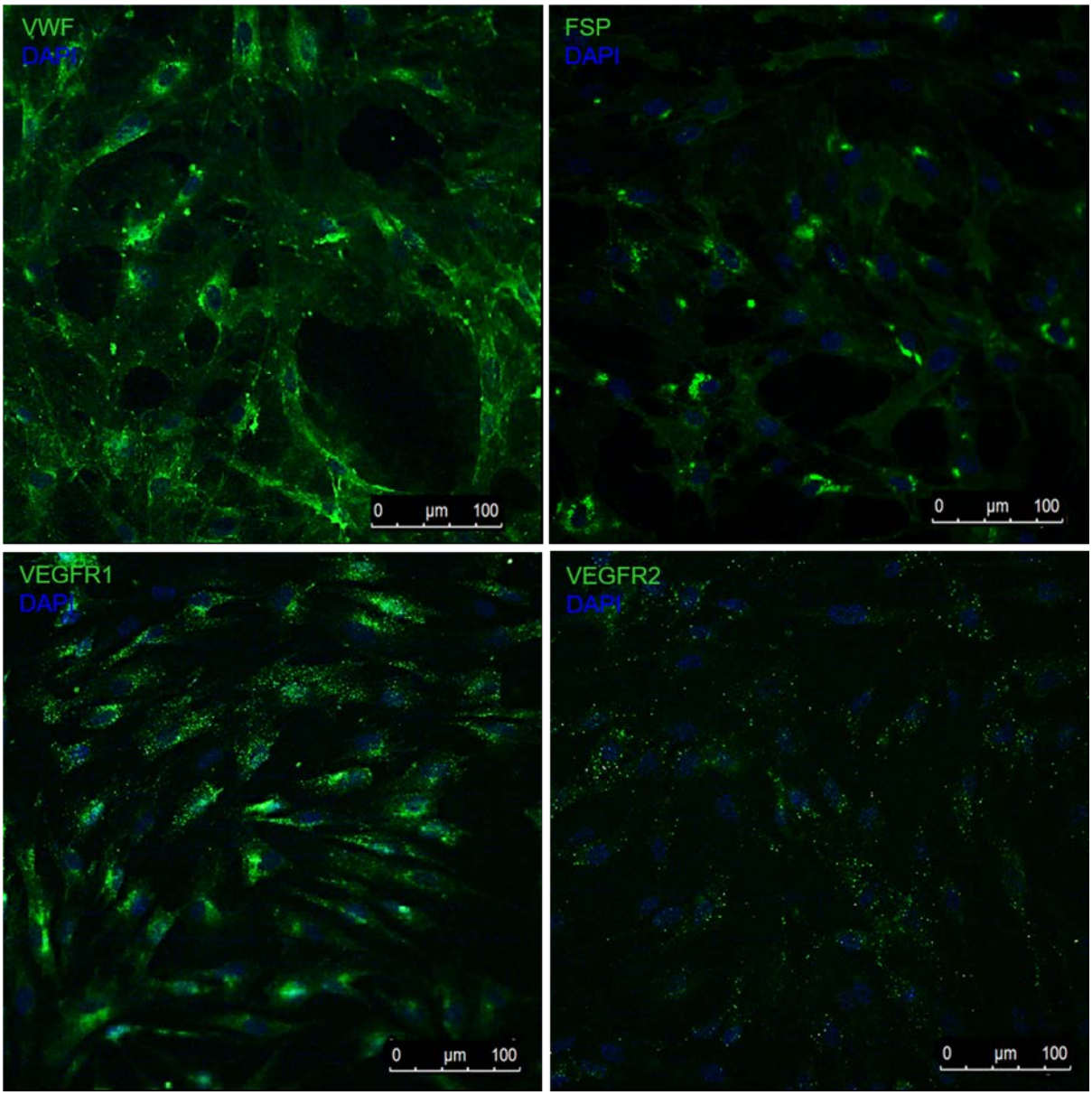

Figure 6-1 Characterisation of HBMECs. [A] HBMECs were immunopositive for VWF. VWF is a marker of endothelial cells. [B] HBMECs were weakly positive for FSP. FSP is a marker of fibroblasts. [C] HBMECs expressed VEGFR1. VEGFR1 appears expressed on the cell surface with some evidence of colocalization around the nucleus in some cells. [D] HBMECs expressed VEGFR2. VEGFR2 appears expressed uniformly on the cell surface. VEGFR2 was expressed to a lesser extent that VEGFR1.

6.3.2 VEGFR1 immunofluorescence in HBMECs exposed to hypoxia, and $A\beta_{1-40}$ or $A\beta_{1-42}$

Immunofluorescence of VEGFR1 after cells were exposed to hypoxia, and $A\beta_{1-40}$ or $A\beta_{1-42}$ (Figure 6-2). Cells were positive for VEGFR1 in all conditions. VEGFR1 expression appeared to be induced by $A\beta_{1-40}$ or $A\beta_{1-42}$, particularly under hypoxic conditions.

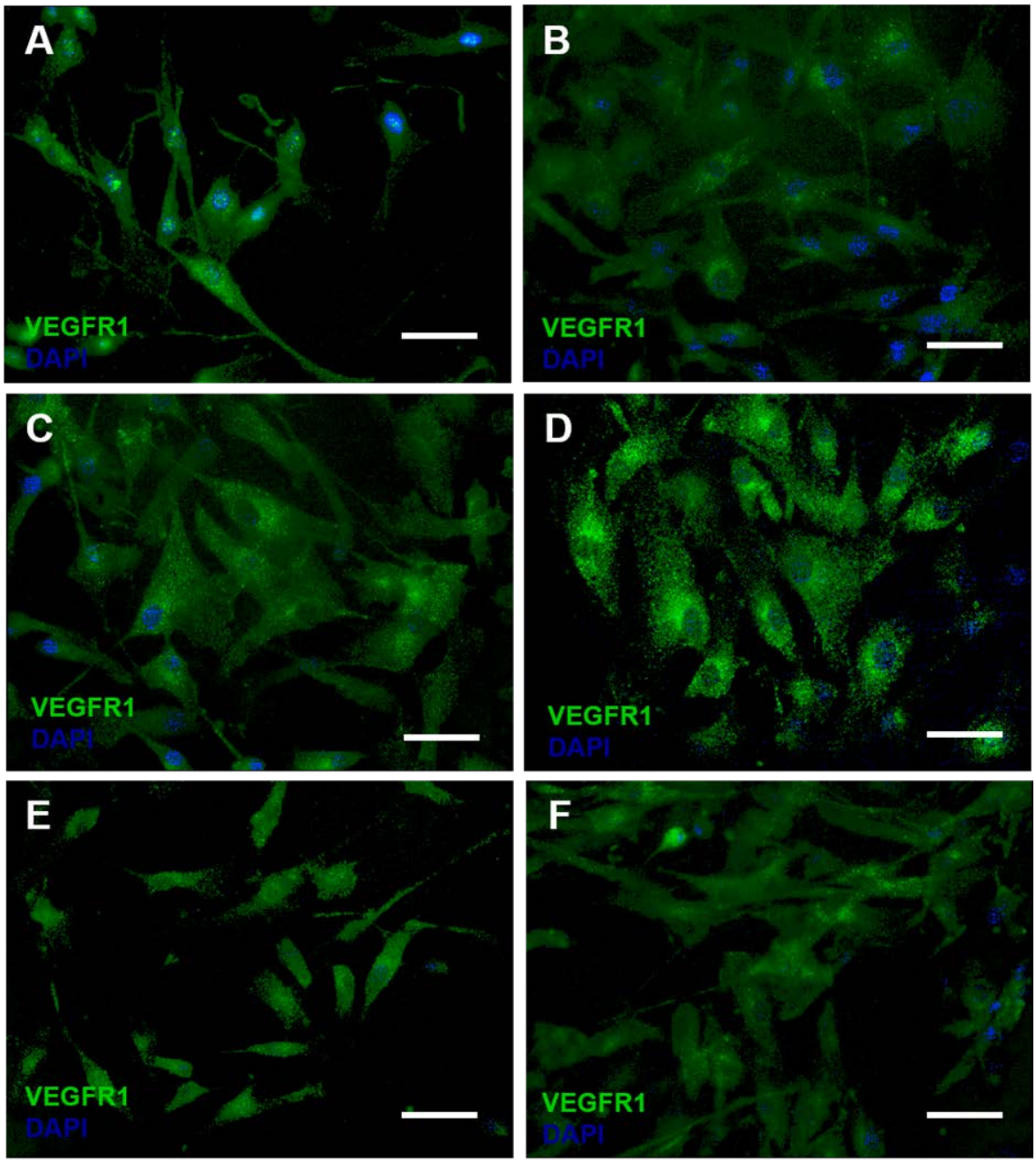

Figure 6-2 VEGFR1 immunofluorescence in HBMECs exposed to hypoxia, $A\beta_{1-40}$ or $A\beta_{1-42}$. [A] VEGFR1 was detected on HBMECs in normoxia. [B] VEGFR2 was detected on HBMECs in hypoxic conditions. There were no observable difference between VEGFR1 expression under hypoxia compared to normoxia. [C] VEGFR1 was detected on HBMECs exposed to $A\beta_{1-40}$. The expression of VEGFR1 appeared induced by $A\beta_{1-40}$ when compared to normoxia. [D] VEGFR1 was detected on HBMECs exposed to $A\beta_{1-40}$ in hypoxic conditions. The expression of VEGFR1 appeared induced by hypoxia and $A\beta_{1-40}$ when compared to normoxia and $A\beta_{1-40}$. [E] VEGFR1 was detected on HBMECs exposed to $A\beta_{1-42}$. The expression of VEGFR1 appeared induced by $A\beta_{1-42}$ when compared to normoxia. [F] VEGFR1 was detected on HBMECs exposed to $A\beta_{1-42}$ in hypoxic conditions. The expression of VEGFR1 appeared induced by hypoxia and $A\beta_{1-42}$ when compared to normoxia and $A\beta_{1-42}$. Scale bar represents 100 µm.

6.3.3 Effect of hypoxia, and Aβ$_{1-40}$ or Aβ$_{1-42}$ on VEGFR1 and sVEGFR1 levels in HBMECs

There was no significant effect of hypoxia, Aβ$_{1-40}$, or Aβ$_{1-42}$ on the level of VEGFR1 in HBMECs (Figure 6-3A). The cell-conditioned culture medium was collected from each treatment group and VEGFR1 ELISA used to measure the level of sVEGFR1. There was a significant difference the groups (p= 0.009, Figure 6-3B). Pairwise analysis revealed a significant increase in sVEGFR1 level in HBMECs under conditions of hypoxia (p< 0.01; M= 129.9, IQR= 41.1, n= 8), hypoxia with Aβ$_{1-40}$ (p< 0.05, M= 125.8, IQR= 44.4, n= 6) and hypoxia with Aβ$_{1-42}$ (p< 0.05, M= 111.6, IQR= 43.3, n= 6) compared to normoxia (M= 100, IQR= 0, n= 8). There was no change in sVEGFR1 level in the presence of Aβ alone. Details of individual values are provided in Appendix 29.

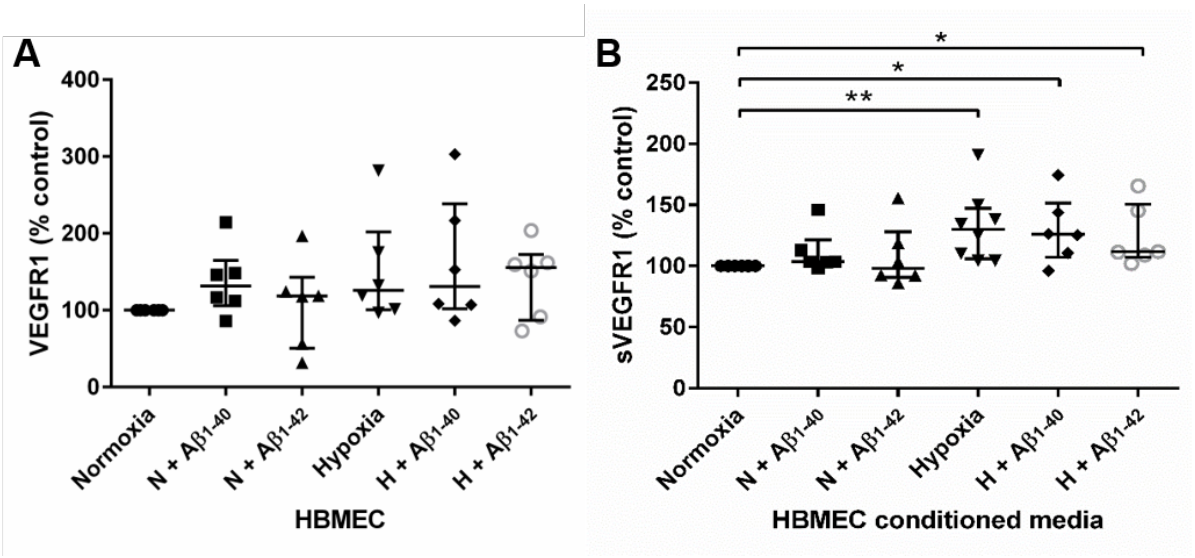

Figure 6-3 VEGFR1 and sVEGFR1 levels in HBMECs lysate and conditioned media as measured by VEGFR1 ELISA. All groups are normalised to the control group (normoxia) and displayed as a percentage of control. [A] VEGFR1 level in HBMEC lysate in the presence of hypoxia ± Aβ$_{1-40}$, or Aβ$_{1-42}$. There was no significant difference between normoxic conditions and cells under incubated in hypoxic conditions with or without the presence of 1μM Aβ$_{1-40}$, or 1μM Aβ$_{1-42}$. [B] sVEGFR1 level in HBMEC-conditioned media under conditions of hypoxia ± Aβ$_{1-40}$ or Aβ$_{1-42}$. Kruskal Wallis test indicated a significant difference between groups compared (p= 0.009) and post-hoc tests revealed a significant increase in the level of sVEGFR1 in hypoxia (p< 0.01), hypoxia with Aβ$_{1-40}$ (p< 0.05) and hypoxia with Aβ$_{1-42}$ (p< 0.05) when compared to normoxic conditions. * = p< 0.05, ** = p<0.01*

6.3.4 VEGFR2 immunofluorescence on HBMECs exposed to hypoxia, and Aβ$_{1-40}$ or Aβ$_{1-42}$

Punctate VEGFR2 immunopositivity was detectable in the cells in all conditions studied. There was no clear change in the expression of VEGFR2 in hypoxia or in the presence of Aβ$_{1-40}$, and Aβ$_{1-42}$.

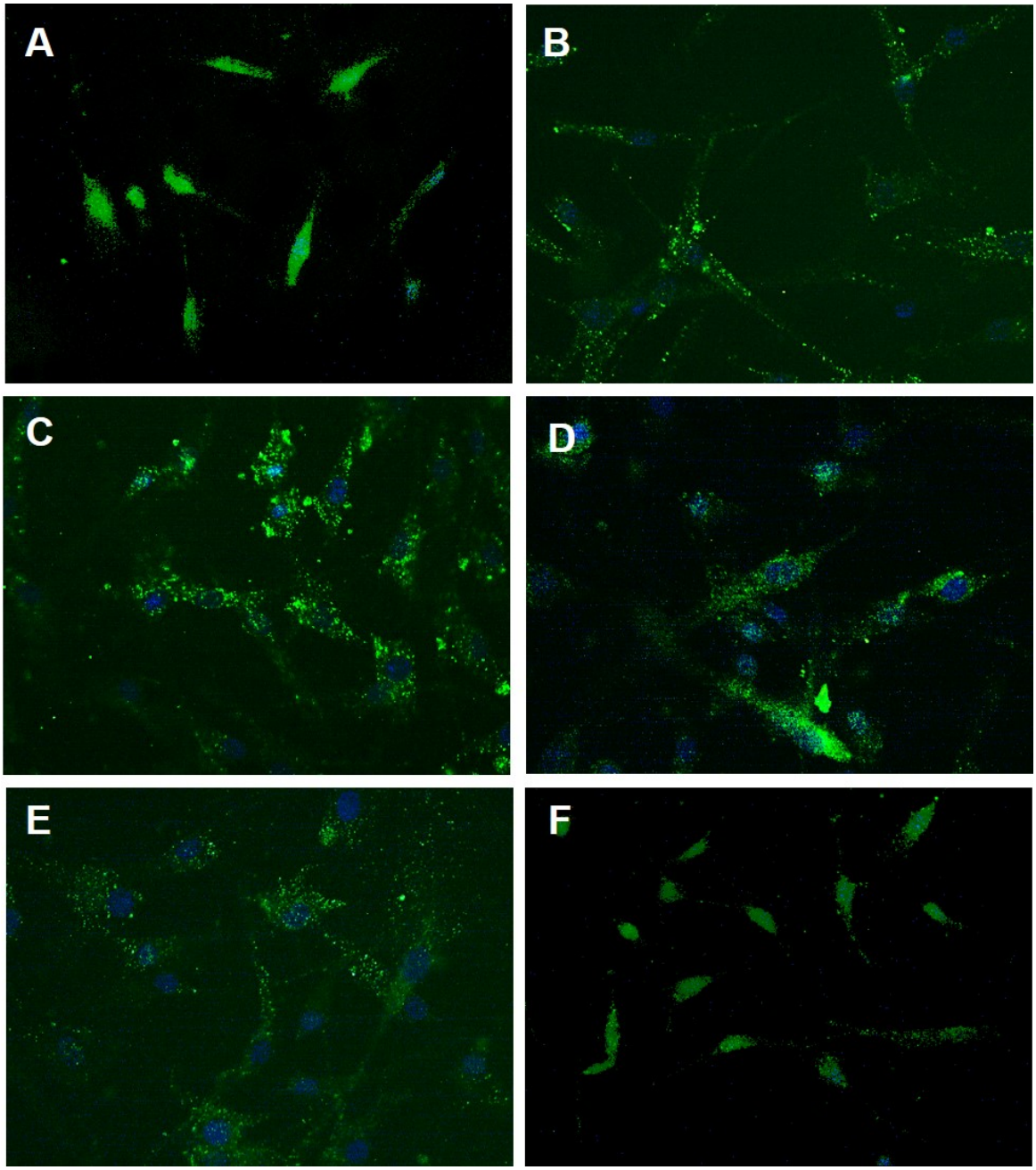

Figure 6-4 VEGFR2 immunofluorescence in HBMECs exposed to hypoxia, $A\beta_{1-40}$ or $A\beta_{1-42}$. [A] VEGFR2 was detected on HBMECs in normoxia. [B] VEGFR2 was detected on HBMECs in hypoxic conditions. There were no observable differences between VEGFR2 expression under hypoxia conditions compared to normoxia. [C] VEGFR2 was detected on HBMECs exposed to $A\beta_{1-40}$. There were no observable differences between VEGFR2 expression in the presence of $A\beta_{1-40}$ when compared to normoxia. [D] VEGFR2 was detected on HBMECs exposed to $A\beta_{1-40}$ in hypoxic conditions. [E] VEGFR2 was detected on HBMECs exposed to $A\beta_{1-42}$. here were no observables difference between VEGFR2 expression in the presence of $A\beta_{1-42}$ compared to normoxia. [F] VEGFR2 was detected on HBMECs exposed to $A\beta_{1-42}$ in hypoxic conditions. Scale bar represents 100 µm.

6.3.5 Characterisation of HVPCs

To establish the phenotype of pericytes, immunofluorescence was used to identify cell markers and the presence of VEGFR1 and VEGFR2. PDGFRβ and SMA are established markers of pericytes and were expressed on cultured pericytes as shown in Figure 6-4. VEGFR1 was strongly expressed on pericytes in normoxia. VEGFR2 was expressed on pericytes but to a lesser extent than VEGFR1. No primary controls are presented in the Appendix 28.

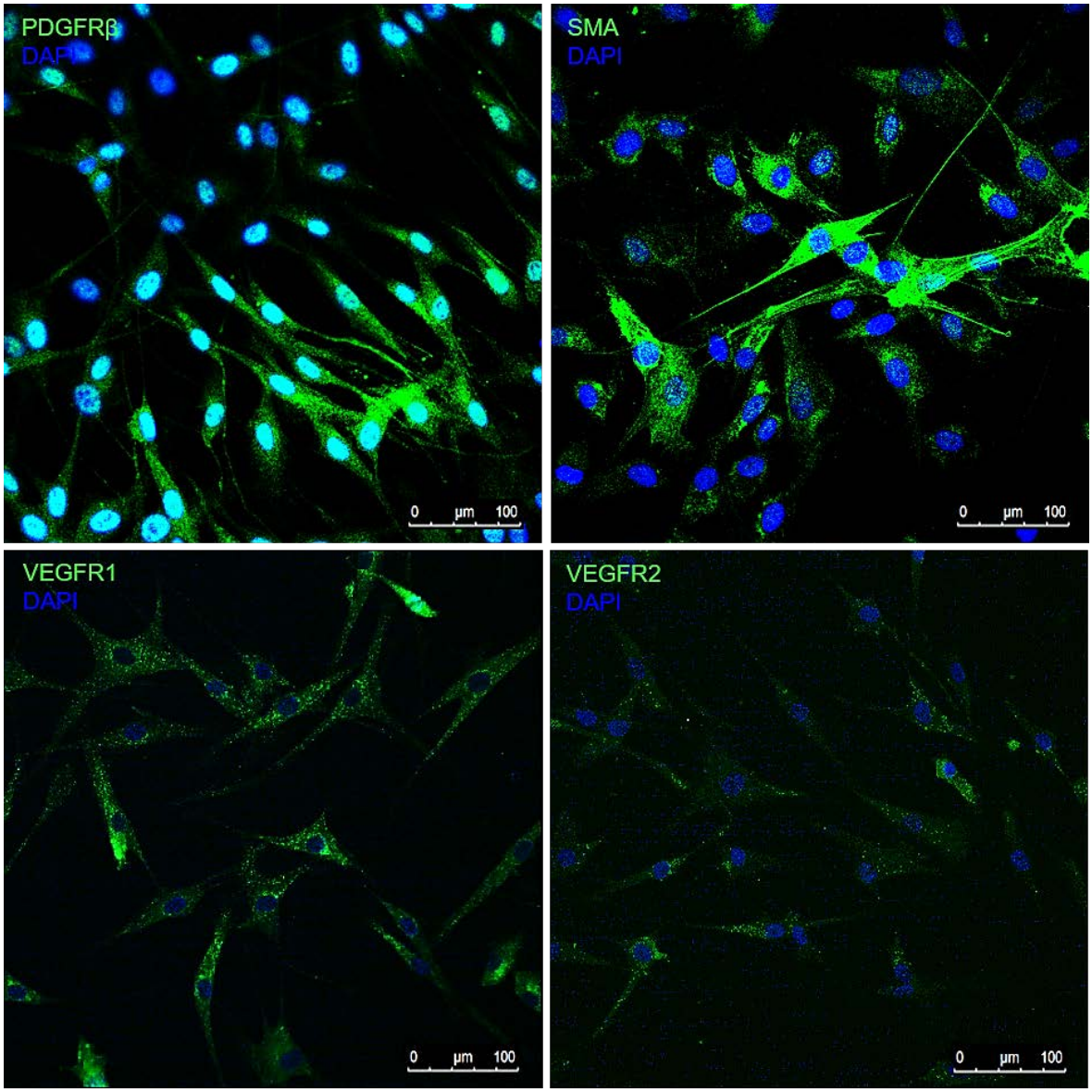

Figure 6-5 Characterisation of HBVPs. [A] HBVPs were positive for PDGFRβ which is a marker of pericytes. [B] HBVPs were positive for SMA which is an additional marker of pericytes. [C] VEGFR1 was clearly detected on HBVPs. [D] VEGFR2 was detected on HBVPs. VEGFR2 expression appeared less than VEGFR1.

6.3.6 VEGFR1 immunofluorescence on HBVPs exposed to hypoxia, and $A\beta_{1-40}$, or $A\beta_{1-42}$

Immunofluorescence showed VEGFR1 in the cells in all conditions (Figure 6-5). There appeared to be a reduction in VEGFR1 under conditions of hypoxia + $A\beta_{1-40}$.

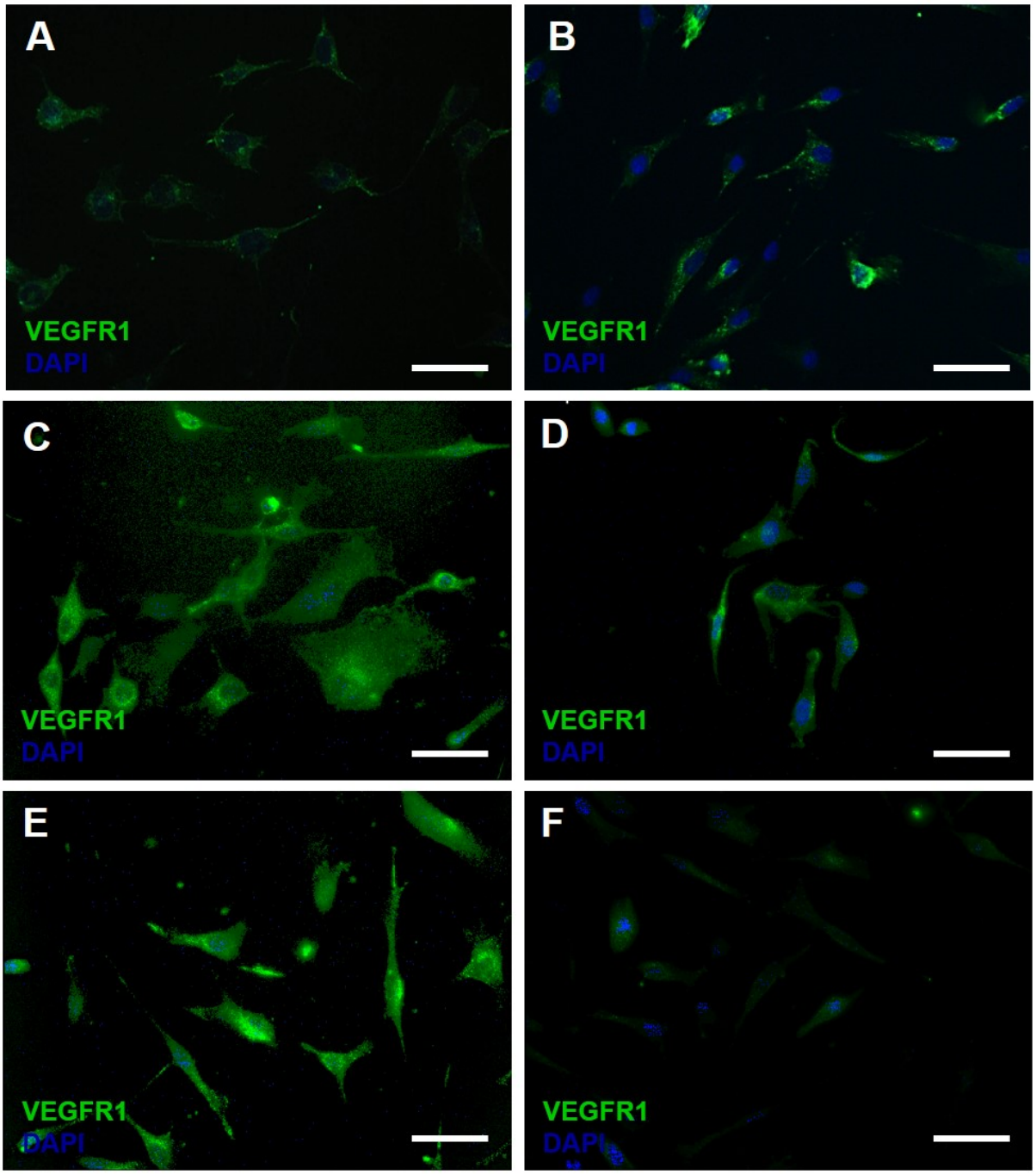

Figure 6-6 VEGFR1 immunofluorescence in HBVPs exposed to hypoxia, $A\beta_{1-40}$ or $A\beta_{1-42}$. [A] VEGFR1 was expressed on HBVPs in normoxia. [B] VEGFR1 was expressed on HBVPs in hypoxic cells. There was no observable visual difference when compared to VEGFR1 expression in normoxia. [C] VEGFR1 was expressed on cells in the presence of $A\beta_{1-40}$. There was no observable visual difference between HBVPs in normoxia alone. [D] VEGFR1 was

expressed on HBVPs in the presence of hypoxia and Aβ$_{1-40}$. There appeared to be a reduction in VEGFR1 under conditions of hypoxia + Aβ$_{1-40}$ when compared to Aβ$_{1-40}$ in normoxia and hypoxia alone. [E] VEGFR1 was expressed on HBVPs in the presence of Aβ$_{1-42}$. There was no observable difference when compared to other conditions. [F] VEGFR1 was expressed on HBVPs in the presence of hypoxia and Aβ$_{1-42}$. There was no observable difference when compared to other conditions. Scale = 50 µm

6.3.7 Effect of hypoxia, and Aβ$_{1-40}$ or Aβ$_{1-42}$, on VEGFR1 and sVEGFR1 in HBVPs

There was no significant change in the level of VEGFR1 in HBVPs under conditions of hypoxia, and Aβ$_{1-40}$ or Aβ$_{1-42}$ (Figure 6-6A). There was a trend towards an increase in VEGFR1 in the presence of hypoxia and either Aβ$_{1-40}$ or Aβ$_{1-42}$, compared to normoxia.

There was a significant difference in sVEGFR1 level between the groups (p= 0.032, Figure 6-6B). Pairwise analysis revealed that the level of sVEGFR1 was significantly increased in hypoxia (p< 0.05, M= 141.4, IQR= 150.9, n= 8) when compared to normoxia (M= 100, IQR= 0, n= 8). There was no significant change in sVEGFR1 level in normoxia or hypoxia, and when Aβ species were present. There seemed to be a reduction in sVEGFR1 level in hypoxia in the presence of Aβ$_{1-40}$, but on analysis this was shown not to be significant. Details of individual values are provided in Appendix 30.

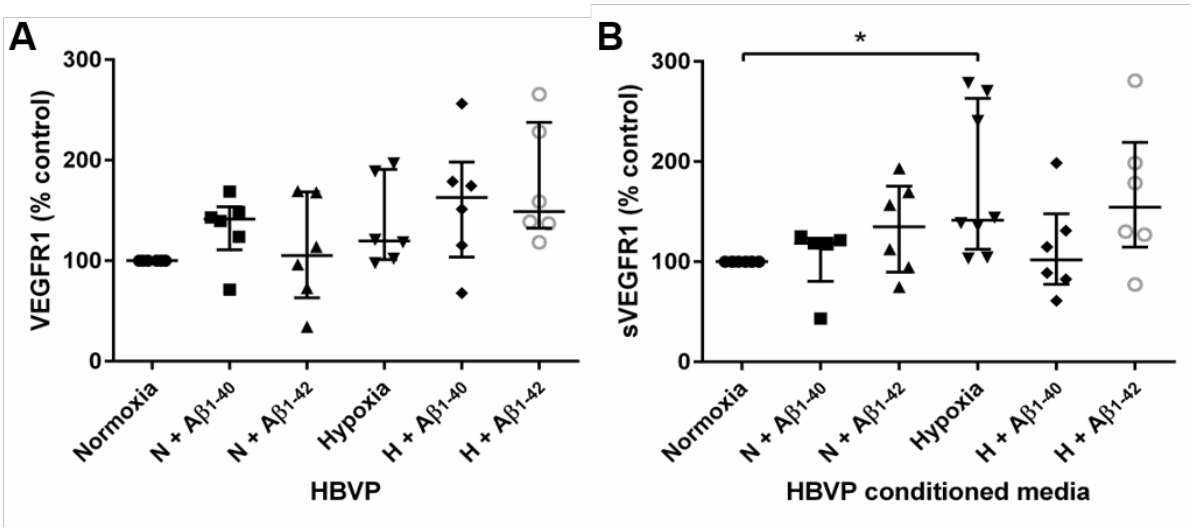

Figure 6-7 VEGFR1 and sVEGFR1 levels in HBVPs lysate and conditioned media as measured by VEGFR1 ELISA. All groups are normalised to the control group (normoxia) and displayed as a percentage of control. [A] VEGFR1 level in HBVP exposed to hypoxia ± Aβ$_{1-40}$, and Aβ$_{1-42}$. No significant difference was reported between the groups (p= 0.078). [B] sVEGFR1 level in HBVP conditioned media exposed to hypoxia ± Aβ$_{1-40}$, and Aβ$_{1-42}$. A significant difference was reported between groups (p= 0.032). Pairwise comparison revealed a significant increase in the level sVEGFR1 in hypoxic conditions (p< 0.05). * p< 0.05.

6.3.8 VEGFR2 immunofluorescence on HVPCs exposed to hypoxia, and $A\beta_{1-40}$ or $A\beta_{1-42}$

There was punctate VEGFR2 immunolabelling of the cells in all conditions (Figure 6-7) but no clear change in the expression of VEGFR2 in hypoxia or in the presence of $A\beta_{1-40}$ or $A\beta_{1-42}$.

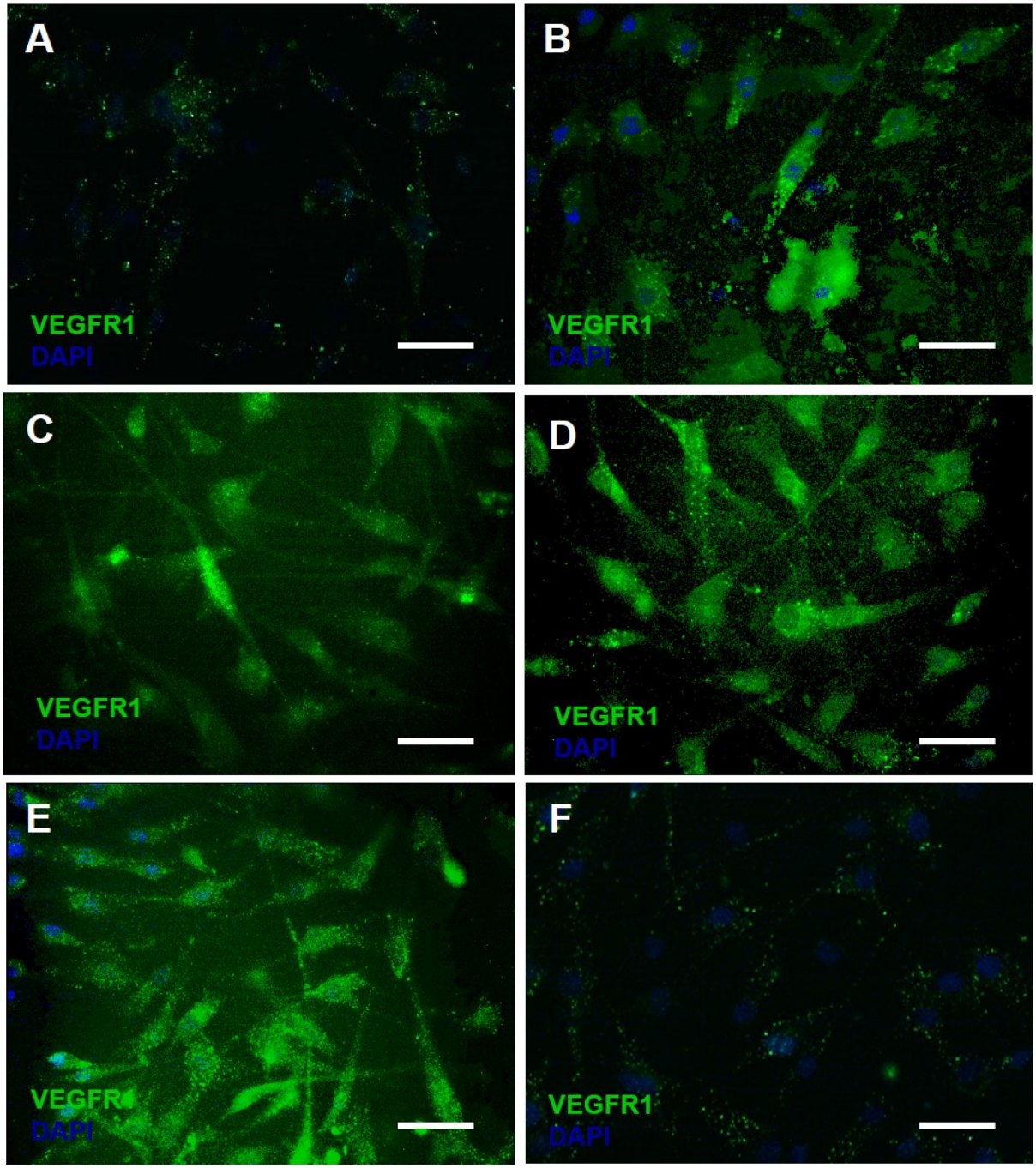

Figure 6-8 VEGFR2 immunofluorescent labelling of HBVPs exposed to hypoxia, $A\beta_{1-40}$ or $A\beta_{1-42}$. [A] VEGFR2 was detectable in the HBVPs in normoxia. [B] VEGFR2 was expressed on HBVPs in hypoxic cells. There was no observable visual difference when compared to VEGFR2 expression in normoxia. [C] VEGFR2 was expressed on cells in the presence of $A\beta_{1-40}$. There

was no observable difference between HBVPs in normoxia alone. [D] VEGFR2 was expressed on HBVPs in the presence of hypoxia and Aβ$_{1-40}$. There was no observable difference compared to Aβ$_{1-40}$ in normoxia and hypoxia alone. [E] VEGFR2 was expressed on HBVPs in the presence of Aβ$_{1-42}$. There was no observable difference when compared to other conditions. [F] VEGFR2 was expressed on HBVPs in the presence of hypoxia and Aβ$_{1-42}$. There was no observable difference when compared to other conditions. Scale = 50 µm

6.3.9 Effect of hypoxia, Aβ$_{1-40}$ and Aβ$_{1-42}$ on VEGFR2 receptor levels in HBVPs

A significant difference in VEGFR2 level was found between groups (p= 0.0002, Figure 6-9). Pairwise analysis revealed a significant decrease in VEGFR2 levels in HBVP in the presence of hypoxia compared to normoxia. This significant decrease was evident with hypoxia alone (p< 0.001, M= 33.03, IQR= 22.61, n= 7), or when combined with Aβ$_{1-40}$ (p< 0.01, M= 44.08, IQR= 35.15, n=7) or Aβ$_{1-42}$ (p< 0.05, M= 41.2, IQR= 47.66, n= 7). There was no change in VEGFR2 level in the presence of Aβ alone. Details of individual values are provided in Appendix 30.

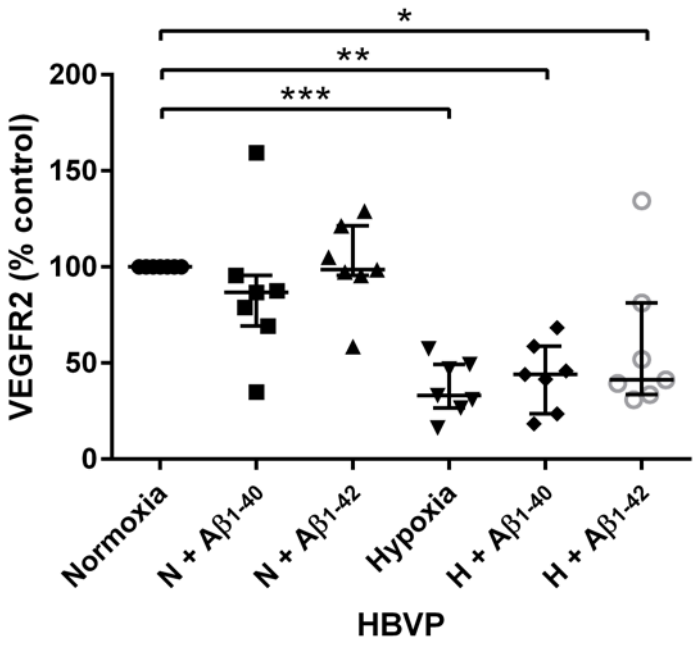

Figure 6-9 VEGFR2 level in HBVP exposed to hypoxia ± 1µM Aβ$_{1-40}$ or 1µM Aβ$_{1-42}$. A significant difference was found between the groups (p= 0.0002). Pairwise comparison revealed a significant decrease in VEGFR2 level in hypoxia (p< 0.001), hypoxia + Aβ$_{1-40}$ (p< 0.01) or hypoxia + Aβ$_{1-42}$ (p< 0.05, compared to normoxia. * p< 0.05, ** p< 0.01, *** p< 0.001.

6.4 Discussion

The HBMECs were characterised before starting any further experimental work. It was confirmed that HBMECs expressed VWF and VEGFR2 which are both makers of endothelial cells. The HBMECs also showed weak immunopositivity for FSP, a marker of fibroblasts.

This may be due to the cell line displaying both endothelial and fibroblastic characteristics at early passage. Despite the presence of the fibroblast marker, the expression of endothelium-specific markers supports their use for in vitro study of hypoxic responses of cerebral endothelial cells.

A VEGFR1 ELISA was used to measure the level of VEGFR1 in cell lysate and the level of sVEGFR1 in conditioned media. Cells were exposed to $A\beta_{1-40,}$ $A\beta_{1-42}$ in normoxic and hypoxic conditions. There was no change in the level of VEGFR1 in HBMECs under any of the conditions studied whereas the level of sVEGFR1 was significantly increased in all hypoxic conditions compared to normoxia. The increase in sVEGFR1 under hypoxic conditions is in keeping with other evidence of the role of the receptor in negative regulation of VEGF in hypoxia [143, 148]. The increase in sVEGFR1 is relevant to my findings on analysis of human brain tissue in AD, in which sVEGFR1 subtypes appeared to be increased [259], possibly in response to reduced oxygenation of the tissue in this disease. However, the unchanged level of VEGFR1 in vitro does not mirror changes in post-mortem brain tissue, in which a decrease in VEGFR1 was observed in AD. Despite repeated attempts, I was unable to measure VEGFR2 in HBMECs by ELISA. This may be due to the reduced expression of VEGFR2 on HBMECs when compared to VEGFR1 meaning the sample was below detection by the VEGFR2 ELISA. In future, it would be beneficial to increase the protein concentration of the lysate by extraction for a great number of cells. This should allow the detection of VEGFR2 by ELISA in all conditions.

Following the completion of this work, a paper was published describing measurement of the level of mbVEGFR1, sVEGFR1 and VEGFR2 mRNA as well as mbVEGFR1 and VEGFR2 protein in HUVECs and HBMECs exposed to $A\beta_{1-40}$ [367]. HUVECs were exposed to 10 μM of $A\beta_{1-40}$ for 8 hours. VEGFR1 mRNA was unchanged between $A\beta_{1-40}$-treated and control cells, while VEGFR2 mRNA was reduced significantly after $A\beta_{1-40}$ exposure. HUVECs were then exposed to 10 μM and 20 μM of $A\beta_{1-40}$ for 24 hours. Western blots displayed no change in mbVEGFR1 protein, but VEGFR2 level fell with increasing $A\beta_{1-40}$ concentration. To investigate sVEGFR1 levels the group looked at HUVECs exposed to 10 μM of $A\beta_{1-40}$ for 8 and 24 hours and HBMECs exposed to 10 μM of $A\beta_{1-40}$ for 24 hours. They found that sVEGFR1 mRNA was significantly reduced in cells exposed to $A\beta_{1-40}$. Data on sVEGFR1 protein levels were not provided. The concentration of Aβ used in that work was at least 10-fold higher than that used in the present study and the findings may therefore be less physiologically relevant. This study did not extract mRNA from cell lysate. It was thought measurement receptor proteins would provide the most physiologically relevant data and it is known that the level of mRNA does not always predict protein levels [368]. The extraction of

VEGFR1 and VEGFR2 mRNA would provide a useful addition to this study and allow direct comparison of the work.

The absence of change in the level of mbVEGFR1 in HUVECs[367] is consistent with my findings that VEGFR1 was unchanged in HBMECs when exposed to $A\beta_{1-40}$. However, as the group measured only mRNA, not protein, the results are not directly comparable and limit the usefulness of speculation as to why the authors found that exposure of the HUVECs to $A\beta_{1-40}$ caused sVEGFR1 mRNA to fall whereas I did not find a corresponding change in sVEGFR1 protein.

The group also measured sVEGFR2 mRNA and protein in HUVECs and HBMECs [367]. In the current study sVEGFR2 could not be detected in cell culture medium conditioned by HBMECs. No band for sVEGFR2 was observed using the ELISA detection antibody (Appendix 17) indicating that the antibody is specific for the intracellular domain, not present in sVEGFR2. sVEGFR2 was not of direct relevance to the investigation of disrupted VEGF angiogenesis as VEGF-C is the main ligand for sVEGFR2 which mediates lymphogenesis (1.2.2.2.1). However further understanding of the VEGF-VEGFR system in the presence of Aβ is needed. Future work could include use of the same sVEGFR2 antibody used by Cho et al. (2017) and a sVEGFR2-specific ELISA to measure sVEGFR2 after hypoxia and Aβ exposure.

HBVPs were immunopositive for two pericyte markers, SMA and PDGFRβ. Immunofluorescence showed mbVEGFR1 expression on HBVPs to be more prominent than VEGFR2 expression. Measurement of protein levels in cell lysates showed that hypoxia upregulated mbVEGFR1 in HBVP while the level of VEGFR2 was reduced. The elevation in sVEGFR1 and mbVEGFR1 in hypoxia was predicted, as hypoxia directly regulates VEGFR1 expression and mbVEGFR1. sVEGFR1 secreted from HBVPs increased in hypoxic conditions, though there was no change in sVEGFR1 in the presence of $A\beta_{1-40}$ and $A\beta_{1-42}$. VEGFR1 level displayed a non-significant trend towards an increase in hypoxic conditions. Immunofluorescence showed stronger labelling of VEGFR1 than of VEGFR2 in HBVP, which supported results of the VEGFR1 and VEGFR2 ELISAs. Upregulation of VEGFR1 in pericytes by hypoxia has previously been reported [214].

Contrary to my initial hypothesis, VEGFR2 level in HBVPs was reduced in hypoxic conditions. Hypoxia alone was enough to reduce VEGFR2 in pericytes and the presence of Aβ did not affect the level of VEGFR2. This work supports a previous study in which VEGFR2 expression in pericytes were reduced by hypoxia [214]. The presence of VEGFR2 on pericytes and its subsequent reduction in hypoxia is in keeping with the role of pericytes as support cells for endothelium in hypoxia. Pericytes are known to secrete VEGF [343] and the

reduction in VEGFR2 in pericytes under hypoxic conditions is likely to favour paracrine signalling of endothelial cells by pericyte-secreted VEGF over its autocrine activity [340].

To develop this work, several variables could be altered in future studies. In this study one hypoxia timepoint and O_2 percentage were used. This does not reflect physiological conditions in the human brain in dementia but was an acute model to gain initial insights into the receptor system. Similarly, one concentration of $A\beta_{1-40}$ or $A\beta_{1-42}$ was used. In future work, it would be of interest to examine the effects of several O_2 and Aβ concentrations to establish the dose responses in both cell types. It would also be useful to quantify the immunofluorescent labelling of mbVEGFR1 and VEGFR2 in both cell types, with or without hypoxia and additional exposure to $A\beta_{1-40}$ or $A\beta_{1-42}$ to complement the ELISA measurements of these receptor proteins. Further investigation into phosphorylation would provide information about the functional level of receptors under hypoxia and in the presence of Aβ. The sVEGFR2 ELISA and/or anti-p-VEGFR2 antibodies could be tested and used to indicate the phosphorylation level in both cell types. In addition, data on the functional implications for hypoxia and Aβ on both types could be measured. A tube-formation assay for could be used to measure the effect of hypoxia and Aβ on HBMEC ability to form capillary-like structures. A proliferation assay combined with a cell live/dead assay could be used to assess the effect of hypoxia and Aβ on pericytes. These assays would provide further insight into the effect of hypoxia and Aβ on the VEGF system, as VEGF is known to stimulate both proliferation and migration by its action on VEGFR1[106] and VEGFR2 [129, 168].

In conclusion, the level of sVEGFR1 increased in hypoxia in HBMECs and pericytes, while there was no change in mbVEGFR1 level. The level of VEGFR2 in pericytes decreased in hypoxia. The findings support other evidence that VEGFR1 is the main VEGF signal mediator in pericytes and is in keeping with the previously described role of pericytes as important vasculotropic cells in hypoxia. Aβ alone did not have a significant effect on the level of receptors in either cell type.

Chapter 7 Discussion

In this thesis, human tissue and cell-based work was used to expand the literature on VEGFR1 and VEGFR2 in AD and VaD. This chapter will provide an overview of the main findings, their implications and future work.

7.1 Are VEGFR1 and VEGFR2 altered in the AD brain?

The localisation, mRNA and protein level of VEGFR1 and VEGFR2 were measured in human control and AD brain tissue, as described in Chapters 3 and 4 respectively. Localisation of receptors was unchanged in the AD brain compared to control. The mRNA level of both proteins was significantly increased in AD compared to control. This was hypothesised as the presence of cerebral hypoperfusion and resulting hypoxia would increase transcription of VEGFR1 and the increase in VEGF concentration would increase VEGFR2 transcription. This study supports previous work in animal models of hypoxia showing elevated VEGFR1 [127, 229-231] and VEGFR2 [253 301 302] levels when compared to normoxia.

Unexpectedly, the level of total VEGFR1 protein was reduced in AD compared to control while the relative level of sVEGFR1 was increased. The increased proportion of sVEGFR1:mbVEGFR1 in AD may contribute to the lack of microvessel growth in AD despite elevated levels of VEGF. The unchanged level of VEGFR2 protein indicates that the impaired angiogenic response in AD is not caused by deficiency of this receptor.

An interpretation of the relevance of VEGFR1 and VEGFR2 in the context of vascular homeostasis and hypoperfusion of the parietal cortex in AD is summarised in Figure 7-1. Numerous factors may contribute to the reduced CBF in early AD, including cerebrovascular pathology, a reduction in cholinergic innervation and an increase in vasoconstrictors (Figure 7-1). Reduced tissue oxygenation is thought to induce the increase in VEGF but is not associated with a corresponding increase in vWF in the parietal lobe. The increase in proportion of sVEGFR1 is a possible contributor to this disparity, but other abnormalities of VEGFR1 or VEGFR2 receptor signalling or VEGF metabolism (see below) cannot be excluded.

In this study only those with late stage, established AD were studied. At this stage of disease, we are limited by the possible ceiling effect of AD. Amyloid deposition and MAPT distribution is established leading to a variety of changes and delirious effects in the brain including neuronal death. Therefore, this study is unable may be too late to detect some changes that may have occurred earlier in disease.

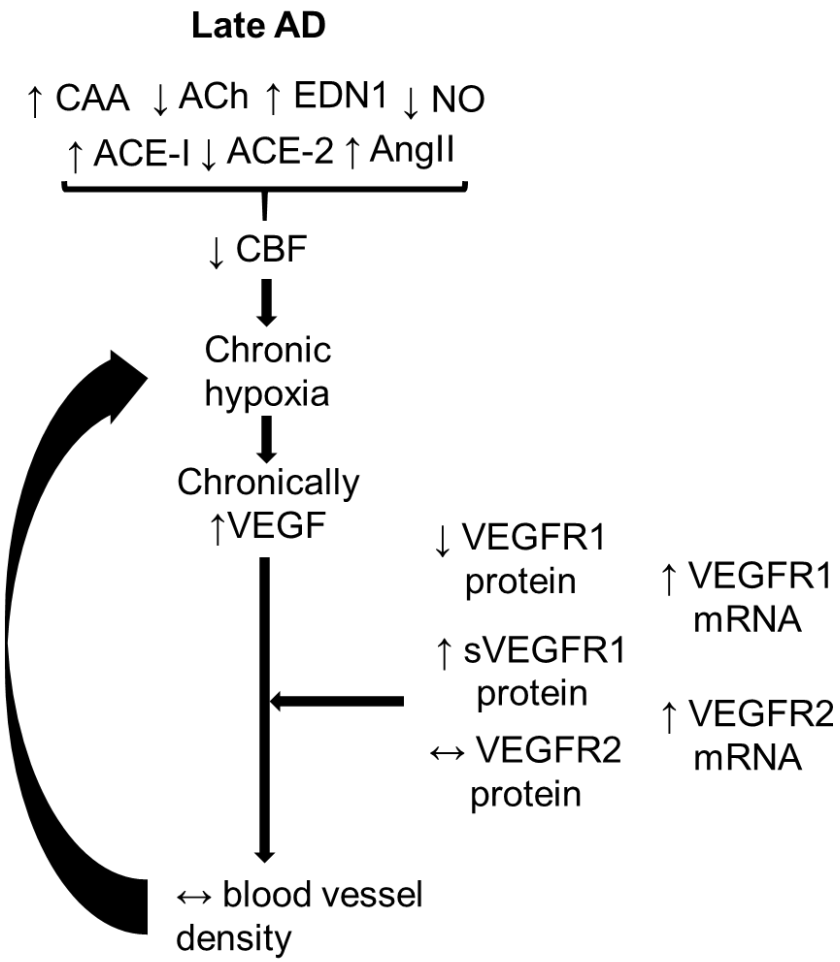

Figure 7-1 The relevance of present findings in the context of vascular homeostasis and hypoperfusion of the parietal cortex in late AD (Braak stages V and IV). CAA, decreased cholinergic innervation of intracerebral blood vessels [94, 95], reduced NO production [92, 93, 369, 370] and an increase in vasoconstrictors EDN1 [90, 226] and AngII, through upregulation of angiotensin-converting enzyme (ACE)-1 and downregulation of ACE-2 [91, 227] may all contribute to reduced CBF. Reduced tissue oxygenation leads to increased VEGF [72, 78, 198, 212, 314] that is not accompanied by an increase in vWF level [78]. Reduction in VEGFR1 is probably a physiological response to reduced oxygenation but an increase in sVEGFR1 may contribute to impaired angiogenesis. VEGFR2 level remains unchanged. Arrows denote an increase (↑) or decrease (↓) in protein in AD compared to control. Horizontal double arrow (↔) indicates no change in AD compared to controls.

As mentioned above the investigation of VEGF receptors was performed in cases with advanced AD, therefore do not reflect the changes that may have occurred in the early stages of AD. Parietal lobe one of the earliest regions of the cortex to be affected by reduced CBF [371]. This made the parietal lobe an area beneficial for investigating hypoperfusion and the chronic effects of hypoxia and Aβ on VEGF and VEGF receptors. To investigate the effect of early hypoperfusion in AD on VEGF receptors and changes over the course of disease it would be beneficial to include samples from early AD and from multiple brain areas.

Figure 7-2 presents the hypothesised changes in receptor. Reduced CBF will lead to hypoxia in the brain and an acute response which could include the upregulation of VEGFR1 and VEGFR2 protein levels. After an initial elevation in VEGFR levels, there would be a reduction in receptor concentration as the hypoxia became chronic.

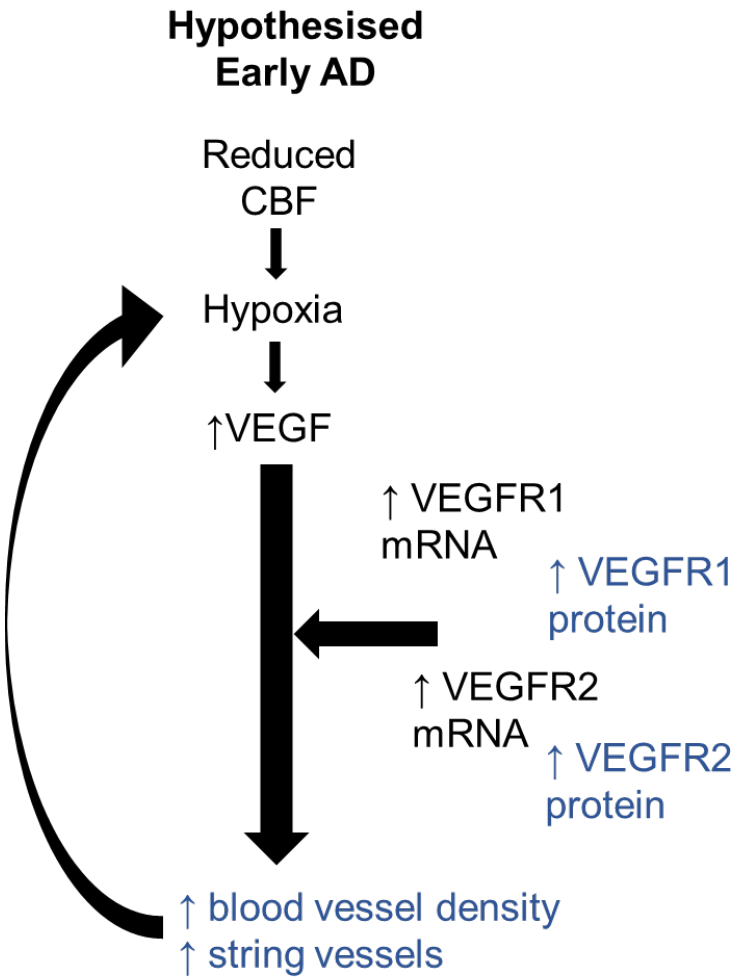

Figure 7-2 Hypothesised mechanisms in the context of vascular homeostasis and hypoperfusion of the parietal cortex in early AD (Braak stages I and II). Changes compared to late AD are written in blue text. Under acute hypoxia in very early stages of AD it is possible that VEGFR1 and VEGFR2 levels may increase resulting in increased blood vessel density.

String vessels have been reported in the AD brain which may be in part due to the initial presence of blood vessel, but due to pathological changes ongoing in AD, including the presence of Aβ. Arrows denote an increase (↑) or decrease (↓) in protein in AD compared to control. Horizontal double arrow (↔) indicates no change in AD compared to controls.

7.2 Are VEGFR1 and VEGFR2 altered in the VaD brain?

This study investigated the levels of VEGFR1 and VEGFR2 protein in VaD brain. Initial studies had found that the level of microvessel density increased as the level of VEGF increased in VaD[72]. It was hypothesised that the increase VEGF would accompany an increase microvessel density. Since VaD is defined by reduced CBF in the brain due to CAA and SVD, any increase in blood vessel density would be unlikely to result in reperfusion for large areas of the brain.

The level of VEGFR1 in VaD was not measured in this study. The level of VEGFR2 protein was unchanged compared to control and AD samples in the parietal cortex. There was a reduction in VEGFR2 level in the VaD white matter compared to AD. This indicates that the receptor level remains unchanged due to chronic hypoperfusion. In the *in vitro* experiments in this study the level of VEGFR1 and VEGFR2 were increased on endothelial cells in acute hypoxia. There may be an increase in VEGFR2 in the early stages of disease when hypoxia is acute as described above in AD.

VaD samples in this study had low levels of AD pathology and were therefore a ‘pure VaD’ cohort. VaD was studied in order to determine the effect of AD pathology on receptor expression. Aβ pathology was not present, or present in minimal amounts, compared to AD. As both AD and VaD samples showed no change in VEGFR2 level when compared to control it could be determined that VEGFR2 level is not influenced by Aβ pathology.

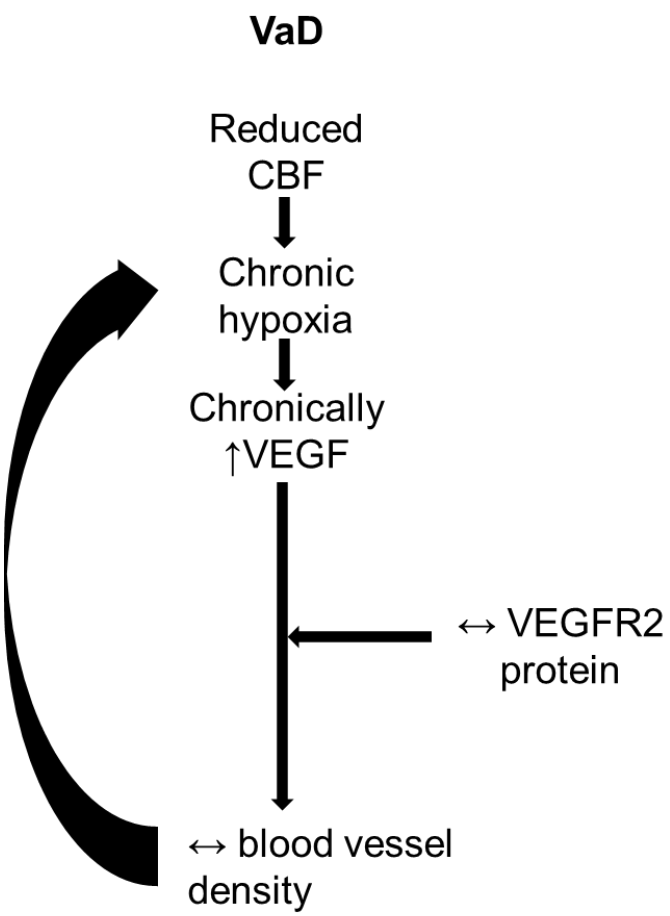

Figure 7-3 VaD mechanisms in the context of vascular homeostasis and hypoperfusion of the parietal cortex in VaD. CBF in VaD is reduced leading to chronic hypoxia and neuronal death in VaD. Chronically elevated would result from ongoing hypoxic conditions. Despite increased VEGF There was no change in blood vessel density in VaD. With no increase in blood vessel density the hypoxic condition remains. Arrows denote an increase (↑) or decrease (↓) in protein in VaD compared to control. Horizontal double arrow (↔) indicates no change in VaD compared to controls.

7.3 Does Aβ interfere with VEGF-VEGFR signalling?

There have been several reports of VEGF binding to Aβ in AD brain [222, 372] and of Aβ binding to VEGFR2 in vitro and in vivo [307, 308]. VEGF has been found sequestered in Aβ plaques in human AD brain and VEGF was found to bind to Aβ with the same affinity as it binds to its own receptors [222]. This would reduce the bioavailiblity of VEGF despite it being present in higher concentrations. In HUVECs and HBMECs, Aβ was found to bind to VEGFR2 and VEGFR2 phosphorylation was reduced with increasing Aβ concentration. This reduced the ability of cells to migrate and form tubules as tested with a tube formation assay. Therefore VEGF could be present in high concentrations but not have access to the receptors due to the presence of Aβ binding to VEGFR2. Despite elevated VEGF levels there is no increase

in microvessel density in the AD brain. This raises the possibility that VEGF signalling may be altered in AD. It seems likely that a combination of VEGF sequestration and lack of access to receptors could contribute to reduced VEGF-VEGFR signalling.

At the time of this study there had been no investigation into the interaction between VEGFR1 and Aβ binding. This is due to the minimal role of VEGFR1 in cellular signalling when compared to VEGFR2. VEGFR1 and VEGFR2 share 33.3% sequence homology in the extracellular domain[125] and are structural analysis has shown VEGFR1 able to bind VEGF similarly to VEGFR2 [373]. As Aβ is able to bind to VEGFR2 it is hypothesised that Aβ could bind to VEGFR1. In a recent study the effect of Aβ on HUVEC VEGFR levels was investigated and found that VEGFR1 levels were significantly increased. This was then attributed to increased cell death. This contradicts the work in this study and provides grounds for further investigation of the interaction between VEGFR1 and Aβ [374]. This would be of interest due to the presence of VEGFR1 on endothelial cells where they regulate VEGF mediated angiogenesis [375]. VEGFR1 is also present neurons where it is hypothesised to have a similar role in regulating VEGF as a neurotrophic factor and on microglia [142].

This study established that the level of VEGFR2 in parietal lobe was unchanged between control and AD indicating that it is an alteration in ligand binding or downstream signalling that is occurring rather than a lack of binding sites.

After establishing that receptor levels were unchanged the role of Aβ in VEGF-VEGFR signalling was investigated. There was no change to the levels of VEGFR1 and VEGFR2 when endothelial cells and pericytes were exposed to $A\beta_{1\text{-}40}$ and $A\beta_{1\text{-}42}$ alone. It was only when cells were exposed to hypoxia that an effect on receptor level was reported. Despite efforts to measure the phosphorylation level of VEGFR2 in human tissue via assay and western blot, no suitable methods were optimised. In vitro work determined that the effects of VEGFR1 and VEGFR2 levels were dictated by hypoxia, Aβ itself having no effect. It is however possible for Aβ to be affecting receptor signalling though due to a lack of suitable antibody to p-VEGFR2 this was not investigated in this project.

This thesis has focused on the VEGF-VEGFR system in blood vessel maintenance and formation; however, there are several other receptor systems and signalling pathways involved in these processes. Notch signalling is vital in angiogenesis and interaction with VEGFR signalling well characterised [130]. Notch can control the level of VEGFR expression and high levels of VEGFR1 expression can result in blood vessel regression [376] Notch and VEGF signalling are also known to interact in neurogenesis in the SVZ [376]. Alteration of signalling of VEGFR can have other effects on the activity of Notch signalling. The role of pericytes was investigated in the final results chapter. PDGFRβ is used as a pericyte marker

and one of the receptors for platelet derived growth factor (PDGF). VEGFR1, VEGFR2 and PDGFRβ were shown to be co-expressed by pericytes, as reported in this thesis. Not only is VEGF able to bind to PDGFRβ [377] but there is evidence that PDGF can bind to VEGFR2 [378]. The changes in bioavailability of VEGF could reduce PDGF signalling by pericytes as well as endothelial cells, neurons and astrocytes, from which PDGF is also released.

7.4 What are the implications of VEGF–VEGFR dysfunction on the AD brain?

The role of VEGF system in disrupted angiogenesis motivated investigation of the receptors in the control, AD and VaD brain. VEGF, however, has several other roles in nervous system tissue, so disruption to VEGF signal transduction could lead to multiple adverse effects in AD. These include disruption to the BBB, astrocytic and neuronal function.

This study did not have the scope to address impacts of increased VEGF on the blood brain barrier or alter flow and consequences of BBB damage and permeability. This would be of particular interest in early AD when BBB changes are first thought to occur. Endothelial cells are a key component of the BBB and disrupted signalling, as described in 7.3 could reduce the ability of these endothelial cells to proliferate and migrate to maintain the BBB. Indeed the death of endothelial cells has been suggested as a contributing factor to BBB breakdown[379]. VEGF was first discovered as a permeability factor and Increases in the concentration of VEGF could be a contributing factor to the breakdown of the BBB. Alterations in VEGF level on BBB breakdown have been consistently reported in AD. Increased permeability would lead to infiltration of neurotoxic molecules from the periphery, immunoglobulins and immune cells which can result in increased oxidative stress and inflammation contributing to neurodegeneration [380].

It has been proposed that the main role for VEGF in the adult nervous system is not angiogenesis. This study observed VEGFR1 and VEGFR2 on endothelial cells in the AD brain, as expected. Furthermore, VEGFR1 is present on neurons (Chapter 3) and VEGFR2 is present on both neurons and astrocytes in control and AD (Chapter 4). Despite the major role of VEGF in angiogenesis via endothelial cells, it has been noted that astrocytes are a major producer of VEGF. The role of astrocytes in neuronal and endothelial signalling has been well established but the role of VEGF in these interactions is not entirely clear.

VEGF mediates both LTP and hippocampal neurogenesis. VEGF is essential for LTP and increases synaptic strength independent of its effects on angiogenesis and neurogenesis [211, 381]. A more recent study has shown VEGF to mediates its effect by causing the redistribution of NMDA type glutamate receptors on neurons [382]. VEGF acts on VEGFR2 on hippocampal

neurons. The silencing of VEGFR2 lead to impaired synaptic plasticity and memory consolidation [382].

If VEGF-VEGFR signalling is disrupted, by hypoxia or Aβ, this could have a direct effect on synaptic function. As the reduction in CBF and resultant reduced perfusion of brain tissue is one of the first changes in AD, changes in the level of sVEGFR1 may occur early in disease. Following reduced CBF, increases in $A\beta_{1-42}$ may have a direct effect on the receptor system on neurons [308] or the binding of VEGF with $A\beta_{1-42}$[222] may reduce the bioavailability of VEGF resulting in reduced VEGFR2 signalling and therefore reduced LTP and neurogenesis in the AD brain. Furthermore, the interference with VEGF signalling may also contribute to the inhibitory effects of $A\beta_{1-42}$ on synaptic transmission [383-385].

7.5 Does promotion of angiogenesis offer therapeutic potential in AD?

Due to the overlap of clinical symptoms and involvement of the vascular system in dementia, understanding the role of brain perfusion and its dysfunction in disease could provide novel clinical insights to slow the progression of disease. Indeed, VEGF administration has been investigated as a neuroprotective, proangiogenic therapy in AD [134, 386, 387].

Increasing CBF in early disease has the potential to slow the progression of AD. Reduced CBF is one of the first changes in disease and Aβ is increased in ischaemic conditions so preventing hypoxia may well slow Aβ accumulation in the brain.

Initiating angiogenesis via the VEGF system by either VEGF administration or VEGFR agonists may be beneficial in disease. There are however, significant drawbacks due to the potent effect of this ligand-receptor system and dosing would need to be carefully targeted and regulated. Elevated VEGF levels would risk aberrant angiogenesis, a known cause of disease and increased permeability of the BBB leading to further neuronal damage. Targeted delivery of VEGF containing biodegradable nanospheres to the CNS has been trialled in mice [386]. This direct administration of nanospheres to the brain promoted angiogenesis, and reduced neuronal loss and cerebrovascular abnormalities [386]. This offers therapeutic potential, though delivery through the BBB would need to be optimised to be of benefit.

The caveats for increasing VEGF level may prohibit its use in the CNS but it is possible that other members of this ligand family may be more clinically appropriate. VEGF-B is only able to activate VEGFR1 resulting in weaker angiogenic activity than VEGF while retaining neuroprotective effects. As a result, VEGF-B has been suggested as an alternative ligand for increasing angiogenesis and neuronal survival in the CNS. VEGF-B was found to have neuroprotective effects both in primary cultured motor neurons and in a mouse model of

motor neurone disease [244]. In the same study VEGF-B did not cause BBB permeability or aberrant vessel growth seen with a similar dose of VEGF [244]. In a more recent study, VEGF-B was administered to a mouse model of ischaemic stroke which resulted in the formation of stable microvasculature [388]. The authors found this was effect was mediated by the activation of VEGFR1 on pericytes, as opposed to endothelial cells.

The apparent specificity of VEGF-A isoforms offers a useful opportunity to be able to enact changes to the system with minimal side effects. Subtypes of $VEGF_{xxx}a$, in particular or VEGF-Ax. The $VEGF_{xxx}b$ family are unlikely to be suitable as there is evidence they are antiangiogenic and increase permeability [389]. As although they have been shown to be neuroprotective [125]. To take full advantage the system must first be understood in the CNS.

Possible therapeutic options are also offered from existing registered drugs. For example, a combination treatment of memantine, an NMDA inhibitor, and rosuvastatin, a statin, were administered to a rat model of permanent cerebral hypoperfusion [390]. The paper reported the NMDA inhibitor upregulated brain derived neurotrophic factor (BDNF) and the statin upregulated VEGF, inducing cell proliferation and leading to neovascularisation. The two drugs in combination increased LTP and level of growth factors more than either treatment alone. The authors point out that the treatment should be further validated in newly developed models of cerebral hypoperfusion that do not induce acute brain damage [391, 392]. This provides evidence that combination treatment could provide an effective way of modulating brain function.

This use of existing drug treatments provides a clear opportunity to avoiding severe side effects of administering VEGF directly while still benefitting from the role of the growth factor in angiogenesis and LTP.

Prior to the investigation of these as therapeutics in the CNS, more must be elucidated about the function and effect of these subtypes on receptors both within the VEGFR system and possible cross-reactivity with other receptor systems.

7.6 Future work

This thesis investigated VEGFR1 and VEGFR2 in the grey and white matter of the parietal lobe. VEGF expression level has shown regional variation in human brain post-mortem studies [78] so it would be beneficial to study the expression of the receptors in multiple brain regions.

A further study would also benefit from using human brain tissue at an earlier stage of disease. As indicated in Figure 7-2**,** the use of an AD cohort at Braak stages I-III would allow

changes in VEGF receptor levels to be investigated when cerebral hypoperfusion will be present but before extensive deposition of tau and Aβ. Detection of changes in the receptor system at this stage would provide evidence for the role in VEGF disruption in the pathophysiology of AD.

Other areas of work arising immediately from this study include the exploration of sVEGFR1 mRNA levels in human brain tissue by qPCR. The levels of sVEGFR1 isoforms have been measured by qPCR in other studies and this would add to the understanding of the possible increase in sVEGFR1 as a negative regulator of VEGF function in AD.

Two methods for measuring p-VEGFR2 were tested in this thesis. Neither the p-VEGFR2 ELISA or antibody could be optimised adequately to be used on human tissue or cell lysate. Further work should include further optimisation of a method for measuring p-VEGFR2 *in vitro* to clarify the effect of Aβ and hypoxia on VEGFR signalling.

Further work arising from the cell studies include the measurement of cell proliferation and migration. A cell proliferation assay combined with a cell live and death assay could be used assess the effect of hypoxia and, or, Aβ on cell proliferation and viability. Migration can could be assessed in HBMECs using a tube formation assay. This would assess any functional effect hypoxia and, or, Aβ would have on cell migration.

The work in this thesis relates to VEGF, with no attempt to discriminate between $VEGF_{xxx}a$ and $VEGF_{xxx}b$ subtypes. The has been no detailed investigation of $VEGF_{xxx}a$ isoforms in the brain, with the focus of this study on $VEGF_{165}a$. There has been one investigation of the anti-angiogenic splice variant, $VEGF_{165}b$ in the AD brain to date [125]. Further studies would be of interest, as the ratio of $VEGF_{165}a$: $VEGF_{165}b$ subtypes was found to be altered in lung disease [393] and an alteration in the ratio of these subtypes might have a significant impact on angiogenesis in AD.

The other members of the VEGF family, VEGFR3 and their neuropilin co-receptors are all yet to be investigated in dementia. VEGF-B and VEGF-C are known to have direct effects on neurons but the effect of dementia on the localisation, level and activity of these proteins is still to be elucidated.

Chronic cerebral hypoperfusion is a key abnormality leading to vascular cognitive impairment and dementia. Closing the translational gap between rodent models and human vascular cognitive impairment and dementia is likely to be a key step in making progress in this field [394]. Current models can reduce blood flow following implementation of microcoils[395] or constrictors around the carotid arteries [391] to mimic hypoperfusion in AD or VaD. However,

there are limitations of these animal models of cerebral hypoperfusion and the development of better models would allow translational work to proceed more effectively.

7.7 Final conclusions

Data in this thesis support the hypothesis that VEGF receptor signalling is disrupted in AD and this may affect the progression of AD. This has implications of the role of reduced blood flow in the pathogenesis of AD. The disruption of signalling may also have wider impact on neuronal, astrocyte and pericyte function in disease, though further investigation is needed. This work adds to the understanding of VEGF-VEGFR system in dementia. Further work is needed to elucidate the receptor system in VaD and to determine precisely why this signalling pathway does not function normally in AD.

References

1. PHE. Health matters: midlife approaches to reduce dementia risk: Public Health England;2016.
2. Prince M, Wimo A, Guerchet M, Ali G-C, Wu Y-T, Prina M. World Alzheimer Report 2015. London: Alzheimer's Disease International (ADI);2015.
3. Prince M, Knapp M, Guerchet M, McCrone P, Prina M, Comas-Herrera A*, et al.* Dementia UK: Second Edition - Overview.;2014.
4. Folstein MF, Folstein SE, McHugh PR. "Mini-mental state". A practical method for grading the cognitive state of patients for the clinician. J Psychiatr Res. 1975, 12: 189-98.
5. NICE. Donepezil, galantamine, rivastigmine and memantine for the treatment of Alzheimer's disease;2011.
6. Fillit H, Nash DT, Rundek T, Zuckerman A. Cardiovascular risk factors and dementia. Am J Geriatr Pharmacother. 2008, 6: 100-18.
7. Davies P, Maloney AJ. Selective loss of central cholinergic neurons in Alzheimer's disease. Lancet. 1976, 2: 1403.
8. Bartus RT, Dean RL, 3rd, Beer B, Lippa AS. The cholinergic hypothesis of geriatric memory dysfunction. Science. 1982, 217: 408-14.
9. Hardy J, Cowburn R, Barton A, Reynolds G, Lofdahl E, O'Carroll AM*, et al.* Region-specific loss of glutamate innervation in Alzheimer's disease. Neurosci Lett. 1987, 73: 77-80.
10. Terry RD, Gonatas NK, Weiss M. Ultrastructural Studies in Alzheimer's Presenile Dementia. Am J Pathol. 1964, 44: 269-97.
11. Müller UC, Zheng H. Physiological Functions of APP Family Proteins. Cold Spring Harb Perspect Med. 2012, 2.
12. van der Kant R, Goldstein LS. Cellular functions of the amyloid precursor protein from development to dementia. Dev Cell. 2015, 32: 502-15.
13. O'Brien RJ, Wong PC. Amyloid precursor protein processing and Alzheimer's disease. Annu Rev Neurosci. 2011, 34: 185-204.
14. Bergmans BA, De Strooper B. gamma-secretases: from cell biology to therapeutic strategies. Lancet Neurol. 2010, 9: 215-26.
15. Goedert M, Spillantini MG. A century of Alzheimer's disease. Science. 2006, 314: 777-81.
16. Hardy JA, Higgins GA. Alzheimer's disease: the amyloid cascade hypothesis. Science. 1992, 256: 184-5.
17. Hardy J, Selkoe DJ. The Amyloid Hypothesis of Alzheimer's Disease: Progress and Problems on the Road to Therapeutics. Science. 2002, 297: 353-6.
18. Sengupta U, Nilson AN, Kayed R. The Role of Amyloid-β Oligomers in Toxicity, Propagation, and Immunotherapy. EBioMedicine. 2016, 6: 42-9.
19. Haass C, Selkoe DJ. Soluble protein oligomers in neurodegeneration: lessons from the Alzheimer's amyloid beta-peptide. Nat Rev Mol Cell Biol. 2007, 8: 101-12.
20. Deane R, Bell R, Sagare A, Zlokovic B. Clearance of amyloid-β peptide across the blood-brain barrier: Implication for therapies in Alzheimer's disease. CNS Neurol Disord Drug Targets. 2009, 8: 16-30.
21. Tarasoff-Conway JM, Carare RO, Osorio RS, Glodzik L, Butler T, Fieremans E*, et al.* Clearance systems in the brain—implications for Alzheimer disease. Nat Rev Neurol. 2015, 11: 457-70.
22. Baranello RJ, Bharani KL, Padmaraju V, Chopra N, Lahiri DK, Greig NH*, et al.* Amyloid-beta protein clearance and degradation (ABCD) pathways and their role in Alzheimer's disease. Curr Alzheimer Res. 2015, 12: 32-46.
23. Oddo S. The ubiquitin-proteasome system in Alzheimer's disease. J Cell Mol Med. 2008, 12: 363-73.

24. Orr ME, Oddo S. Autophagic/lysosomal dysfunction in Alzheimer's disease. Alzheimers Res Ther. 2013, 5: 53.
25. Stewart PA, Hayakawa K, Akers MA, Vinters HV. A morphometric study of the blood-brain barrier in Alzheimer's disease. Lab Invest. 1992, 67: 734-42.
26. Deane R, Yan SD, Submamaryan RK, LaRue B, Jovanovic S, Hogg E*, et al.* RAGE mediates amyloid-β peptide transport across the blood-brain barrier and accumulation in brain. Nature medicine. 2003, 9: 907.
27. Sweeney MD, Sagare AP, Zlokovic BV. Blood–brain barrier breakdown in Alzheimer's disease and other neurodegenerative disorders. Nat Rev Neurol. 2018, 14: 133-50.
28. Kidd. Paired Helical Filaments in Electron Microscopy of Alzheimer's Disease. Nature. 1963, 197: 192-3.
29. Wischik CM, Novak M, Edwards PC, Klug A, Tichelaar W, Crowther RA. Structural characterization of the core of the paired helical filament of Alzheimer disease. Proc Natl Acad Sci U S A. 1988, 85: 4884-8.
30. Braak H, Braak E. Neuropathological stageing of Alzheimer-related changes. Acta Neuropathol. 1991, 82: 239-59.
31. Braak H, Braak E. Staging of Alzheimer's disease-related neurofibrillary changes. Neurobiol Aging. 1995, 16: 271-8; discussion 8-84.
32. Virginia M-Y Lee, Michel Goedert, Trojanowski JQ. Neurodegenerative Tauopathies. Annu Rev Neurosci. 2003, 24: 1121-59.
33. Love S, Nicoll JA, Hughes A, Wilcock GK. APOE and cerebral amyloid angiopathy in the elderly. Neuroreport. 2003, 14: 1535-6.
34. Smith EE. Cerebral amyloid angiopathy as a cause of neurodegeneration. J Neurochem. 2018, 144: 651-8.
35. Viswanathan A, Greenberg SM. Cerebral amyloid angiopathy in the elderly. Ann Neurol. 2011, 70: 871-80.
36. Banerjee G, Carare R, Cordonnier C, Greenberg SM, Schneider JA, Smith EE*, et al.* The increasing impact of cerebral amyloid angiopathy: essential new insights for clinical practice. J Neurol Neurosurg Psychiatry. 2017, 88: 982-94.
37. Sweeney MD, Sagare AP, Zlokovic BV. Cerebrospinal fluid biomarkers of neurovascular dysfunction in mild dementia and Alzheimer's disease. J Cereb Blood Flow Metab. 2015, 35: 1055-68.
38. Pfeifer LA, White LR, Ross GW, Petrovitch H, Launer LJ. Cerebral amyloid angiopathy and cognitive function: the HAAS autopsy study. Neurology. 2002, 58: 1629-34.
39. Esiri MM, Nagy Z, Smith MZ, Barnetson L, Smith AD. Cerebrovascular disease and threshold for dementia in the early stages of Alzheimer's disease. Lancet. 1999, 354: 919-20.
40. Heyman A, Fillenbaum GG, Welsh-Bohmer KA, Gearing M, Mirra SS, Mohs RC*, et al.* Cerebral infarcts in patients with autopsy-proven Alzheimer's disease: CERAD, part XVIII. Consortium to Establish a Registry for Alzheimer's Disease. Neurology. 1998, 51: 159-62.
41. Reijmer YD, van Veluw SJ, Greenberg SM. Ischemic brain injury in cerebral amyloid angiopathy. J Cereb Blood Flow Metab. 2016, 36: 40-54.
42. Iadecola C. Neurovascular regulation in the normal brain and in Alzheimer's disease. Nat Rev Neurosci. 2004, 5: 347-60.
43. Wang F, Gordon BA, Ryman DC, Ma S, Xiong C, Hassenstab J*, et al.* Cerebral amyloidosis associated with cognitive decline in autosomal dominant Alzheimer disease. Neurology. 2015, 85: 790-8.
44. Rocchi A, Pellegrini S, Siciliano G, Murri L. Causative and susceptibility genes for Alzheimer's disease: a review. Brain Res Bull. 2003, 61: 1-24.
45. Hardy J. Amyloid, the presenilins and Alzheimer's disease. Trends Neurosci. 1997, 20: 154-9.

46. http://www.molgen.vib-ua.be/ADMutations. Alzheimer Disease & Frontotemporal Dementia Mutation Database.
47. Cruts M, Theuns J, Van Broeckhoven C. Locus-specific mutation databases for neurodegenerative brain diseases. Hum Mutat. 2012, 33: 1340-4.
48. Clark RF, Hutton M, Fuldner M, Froelich S, Karran E, Talbot C*, et al.* The structure of the presenilin 1 (S182) gene and identification of six novel mutations in early onset AD families. Nat Genet. 1995, 11: 219-22.
49. Ballard C, Gauthier S, Corbett A, Brayne C, Aarsland D, Jones E. Alzheimer's disease. Lancet. 2011, 377: 1019-31.
50. Cuyvers E, Sleegers K. Genetic variations underlying Alzheimer's disease: evidence from genome-wide association studies and beyond. Lancet Neurol. 2016, 15: 857-68.
51. Bertram L, McQueen MB, Mullin K, Blacker D, Tanzi RE. Systematic meta-analyses of Alzheimer disease genetic association studies: the AlzGene database. Nat Genet. 2007, 39: 17-23.
52. Liu CC, Kanekiyo T, Xu H, Bu G. Apolipoprotein E and Alzheimer disease: risk, mechanisms, and therapy. Nat Rev Neurol. 2013, 9: 106-18.
53. Corder EH, Saunders AM, Strittmatter WJ, Schmechel DE, Gaskell PC, Small GW*, et al.* Gene dose of apolipoprotein E type 4 allele and the risk of Alzheimer's disease in late onset families. Science. 1993, 261: 921-3.
54. Hickman SE, El Khoury J. TREM2 and the neuroimmunology of Alzheimer's disease. Biochem Pharmacol. 2014, 88: 495-8.
55. Selkoe DJ, Hardy J. The amyloid hypothesis of Alzheimer's disease at 25 years. EMBO Mol Med. 2016, 8: 595-608.
56. Shepherd C, McCann H, Halliday GM. Variations in the neuropathology of familial Alzheimer's disease. Acta Neuropathol. 2009, 118: 37-52.
57. Iadecola C. The Pathobiology of Vascular Dementia. Neuron. 2013, 80: 844-66.
58. Erkinjuntti T. Cerebrovascular disease, vascular cognitive impairment and dementia. Psychiatry. 2005, 4: 48–51.
59. Roman GC, Tatemichi TK, Erkinjuntti T, Cummings JL, Masdeu JC, Garcia JH*, et al.* Vascular dementia: diagnostic criteria for research studies. Report of the NINDS-AIREN International Workshop. Neurology. 1993, 43: 250-60.
60. Moorhouse P, Rockwood K. Vascular cognitive impairment: current concepts and clinical developments. Lancet Neurol. 2008, 7: 246-55.
61. Joutel A, Corpechot C, Ducros A, Vahedi K, Chabriat H, Mouton P*, et al.* Notch3 mutations in CADASIL, a hereditary adult-onset condition causing stroke and dementia. Nature. 1996, 383: 707.
62. Chabriat H, Joutel A, Dichgans M, Tournier-Lasserve E, Bousser MG. Cadasil. Lancet Neurol. 2009, 8: 643-53.
63. McAleese KE, Alafuzoff I, Charidimou A, De Reuck J, Grinberg LT, Hainsworth AH*, et al.* Post-mortem assessment in vascular dementia: advances and aspirations. BMC Med. 2016, 14: 129.
64. Kalaria RN. Neuropathological diagnosis of vascular cognitive impairment and vascular dementia with implications for Alzheimer’s disease. Acta Neuropathol. 2016, 131: 659-85.
65. Grinberg LT, Thal DR. Vascular pathology in the aged human brain. Acta Neuropathol. 2010, 119: 277-90.
66. Østergaard L, Engedal TS, Moreton F, Hansen MB, Wardlaw JM, Dalkara T*, et al.* Cerebral small vessel disease: Capillary pathways to stroke and cognitive decline. J Cereb Blood Flow Metab. 2016, 36: 302-25.
67. Stelzmann RA, Norman Schnitzlein H, Reed Murtagh F. An English translation of Alzheimer's 1907 paper, “über eine eigenartige erkankung der hirnrinde”. Clinical Anatomy. 1995, 8: 429-31.
68. Miners S, Moulding H, de Silva R, Love S. Reduced vascular endothelial growth factor and capillary density in the occipital cortex in dementia with Lewy bodies. Brain Pathol. 2014, 24: 334-43.

69. Whitmer RA, Sidney S, Selby J, Johnston SC, Yaffe K. Midlife cardiovascular risk factors and risk of dementia in late life. Neurology. 2005, 64: 277-81.
70. Chuang YF, An Y, Bilgel M, Wong DF, Troncoso JC, O'Brien RJ*, et al.* Midlife adiposity predicts earlier onset of Alzheimer's dementia, neuropathology and presymptomatic cerebral amyloid accumulation. Mol Psychiatry. 2015, DOI: 10.1038/mp.2015.129.
71. Liu G, Yao L, Liu J, Jiang Y, Ma G, Chen Z*, et al.* Cardiovascular disease contributes to Alzheimer's disease: evidence from large-scale genome-wide association studies. Neurobiol Aging. 2014, 35: 786-92.
72. Barker R, Ashby EL, Wellington D, Barrow VM, Palmer JC, Kehoe PG*, et al.* Pathophysiology of white matter perfusion in Alzheimer's disease and vascular dementia. Brain. 2014, 137: 1524-32.
73. Zlokovic BV. Neurovascular pathways to neurodegeneration in Alzheimer's disease and other disorders. Nature Reviews Neuroscience. 2011, 12: 723-38.
74. Love S, Miners JS. Cerebral Hypoperfusion and the Energy Deficit in Alzheimer's Disease. Brain Pathol. 2016, 26: 607-17.
75. Tohgi H, Yonezawa H, Takahashi S, Sato N, Kato E, Kudo M*, et al.* Cerebral blood flow and oxygen metabolism in senile dementia of Alzheimer's type and vascular dementia with deep white matter changes. Neuroradiology. 1998, 40: 131-7.
76. Binnewijzend MA, Kuijer JP, Benedictus MR, van der Flier WM, Wink AM, Wattjes MP*, et al.* Cerebral blood flow measured with 3D pseudocontinuous arterial spin-labeling MR imaging in Alzheimer disease and mild cognitive impairment: a marker for disease severity. Radiology. 2013, 267: 221-30.
77. Benzinger TL, Blazey T, Jack CR, Jr., Koeppe RA, Su Y, Xiong C*, et al.* Regional variability of imaging biomarkers in autosomal dominant Alzheimer's disease. Proc Natl Acad Sci U S A. 2013, 110: E4502-9.
78. Thomas T, Miners S, Love S. Post-mortem assessment of hypoperfusion of cerebral cortex in Alzheimer's disease and vascular dementia. Brain. 2015, 138: 1059-69.
79. Miners JS, Palmer JC, Love S. Pathophysiology of hypoperfusion of the precuneus in early Alzheimer's disease. Brain Pathol. 2016, 26: 533-41.
80. Ruitenberg A, den Heijer T, Bakker SL, van Swieten JC, Koudstaal PJ, Hofman A*, et al.* Cerebral hypoperfusion and clinical onset of dementia: the Rotterdam Study. Ann Neurol. 2005, 57: 789-94.
81. Ashby EL, Miners JS, Kehoe PG, Love S. Effects of Hypertension and Anti-Hypertensive Treatment on Amyloid-beta (Abeta) Plaque Load and Abeta-Synthesizing and Abeta-Degrading Enzymes in Frontal Cortex. J Alzheimers Dis. 2016, DOI: 10.3233/jad-150831.
82. Lee S, Viqar F, Zimmerman ME, Narkhede A, Tosto G, Benzinger TL*, et al.* White matter hyperintensities are a core feature of Alzheimer's disease: Evidence from the dominantly inherited Alzheimer network. Ann Neurol. 2016, 79: 929-39.
83. Uryu K, Laurer H, McIntosh T, Pratico D, Martinez D, Leight S*, et al.* Repetitive mild brain trauma accelerates Abeta deposition, lipid peroxidation, and cognitive impairment in a transgenic mouse model of Alzheimer amyloidosis. J Neurosci. 2002, 22: 446-54.
84. Yokota M, Saido TC, Tani E, Yamaura I, Minami N. Cytotoxic fragment of amyloid precursor protein accumulates in hippocampus after global forebrain ischemia. J Cereb Blood Flow Metab. 1996, 16: 1219-23.
85. Koistinaho J, Pyykonen I, Keinanen R, Hokfelt T. Expression of beta-amyloid precursor protein mRNAs following transient focal ischaemia. Neuroreport. 1996, 7: 2727-31.
86. Li L, Zhang X, Yang D, Luo G, Chen S, Le W. Hypoxia increases Abeta generation by altering beta- and gamma-cleavage of APP. Neurobiol Aging. 2009, 30: 1091-8.
87. Zhang X, Zhou K, Wang R, Cui J, Lipton SA, Liao FF*, et al.* Hypoxia-inducible factor 1alpha (HIF-1alpha)-mediated hypoxia increases BACE1 expression and beta-amyloid generation. J Biol Chem. 2007, 282: 10873-80.

88. Niwa K, Kazama K, Younkin L, Younkin SG, Carlson GA, Iadecola C. Cerebrovascular autoregulation is profoundly impaired in mice overexpressing amyloid precursor protein. Am J Physiol Heart Circ Physiol. 2002, 283: H315-23.
89. Niwa K, Porter VA, Kazama K, Cornfield D, Carlson GA, Iadecola C. A beta-peptides enhance vasoconstriction in cerebral circulation. Am J Physiol Heart Circ Physiol. 2001, 281: H2417-24.
90. Palmer JC, Barker R, Kehoe PG, Love S. Endothelin-1 is elevated in Alzheimer's disease and upregulated by amyloid-beta. J Alzheimers Dis. 2012, 29: 853-61.
91. Miners JS, Ashby E, Van Helmond Z, Chalmers KA, Palmer LE, Love S*, et al.* Angiotensin-converting enzyme (ACE) levels and activity in Alzheimer's disease, and relationship of perivascular ACE-1 to cerebral amyloid angiopathy. Neuropathol Appl Neurobiol. 2008, 34: 181-93.
92. Lamoke F, Mazzone V, Persichini T, Maraschi A, Harris MB, Venema RC*, et al.* Amyloid beta peptide-induced inhibition of endothelial nitric oxide production involves oxidative stress-mediated constitutive eNOS/HSP90 interaction and disruption of agonist-mediated Akt activation. J Neuroinflammation. 2015, 12: 84.
93. Tan XL, Xue YQ, Ma T, Wang X, Li JJ, Lan L*, et al.* Partial eNOS deficiency causes spontaneous thrombotic cerebral infarction, amyloid angiopathy and cognitive impairment. Mol Neurodegener. 2015, 10: 24.
94. Blin J, Ivanoiu A, Coppens A, De Volder A, Labar D, Michel C*, et al.* Cholinergic neurotransmission has different effects on cerebral glucose consumption and blood flow in young normals, aged normals, and Alzheimer's disease patients. Neuroimage. 1997, 6: 335-43.
95. Claassen JA, Jansen RW. Cholinergically mediated augmentation of cerebral perfusion in Alzheimer's disease and related cognitive disorders: the cholinergic-vascular hypothesis. J Gerontol A Biol Sci Med Sci. 2006, 61: 267-71.
96. Obermeier B, Daneman R, Ransohoff RM. Development, maintenance and disruption of the blood-brain barrier. Nat Med. 2013, 19: 1584-96.
97. Smith CD, Andersen AH, Kryscio RJ, Schmitt FA, Kindy MS, Blonder LX*, et al.* Altered brain activation in cognitively intact individuals at high risk for Alzheimer's disease. Neurology. 1999, 53: 1391-6.
98. Starr JM, Farrall AJ, Armitage P, McGurn B, Wardlaw J. Blood-brain barrier permeability in Alzheimer's disease: a case-control MRI study. Psychiatry Res. 2009, 171: 232-41.
99. Farrall AJ, Wardlaw JM. Blood-brain barrier: ageing and microvascular disease--systematic review and meta-analysis. Neurobiol Aging. 2009, 30: 337-52.
100. Thambisetty M, Beason-Held L, An Y, Kraut MA, Resnick SM. APOE ε4 Genotype and Longitudinal Changes in Cerebral Blood Flow in Normal Aging. Arch Neurol. 2010, 67: 93-8.
101. Mawuenyega KG, Sigurdson W, Ovod V, Munsell L, Kasten T, Morris JC*, et al.* Decreased clearance of CNS beta-amyloid in Alzheimer's disease. Science. 2010, 330: 1774.
102. Brown WR, Thore CR. Review: cerebral microvascular pathology in ageing and neurodegeneration. Neuropathol Appl Neurobiol. 2011, 37: 56-74.
103. Burke MJ, Nelson L, Slade JY, Oakley AE, Khundakar AA, Kalaria RN. Morphometry of the hippocampal microvasculature in post-stroke and age-related dementias. Neuropathol Appl Neurobiol. 2014, 40: 284-95.
104. Hunter JM, Kwan J, Malek-Ahmadi M, Maarouf CL, Kokjohn TA, Belden C*, et al.* Morphological and pathological evolution of the brain microcirculation in aging and Alzheimer's disease. PLoS ONE. 2012, 7: e36893.
105. Brown WR. A review of string vessels or collapsed, empty basement membrane tubes. J Alzheimers Dis. 2010, 21: 725-39.
106. Wittko-Schneider IM, Schneider FT, Plate KH. Brain homeostasis: VEGF receptor 1 and 2-two unequal brothers in mind. Cell Mol Life Sci. 2013, 70: 1705-25.

107. Olsson AK, Dimberg A, Kreuger J, Claesson-Welsh L. VEGF receptor signalling - in control of vascular function. Nat Rev Mol Cell Biol. 2006, 7: 359-71.
108. Qiu Y, Hoareau-Aveilla C, Oltean S, Harper SJ, Bates DO. The anti-angiogenic isoforms of VEGF in health and disease. Biochem Soc Trans. 2009, 37: 1207-13.
109. Barratt S, Medford AR, Millar AB. Vascular endothelial growth factor in acute lung Injury and acute respiratory distress syndrome. Respiration. 2013, 87: 329-42.
110. Rosenstein JM, Krum JM, Ruhrberg C. VEGF in the nervous system. Organogenesis. 2010, 6: 107-14.
111. Harris S, Craze M, Newton J, Fisher M, Shima DT, Tozer GM*, et al.* Do anti-angiogenic VEGF (VEGFxxxb) isoforms exist? A cautionary tale. PLoS One. 2012, 7: e35231.
112. Bates DO, Mavrou A, Qiu Y, Carter JG, Hamdollah-Zadeh M, Barratt S*, et al.* Detection of VEGF-Axxxb Isoforms in Human Tissues. PLoS ONE. 2013, 8: e68399.
113. Bates DO, Cui TG, Doughty JM, Winkler M, Sugiono M, Shields JD*, et al.* VEGF165b, an inhibitory splice variant of vascular endothelial growth factor, is down-regulated in renal cell carcinoma. Cancer Res. 2002, 62: 4123-31.
114. Grunewald FS, Prota AE, Giese A, Ballmer-Hofer K. Structure-function analysis of VEGF receptor activation and the role of coreceptors in angiogenic signaling. Biochim Biophys Acta. 2010, 1804: 567-80.
115. Senger DR, Galli SJ, Dvorak AM, Perruzzi CA, Harvey VS, Dvorak HF. Tumor Cells Secrete a Vascular Permeability Factor that Promotes Accumulation of Ascites Fluid. Science. 1983, 219: 983-5.
116. Ferrara N, Carver-Moore K, Chen H, Dowd M, Lu L, O'Shea KS*, et al.* Heterozygous embryonic lethality induced by targeted inactivation of the VEGF gene. Nature. 1996, 380: 439-42.
117. Carmeliet P, Ferreira V, Breier G, Pollefeyt S, Kieckens L, Gertsenstein M*, et al.* Abnormal blood vessel development and lethality in embryos lacking a single VEGF allele. Nature. 1996, 380: 435-9.
118. Stone J, Itin A, Alon T, Pe'er J, Gnessin H, Chan-Ling T*, et al.* Development of retinal vasculature is mediated by hypoxia-induced vascular endothelial growth factor (VEGF) expression by neuroglia. J Neurosci. 1995, 15: 4738-47.
119. Alon T, Hemo I, Itin A, Pe'er J, Stone J, Keshet E. Vascular endothelial growth factor acts as a survival factor for newly formed retinal vessels and has implications for retinopathy of prematurity. Nat Med. 1995, 1: 1024-8.
120. Fong GH, Rossant J, Gertsenstein M, Breitman ML. Role of the Flt-1 receptor tyrosine kinase in regulating the assembly of vascular endothelium. Nature. 1995, 376: 66-70.
121. Argandona EG, Bengoetxea H, Ortuzar N, Bulnes S, Rico-Barrio I, Lafuente JV. Vascular endothelial growth factor: adaptive changes in the neuroglialvascular unit. Curr Neurovasc Res. 2012, 9: 72-81.
122. Bates DO, MacMillan PP, Manjaly JG, Qiu Y, Hudson SJ, Bevan HS*, et al.* The endogenous anti-angiogenic family of splice variants of VEGF, VEGFxxxb, are down-regulated in pre-eclamptic placentae at term. Clin Sci (Lond). 2006, 110: 575-85.
123. Rennel ES, Varey AHR, Churchill AJ, Wheatley ER, Stewart L, Mather S*, et al.* VEGF121b, a new member of the VEGFxxxb family of VEGF-A splice isoforms, inhibits neovascularisation and tumour growth in vivo. Br J Cancer. 2009, 101: 1183-93.
124. Miller-Kasprzak E, Jagodzinski PP. 5-Aza-2'-deoxycytidine increases the expression of anti-angiogenic vascular endothelial growth factor 189b variant in human lung microvascular endothelial cells. Biomed Pharmacother. 2008, 62: 158-63.
125. Beazley-Long N, Hua J, Jehle T, Hulse RP, Dersch R, Lehrling C*, et al.* VEGF-A165b Is an Endogenous Neuroprotective Splice Isoform of Vascular Endothelial Growth Factor A in Vivo and in Vitro. Am J Pathol. 2013, 183: 918-29.

126. Eswarappa SM, Potdar AA, Koch WJ, Fan Y, Vasu K, Lindner D*, et al.* Programmed translational readthrough generates antiangiogenic VEGF-Ax. Cell. 2014, 157: 1605-18.
127. Xin H, Zhong C, Nudleman E, Ferrara N. Evidence for Pro-angiogenic Functions of VEGF-Ax. Cell. 2016, 167: 275-84.e6.
128. Eswarappa SM, Fox PL. Antiangiogenic VEGF-Ax: A New Participant in Tumor Angiogenesis. Cancer Res. 2015, 75: 2765-9.
129. Ruiz de Almodovar C, Lambrechts D, Mazzone M, Carmeliet P. Role and therapeutic potential of VEGF in the nervous system. Physiol Rev. 2009, 89: 607-48.
130. Simons M, Gordon E, Claesson-Welsh L. Mechanisms and regulation of endothelial VEGF receptor signalling. Nat Rev Mol Cell Biol. 2016, 17: 611-25.
131. Svensson B, Peters M, König H-G, Poppe M, Levkau B, Rothermundt M*, et al.* Vascular endothelial growth factor protects cultured rat hippocampal neurons against hypoxic injury via an antiexcitotoxic, caspase-independent mechanism. J Cereb Blood Flow Metab. 2002, 22: 1170-5.
132. Lagercrantz J, Farnebo F, Larsson C, Tvrdik T, Weber G, Piehl F. A comparative study of the expression patterns for vegf, vegf-b/vrf and vegf-c in the developing and adult mouse. Biochim Biophys Acta. 1998, 1398: 157-63.
133. Sun Y, Jin K, Childs JT, Xie L, Mao XO, Greenberg DA. Vascular endothelial growth factor-B (VEGFB) stimulates neurogenesis: evidence from knockout mice and growth factor administration. Dev Biol. 2006, 289: 329-35.
134. Lange C, Storkebaum E, Almodóvar CRd, Dewerchin M, Carmeliet P. Vascular endothelial growth factor: a neurovascular target in neurological diseases. Nat Rev Neurol. 2016, 12: 439-54.
135. Jeltsch M, Kaipainen A, Joukov V, Meng X, Lakso M, Rauvala H*, et al.* Hyperplasia of lymphatic vessels in VEGF-C transgenic mice. Science. 1997, 276: 1423-5.
136. Bras BL, Barallobre M-J, Homman-Ludiye J, Ny A, Wyns S, Tammela T*, et al.* VEGF-C is a trophic factor for neural progenitors in the vertebrate embryonic brain. Nat Neurosci. 2006, 9: 340-8.
137. Calvo CF, Fontaine RH, Soueid J, Tammela T, Makinen T, Alfaro-Cervello C*, et al.* Vascular endothelial growth factor receptor 3 directly regulates murine neurogenesis. Genes Dev. 2011, 25: 831-44.
138. Eichmann A, Simons M. VEGF signaling inside vascular endothelial cells and beyond. Curr Opin Cell Biol. 2012, 24: 188-93.
139. de Vries C, Escobedo JA, Ueno H, Houck K, Ferrara N, Williams LT. The fms-like tyrosine kinase, a receptor for vascular endothelial growth factor. Science. 1992, 255: 989-91.
140. Rahimi N. VEGFR-1 and VEGFR-2: two non-identical twins with a unique physiognomy. Front Biosci. 2006, 11: 818-29.
141. Forstreuter F, Lucius R, Mentlein R. Vascular endothelial growth factor induces chemotaxis and proliferation of microglial cells. J Neuroimmunol. 2002, 132: 93-8.
142. Ryu JK, Cho T, Choi HB, Wang YT, McLarnon JG. Microglial VEGF receptor response is an integral chemotactic component in Alzheimer's disease pathology. J Neurosci. 2009, 29: 3-13.
143. Hiratsuka S, Minowa O, Kuno J, Noda T, Shibuya M. Flt-1 lacking the tyrosine kinase domain is sufficient for normal development and angiogenesis in mice. Proc Natl Acad Sci U S A. 1998, 95: 9349-54.
144. Kanno S, Oda N, Abe M, Terai Y, Ito M, Shitara K*, et al.* Roles of two VEGF receptors, Flt-1 and KDR, in the signal transduction of VEGF effects in human vascular endothelial cells. Oncogene. 2000, 19: 2138-46.
145. Gerber HP, Condorelli F, Park J, Ferrara N. Differential transcriptional regulation of the two vascular endothelial growth factor receptor genes. Flt-1, but not Flk-1/KDR, is up-regulated by hypoxia. J Biol Chem. 1997, 272: 23659-67.

146. Mezquita B, Mezquita J, Pau M, Mezquita C. A novel intracellular isoform of VEGFR-1 activates Src and promotes cell invasion in MDA-MB-231 breast cancer cells. J Cell Biochem. 2010, 110: 732-42.
147. Kendall RL, Thomas KA. Inhibition of vascular endothelial cell growth factor activity by an endogenously encoded soluble receptor. Proc Natl Acad Sci U S A. 1993, 90: 10705-9.
148. Shibuya M. Structure and dual function of vascular endothelial growth factor receptor-1 (Flt-1). Int J Biochem Cell Biol. 2001, 33: 409-20.
149. Wu FTH, Stefanini MO, Gabhann FM, Kontos CD, Annex BH, Popel AS. A systems biology perspective on sVEGFR1: its biological function, pathogenic role and therapeutic use. J Cell Mol Med. 2010, 14: 528-52.
150. Hornig C, Barleon B, Ahmad S, Vuorela P, Ahmed A, Weich HA. Release and complex formation of soluble VEGFR-1 from endothelial cells and biological fluids. Lab Invest. 2000, 80: 443-54.
151. Wu FT, Stefanini MO, Mac Gabhann F, Kontos CD, Annex BH, Popel AS. A systems biology perspective on sVEGFR1: its biological function, pathogenic role and therapeutic use. J Cell Mol Med. 2010, 14: 528-52.
152. Thomas CP, Andrews JI, Liu KZ. Intronic polyadenylation signal sequences and alternate splicing generate human soluble Flt1 variants and regulate the abundance of soluble Flt1 in the placenta. Faseb j. 2007, 21: 3885-95.
153. Sela S, Itin A, Natanson-Yaron S, Greenfield C, Goldman-Wohl D, Yagel S*, et al.* A novel human-specific soluble vascular endothelial growth factor receptor 1: cell-type-specific splicing and implications to vascular endothelial growth factor homeostasis and preeclampsia. Circ Res. 2008, 102: 1566-74.
154. Barleon B, Totzke F, Herzog C, Blanke S, Kremmer E, Siemeister G*, et al.* Mapping of the sites for ligand binding and receptor dimerization at the extracellular domain of the vascular endothelial growth factor receptor FLT-1. J Biol Chem. 1997, 272: 10382-8.
155. Gu Y, Lewis DF, Wang Y. Placental Productions and Expressions of Soluble Endoglin, Soluble fms-Like Tyrosine Kinase Receptor-1, and Placental Growth Factor in Normal and Preeclamptic Pregnancies. J Clin Endocrinol Metab. 2008, 93: 260-6.
156. Jebbink J, Keijser R, Veenboer G, van der Post J, Ris-Stalpers C, Afink G. Expression of placental FLT1 transcript variants relates to both gestational hypertensive disease and fetal growth. Hypertension. 2011, 58: 70-6.
157. Szalai G, Romero R, Chaiworapongsa T, Xu Y, Wang B, Ahn H*, et al.* Full-length human placental sFlt-1-e15a isoform induces distinct maternal phenotypes of preeclampsia in mice. PLoS ONE. 2015, 10: e0119547.
158. Heydarian M, McCaffrey T, Florea L, Yang Z, Ross MM, Zhou W*, et al.* Novel splice variants of sFlt1 are upregulated in preeclampsia. Placenta. 2009, 30: 250-5.
159. Jin P, Zhang J, Sumariwalla PF, Ni I, Jorgensen B, Crawford D*, et al.* Novel splice variants derived from the receptor tyrosine kinase superfamily are potential therapeutics for rheumatoid arthritis. Arthritis Res Ther. 2008, 10: R73.
160. Thomas CP, Andrews JI, Raikwar NS, Kelley EA, Herse F, Dechend R*, et al.* A recently evolved novel trophoblast-enriched secreted form of fms-like tyrosine kinase-1 variant is up-regulated in hypoxia and preeclampsia. J Clin Endocrinol Metab. 2009, 94: 2524-30.
161. Thomas CP, Raikwar NS, Kelley EA, Liu KZ. Alternate processing of Flt1 transcripts is directed by conserved cis-elements within an intronic region of FLT1 that reciprocally regulates splicing and polyadenylation. Nucleic Acids Res. 2010, 38: 5130-40.
162. Cai J, Jiang WG, Ahmed A, Boulton M. Vascular endothelial growth factor-induced endothelial cell proliferation is regulated by interaction between VEGFR-2, SH-PTP1 and eNOS. Microvasc Res. 2006, 71: 20-31.

163. Rahimi N, Golde TE, Meyer RD. Identification of ligand-induced proteolytic cleavage and ectodomain shedding of VEGFR-1/FLT1 in leukemic cancer cells. Cancer Res. 2009, 69: 2607-14.
164. Raikwar NS, Liu KZ, Thomas CP. Protein kinase C regulates FLT1 abundance and stimulates its cleavage in vascular endothelial cells with the release of a soluble PlGF/VEGF antagonist. Exp Cell Res. 2013, 319: 2578-87.
165. Raikwar NS, Liu KZ, Thomas CP. N-terminal cleavage and release of the ectodomain of Flt1 is mediated via ADAM10 and ADAM 17 and regulated by VEGFR2 and the Flt1 intracellular domain. PLoS One. 2014, 9: e112794.
166. Chen MK, Hung MC. Proteolytic cleavage, trafficking, and functions of nuclear receptor tyrosine kinases. Febs j. 2015, 282: 3693-721.
167. Huckle WR, Roche RI. Post-transcriptional control of expression of sFlt-1, an endogenous inhibitor of vascular endothelial growth factor. J Cell Biochem. 2004, 93: 120-32.
168. Holmes K, Roberts OL, Thomas AM, Cross MJ. Vascular endothelial growth factor receptor-2: structure, function, intracellular signalling and therapeutic inhibition. Cell Signal. 2007, 19: 2003-12.
169. Cudmore MJ, Hewett PW, Ahmad S, Wang K-Q, Cai M, Al-Ani B*, et al.* The role of heterodimerization between VEGFR-1 and VEGFR-2 in the regulation of endothelial cell homeostasis. Nat Commun. 2012, 3: 972.
170. Millauer B, Wizigmann-Voos S, Schnurch H, Martinez R, Moller NP, Risau W*, et al.* High affinity VEGF binding and developmental expression suggest Flk-1 as a major regulator of vasculogenesis and angiogenesis. Cell. 1993, 72: 835-46.
171. Ahmed-Jushuf F, Jiwa NS, Arwani AS, Foot P, Bridges LR, Kalaria RN*, et al.* Age-dependent expression of VEGFR2 in deep brain arteries in small vessel disease, CADASIL and healthy brains. Neurobiol Aging. 2016, 42: 110-5.
172. Mani N, Khaibullina A, Krum JM, Rosenstein JM. Astrocyte growth effects of vascular endothelial growth factor (VEGF) application to perinatal neocortical explants: receptor mediation and signal transduction pathways. Exp Neurol. 2005, 192: 394-406.
173. Albuquerque RJ, Hayashi T, Cho WG, Kleinman ME, Dridi S, Takeda A*, et al.* Alternatively spliced vascular endothelial growth factor receptor-2 is an essential endogenous inhibitor of lymphatic vessel growth. Nat Med. 2009, 15: 1023-30.
174. Corti F, Simons M. Modulation of VEGF receptor 2 signaling by protein phosphatases. Pharmacol Res. 2016, 115: 107-23.
175. Dumont DJ, Jussila L, Taipale J, Lymboussaki A, Mustonen T, Pajusola K*, et al.* Cardiovascular failure in mouse embryos deficient in VEGF receptor-3. Science. 1998, 282: 946-9.
176. Deng Y, Zhang X, Simons M. Molecular controls of lymphatic VEGFR3 signaling. Arterioscler Thromb Vasc Biol. 2015, 35: 421-9.
177. Valtola R, Salven P, Heikkila P, Taipale J, Joensuu H, Rehn M*, et al.* VEGFR-3 and its ligand VEGF-C are associated with angiogenesis in breast cancer. Am J Pathol. 1999, 154: 1381-90.
178. Paavonen K, Puolakkainen P, Jussila L, Jahkola T, Alitalo K. Vascular endothelial growth factor receptor-3 in lymphangiogenesis in wound healing. Am J Pathol. 2000, 156: 1499-504.
179. Benedito R, Rocha SF, Woeste M, Zamykal M, Radtke F, Casanovas O*, et al.* Notch-dependent VEGFR3 upregulation allows angiogenesis without VEGF-VEGFR2 signalling. Nature. 2012, 484: 110-4.
180. Shin YJ, Choi JS, Choi JY, Cha JH, Chun MH, Lee MY. Enhanced expression of vascular endothelial growth factor receptor-3 in the subventricular zone of stroke-lesioned rats. Neurosci Lett. 2010, 469: 194-8.
181. Ward MC, Cunningham AM. Developmental expression of vascular endothelial growth factor receptor 3 and vascular endothelial growth factor C in forebrain. Neuroscience. 2015, 303: 544-57.

182. Baeyens N, Nicoli S, Coon BG, Ross TD, Van den Dries K, Han J*, et al.* Vascular remodeling is governed by a VEGFR3-dependent fluid shear stress set point. Elife. 2015, 4.
183. Coon BG, Baeyens N, Han J, Budatha M, Ross TD, Fang JS*, et al.* Intramembrane binding of VE-cadherin to VEGFR2 and VEGFR3 assembles the endothelial mechanosensory complex. J Cell Biol. 2015, 208: 975-86.
184. Soker S, Takashima S, Miao HQ, Neufeld G, Klagsbrun M. Neuropilin-1 is expressed by endothelial and tumor cells as an isoform-specific receptor for vascular endothelial growth factor. Cell. 1998, 92: 735-45.
185. Gagnon ML, Bielenberg DR, Gechtman Z, Miao HQ, Takashima S, Soker S*, et al.* Identification of a natural soluble neuropilin-1 that binds vascular endothelial growth factor: In vivo expression and antitumor activity. Proc Natl Acad Sci U S A. 2000, 97: 2573-8.
186. Oosthuyse B, Moons L, Storkebaum E, Beck H, Nuyens D, Brusselmans K*, et al.* Deletion of the hypoxia-response element in the vascular endothelial growth factor promoter causes motor neuron degeneration. Nat Genet. 2001, 28: 131-8.
187. Muche A, Bigl M, Arendt T, Schliebs R. Expression of vascular endothelial growth factor (VEGF) mRNA, VEGF receptor 2 (Flk-1) mRNA, and of VEGF co-receptor neuropilin (Nrp)-1 mRNA in brain tissue of aging Tg2576 mice by in situ hybridization. Int J Dev Neurosci. 2015, 43: 25-34.
188. Potente M, Gerhardt H, Carmeliet P. Basic and therapeutic aspects of angiogenesis. Cell. 2011, 146: 873-87.
189. Krock BL, Skuli N, Simon MC. Hypoxia-induced angiogenesis: good and evil. Genes Cancer. 2011, 2: 1117-33.
190. Forsythe JA, Jiang BH, Iyer NV, Agani F, Leung SW, Koos RD*, et al.* Activation of vascular endothelial growth factor gene transcription by hypoxia-inducible factor 1. Mol Cell Biol. 1996, 16: 4604-13.
191. Carmeliet P. Angiogenesis in health and disease. Nat Med. 2003, 9: 653-60.
192. Pronto-Laborinho AC, Pinto S, de Carvalho M. Roles of vascular endothelial growth factor in amyotrophic lateral sclerosis. Biomed Res Int. 2014, 2014: 947513.
193. Lambrechts D, Storkebaum E, Morimoto M, Del-Favero J, Desmet F, Marklund SL*, et al.* VEGF is a modifier of amyotrophic lateral sclerosis in mice and humans and protects motoneurons against ischemic death. Nat Genet. 2003, 34: 383-94.
194. Rosenstein JM, Krum JM, Ruhrberg C. VEGF in the nervous system. Organogenesis2010. 107-14.
195. Pharmaceuticals N. Newron initiates Phase II study of sNN0029 in patients with Amyotrophic Lateral Sclerosis. Milan, Italy2015.
196. Chiappelli M, Borroni B, Archetti S, Calabrese E, Corsi MM, Franceschi M*, et al.* VEGF gene and phenotype relation with Alzheimer's disease and mild cognitive impairment. Rejuvenation Res. 2006, 9: 485-93.
197. Mateo I, Llorca J, Infante J, Rodríguez-Rodríguez E, Fernández-Viadero C, Peña N*, et al.* Low serum VEGF levels are associated with Alzheimer's disease. Acta Neurol Scand. 2007, 116: 56-8.
198. Tarkowski E, Issa R, Sjogren M, Wallin A, Blennow K, Tarkowski A*, et al.* Increased intrathecal levels of the angiogenic factors VEGF and TGF-beta in Alzheimer's disease and vascular dementia. Neurobiol Aging. 2002, 23: 237-43.
199. Hu WT, Chen-Plotkin A, Arnold SE, Grossman M, Clark CM, Shaw LM*, et al.* Novel CSF biomarkers for Alzheimer's disease and mild cognitive impairment. Acta Neuropathol. 2010, 119: 669-78.
200. Chakraborty A, Chatterjee M, Twaalfhoven H, Milan MDC, Teunissen CE, Scheltens P*, et al.* Vascular Endothelial Growth Factor remains unchanged in cerebrospinal fluid of patients with Alzheimer's disease and vascular dementia. Alzheimers Res Ther. 2018, 10: 58.

201. Kim Y, Nam YJ, Lee C. Haplotype analysis of single nucleotide polymorphisms in VEGF gene for vascular dementia. Am J Med Genet B Neuropsychiatr Genet. 2006, 141B: 332-5.
202. Stevens A, Soden J, Brenchley PE, Ralph S, Ray DW. Haplotype analysis of the polymorphic human vascular endothelial growth factor gene promoter. Cancer Res. 2003, 63: 812-6.
203. Del Bo R, Scarlato M, Ghezzi S, Martinelli Boneschi F, Fenoglio C, Galbiati S*, et al.* Vascular endothelial growth factor gene variability is associated with increased risk for AD. Ann Neurol. 2005, 57: 373-80.
204. Mateo I, Llorca J, Infante J, Rodriguez-Rodriguez E, Sanchez-Quintana C, Sanchez-Juan P*, et al.* Case-control study of vascular endothelial growth factor (VEGF) genetic variability in Alzheimer's disease. Neurosci Lett. 2006, 401: 171-3.
205. Chapuis J, Tian J, Shi J, Bensemain F, Cottel D, Lendon C*, et al.* Association study of the vascular endothelial growth factor gene with the risk of developing Alzheimer's disease. Neurobiol Aging. 2006, 27: 1212-5.
206. Landgren S, Palmer MS, Skoog I, Minthon L, Wallin A, Andreasen N*, et al.* No association of VEGF polymorphims with Alzheimer's disease. Neuromolecular Med. 2010, 12: 224-8.
207. He D, Lu W, Chang K, Liu Y, Zhang J, Zeng Z. Vascular endothelial growth factor polymorphisms and risk of Alzheimer's disease: a meta-analysis. Gene. 2013, 518: 296-302.
208. Liu SY, Zeng FF, Chen ZW, Wang CY, Zhao B, Li KS. Vascular endothelial growth factor gene promoter polymorphisms and Alzheimer's disease risk: a meta-analysis. CNS Neurosci Ther. 2013, 19: 469-76.
209. Argaw AT, Asp L, Zhang J, Navrazhina K, Pham T, Mariani JN*, et al.* Astrocyte-derived VEGF-A drives blood-brain barrier disruption in CNS inflammatory disease. J Clin Investig. 2012, DOI: 10.1172/JCI60842.
210. Licht T, Keshet E. Delineating multiple functions of VEGF-A in the adult brain. Cell Mol Life Sci. 2013, 70: 1727-37.
211. Licht T, Goshen I, Avital A, Kreisel T, Zubedat S, Eavri R*, et al.* Reversible modulations of neuronal plasticity by VEGF. Proc Natl Acad Sci U S A. 2011, 108: 5081-6.
212. Kalaria RN, Cohen DL, Premkumar DR, Nag S, LaManna JC, Lust WD. Vascular endothelial growth factor in Alzheimer's disease and experimental cerebral ischemia. Brain Res Mol Brain Res. 1998, 62: 101-5.
213. Behzadian MA, Wang XL, Al-Shabrawey M, Caldwell RB. Effects of hypoxia on glial cell expression of angiogenesis-regulating factors VEGF and TGF-beta. Glia. 1998, 24: 216-25.
214. Yamagishi S, Yonekura H, Yamamoto Y, Fujimori H, Sakurai S, Tanaka N*, et al.* Vascular endothelial growth factor acts as a pericyte mitogen under hypoxic conditions. Lab Invest. 1999, 79: 501-9.
215. Nomura M, Yamagishi S, Harada S, Hayashi Y, Yamashima T, Yamashita J*, et al.* Possible participation of autocrine and paracrine vascular endothelial growth factors in hypoxia-induced proliferation of endothelial cells and pericytes. J Biol Chem. 1995, 270: 28316-24.
216. Greenberg JI, Shields DJ, Barillas SG, Acevedo LM, Murphy E, Huang J*, et al.* A Role for VEGF as a Negative Regulator of Pericyte Function and Vessel Maturation. Nature. 2008, 456: 809-13.
217. Rengo G, Cannavo A, Liccardo D, Zincarelli C, de Lucia C, Pagano G*, et al.* Vascular endothelial growth factor blockade prevents the beneficial effects of beta-blocker therapy on cardiac function, angiogenesis, and remodeling in heart failure. Circ Heart Fail. 2013, 6: 1259-67.
218. Biron KE, Dickstein DL, Gopaul R, Jefferies WA. Amyloid triggers extensive cerebral angiogenesis causing blood brain barrier permeability and hypervascularity in Alzheimer's disease. PLoS ONE. 2011, 6: e23789.

219. Zhu Y, Sun Y, Xie L, Jin K, Sheibani N, Greenberg DA. Hypoxic induction of endoglin via mitogen-activated protein kinases in mouse brain microvascular endothelial cells. Stroke. 2003, 34: 2483-8.
220. Palu E, Liesi P. Differential distribution of laminins in Alzheimer disease and normal human brain tissue. J Neurosci Res. 2002, 69: 243-56.
221. Baloyannis SJ. Brain capillaries in Alzheimer's disease. Hell J Nucl Med. 2015, 18 Suppl 1: 152.
222. Yang SP, Bae DG, Kang HJ, Gwag BJ, Gho YS, Chae CB. Co-accumulation of vascular endothelial growth factor with beta-amyloid in the brain of patients with Alzheimer's disease. Neurobiol Aging. 2004, 25: 283-90.
223. Chiarini A, Whitfield J, Bonafini C, Chakravarthy B, Armato U, Dal Prà I. Amyloid-β(25-35), an amyloid-β(1-42) surrogate, and proinflammatory cytokines stimulate VEGF-A secretion by cultured, early passage, normoxic adult human cerebral astrocytes. J Alzheimers Dis. 2010, 21: 915-26.
224. Soucek T, Cumming R, Dargusch R, Maher P, Schubert D. The regulation of glucose metabolism by HIF-1 mediates a neuroprotective response to amyloid beta peptide. Neuron. 2003, 39: 43-56.
225. Park SY, Chae CB. Toxic levels of amyloid beta peptide do not induce VEGF synthesis. Mol Cells. 2007, 24: 69-75.
226. Palmer JC, Tayler HM, Love S. Endothelin-converting enzyme-1 activity, endothelin-1 production, and free radical-dependent vasoconstriction in Alzheimer's disease. J Alzheimers Dis. 2013, 36: 577-87.
227. Miners S, Ashby E, Baig S, Harrison R, Tayler H, Speedy E*, et al.* Angiotensin-converting enzyme levels and activity in Alzheimer's disease: differences in brain and CSF ACE and association with ACE1 genotypes. Am J Transl Res. 2009, 1: 163-77.
228. Mirra SS, Heyman A, McKeel D, Sumi SM, Crain BJ, Brownlee LM*, et al.* The Consortium to Establish a Registry for Alzheimer's Disease (CERAD). Part II. Standardization of the neuropathologic assessment of Alzheimer's disease. Neurology. 1991, 41: 479-86.
229. Fillenbaum GG, van Belle G, Morris JC, Mohs RC, Mirra SS, Davis PC*, et al.* CERAD (Consortium to Establish a Registry for Alzheimer's Disease) The first 20 years. Alzheimers Dement. 2008, 4: 96-109.
230. Olichney JM, Hansen LA, Hofstetter CR, Lee JH, Katzman R, Thal LJ. Association between severe cerebral amyloid angiopathy and cerebrovascular lesions in Alzheimer disease is not a spurious one attributable to apolipoprotein E4. Arch Neurol. 2000, 57: 869-74.
231. Ellis RJ, Olichney JM, Thal LJ, Mirra SS, Morris JC, Beekly D*, et al.* Cerebral amyloid angiopathy in the brains of patients with Alzheimer's disease: the CERAD experience, Part XV. Neurology. 1996, 46: 1592-6.
232. Schnell SA, Staines WA, Wessendorf MW. Reduction of Lipofuscin-like Autofluorescence in Fluorescently Labeled Tissue. J Histochem Cytochem. 1999, 47: 719-30.
233. Baschong W, Suetterlin R, Laeng RH. Control of autofluorescence of archival formaldehyde-fixed, paraffin-embedded tissue in confocal laser scanning microscopy (CLSM). J Histochem Cytochem. 2001, 49: 1565-72.
234. Sun Y, Yu H, Zheng D, Cao Q, Wang Y, Harris D. Sudan black B reduces autofluorescence in murine renal tissue. Arch Pathol Lab Med. 2011, 135: 1335-42.
235. Livak KJ, Schmittgen TD. Analysis of relative gene expression data using real-time quantitative PCR and the 2(-Delta Delta C(T)) Method. Methods. 2001, 25: 402-8.
236. D'Agostino RB, Stephens MA. Goodness-of-Fit Techniques. New York, USA: Macel Dekker Inc.; 1986.
237. Ferrara N, Heinsohn H, Walder CE, Bunting S, Thomas GR. The regulation of blood vessel growth by vascular endothelial growth factor. Ann N Y Acad Sci. 1995, 752: 246-56.

238. Liu Y, Cox SR, Morita T, Kourembanas S. Hypoxia regulates vascular endothelial growth factor gene expression in endothelial cells. Identification of a 5' enhancer. Circ Res. 1995, 77: 638-43.
239. Pham I, Uchida T, Planes C, Ware LB, Kaner R, Matthay MA*, et al.* Hypoxia upregulates VEGF expression in alveolar epithelial cells in vitro and in vivo. Am J Physiol Lung Cell Mol Physiol. 2002, 283: L1133-42.
240. Waltenberger J, Claesson-Welsh L, Siegbahn A, Shibuya M, Heldin CH. Different signal transduction properties of KDR and Flt1, two receptors for vascular endothelial growth factor. J Biol Chem. 1994, 269: 26988-95.
241. Shibuya M. Vascular endothelial growth factor receptor-1 (VEGFR-1/Flt-1): a dual regulator for angiogenesis. Angiogenesis. 2006, 9: 225-30; discussion 31.
242. Roberts DM, Kearney JB, Johnson JH, Rosenberg MP, Kumar R, Bautch VL. The vascular endothelial growth factor (VEGF) receptor Flt-1 (VEGFR-1) modulates Flk-1 (VEGFR-2) signaling during blood vessel formation. Am J Pathol. 2004, 164: 1531-5.
243. Li Y, Zhang F, Nagai N, Tang Z, Zhang S, Scotney P*, et al.* VEGF-B inhibits apoptosis via VEGFR-1-mediated suppression of the expression of BH3-only protein genes in mice and rats. J Clin Invest. 2008, 118: 913-23.
244. Poesen K, Lambrechts D, Van Damme P, Dhondt J, Bender F, Frank N*, et al.* Novel role for vascular endothelial growth factor (VEGF) receptor-1 and its ligand VEGF-B in motor neuron degeneration. J Neurosci. 2008, 28: 10451-9.
245. Wittko IM, Schanzer A, Kuzmichev A, Schneider FT, Shibuya M, Raab S*, et al.* VEGFR-1 regulates adult olfactory bulb neurogenesis and migration of neural progenitors in the rostral migratory stream in vivo. J Neurosci. 2009, 29: 8704-14.
246. Shweiki D, Itin A, Soffer D, Keshet E. Vascular endothelial growth factor induced by hypoxia may mediate hypoxia-initiated angiogenesis. Nature. 1992, 359: 843-5.
247. Pugh CW, Ratcliffe PJ. Regulation of angiogenesis by hypoxia: role of the HIF system. Nat Med. 2003, 9: 677-84.
248. Tuder RM, Flook BE, Voelkel NF. Increased gene expression for VEGF and the VEGF receptors KDR/Flk and Flt in lungs exposed to acute or to chronic hypoxia. Modulation of gene expression by nitric oxide. J Clin Invest. 1995, 95: 1798-807.
249. Sandner P, Wolf K, Bergmaier U, Gess B, Kurtz A. Hypoxia and cobalt stimulate vascular endothelial growth factor receptor gene expression in rats. Pflugers Arch. 1997, 433: 803-8.
250. Lennmyr F, Ata KA, Funa K, Olsson Y, Terent A. Expression of vascular endothelial growth factor (VEGF) and its receptors (Flt-1 and Flk-1) following permanent and transient occlusion of the middle cerebral artery in the rat. J Neuropathol Exp Neurol. 1998, 57: 874-82.
251. Choi JS, Kim HY, Cha JH, Choi JY, Park SI, Jeong CH*, et al.* Upregulation of vascular endothelial growth factor receptors Flt-1 and Flk-1 following acute spinal cord contusion in rats. J Histochem Cytochem. 2007, 55: 821-30.
252. Widenfalk J, Lipson A, Jubran M, Hofstetter C, Ebendal T, Cao Y*, et al.* Vascular endothelial growth factor improves functional outcome and decreases secondary degeneration in experimental spinal cord contusion injury. Neuroscience. 2003, 120: 951-60.
253. Ara J, Shukla P, Frank M. Enhanced expression of the Flt-1 and Flk-1 receptor tyrosine kinases in a newborn piglet model of ischemic tolerance. J Neurochem. 2013, 124: 735-46.
254. Krum JM, Mani N, Rosenstein JM. Angiogenic and astroglial responses to vascular endothelial growth factor administration in adult rat brain. Neuroscience. 2002, 110: 589-604.
255. Krum JM, Mani N, Rosenstein JM. Roles of the endogenous VEGF receptors flt-1 and flk-1 in astroglial and vascular remodeling after brain injury. Exp Neurol. 2008, 212: 108-17.

256. Krum JM, Rosenstein JM. VEGF mRNA and its receptor flt-1 are expressed in reactive astrocytes following neural grafting and tumor cell implantation in the adult CNS. Exp Neurol. 1998, 154: 57-65.
257. Hai J, Li ST, Lin Q, Pan QG, Gao F, Ding MX. Vascular endothelial growth factor expression and angiogenesis induced by chronic cerebral hypoperfusion in rat brain. Neurosurgery. 2003, 53: 963-70; 70-2.
258. Marti HH, Risau W. Systemic hypoxia changes the organ-specific distribution of vascular endothelial growth factor and its receptors. Proc Natl Acad Sci U S A. 1998, 95: 15809-14.
259. Harris R, Miners JS, Allen S, Love S. VEGFR1 and VEGFR2 in Alzheimer's Disease. J Alzheimers Dis. 2018, 61: 741-52.
260. Yingzhong Yang WF, Lingling Zhu, Tong Zhao, Lan Ma, Yan Wu, Rili Ge, Ming Fan. Effects of hypoxia on mRNA expression of housekeeping genes in rat braain tissue and primary cultured neural cells. Front Med China. 2008, 2: 239-43.
261. Zhong H, Simons JW. Direct comparison of GAPDH, beta-actin, cyclophilin, and 28S rRNA as internal standards for quantifying RNA levels under hypoxia. Biochem Biophys Res Commun. 1999, 259: 523-6.
262. Penna I, Vella S, Gigoni A, Russo C, Cancedda R, Pagano A. Selection of Candidate Housekeeping Genes for Normalization in Human Postmortem Brain Samples. Int J Mol Sci. 2011, 12: 5461-70.
263. Kim KK, Adelstein RS, Kawamoto S. Identification of neuronal nuclei (NeuN) as Fox-3, a new member of the Fox-1 gene family of splicing factors. J Biol Chem. 2009, 284: 31052-61.
264. Mullen RJ, Buck CR, Smith AM. NeuN, a neuronal specific nuclear protein in vertebrates. Development. 1992, 116: 201-11.
265. Wang Y, Su X, Sorenson CM, Sheibani N. Tissue-specific distributions of alternatively spliced human PECAM-1 isoforms. Am J Physiol Heart Circ Physiol. 2003, 284: H1008-17.
266. Wong D, Dorovini-Zis K. Platelet/endothelial cell adhesion molecule-1 (PECAM-1) expression by human brain microvessel endothelial cells in primary culture. Brain Res. 1996, 731: 217-20.
267. Jin K, Zhu Y, Sun Y, Mao XO, Xie L, Greenberg DA. Vascular endothelial growth factor (VEGF) stimulates neurogenesis in vitro and in vivo. Proc Natl Acad Sci U S A. 2002, 99: 11946-50.
268. Jin KL, Mao XO, Greenberg DA. Vascular endothelial growth factor: direct neuroprotective effect in in vitro ischemia. Proc Natl Acad Sci U S A. 2000, 97: 10242-7.
269. Harris AL. Hypoxia: a key regulatory factor in tumour growth. Nat Rev Cancer. 2002, 2: 38-47.
270. Katzman R, Saitoh T. Advances in Alzheimer's disease. Faseb j. 1991, 5: 278-86.
271. Shibuya M. Vascular endothelial growth factor and its receptor system: physiological functions in angiogenesis and pathological roles in various diseases. J Biochem. 2013, 153: 13-9.
272. Kalinowska A, Losy J. PECAM-1, a key player in neuroinflammation. Eur J Neurol. 2006, 13: 1284-90.
273. Ikeda T, Sun L, Tsuruoka N, Ishigaki Y, Yoshitomi Y, Yoshitake Y*, et al.* Hypoxia down-regulates sFlt-1 (sVEGFR-1) expression in human microvascular endothelial cells by a mechanism involving mRNA alternative processing. Biochem J. 2011, 436: 399-407.
274. Saito T, Takeda N, Amiya E, Nakao T, Abe H, Semba H*, et al.* VEGF-A induces its negative regulator, soluble form of VEGFR-1, by modulating its alternative splicing. FEBS Lett. 2013, 587: 2179-85.
275. Ahmad S, Ahmed A. Elevated placental soluble vascular endothelial growth factor receptor-1 inhibits angiogenesis in preeclampsia. Circ Res. 2004, 95: 884-91.

276. Shibuya M. Involvement of Flt-1 (VEGF receptor-1) in cancer and preeclampsia. Proc Jpn Acad Ser B Phys Biol Sci. 2011, 87: 167-78.
277. Maynard SE, Min JY, Merchan J, Lim KH, Li J, Mondal S*, et al.* Excess placental soluble fms-like tyrosine kinase 1 (sFlt1) may contribute to endothelial dysfunction, hypertension, and proteinuria in preeclampsia. J Clin Invest. 2003, 111: 649-58.
278. Fischer VW, Siddiqi A, Yusufaly Y. Altered angioarchitecture in selected areas of brains with Alzheimer's disease. Acta Neuropathol. 1990, 79: 672-9.
279. Buee L, Hof PR, Bouras C, Delacourte A, Perl DP, Morrison JH*, et al.* Pathological alterations of the cerebral microvasculature in Alzheimer's disease and related dementing disorders. Acta Neuropathol. 1994, 87: 469-80.
280. Buee L, Hof PR, Delacourte A. Brain microvascular changes in Alzheimer's disease and other dementias. Ann N Y Acad Sci. 1997, 826: 7-24.
281. Bailey TL, Rivara CB, Rocher AB, Hof PR. The nature and effects of cortical microvascular pathology in aging and Alzheimer's disease. Neurol Res. 2004, 26: 573-8.
282. Silverman WF, Krum JM, Mani N, Rosenstein JM. Vascular, glial and neuronal effects of vascular endothelial growth factor in mesencephalic explant cultures. Neuroscience. 1999, 90: 1529-41.
283. Freitas-Andrade M, Carmeliet P, Stanimirovic DB, Moreno M. VEGFR-2-mediated increased proliferation and survival in response to oxygen and glucose deprivation in PlGF knockout astrocytes. J Neurochem. 2008, 107: 756-67.
284. Wuestefeld R, Chen J, Meller K, Brand-Saberi B, Theiss C. Impact of vegf on astrocytes: Analysis of gap junctional intercellular communication, proliferation, and motility. Glia. 2012, 60: 936-47.
285. Kremer C, Breier G, Risau W, Plate KH. Up-regulation of flk-1/vascular endothelial growth factor receptor 2 by its ligand in a cerebral slice culture system. Cancer Res. 1997, 57: 3852-9.
286. Shen BQ, Lee DY, Gerber HP, Keyt BA, Ferrara N, Zioncheck TF. Homologous up-regulation of KDR/Flk-1 receptor expression by vascular endothelial growth factor in vitro. J Biol Chem. 1998, 273: 29979-85.
287. Elvert G, Kappel A, Heidenreich R, Englmeier U, Lanz S, Acker T*, et al.* Cooperative interaction of hypoxia-inducible factor-2alpha (HIF-2alpha) and Ets-1 in the transcriptional activation of vascular endothelial growth factor receptor-2 (Flk-1). J Biol Chem. 2003, 278: 7520-30.
288. Koch S, Claesson-Welsh L. Signal Transduction by Vascular Endothelial Growth Factor Receptors. Cold Spring Harb Perspect Med. 2012, 2.
289. Sentilhes L, Michel C, Lecourtois M, Catteau J, Bourgeois P, Laudenbach V*, et al.* Vascular endothelial growth factor and its high-affinity receptor (VEGFR-2) are highly expressed in the human forebrain and cerebellum during development. J Neuropathol Exp Neurol. 2010, 69: 111-28.
290. Sentilhes L, Marret S, Leroux P, Gonzalez BJ, Laquerriere A. Vascular-endothelial growth factor and its high affinity receptor VEGFR-2 in the normal versus destructive lesions human forebrain during development: an immuno-histochemical comparative study. Brain Res. 2011, 1385: 77-86.
291. Fernando MS, Simpson JE, Matthews F, Brayne C, Lewis CE, Barber R*, et al.* White matter lesions in an unselected cohort of the elderly: molecular pathology suggests origin from chronic hypoperfusion injury. Stroke. 2006, 37: 1391-8.
292. Bernal GM, Peterson DA. Phenotypic and gene expression modification with normal brain aging in GFAP-positive astrocytes and neural stem cells. Aging Cell. 2011, 10: 466-82.
293. Wang WY, Dong JH, Liu X, Wang Y, Ying GX, Ni ZM*, et al.* Vascular endothelial growth factor and its receptor Flk-1 are expressed in the hippocampus following entorhinal deafferentation. Neuroscience. 2005, 134: 1167-78.
294. Koyama Y, Nagae R, Tokuyama S, Tanaka K. I.c.v administration of an endothelin ET(B) receptor agonist stimulates vascular endothelial growth factor-A production

and activates vascular endothelial growth factor receptors in rat brain. Neuroscience. 2011, 192: 689-98.
295. Wang P, Xie ZH, Guo YJ, Zhao CP, Jiang H, Song Y*, et al.* VEGF-induced angiogenesis ameliorates the memory impairment in APP transgenic mouse model of Alzheimer's disease. Biochem Biophys Res Commun. 2011, 411: 620-6.
296. Boer K, Troost D, Spliet WG, van Rijen PC, Gorter JA, Aronica E. Cellular distribution of vascular endothelial growth factor A (VEGFA) and B (VEGFB) and VEGF receptors 1 and 2 in focal cortical dysplasia type IIB. Acta Neuropathol. 2008, 115: 683-96.
297. Waltenberger J, Mayr U, Pentz S, Hombach V. Functional upregulation of the vascular endothelial growth factor receptor KDR by hypoxia. Circulation. 1996, 94: 1647-54.
298. Olszewska-Pazdrak B, Hein TW, Olszewska P, Carney DH. Chronic hypoxia attenuates VEGF signaling and angiogenic responses by downregulation of KDR in human endothelial cells. Am J Physiol Cell Physiol. 2009, 296: C1162-70.
299. Brogi E, Schatteman G, Wu T, Kim EA, Varticovski L, Keyt B*, et al.* Hypoxia-induced paracrine regulation of vascular endothelial growth factor receptor expression. J Clin Invest. 1996, 97: 469-76.
300. Rosenstein JM, Mani N, Khaibullina A, Krum JM. Neurotrophic effects of vascular endothelial growth factor on organotypic cortical explants and primary cortical neurons. J Neurosci. 2003, 23: 11036-44.
301. Lee HT, Chang YC, Tu YF, Huang CC. VEGF-A/VEGFR-2 signaling leading to cAMP response element-binding protein phosphorylation is a shared pathway underlying the protective effect of preconditioning on neurons and endothelial cells. J Neurosci. 2009, 29: 4356-68.
302. Stowe AM, Plautz EJ, Nguyen P, Frost SB, Eisner-Janowicz I, Barbay S*, et al.* Neuronal HIF-1 alpha protein and VEGFR-2 immunoreactivity in functionally related motor areas following a focal M1 infarct. J Cereb Blood Flow Metab. 2008, 28: 612-20.
303. Cebe-Suarez S, Zehnder-Fjallman A, Ballmer-Hofer K. The role of VEGF receptors in angiogenesis; complex partnerships. Cell Mol Life Sci. 2006, 63: 601-15.
304. Dougher M, Terman BI. Autophosphorylation of KDR in the kinase domain is required for maximal VEGF-stimulated kinase activity and receptor internalization. Oncogene. 1999, 18: 1619-27.
305. Meyer RD, Dayanir V, Majnoun F, Rahimi N. The presence of a single tyrosine residue at the carboxyl domain of vascular endothelial growth factor receptor-2/FLK-1 regulates its autophosphorylation and activation of signaling molecules. J Biol Chem. 2002, 277: 27081-7.
306. Paris D, Townsend K, Quadros A, Humphrey J, Sun J, Brem S*, et al.* Inhibition of angiogenesis by Abeta peptides. Angiogenesis. 2004, 7: 75-85.
307. Patel NS, Quadros A, Brem S, Wotoczek-Obadia M, Mathura VS, Laporte V*, et al.* Potent anti-angiogenic motifs within the Alzheimer beta-amyloid peptide. Amyloid. 2008, 15: 5-19.
308. Patel NS, Mathura VS, Bachmeier C, Beaulieu-Abdelahad D, Laporte V, Weeks O*, et al.* Alzheimer's beta-amyloid peptide blocks vascular endothelial growth factor mediated signaling via direct interaction with VEGFR-2. J Neurochem. 2010, 112: 66-76.
309. Terman BI, Dougher-Vermazen M, Carrion ME, Dimitrov D, Armellino DC, Gospodarowicz D*, et al.* Identification of the KDR tyrosine kinase as a receptor for vascular endothelial cell growth factor. Biochem Biophys Res Commun. 1992, 187: 1579-86.
310. Takahashi T, Shibuya M. The 230 kDa mature form of KDR/Flk-1 (VEGF receptor-2) activates the PLC-gamma pathway and partially induces mitotic signals in NIH3T3 fibroblasts. Oncogene. 1997, 14: 2079-89.

311. Cahoy JD, Emery B, Kaushal A, Foo LC, Zamanian JL, Christopherson KS*, et al.* A Transcriptome Database for Astrocytes, Neurons, and Oligodendrocytes: A New Resource for Understanding Brain Development and Function. J Neurosci. 2008, 28: 264-78.
312. Sekar S, McDonald J, Cuyugan L, Aldrich J, Kurdoglu A, Adkins J*, et al.* Alzheimer's disease is associated with altered expression of genes involved in immune response and mitochondrial processes in astrocytes. Neurobiol Aging. 2015, 36: 583-91.
313. Spliet WG, Aronica E, Ramkema M, Witmer AN, Schlingemann RO, de Jong JM*, et al.* Immunohistochemical localization of vascular endothelial growth factor receptors-1, -2 and -3 in human spinal cord: altered expression in amyotrophic lateral sclerosis. Neuropathol Appl Neurobiol. 2004, 30: 351-9.
314. Barker R, Wellington D, Esiri MM, Love S. Assessing white matter ischemic damage in dementia patients by measurement of myelin proteins. J Cereb Blood Flow Metab. 2013, 33: 1050-7.
315. Ashby EL, Kehoe PG, Love S. Kallikrein-related peptidase 6 in Alzheimer's disease and vascular dementia. Brain Res. 2010, 1363: 1-10.
316. Miners JS, Palmer JC, Tayler H, Palmer LE, Ashby E, Kehoe PG*, et al.* Abeta degradation or cerebral perfusion? Divergent effects of multifunctional enzymes. Front Aging Neurosci. 2014, 6: 238.
317. Attems J, Quass M, Jellinger KA, Lintner F. Topographical distribution of cerebral amyloid angiopathy and its effect on cognitive decline are influenced by Alzheimer disease pathology. J Neurol Sci. 2007, 257: 49-55.
318. Jellinger KA. Alzheimer disease and cerebrovascular pathology: an update. J Neural Transm (Vienna). 2002, 109: 813-36.
319. Thal DR, Capetillo-Zarate E, Larionov S, Staufenbiel M, Zurbruegg S, Beckmann N. Capillary cerebral amyloid angiopathy is associated with vessel occlusion and cerebral blood flow disturbances. Neurobiol Aging. 2009, 30: 1936-48.
320. Biffi A, Greenberg SM. Cerebral amyloid angiopathy: a systematic review. J Clin Neurol. 2011, 7: 1-9.
321. Suzuki N, Iwatsubo T, Odaka A, Ishibashi Y, Kitada C, Ihara Y. High tissue content of soluble beta 1-40 is linked to cerebral amyloid angiopathy. Am J Pathol. 1994, 145: 452-60.
322. Shi Y, Thrippleton MJ, Makin SD, Marshall I, Geerlings MI, de Craen AJ*, et al.* Cerebral blood flow in small vessel disease: A systematic review and meta-analysis. J Cereb Blood Flow Metab. 2016, 36: 1653-67.
323. Arba F, Mair G, Carpenter T, Sakka E, Sandercock PAG, Lindley RI*, et al.* Cerebral White Matter Hypoperfusion Increases with Small-Vessel Disease Burden. Data From the Third International Stroke Trial. J Stroke Cerebrovasc Dis. 2017, 26: 1506-13.
324. van Dijk EJ, Prins ND, Vrooman HA, Hofman A, Koudstaal PJ, Breteler MM. Progression of cerebral small vessel disease in relation to risk factors and cognitive consequences: Rotterdam Scan study. Stroke. 2008, 39: 2712-9.
325. van der Flier WM, van Straaten EC, Barkhof F, Verdelho A, Madureira S, Pantoni L*, et al.* Small vessel disease and general cognitive function in nondisabled elderly: the LADIS study. Stroke. 2005, 36: 2116-20.
326. Study NGMRCCFaA. Pathological correlates of late-onset dementia in a multicentre, community-based population in England and Wales. Neuropathology Group of the Medical Research Council Cognitive Function and Ageing Study (MRC CFAS). Lancet. 2001, 357: 169-75.
327. Hainsworth AH, Oommen AT, Bridges LR. Endothelial cells and human cerebral small vessel disease. Brain Pathol. 2015, 25: 44-50.
328. Grinberg LT, Korczyn AD, Heinsen H. Cerebral amyloid angiopathy impact on endothelium. Exp Gerontol. 2012, 47: 838-42.

329. Poggesi A, Pasi M, Pescini F, Pantoni L, Inzitari D. Circulating biologic markers of endothelial dysfunction in cerebral small vessel disease: A review. J Cereb Blood Flow Metab. 2016, 36: 72-94.
330. Magrane J, Christensen RA, Rosen KM, Veereshwarayya V, Querfurth HW. Dissociation of ERK and Akt signaling in endothelial cell angiogenic responses to beta-amyloid. Exp Cell Res. 2006, 312: 996-1010.
331. Sadler JE. Biochemistry and genetics of von Willebrand factor. Annu Rev Biochem. 1998, 67: 395-424.
332. Sternberger NH, Quarles RH, Itoyama Y, Webster HD. Myelin-associated glycoprotein demonstrated immunocytochemically in myelin and myelin-forming cells of developing rat. Proc Natl Acad Sci U S A. 1979, 76: 1510-4.
333. Trapp BD, Andrews SB, Cootauco C, Quarles R. The myelin-associated glycoprotein is enriched in multivesicular bodies and periaxonal membranes of actively myelinating oligodendrocytes. J Cell Biol. 1989, 109: 2417-26.
334. Hudson LD, Friedrich VL, Jr., Behar T, Dubois-Dalcq M, Lazzarini RA. The initial events in myelin synthesis: orientation of proteolipid protein in the plasma membrane of cultured oligodendrocytes. J Cell Biol. 1989, 109: 717-27.
335. Quarles RH. Myelin-associated glycoprotein (MAG): past, present and beyond. J Neurochem. 2007, 100: 1431-48.
336. Aboul-Enein F, Rauschka H, Kornek B, Stadelmann C, Stefferl A, Bruck W*, et al.* Preferential loss of myelin-associated glycoprotein reflects hypoxia-like white matter damage in stroke and inflammatory brain diseases. J Neuropathol Exp Neurol. 2003, 62: 25-33.
337. Lucchinetti C, Bruck W, Parisi J, Scheithauer B, Rodriguez M, Lassmann H. Heterogeneity of multiple sclerosis lesions: implications for the pathogenesis of demyelination. Ann Neurol. 2000, 47: 707-17.
338. Wallin A, Gottfries CG, Karlsson I, Svennerholm L. Decreased myelin lipids in Alzheimer's disease and vascular dementia. Acta Neurol Scand. 1989, 80: 319-23.
339. Thomas T, Miners, SJ, Kehoe, PG. Correlation between levels of VEGF and insoluble Aβ(1-42) in the cerebral cortex in Alzheimer's disease. Neuropathol Appl Neurobiol. 2015, 41: 8-29.
340. Sweeney MD, Ayyadurai S, Zlokovic BV. Pericytes of the neurovascular unit: key functions and signaling pathways. Nat Neurosci. 2016, 19: 771-83.
341. Attwell D, Mishra A, Hall CN, O'Farrell FM, Dalkara T. What is a pericyte? J Cereb Blood Flow Metab. 2016, 36: 451-5.
342. Bergers G, Song S. The role of pericytes in blood-vessel formation and maintenance. Neuro Oncol. 2005, 7: 452-64.
343. Winkler EA, Sagare AP, Zlokovic BV. The pericyte: a forgotten cell type with important implications for Alzheimer's disease? Brain Pathol. 2014, 24: 371-86.
344. Armulik A, Genove G, Mae M, Nisancioglu MH, Wallgard E, Niaudet C*, et al.* Pericytes regulate the blood-brain barrier. Nature. 2010, 468: 557-61.
345. Bell RD, Winkler EA, Sagare AP, Singh I, LaRue B, Deane R*, et al.* Pericytes control key neurovascular functions and neuronal phenotype in the adult brain and during brain aging. Neuron. 2010, 68: 409-27.
346. Lindahl P, Johansson BR, Leveen P, Betsholtz C. Pericyte loss and microaneurysm formation in PDGF-B-deficient mice. Science. 1997, 277: 242-5.
347. Sagare AP, Bell RD, Zhao Z, Ma Q, Winkler EA, Ramanathan A*, et al.* Pericyte loss influences Alzheimer-like neurodegeneration in mice. Nat Commun. 2013, 4: 2932.
348. Rustenhoven J, Jansson D, Smyth LC, Dragunow M. Brain Pericytes As Mediators of Neuroinflammation. Trends Pharmacol Sci. 2017, 38: 291-304.
349. Baloyannis SJ, Baloyannis IS. The vascular factor in Alzheimer's disease: a study in Golgi technique and electron microscopy. J Neurol Sci. 2012, 322: 117-21.
350. Miners JS, Schulz I, Love S. Differing associations between Abeta accumulation, hypoperfusion, blood-brain barrier dysfunction and loss of PDGFRB pericyte marker

in the precuneus and parietal white matter in Alzheimer's disease. J Cereb Blood Flow Metab. 2017: 103-15.
351. Kisler K, Nelson AR, Rege SV, Ramanathan A, Wang Y, Ahuja A*, et al.* Pericyte degeneration leads to neurovascular uncoupling and limits oxygen supply to brain. Nat Neurosci. 2017, 20: 406-16.
352. Verbeek MM, de Waal RM, Schipper JJ, Van Nostrand WE. Rapid degeneration of cultured human brain pericytes by amyloid beta protein. J Neurochem. 1997, 68: 1135-41.
353. Wisniewski HM, Wegiel J, Wang KC, Lach B. Ultrastructural studies of the cells forming amyloid in the cortical vessel wall in Alzheimer's disease. Acta Neuropathol. 1992, 84: 117-27.
354. Vinters HV, Secor DL, Read SL, Frazee JG, Tomiyasu U, Stanley TM*, et al.* Microvasculature in brain biopsy specimens from patients with Alzheimer's disease: an immunohistochemical and ultrastructural study. Ultrastruct Pathol. 1994, 18: 333-48.
355. Bell RD, Winkler EA, Singh I, Sagare AP, Deane R, Wu Z*, et al.* Apolipoprotein E controls cerebrovascular integrity via cyclophilin A. Nature. 2012, 485: 512-6.
356. Halliday MR, Pomara N, Sagare AP, Mack WJ, Frangione B, Zlokovic BV. Relationship between cyclophilin a levels and matrix metalloproteinase 9 activity in cerebrospinal fluid of cognitively normal apolipoprotein e4 carriers and blood-brain barrier breakdown. JAMA Neurol. 2013, 70: 1198-200.
357. Halliday MR, Rege SV, Ma Q, Zhao Z, Miller CA, Winkler EA*, et al.* Accelerated pericyte degeneration and blood-brain barrier breakdown in apolipoprotein E4 carriers with Alzheimer's disease. J Cereb Blood Flow Metab. 2016, 36: 216-27.
358. Franco M, Roswall P, Cortez E, Hanahan D, Pietras K. Pericytes promote endothelial cell survival through induction of autocrine VEGF-A signaling and Bcl-w expression. Blood. 2011, 118: 2906-17.
359. Darland DC, Massingham LJ, Smith SR, Piek E, Saint-Geniez M, D'Amore PA. Pericyte production of cell-associated VEGF is differentiation-dependent and is associated with endothelial survival. Dev Biol. 2003, 264: 275-88.
360. Winkler EA, Bell RD, Zlokovic BV. Central nervous system pericytes in health and disease. Nat Neurosci. 2011, 14: 1398-405.
361. Dore-Duffy P, Wang X, Mehedi A, Kreipke CW, Rafols JA. Differential expression of capillary VEGF isoforms following traumatic brain injury. Neurol Res. 2007, 29: 395-403.
362. Zechariah A, ElAli A, Doeppner TR, Jin F, Hasan MR, Helfrich I*, et al.* Vascular endothelial growth factor promotes pericyte coverage of brain capillaries, improves cerebral blood flow during subsequent focal cerebral ischemia, and preserves the metabolic penumbra. Stroke. 2013, 44: 1690-7.
363. Gonul E, Duz B, Kahraman S, Kayali H, Kubar A, Timurkaynak E. Early pericyte response to brain hypoxia in cats: an ultrastructural study. Microvasc Res. 2002, 64: 116-9.
364. Eilken HM, Dieguez-Hurtado R, Schmidt I, Nakayama M, Jeong HW, Arf H*, et al.* Pericytes regulate VEGF-induced endothelial sprouting through VEGFR1. Nat Commun. 2017, 8: 1574.
365. Flores-Nascimento MC, Alessio AM, de Andrade Orsi FL, Annichino-Bizzacchi JM. CD144, CD146 and VEGFR-2 properly identify circulating endothelial cell. Rev Bras Hematol Hemoter. 2015, 37: 98-102.
366. Yoder MC. Human Endothelial Progenitor Cells. Cold Spring Harb Perspect Med. 2012, 2.
367. Cho SJ, Park MH, Han C, Yoon K, Koh YH. VEGFR2 alteration in Alzheimer's disease. Sci Rep. 2017, 7: 17713.
368. Greenbaum D, Colangelo C, Williams K, Gerstein M. Comparing protein abundance and mRNA expression levels on a genomic scale. Genome Biol. 2003, 4: 117.

369. Gentile MT, Vecchione C, Maffei A, Aretini A, Marino G, Poulet R*, et al.* Mechanisms of soluble beta-amyloid impairment of endothelial function. J Biol Chem. 2004, 279: 48135-42.
370. Suhara T, Magrane J, Rosen K, Christensen R, Kim HS, Zheng B*, et al.* Abeta42 generation is toxic to endothelial cells and inhibits eNOS function through an Akt/GSK-3beta signaling-dependent mechanism. Neurobiol Aging. 2003, 24: 437-51.
371. Jacobs HI, Van Boxtel MP, Jolles J, Verhey FR, Uylings HB. Parietal cortex matters in Alzheimer's disease: an overview of structural, functional and metabolic findings. Neurosci Biobehav Rev. 2012, 36: 297-309.
372. Yang SP, Kwon BO, Gho YS, Chae CB. Specific interaction of VEGF165 with beta-amyloid, and its protective effect on beta-amyloid-induced neurotoxicity. J Neurochem. 2005, 93: 118-27.
373. Markovic-Mueller S, Stuttfeld E, Asthana M, Weinert T, Bliven S, Goldie KN*, et al.* Structure of the Full-length VEGFR-1 Extracellular Domain in Complex with VEGF-A. Structure. 2017, 25: 341-52.
374. Singh Angom R, Wang Y, Wang E, Pal K, Bhattacharya S, Watzlawik JO*, et al.* VEGF receptor-1 modulates amyloid beta 1-42 oligomer-induced senescence in brain endothelial cells. Faseb j. 2019, 33: 4626-37.
375. Cao Y. Positive and negative modulation of angiogenesis by VEGFR1 ligands. Sci Signal. 2009, 2: re1.
376. Thomas JL, Baker K, Han J, Calvo C, Nurmi H, Eichmann AC*, et al.* Interactions between VEGFR and Notch signaling pathways in endothelial and neural cells. Cell Mol Life Sci. 2013, 70: 1779-92.
377. Ball SG, Shuttleworth CA, Kielty CM. Vascular endothelial growth factor can signal through platelet-derived growth factor receptors. J Cell Biol. 2007, 177: 489-500.
378. Mamer SB, Chen S, Weddell JC, Palasz A, Wittenkeller A, Kumar M*, et al.* Discovery of High-Affinity PDGF-VEGFR Interactions: Redefining RTK Dynamics. Sci Rep. 2017, 7: 16439.
379. Yamazaki Y, Baker DJ, Tachibana M, Liu CC, van Deursen JM, Brott TG*, et al.* Vascular Cell Senescence Contributes to Blood-Brain Barrier Breakdown. Stroke. 2016, 47: 1068-77.
380. Erickson MA, Banks WA. Blood-brain barrier dysfunction as a cause and consequence of Alzheimer's disease. J Cereb Blood Flow Metab. 2013, 33: 1500-13.
381. Cao L, Jiao X, Zuzga DS, Liu Y, Fong DM, Young D*, et al.* VEGF links hippocampal activity with neurogenesis, learning and memory. Nat Genet. 2004, 36: 827-35.
382. De Rossi P, Harde E, Dupuis JP, Martin L, Chounlamountri N, Bardin M*, et al.* A critical role for VEGF and VEGFR2 in NMDA receptor synaptic function and fear-related behavior. Mol Psychiatry. 2016, 21: 1768-80.
383. Walsh DM, Klyubin I, Fadeeva JV, Cullen WK, Anwyl R, Wolfe MS*, et al.* Naturally secreted oligomers of amyloid |[beta]| protein potently inhibit hippocampal long-term potentiation in vivo. Nature. 2002, 416: 535-9.
384. Rowan MJ, Klyubin I, Cullen WK, Anwyl R. Synaptic plasticity in animal models of early Alzheimer's disease. Philos Trans R Soc Lond B Biol Sci. 2003, 358: 821-8.
385. Jo J, Whitcomb DJ, Olsen KM, Kerrigan TL, Lo S-C, Bru-Mercier G*, et al.* A[beta]1-42 inhibition of LTP is mediated by a signaling pathway involving caspase-3, Akt1 and GSK-3[beta]. Nat Neurosci. 2011, 14: 545-7.
386. Herran E, Perez-Gonzalez R, Igartua M, Pedraz JL, Carro E, Hernandez RM. VEGF-releasing biodegradable nanospheres administered by craniotomy: a novel therapeutic approach in the APP/Ps1 mouse model of Alzheimer's disease. J Control Release. 2013, 170: 111-9.
387. Garcia KO, Ornellas FL, Martin PK, Patti CL, Mello LE, Frussa-Filho R*, et al.* Therapeutic effects of the transplantation of VEGF overexpressing bone marrow mesenchymal stem cells in the hippocampus of murine model of Alzheimer's disease. Front Aging Neurosci. 2014, 6: 30.

388. Jean LeBlanc N, Guruswamy R, ElAli A. Vascular Endothelial Growth Factor Isoform-B Stimulates Neurovascular Repair After Ischemic Stroke by Promoting the Function of Pericytes via Vascular Endothelial Growth Factor Receptor-1. Mol Neurobiol. 2017: 1-16.
389. Glass CA, Harper SJ, Bates DO. The anti-angiogenic VEGF isoform VEGF165b transiently increases hydraulic conductivity, probably through VEGF receptor 1 in vivo. J Physiol. 2006, 572: 243-57.
390. Zhang N, Song C, Zhao B, Xing M, Luo L, Gordon ML*, et al.* Neovascularization and Synaptic Function Regulation with Memantine and Rosuvastatin in a Rat Model of Chronic Cerebral Hypoperfusion. J Mol Neurosci. 2017, DOI: 10.1007/s12031-017-0974-1.
391. Kitamura A, Saito S, Maki T, Oishi N, Ayaki T, Hattori Y*, et al.* Gradual cerebral hypoperfusion in spontaneously hypertensive rats induces slowly evolving white matter abnormalities and impairs working memory. J Cereb Blood Flow Metab. 2016, 36: 1592-602.
392. Hattori Y, Enmi J, Iguchi S, Saito S, Yamamoto Y, Tsuji M*, et al.* Gradual Carotid Artery Stenosis in Mice Closely Replicates Hypoperfusive Vascular Dementia in Humans. J Am Heart Assoc. 2016, 5.
393. Varet J, Douglas SK, Gilmartin L, Medford ARL, Bates DO, Harper SJ*, et al.* VEGF in the lung: a role for novel isoforms. American Journal of Physiology - Lung Cellular and Molecular Physiology. 2010, 298: L768-L74.
394. Duncombe J, Kitamura A, Hase Y, Ihara M, Kalaria RN, Horsburgh K. Chronic cerebral hypoperfusion: a key mechanism leading to vascular cognitive impairment and dementia. Closing the translational gap between rodent models and human vascular cognitive impairment and dementia. Clin Sci (Lond). 2017, 131: 2451-68.
395. Hase Y, Craggs L, Hase M, Stevenson W, Slade J, Lopez D*, et al.* Effects of environmental enrichment on white matter glial responses in a mouse model of chronic cerebral hypoperfusion. J Neuroinflammation. 2017, 14: 81.
396. Basagiannis D, Christoforidis S. Constitutive Endocytosis of VEGFR2 Protects the Receptor against Shedding. J Biol Chem. 2016, 291: 16892-903.
397. Smith GA, Fearnley GW, Abdul-Zani I, Wheatcroft SB, Tomlinson DC, Harrison MA*, et al.* VEGFR2 Trafficking, Signaling and Proteolysis is Regulated by the Ubiquitin Isopeptidase USP8. Traffic. 2016, 17: 53-65.
398. Bruns AF, Herbert SP, Odell AF, Jopling HM, Hooper NM, Zachary IC*, et al.* Ligand-stimulated VEGFR2 signaling is regulated by co-ordinated trafficking and proteolysis. Traffic. 2010, 11: 161-74.

Appendix

Appendix 1 Chemicals and reagents

Consumables	Manufacturer
10x Trypsin-EDTA	Sigma
2 ml screw-top tubes	ThermoFisher Scientific
24-well plates	Starstdt
30% Acrylamide	Bio-Rad Laboratories
96 well plate – Black	Nunc
96 well plate – Clear	Nunc
96 well plate - Clear removable strips (ELISA)	Biotechne
Accutase	Sigma
Acetonitrile	ThermoFisher Scientific
Aprotinin	Sigma
APS	Sigma
Avidin-biotin complex (ABC) Elite-Peroxidase kit (universal)	Vector Laboratories
$A\beta_{1-40}$	Anaspec
$A\beta_{1-42}$	Anaspec
Bijoux (7ml)	Greiner
Biotinylated Goat anti-Rabbit IgG (H+L)	Vector Laboratories,
BLUeye prestained protein ladder	Geneflow
Bovine serum albumin	Sigma
Cell culture flasks (vented)- T25 and T75	Greiner
CelLytic M Cell Lysis Reagent	Sigma-Aldrich
Chloroform	Sigma
Clearene	Leica
Compressed gas (O_2, Air, N_2)	BOC
Copper sulphate ($CuSO_4$)	BDH Merck
Coverslips	Surgipath
Cryovials	Greiner
DAB peroxidase (HRP) substrate kit (with nickel), 3,3'-diaminobenzidine	Vector Laboratories
Di-sodium hydrogen orthophosphate 12-hydrate	Sigma
Disposible pipettes (sterile) - 5ml, 10ml, 25ml	Greiner
DMSO	Sigma
DNase I recombinant	Roche
DPX mountant	Sigma
Dried skimmed milk powder	Marvel
Dulbecco's Phosphate Buffered Saline (without calcium or magnesium)	Sigma
Eagle's Minimum Essential Medium	Sigma
EDTA	BDG
Endothelial cell medium (Complete kit)	ScienCell

Enhanced chemiluminescence (ECL) western blotting substrate	ThermoFisher Scientific
Eppendorf tubes - 0.2ml, 1.5ml, 2ml	Eppendorf
Ethanol	ThermoFisher Scientific
Falcon tubes (15 ml, 50 ml)	Greiner
Fast Taqman qPCR master mix	Applied Biosystems
Fetal bovine serum	ThermoFisher Scientific
Fibroblast surface protein antibody	Abcam
Fibronectin	ScienCell
Foetal bovine serum (FBS)	Gibco
GFAP	Dako
Gill II Hematoxylin	Leica
Glycogen from Mytilus edulis (Blue mussel)	Sigma
Goat anti-Mouse IgG (H+L), Alexa Fluor 488 conjugate	ThermoFisher Scientific
Goat anti-Mouse IgM (μ chain), Alexa Fluor 488 conjugate	Abcam
Goat anti-Rabbit IgG (H+L), Alexa Fluor 546 conjugate	ThermoFisher Scientific
High capacity cDNA reverse transcription kit	ThermoFisher Scientific
HLA-DP, DQ, DR	Dako
HRP Goat Anti-Rabbit IgG Antibody (Peroxidase)	Vector Laboratories,
HRP Horse Anti-Mouse IgG Antibody (Peroxidase)	Vector Laboratories,
Human brain microvascular endothelial cells	ScienCell
Human brain vascular pericytes	ScienCell
Human phospho-VEGF R2/KDR DuoSet IC ELISA kit	R&D Systems
Human total VEGFR2 (KDR) DuoSet IC ELISA kit	R&D Systems
Human VEGF-A DuoSet ELISA kit	R&D Systems
Human VEGFR1 (Flt1) DuoSet ELISA kit	R&D Systems
Human Von Willebrand factor ELISA kit	Abcam
Hydrogen peroxide (30%)	ThermoFisher Scientific
Isopropranol	ThermoFisher Scientific
Leupeptin	Sigma
MAG recombinant	Abnova
Magnesium chloride ($MgCl_2$)	ThermoFisher Scientific
Methanol	ThermoFisher Scientific
MicroAmp fast optical 96-well reaction plate	ThermoFisher Scientific
MicroAmp optical adhesive film	ThermoFisher Scientific
Microscope slides Superfrost Plus	ThermoFisher Scientific
Myelin-associated glycoprotein (MAG) antibody	Abcam
Nitrocellulose membrane	Thermo Fisher Scientific
Normal goat serum	Vector Laboritories
PAP pen	Daido Sangyo Co.
PDGFRβ antibody	ThermoFisher Scientific
Pericyte medium (Complete kit)	ScienCell
Peroxidase substrate for ELISA	R&D systems
Pipette tips (10 µl, 200 µl 1000 µl)	STARLAB
PipetteBoy	NovaVeth

Polyacrilimide gels (7.5%, 4-20%)	BioRad
Poly-L-lysine	ScienCell
PureLink RNA Mini Kit	ThermoFisher Scientific
Quant-iT PicoGreen Kit	Invitrogen
Rabbit (DA1E) mAb IgG XP Isotype Control	Cell Signalling
Restore western blot stripping buffer	ThermoFisher Scientific
RNase- free water	Sigma
RNAse-free filter tips (10 µl, 20µl, 200 µl 1000 µl	STARLAB
Scalpels	Apelton woods
SDS	Sigma
Sodium chloride (NaCl)	Sigma
Sodium dihydrogen orthophosphate dihydrate	Sigma
Streptavidin, Alexa Fluor® 555 Conjugate	Invitrogen
Sudan Black	Sigma
Sulfuric Acid (2N)	Sigma
Taqman Fast Advanced Master Mix	ThermoFisher Scientific
Taqman primers	ThermoFisher Scientific
TEMED	Bio-Rad Laboratories
Total protein kit	Sigma
Tris	Sigma
Trisodium citrate	ThermoFisher Scientific
TRIzol	ThermoFisher Scientific
Trypan blue solution, 0.4%	ThermoFisher Scientific
Tween 20	Sigma
Vectorsheild mounting medium	Vector Laboratories
Vectorsheild mounting medium with DAPI	Vector Laboritories
Vectorstain Elite ABC kit (Universal)	Vector Laboratories
VEGFR1 antibody	Abcam
VEGFR2 antibody	Cell Signalling
Very intense purple substrate kit	Vector Laboratories
Virkon disinfectant tablets	ThermoFisher Scientific
Von Willebrand factor (vWF) antibody	Dako
Von Willebrand factor (vWF) ELISA kit	Abcam
Zirconia/Silica (ceramic) beads (2.3 mm diameter)	Stratech Scientific
α-Smooth muscle actin antibody	Abcam
β-Actin antibody	Sigma

Details of consumable and reagent suppliers.

Appendix 2 Equipment

Details of laboratory equipment	Manufacturer
Autoclave	Priorclave
Balance	Sartorius
Bench top centrifuge (cell culture)	ThermoFisher Scientific
Bio-Rad Laboratories Mini-PROTEAN 3, electrophoresis module	Bio-Rad Laboratories
Class II laminar flow hood	MDH InterMed
CO_2 incubator	Sanyo Electric co.
CoolCell LX controlled-rate alcohol-free cell freezing container	Biocision
CTR6000 Fluorescence Microscope	Leica
DFC350FX Camera - Fluorescence Microscope	Leica
DMR Light microscope	Leica
Dot blot manifold	BioRad
Eclipse TS100 Inverted microscope	Nikon
Fine Balance BR221S	Sartorius
FLUOstar OPTIMA, microplate reader	BMG Labtech
Fume hood	Surgipath Europe
Haematocytometer	Hawksley
Hypoxic chamber (SCI-tive)	Baker Ruskinn
Magnetic stirrer	Bibby
Microcentrifuge	Scotlab
Mini-Sub Cell GT Cell electrophoresis tank	Bio-Rad Laboratories
Molecular Imager Gel Doc XR System	Bio-Rad Laboratories
Orbital shaker platform	GrantBio
pH meter	Hanna instruments
Pico17 Heraeus Centrifuge	Thermo Scientific
Plate spinner	Labnet
Power Pack	Bio-Rad Laboratories
Precellys 24, mechanical homogeniser	Bertin Technologies
QICAM digital camera	QImaging
Refrigerated centrifuge	Biofuge
Thermal cycler	Applied Biosystems
ViiA7 Real-Time PCR system	Applied Biosystems
Vortex	HATi
Water Still	Purite Select Fusion

Details of equipment and manufacturers.

Appendix 3 Software and publishers

Software	Version	Publisher
GraphPad Prism	6.07	GraphPad Software, La Jolla California USA
BioRad ImageLab	5.2	Bio-Rad Laboratories, Hercules, California, United States
BMG Labtech Optima	2.2 R2	BMG LABTECH GmbH Ortenberg, Germany
MARS Data Analysis	3.01 R2	BMG LABTECH GmbH Ortenberg, Germany

Details of software and publishers.

Appendix 4 Solution compositions

Solution	Composition	Technique
10x Running Buffer	0.25 M Tris 1.92 M Glycine 1% w/v SDS	Western blotting
10x Blotting buffer	0.25M Tris (0.25 M) 1.92 glycine (1.92M)	Western blotting
1x Blotting buffer	10% v/v 10x blotting buffer 20% v/v methanol	Western blotting
10x TBS	0.2 M Tris base 5 M NaCl pH 7.6	Western blotting Dot blotting
1x TBS	10% v/v TBS	Western blotting Dot blotting
0.05% TBST	0.05% v/v Tween 20 TBS	Western blotting
Blocking buffer	10% w/v milk powder TBST	Western blotting
BSA block/antibody buffer	3% w/v BSA TBST	Western blotting Dot blotting
BSA block/antibody buffer	5% w/v BSA PBST	Immunofluorescence
Citrate buffer	10 mM trisodium citrate 0.05% v/v Tween 20 pH 6.0	Immunohistochemisty Immunofluorescence
EDTA buffer	1 mM EDTA, 0.05% v/v Tween 20, pH 8.0	Immunohistochemisty Immunofluorescence
Copper sulphate	0.5 mM $CuSO_4$ 50 mM ammonium acetate pH 5.0	Immunofluorescence

Phosphate Buffered Saline (PBS)	0.15 M NaCl 7.5 mM Di-sodium hydrogen orthophosphate 12-hydrate 1.9 mM Sodium dihydrogen orthophosphate dihydrate	Immunohistochemisty
Sudan black	0.1% w/v Sudan Black 70% ethanol	Immunofluorescence
PBS-T	0.05% v/v Tween 20 PBS	ELISA
SDS Buffer	1% SDS, 10 mM Tris base (pH 6.0) 0.1 mM NaCl 1 µM PMSF, 1 µg/ml aprotinin	Protein extraction
PBS	137 mM NaCl 2.7 mM KCl 8.1 mM Na2HPO4 1.5 mM KH2PO4, pH 7.2 - 7.4 0.2 µm filtered	VEGFR1 ELISA VEGFR2 ELISA p-VEGFR2 ELISA
Reagent diluent #12	1% NP-40 20 mM Tris (pH 8.0) 137 mM NaCl, 10% glycerol 2 mM EDTA 1 mM activated sodium orthovanadate	VEGFR2 ELISA p-VEGFR2 ELISA
Reagent diluent #14	20 mM Tris, 137 mM NaCl 0.05% Tween 20 0.1% BSA pH 7.2 - 7.4.	VEGFR2 ELISA p-VEGFR2 ELISA
Lysis Buffer #9	1% NP-40 20 mM Tris (pH 8.0) 137 mM NaCl, 10% glycerol 2 mM EDTA 1 mM activated sodium orthovanadate 10 µg/mL aprotinin 10 µg/mL leupeptin	VEGFR2 ELISA p-VEGFR2 ELISA

Details of solution constituents.

Appendix 5 Commercial kit components

Name	Contents	Supplier
DAB Peroxidase (HRP) Substrate Kit (with Nickel), 3,3'-diaminobenzidine	Buffer stock solution	Vector Laboratories SK-4100
	Hydrogen peroxide solution	
	DAB stock solution	
	Nickel solution	
Endothelial cell medium (Complete kit)	Basal medium	ScienCell 1001
	Penicillin/Streptomycin solution, 5 ml	
	Fetal bovine serum, 10 ml	
	Endothelial cell growth supplement	
High capacity cDNA kit	10X RT buffer	Applied Biosystems 4368814
	10X RT random primers	
	25X dNTP mix (100 mM)	
	MultiScribe® reverse transcriptase (50 U/µL)	
Human VEGF-A DuoSet ELISA	Mouse anti-human VEGF capture antibody	R&D Systems DY293B
	Biotinylated goat anti-human VEGF detection antibody	
	Recombinant human VEGF standard	
	Streptavidin-HRP	
Human VEGFR1 (Flt1) DuoSet ELISA	Mouse anti-human VEGF R1 capture antibody:	R&D Systems DY321B
	Biotinylated mouse anti-human VEGF R1 detection antibody	
	Recombinant human VEGF R1 standard	
	Streptavidin-HRP	
Human phospho-VEGF R2/KDR DuoSet IC ELISA	Human phospho-VEGF R2/KDR capture antibody	R&D Systems DYC1766-5
	Anti-phospho-tyrosine-HRP	
	Human phospho-VEGF R2/KDR control	
Human total VEGFR2 (KDR) DuoSet IC ELISA	Total VEGF R2 capture antibody	R&D Systems DYC1780-5
	Total VEGF R2 detection antibody	
	Total VEGF R2 standard	
	Streptavidin-HRP	
Human Von Willebrand Factor ELISA Kit	Von Willebrand factor microplate (12 x 8 well strips) 96 wells	Abcam ab108918
	Von Willebrand factor standard 1 vial	
	10X Diluent N concentrate	
	50X Biotinylated human von Willebrand factor antibody	
	100X Streptavidin-peroxidase conjugate	
	Chromogen substrate	
	20X Wash buffer concentrate	
	Stop solution	
	Sealing tapes	
Pericyte medium (Complete kit)	Basal medium	ScienCell 1201
	Penicillin/Streptomycin solution, 5 ml	

	Fetal bovine serum, 10 ml	
	Pericyte growth supplement	
PureLink® RNA Mini Kit	Lysis buffer	Ambion 12183018A
	Wash buffer I	
	Wash buffer II	
	RNase-free water	
	Spin cartridges (with collection tubes)	
	Collection tubes	
	Recovery tubes	
Quant-iT Picogreen DNA Assay Kit	Quant-iT PicoGreen dsDNA reagent	Invitrogen P11496
	20X TE buffer	
	Lambda DNA standard	
Quant-iT RiboGreen RNA Assay Kit	Quant-iT RiboGreen RNA reagent	Invitrogen R11490
	20X TE buffer	
	Ribosomal RNA standard - 16S and 23S rRNA from E. coli	
Total protein kit	Protein standard (human albumin)	Sigma TP0100
	Brilliant Blue protein reagent	
Vectorstain Elite ABC kit (Universal)	Normal horse serum	Vector Laboratories PK-6200
	Concentrated universal biotinylated anti-mouse/rabbit IgG secondary antibody	
	Concentrated A and B reagents	
Very intense purple (VIP) substrate kit	Reagent 1	Vector Laboratories SK-4600
	Reagent 2	
	Reagent 3	
	Hydrogen peroxide solution	

Details of commercial kit components and manufacturers.

Appendix 6 Recombinant proteins

Protein	Origin	Catalogue #	Manufacturer
VEGFR1	N terminus of Human VEGF receptor 1	842596	R&D Systems
VEGFR2	Recombinant fragment corresponding to Human VEGF Receptor 2 aa 20-757	841436	R&D Systems
MAG	Human MAG full-length ORF (NP_002352.1, 1 a.a. - 626 a.a.) recombinant protein with GST-tag at N-terminal.	H00004099-P01	Abnova
$A\beta_{1-40}$	-	AS-24236	Anaspec
$A\beta_{1-42}$	-	AS-24224	Anaspec

Details of recombinant proteins.

Appendix 7 Primary antibodies

Name of Antibody	Immunogen	Clone	Host and type	Catalogue #	Manufacturer
Fibroblast surface protein	Tissue, cells or virus corresponding to human fibroblast surface protein	1B10	Mouse, monoclonal	ab11333	Abcam
GFAP	GFAP from human brain	6F2	Mouse, monoclonal	M0761	Dako
HLA-DP, DQ, DR	ß-chain of the α ß heterodimer of all products of the gene families DP, DQ and DR	CR3/43	Mouse, Monoclonal	M0775	Dako
Myelin-associated glycoprotein	Recombinant fragment corresponding to amino acids 119-208 of human MAG with a proprietary tag.	-	Mouse, Monoclonal	ab89780	Abcam
PDGFRβ	A synthetic peptide derived from near the C-terminus of human PDGFRβ	-	Rabbit, polyclonal	RB-1692	ThermoFisher Scientific
Rabbit IgG	Isotype control is not directed against any known antigen	DA1E	Rabbit, monoclonal	3900	Cell Signalling
VEGFR1	N terminus of Human VEGF receptor 1	Y103	Rabbit, monoclonal	Ab32152	Abcam
VEGFR2	Recombinant fragment corresponding to Human VEGF Receptor 2 aa 20-757	-	Mouse, monoclonal	Ab9530	Abcam
VEGFR2	Carboxy-terminal 150 amino acid residues of human VEGF receptor 2	55B11	Rabbit, monoclonal	2479	Cell Signalling
Von willebrand factor	Von Willebrand Factor isolated from human plasma.	-	Polyclonal, rabbit	A0082	Dako
α-Smooth muscle actin	a synthetic peptide corresponding to N-terminus of actin from human smooth muscle	-	Rabbit, polyclonal	ab5694	Abcam
β-Actin	N-terminal end of the β-isoform of actin	-	Mouse, monoclonal	A1978	Sigma
β-Amyloid, 1-16	Amino acid residue 1-16 of beta amyloid. The epitope lies within amino acids 3-8 of beta amyloid (EFRHDS)	6E10	Mouse, monoclonal	803001	Covance

β-Amyloid, 1-40	C-terminus of β-amyloid and is specific for the isoform ending at the 40th amino acid	11A50-B10	Mouse, monoclonal	805401	Covance
β-Amyloid, 1-42	C-terminus of β-amyloid and is specific for the isoform ending at the 42nd amino acid	12F4	Mouse, monoclonal	805501	Covance

Details of primary antibodies.

Appendix 8 Secondary antibodies

Name of Antibody	Manufacturer and Catalogue #	Application
HRP Goat Anti-Rabbit IgG Antibody (Peroxidase)	Vector Laboratories, PI-1000	Western blotting, Immunohistochemistry, Dot blotting
HRP Horse Anti-Mouse IgG Antibody (Peroxidase)	Vector Laboratories, PI-2000	Western blotting, Immunohistochemistry
Donkey anti-Rabbit IgG (H+L), Alexa Fluor 488 conjugate	Invitrogen,	Immunofluorescence
Goat anti-Mouse IgG (H+L), Alexa Fluor 488 conjugate	Thermo Fisher, A-11001	Immunofluorescence
Goat anti-Rabbit IgG (H+L), Alexa Fluor 546 conjugate	Thermo Fisher, A-11035	Immunofluorescence
Biotinylated Goat anti-Rabbit IgG (H+L)	Vector Laboratories, BA-1000	Immunofluorescence
Streptavidin, Alexa Fluor 555 Conjugate	Invitrogen S32355	Immunofluorescence
Goat anti-Mouse IgM (μ chain), Alexa Fluor 488 conjugate	Abcam ab150121	Immunofluorescence
Concentrated universal biotinylated anti-mouse/rabbit IgG secondary antibody	Vector Laboratories PK-6200	Immunohistochemistry

Details of secondary antibodies.

Appendix 9 Cohort demographic and neuropathological details

Diagnosis	BBNid	Age-at-death (years)	Gender	Post-mortem delay (hours)	Braak Stage	CAA score Parietal	SVD score Parietal
Control	BBN_4205	87	M	24	2	1	1
	BBN_4229	87	F	47	3	0	1
	BBN_8651	95	F	46	2		
	BBN_8671	78	F	24	2	1	2
	BBN_8700	64	M	12	2	0	0
	BBN_8702	58	M	20	0	0	0
	BBN_8706	72	M	42	1	0	1
	BBN_8708	90	M	45	2	0	0
	BBN_8717	77	M	55	1	0	1
	BBN_8722	78	M	12	2	0	1
	BBN_8723	80	M	67	3	2	2
	BBN_8725	73	M	36	2	0	0
	BBN_8739	93	F	18	2	0	1
	BBN_8751	82	M	30	2	0	2
	BBN_8759	75	M	48	2		1
	BBN_8776	73	M	33	1	0	1
	BBN_8779	69	M	66	2	0	1
	BBN_8835	73	F	59	1	0	1
	BBN_8898	83	F	24	2	0	0
	BBN_8923	82	M	3	2	1	1
	BBN_8949	79	M	24	-	-	-
	BBN_8957	76	F	12	-	-	-
	BBN_8980	72	F	24	0	0	2
	BBN_8983	78	M	48	1	0	1
	BBN_9028	76	M	23	2	0	1
	BBN_9092	75	M	6	3		
	BBN_9292	73	M	35	3	0	1
	BBN_9299	90	M	5.5	2	0	1
	BBN_9311	93	M	37.75	3	1	2
	BBN_9329	80	M	45.75	0	2	2
	BBN_9340	94	F	21	2	2	2
	BBN_9344	92	M	34.25	2	0	2
	BBN_9354	85	M	30.5	2	0	0
	BBN_9359	77	M	42	1	2	1
	BBN_9365	86	F	32	2	3	1
	BBN_9389	68	F	38.75	0	0	0

Demographic and Neuropathological details for control cohort.

Diagnosis	BBNid	Age-at-death (years)	Gender	Post-mortem delay (hours)	Braak Stage	CAA score Parietal	SVD score Parietal
AD	BBN_4202	64	M	66.5	5	0	0
	BBN_4204	65	M	38.5	4	0	2
	BBN_4215	80	F	26	5	2	0
	BBN_8834	78	F	9	5	0	2
	BBN_8848	77	F	43	4	0	0
	BBN_8883	90	M	40	6	0	1
	BBN_8910	71	M	30	6	2	2
	BBN_8912	82	F	24	6	3	1
	BBN_8921	75	F	40	6	3	1
	BBN_8997	74	F	12	6	3	1
	BBN_9005	89	F	4	6	3	1
	BBN_9026	79	M	28	6	1	1
	BBN_9030	65	M	27	6	2	1
	BBN_9031	85	M	66	6	3	1
	BBN_9044	86	M	48	5	0	2
	BBN_9052	57	F	24	5	0	1
	BBN_9076	84	F	20	6	0	3
	BBN_9106	93	M	20	5	0	1
	BBN_9112	74	F	52.5	5	3	1
	BBN_9122	83	F	5	5	0	2
	BBN_9123	74	F	35	6	3	2
	BBN_9136	77	F	26	6	3	1
	BBN_9155	79	M	27	6	1	2
	BBN_9162	63	M	43	6	0	0
	BBN_9163	69	F	71	5	3	1
	BBN_9164	92	F	24	5	3	0
	BBN_9173	86	F	31	6	2	2
	BBN_9179	64	M	9	5	1	1
	BBN_9181	80	F	48	5	2	1
	BBN_9182	74	M	24	6	1	2
	BBN_9186	75	F	21	6	1	1
	BBN_9189	78	F	21	5	3	2
	BBN_9194	89	F	39	6	3	2
	BBN_9198	77	F	14	6	0	2
	BBN_9205	85	F	85	5	3	2
	BBN_9261	83	M	48	6	2	2
	BBN_9262	81	M	4	5	3	2
	BBN_9263	74	M	48	5-6	1	3
	BBN_9266	80	M	72	6	2	1
	BBN_9274	78	M	49	6	2	0
	BBN_9275	87	M	36	5	0	1

	BBN_9280	76	M	11	6	0	3
	BBN_9295	85	M	49.5	5	0	3
	BBN_9303	69	M	12	6	0	1
	BBN_9315	67	F	24.25	6	1	2
	BBN_9323	84	F	20.5	6	2	3
	BBN_9342	65	F	11.5	5	2	1
	BBN_9361	83	M	11	6	0	1
	BBN_9367	77	M	19	5	3	1
	BBN_9378	84	F	22	3	1	2

Demographic and Neuropathological details for AD cohort.

Diagnosis	BBNid	Age-at-death (years)	Gender	Post-mortem delay (hours)	Braak Stage	CAA score Parietal	SVD score Parietal
VaD	BBN_4208	78	F	54	-	0	3
	BBN_8642	84	F	60	-	-	2
	BBN_8662	81	M	66	-	0	2
	BBN_8667	84	F	20	-	1	3
	BBN_8669	93	M	30	-	2	3
	BBN_8711	80	F	70	-	1	2
	BBN_8724	72	M	41	-	0	2
	BBN_8760	86	F	28	-	-	1
	BBN_8787	77	F	85	-	0	3
	BBN_8799	90	F	31	-	0	2
	BBN_8861	89	M	30	-	0	1
	BBN_8927	67	M	54	-	0	2
	BBN_8944	97	F	66	-	0	2
	BBN_8952	84	M	30	-	0	3
	BBN_8975	76	M	40	-	0	3
	BBN_9108	79	M	56	-	2	3
	BBN_9192	79	M	77	-	-	3
	BBN_9224	89	F	22	-	0	1
	BBN_9387	90	M	45		1	3

Demographic and Neuropathological details for VaD cohort.

Appendix 10 AD and control demographic details for FFPE cases

Diagnosis	MRC Identifier	Age-at-death (years)	Post-mortem delay (hours)	Gender
Control	BBN_8732	75	48	M
	BBN_8741	80	92	F
	BBN_9028	76	23	M
	BBN_9354	85	30.5	M
AD	BBN_4215	80	26	F
	BBN_9164	92	24	F
	BBN_9268	72	65	M
	BBN_9304	60	37.5	M
	BBN_9331	97	34	M

Demographic data for FFPE frontal lobe cases used for single and double immunohistochemistry.

Appendix 11 Correlation between cycle threshold and cDNA volume added to qPCR reaction for all genes of interest

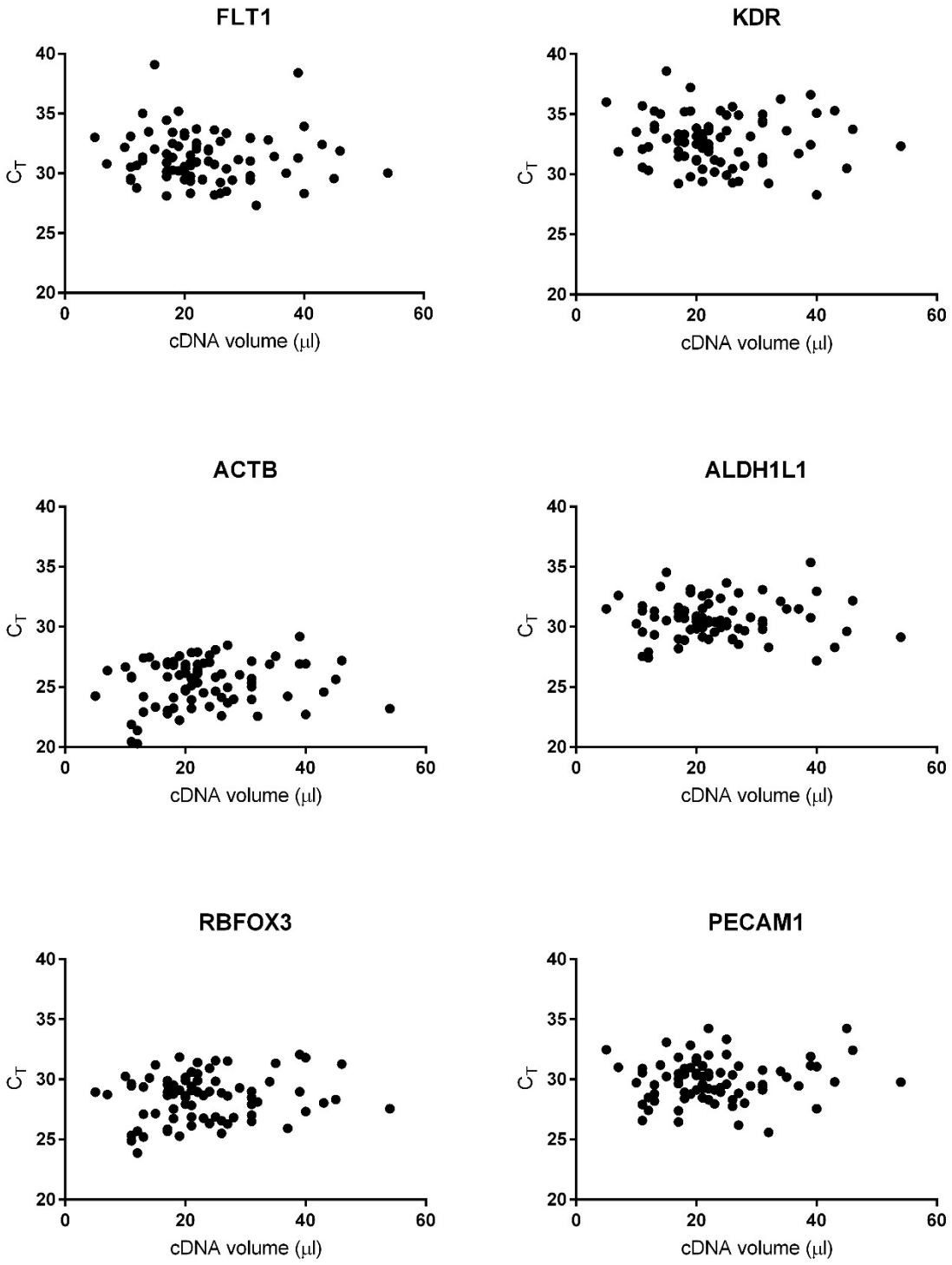

Correlation between cycle threshold and cDNA volume added to qPCR reaction for all genes of interest. Cycle threshold (C_T) values fell between the range of 20-39 for all genes of interest. There was no correlation between cDNA volume added to reaction and resulting C_T, meaning PCR reaction was not overloaded.

Appendix 12 VEGFR1 immunofluorescence

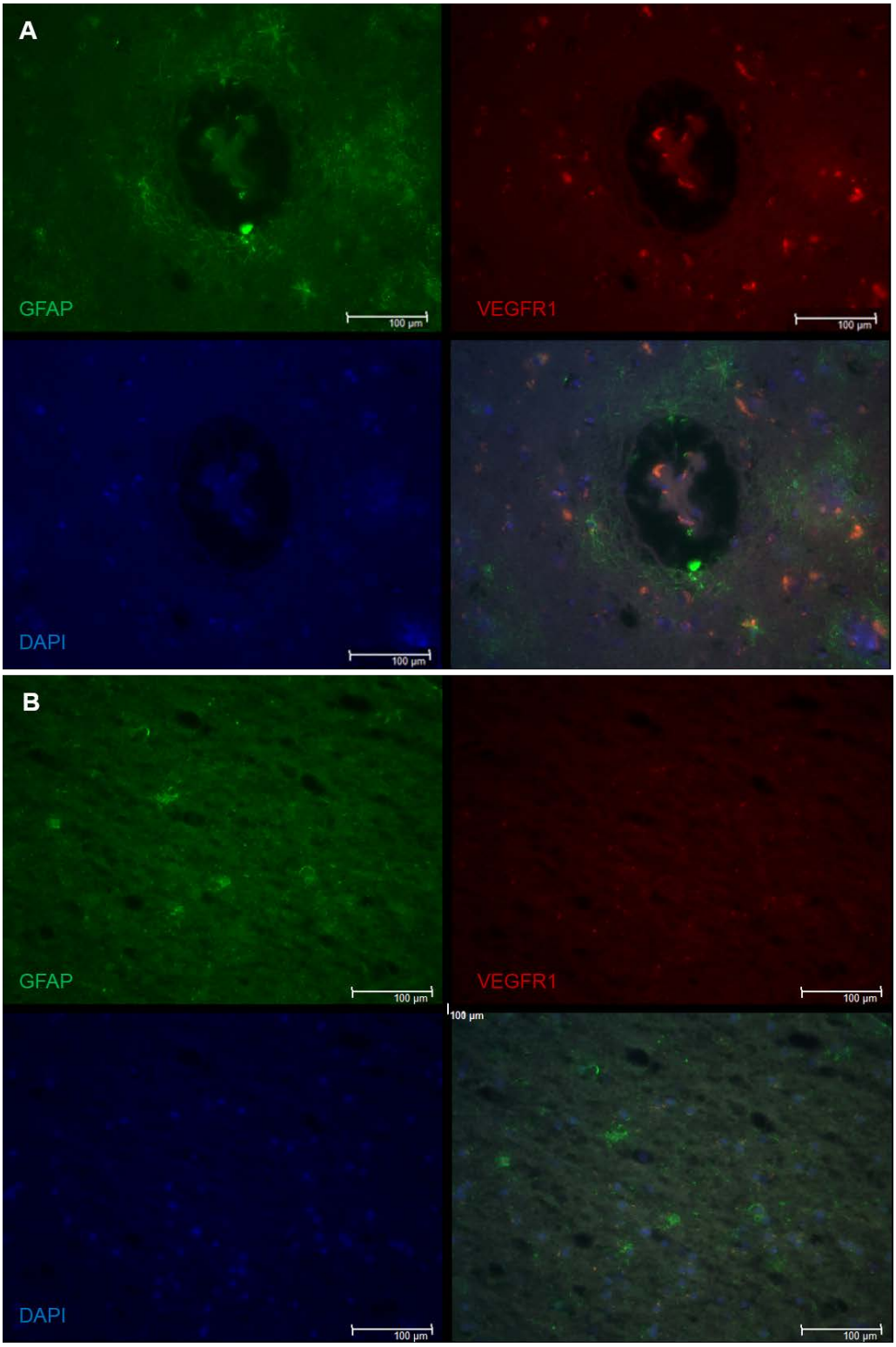

VEGFR1 immunofluorescence was attempted to confirm co-localisation of VEGFR1 on glial cells. (A) No treatment. VEGFR1 applied at 1:200 GFAP applied at 1:200 (B) Copper sulphate pretreatment and sudan black post treatment (not shown) were used to minimise lipofuscin-like fluorescence. DAPI used to stain cell nuclei. Levels background fluorescence remained elevated and double immunohistochemistry was used to confirm cellular localisation of VEGFR1.

Appendix 13 qPCR Primer alignment maps

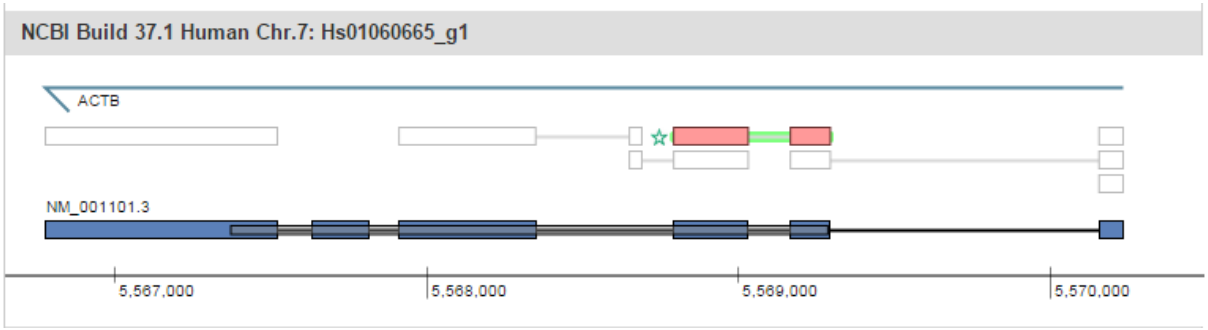

Primer for ACTB. Designed to bind to all isoforms of ACTB. Adapted from ThermoFisher Genomic Map.

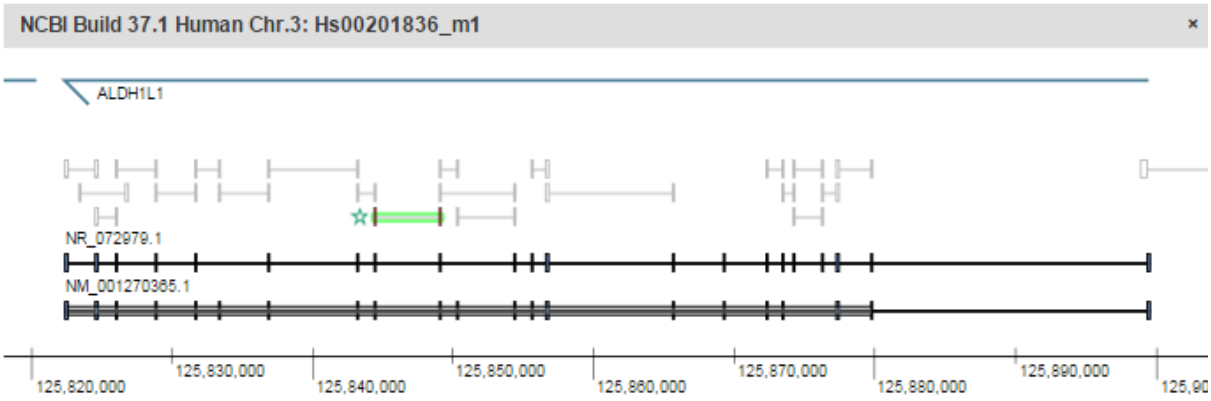

Primer for ALDH1L1. Designed to bind to all isoforms of ALDH1L1. Adapted from ThermoFisher Genomic Map.

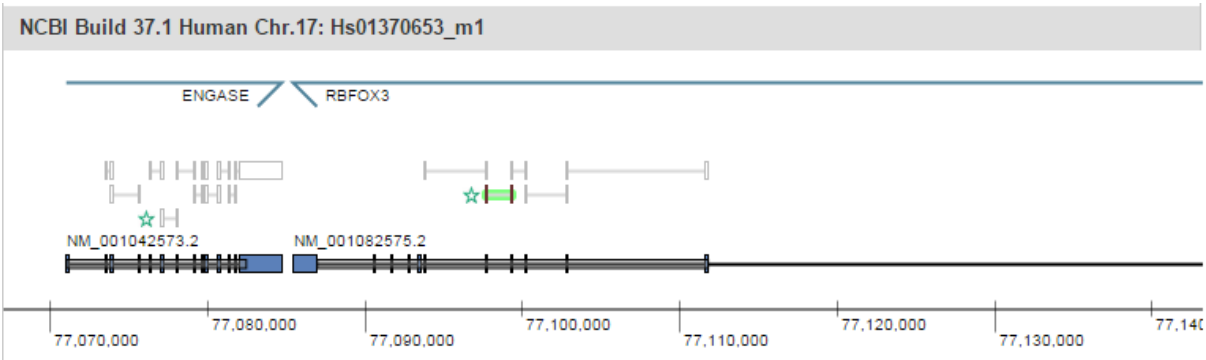

Primer for RBFOX3. Designed to bind to all isoforms of. Adapted from ThermoFisher Genomic Map.

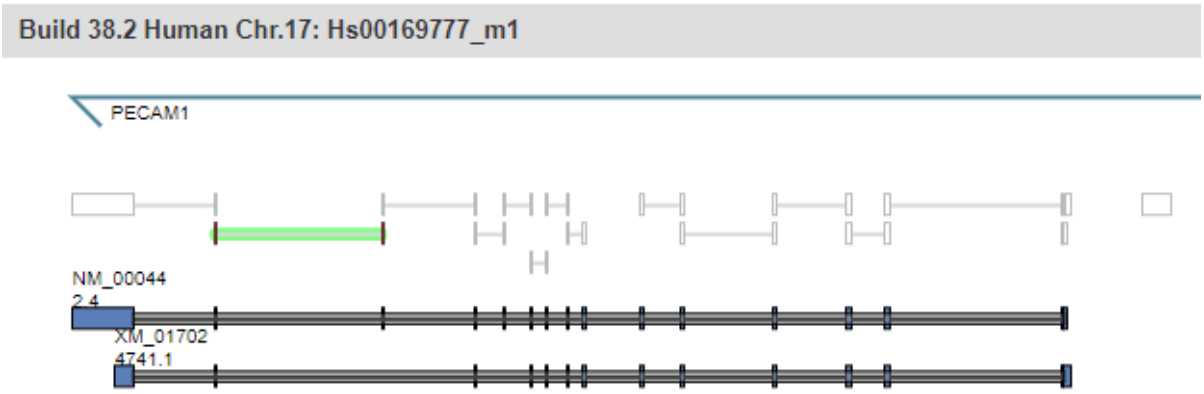

Primer for PECAM1. Adapted from ThermoFisher Genomic Map.

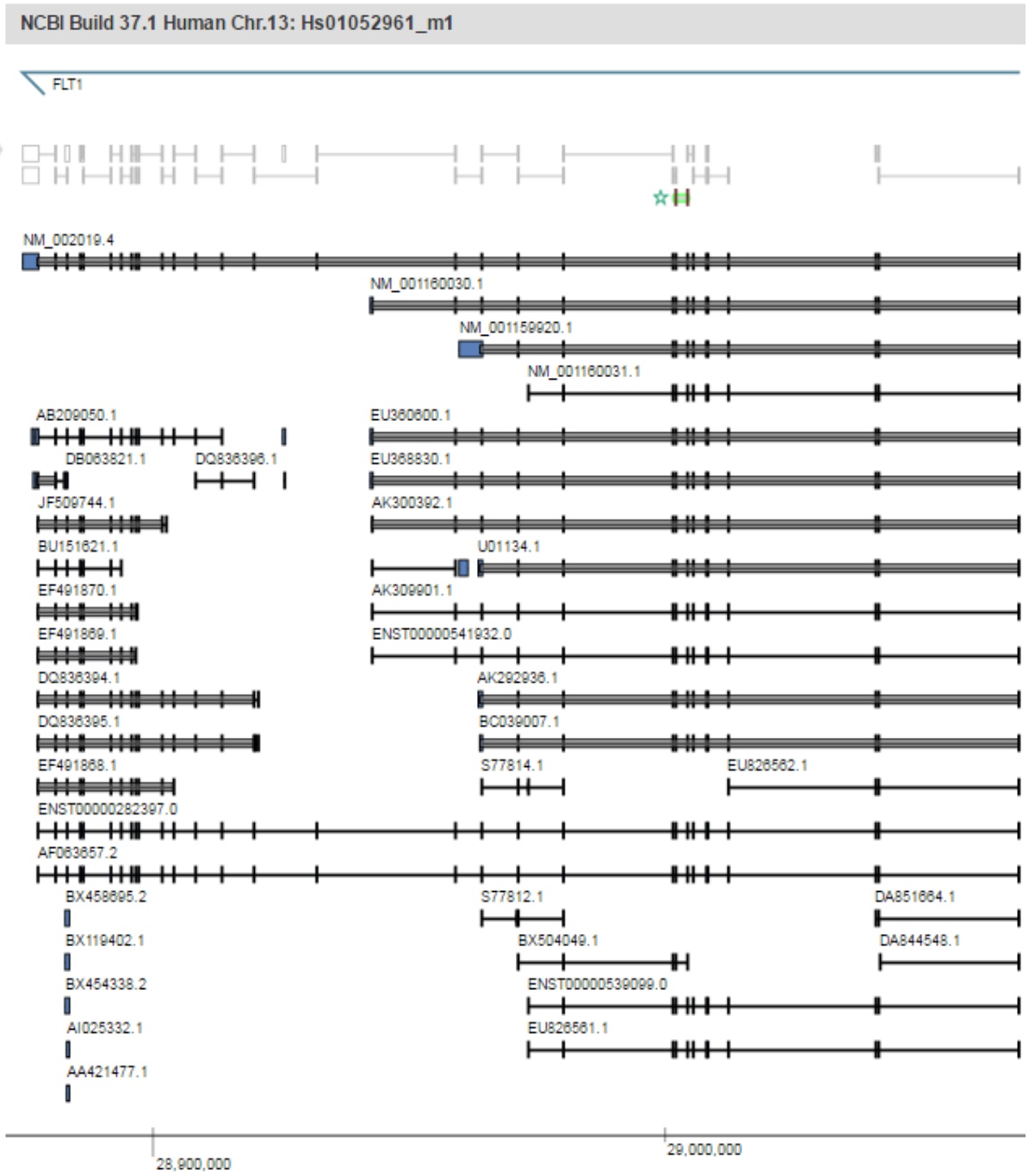

Primer for FLT1. Designed to bind to mbVEGFR1 and sVEGFR1 (not intracellular VEGFR1). Adapted from ThermoFisher Genomic Map.

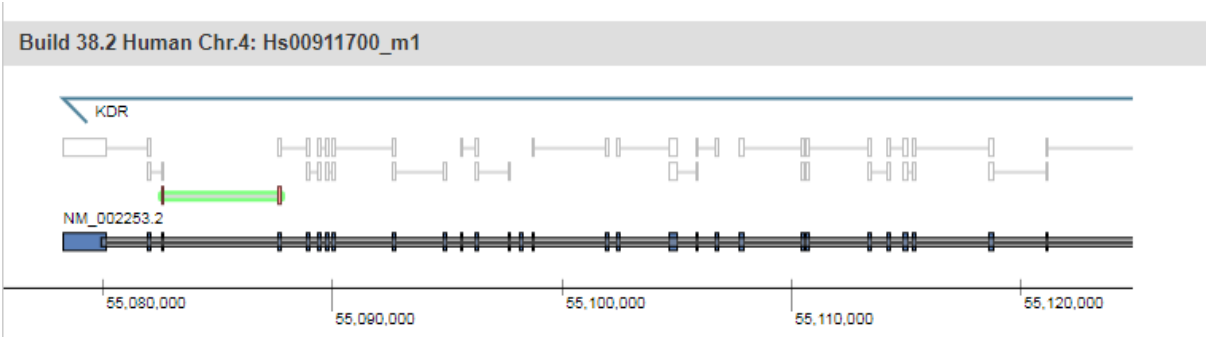

Primer for KDR. Designed to bind to VEGFR2. Adapted from ThermoFisher Genomic Map.

Appendix 14 AD and control: demographic details of cases used for VEGFR1 western blot

Diagnosis	MRC Identifier	Age-at-death (years)	Post-mortem delay (hours)	Gender
Control	BBN_8651	95	46	F
	BBN_8671	78	24	F
	BBN_8706	72	42	M
	BBN_8722	78	12	M
	BBN_8739	93	18	F
	BBN_8751	82	30	M
	BBN_8776	73	33	M
	BBN_8898	83	24	F
	BBN_8923	82	3	M
	BBN_8949	79	24	M
	BBN_8957	76	12	F
	BBN_8980	72	24	F
AD	BBN_8848	77	43	F
	BBN_8910	71	30	M
	BBN_8921	75	40	F
	BBN_8997	74	12	F
	BBN_9112	74	52.5	F
	BBN_9136	77	26	F
	BBN_9164	92	24	F
	BBN_9261	83	48	M
	BBN_9315	67	24.25	F
	BBN_9342	65	11.5	F
	BBN_4215	80	26	F
	BBN_9361	83	11	M

Demographic data for parietal cortex cases used for VEGFR1 western blots.

Appendix 15 VEGFR1 western blot – whole membrane

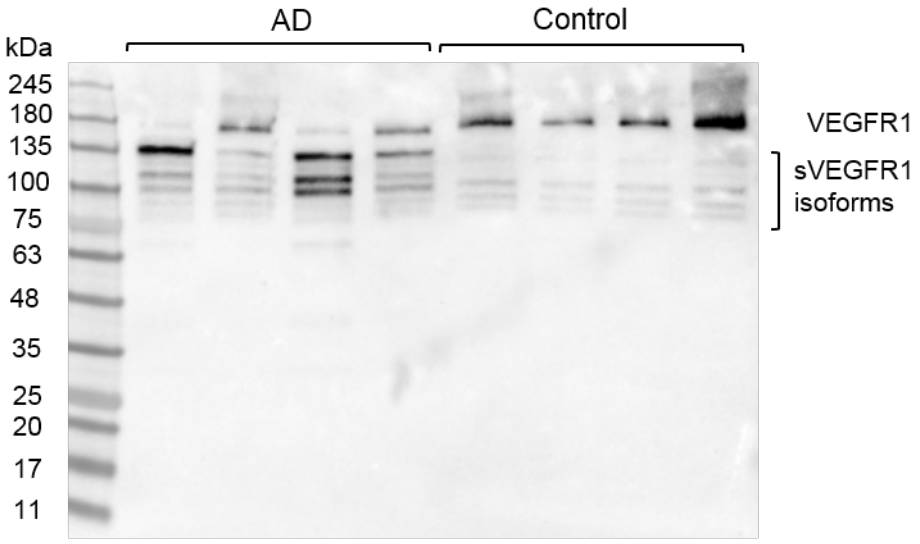

The whole membrane of a VEGFR1 western blot used for mbVEGR1:sVEGFR1 analysis. VEGFR1 was detected at 180 kDa, and sVEGFR1 isoforms were detected from 80 - 135 kDa in the brain homogenates. No prominent bands were observed below 75 kDa.

Appendix 16 VEGFR2 immunofluorescence

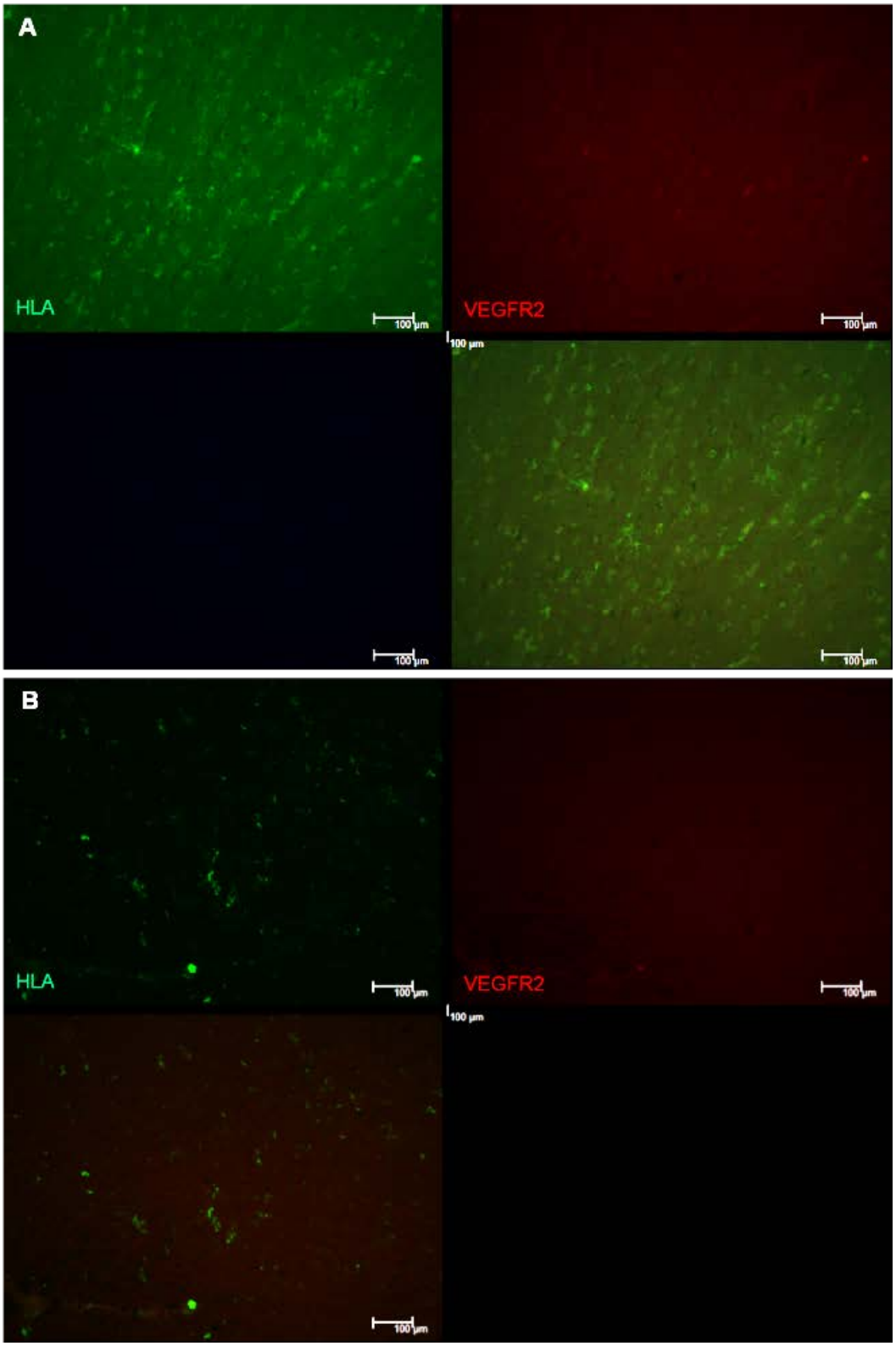

Double immunofluorescence of VEGFR2 and GFAP on AD frontal lobe FFPE. [A] Double IF showed high levels of autofluorescence with no autofluorescence pre-treatment or sudan black post-treatment. [B] Biotinylation to amplify VEGFR2 signal improved images but autofluorescence remained making colocalisation difficult. Double immunohistochemistry was used as an alternative.

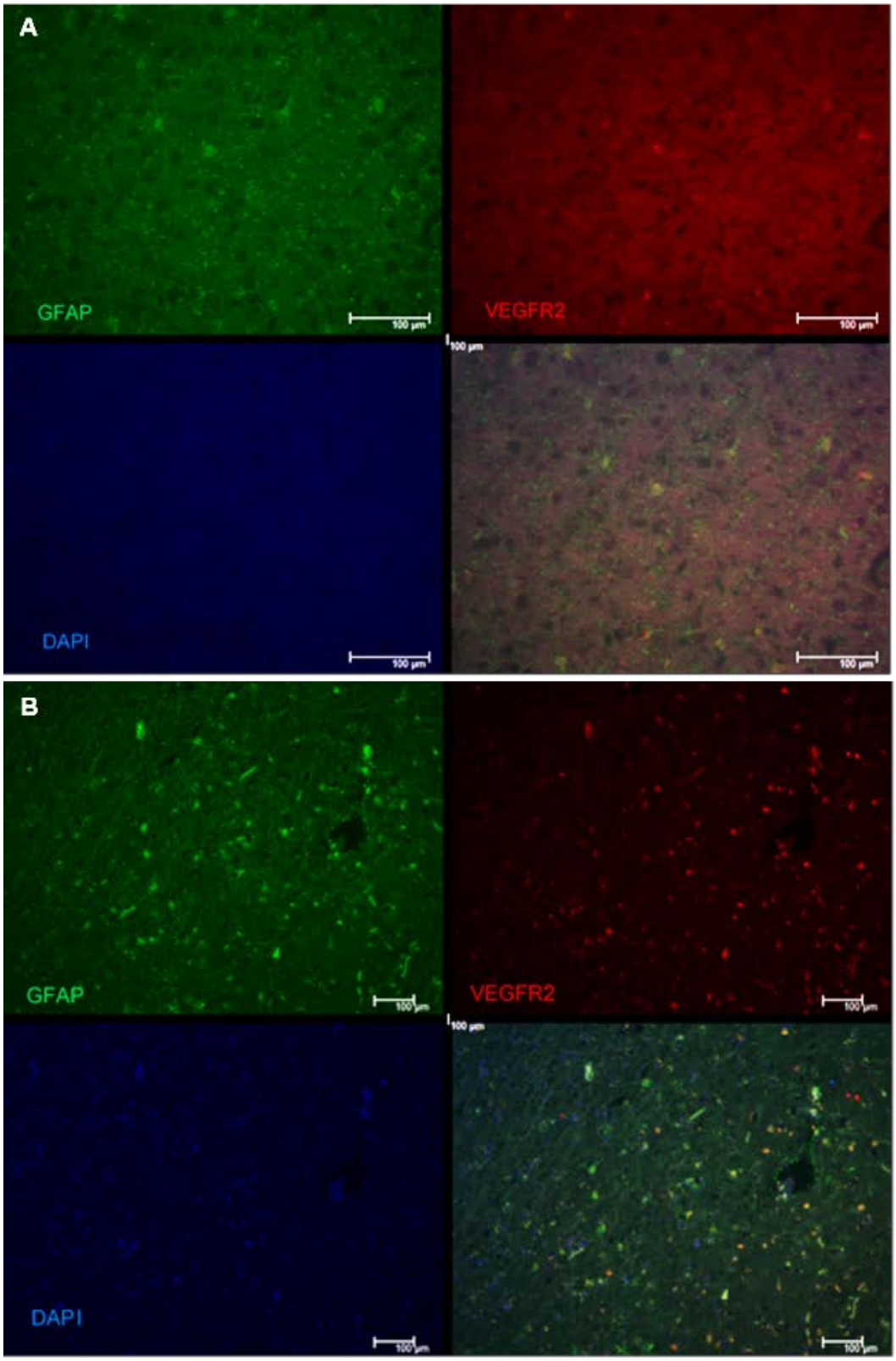

Double immunofluorescence of VEGFR2 and HLA on AD frontal lobe FFPE. [A] VEGFR2 displayed minimal signal and autofluorescence was present when no autofluorescence pre-treatment or sudan black post-treatment was used. [B] Autofluorescence was reduced when sudan black post-treatment was used, however this also reduced VEGFR2 signal making it difficult to establish receptor colocalisation. Double immunohistochemistry was used as an alternative.

Appendix 17 VEGFR2 ELISA detection antibody validation on human tissue

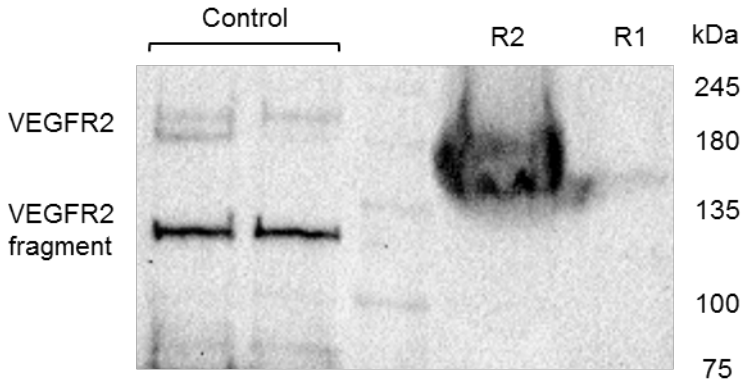

VEGFR2 ELISA detection antibody validation in human tissue. Bands were observed at 230 kDa and 210 kDa corresponding to glycosylated receptor and non-glycosylated form respectively. Bands observed at 120 kDa are attributed to proteolytic cleavage of VEGFR2 [396, 397]. VEGFR1 and VEGFR2 recombinant proteins were used to validate specificity. No crossover was seen with VEGFR1 recombinant.

Appendix 18 p-VEGFR2 ELISA spike and recovery testing on human tissue

	% Recovery		
	Spiked	Unspiked	Control
Neat	56.5	-	-
1:2	159.7	132.6	129.8
1:4	248.1	151.1	137.0

The p-VEGFR2 ELISA was validated on human brain tissue homogenates. Spike, recovery and linearity measurements did not fall within the manufactures accepted range (80-120%).

Appendix 19 p-VEGFR2 (Tyr996) antibody validation

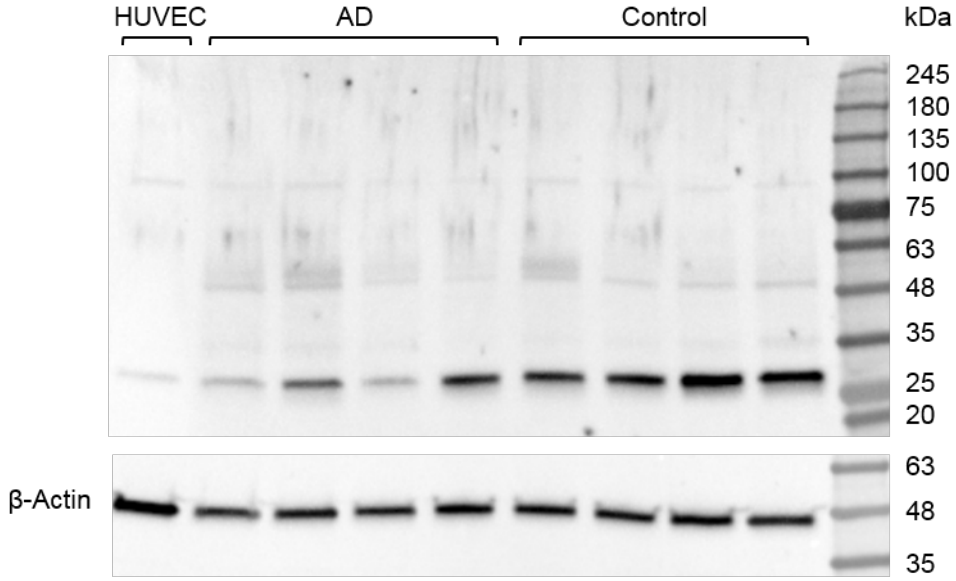

p-VEGFR2 (Tyr996) antibody was used to identify p-VEGFR2 in human brain tissue and HUVEC lysate. No bands were observed at the predicted molecular weight of immature p-VEGFR2 (150 kDa), intermediate glycosylated p-Flk-1 (200 kDa) or mature glycosylated p-Flk-1 (230 kDa). The antibody could not be used to identify p-VEGFR2 levels in human tissue or cell lysate. Bands have been observed at 160 kDa [398] and at 120-130 kDa due to proteolytic cleavage [396, 397]. Bands and 90 kDa, 50 kDa and 30 kDa could be due to further proteolytic cleavage or non-specific binding to another protein with a similar epitope, such as a phosphorylated tyrosine.

Appendix 20 Inter-assay reliability for VWF dot blot.

MRC Identifier	VWF		CoV (%)
	Blot 1	Blot 2	
BBN_4229	226.8	139.7	33.6
BBN_8923	81.3	180.8	53.7
BBN_8980	227.3	105.2	51.9
BBN_9205	282.9	665.0	57.0
BBN_9261	167.0	374.7	54.2
BBN_9262	95.9	373.8	83.7
BBN_9361	133.4	85.8	30.7
BBN_9365	222.5	118.0	43.4

Inter-assay reliability for VWF dot blot. Homogenates from the same samples were measured on in triplicate on two different blots. CoV was performed to assess the relative variability of sample readings. CoV readings show the dot blot is not reliable and as a result the vWF ELISA was optimised.

Appendix 21 Summary statistics for VEGF correlations with VWF

VEGF and vWF	Control			AD			VaD		
	p	**r**	**n**	***p***	**r**	**n**	***p***	**r**	**n**
cortex	0.525	-0.119	31	0.437	-0.119	45	-	-	-
White matter	0.956	-0.01	36	0.132	0.226	48	0.037	0.481	19

Summary statistics for VEGF correlations with VWF in cortex and white matter.

Appendix 22 VEGFR1 correlations in parietal cortex

Cortex	VEGFR1					
	Control			AD		
	p	**r**	**n**	***p***	**r**	**n**
vWF	0.192	0.229	34	0.003	0.438	44
VEGF	0.11	0.303	29	0.413	-0.133	29
Soluble $A\beta_{1\text{-}40}$	0.549	0.118	28	0.48	-0.115	40
Insoluble $A\beta_{1\text{-}40}$	0.22	0.235	29	0.227	0.2	40
Soluble $A\beta_{1\text{-}42}$	0.388	-0.167	29	0.8	0.042	39
Insoluble $A\beta_{1\text{-}42}$	0.518	-0.125	29	0.532	0.102	40
Soluble $A\beta_{42:40}$	0.337	-0.188	28	0.405	0.137	39
Insoluble $A\beta_{42:40}$	0.135	-0.284	29	0.69	-0.065	40
Age	0.428	0.141	34	0.133	0.23	44
Post-mortem delay	0.66	0.072	34	0.979	-0.004	44

Summary statistics for VEGFR1 correlations with variables in parietal cortex.

Appendix 23 VEGFR2 correlations in parietal cortex

Cortex	VEGFR2								
	Control			AD			VaD		
	p	r	n	*p*	r	n	*p*	r	n
vWF	0.135	0.254	36	0.048	0.287	48	0.074	0.764	19
VEGF	0.071	0.328	31	0.013	0.366	45	-	-	-
Soluble $A\beta_{1\text{-}40}$	0.144	-0.273	30	0.129	-0.23	45	-	-	-
Insoluble $A\beta_{1\text{-}40}$	0.98	0.005	31	0.38	-0.135	45	-	-	-
Soluble $A\beta_{1\text{-}42}$	0.011	-0.449	31	0.414	0.126	44	-	-	-
Insoluble $A\beta_{1\text{-}42}$	0.292	-0.195	31	0.222	0.186	45	-	-	-
Soluble $A\beta_{42:40}$	0.005	-0.503	30	0.152	0.22	44	-	-	-
Insoluble $A\beta_{42:40}$	0.993	0.002	31	0.47	0.298	44	-	-	-
Age	0.23	0.205	36	0.094	0.24	50	0.838	-0.05	19
Post-mortem delay	0.23	0.205	36	0.883	-0.022	48	0.451	-0.184	19

Summary statistics for VEGFR2 correlations with variables in parietal cortex.

Appendix 24 VEGFR2 correlations in parietal white matter

White matter	VEGFR2								
	Control			AD			VaD		
	p	r	n	*p*	r	n	*p*	r	n
vWF	0.475	0.123	36	0.917	0.016	48	0.473	-0.175	19
VEGF	0.918	-0.018	36	0.956	-0.008	48	0.3	0.251	19
Soluble $A\beta_{1\text{-}40}$	0.549	0.118	32	0.48	-0.115	45	-	-	-
Insoluble $A\beta_{1\text{-}40}$	0.22	0.235	31	0.227	0.195	43	-	-	-
Soluble $A\beta_{1\text{-}42}$	0.388	-0.167	32	0.799	0.042	44	-	-	-
Insoluble $A\beta_{1\text{-}42}$	0.518	-0.125	32	0.532	0.102	44	-	-	-
Soluble $A\beta_{42:40}$	0.337	-0.188	32	0.405	0.137	45	-	-	-
Insoluble $A\beta_{42:40}$	0.135	-0.284	31	0.69	-0.065	43	-	-	-
Age	0.423	-0.136	36	0.364	0.131	50	0.772	0.071	19
Post-mortem delay	0.684	-0.07	36	0.41	-0.12	48	0.201	0.31	19

Summary statistics for VEGFR2 correlations with variables in parietal white matter.

Appendix 25 Summary statistics for CAA score and VEGFR1 and VEGFR2 levels

CAA		0-1						2-3					
		Median	IQR	n				Median	IQR	n			
				Total	C	AD	VaD			Total	C	AD	VaD
Cortex	VEGFR1	70.6	43.5	46	24	21	-	67.99	30.39	28	5	23	-
	VEGFR2	340.8	476.9	65	14	25	14	490.9	475.3	32	4	25	2
White matter	VEGFR2	166.4	108.5	64	26	24	14	154.7	145.9	31	5	24	2

Summary statistics for CAA score and VEGFR1 and VEGFR2 levels in parietal cortex and white matter.

Appendix 26 Summary statistics for SVD score and VEGFR1 and VEGFR2 levels

SVD		0-1						2-3					
		Median	IQR	n				Median	IQR	n			
				Total	C	AD	VaD			Total	C	AD	VaD
Cortex	VEGFR1	72.87	33.69	46	15	23	-	60.59	49.26	28	3	20	-
	VEGFR2	328.9	499.2	55	25	27	3	391.1	443	46	8	22	16
White matter	VEGFR2	157.8	144.8	53	24	26	4	155.4	102.3	46	9	23	15

Summary statistics for SVD score and VEGFR1 and VEGFR2 levels in parietal cortex and white matter.

Appendix 27 Summary statistics for Braak stage and VEGFR1 and VEGFR2 levels

Braak stage		0-II					II-IV					V-VI				
		Median	IQR	n			Median	IQR	n			Median	IQR	n		
				Total	C	AD			Total	C	AD			Total	C	AD
Cortex	VEGFR1	78.21	37.36	30	28	0	65.6	46.82	7	4	3	59.59	45.71	41	0	41
	VEGFR2	326.8	232.9	31	29	0	495.4	551.2	8	5	3	395.4	489.1	47	0	47
White matter	VEGFR2	169.1	133.2	29	29	0	137.2	108.44	8	5	3	178.2	114.2	45	0	45

Summary statistics for Braak stage and VEGFR1 and VEGFR2 levels in parietal cortex and white matter.

Appendix 28 No primary control for HBMEC and HBVP immunofluorescence

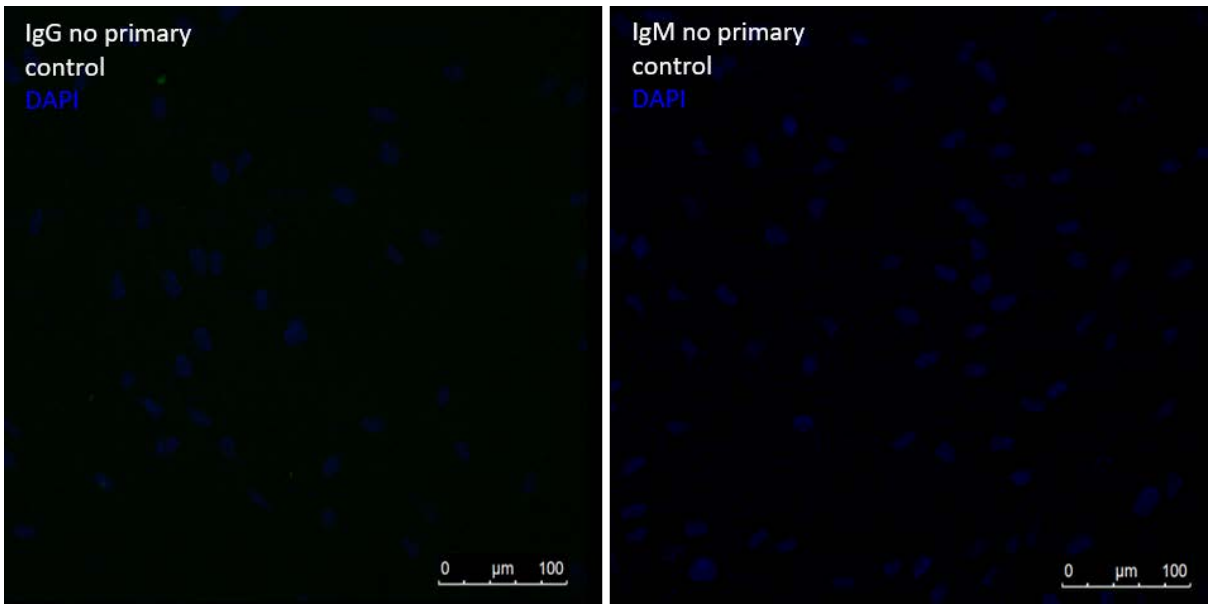

No primary antibody control immunofluorescence. Cells were incubated with primary antibody diluent and secondary antibodies specific for primary antibody immunogloblin subtypes. DAPI positivity is present in the cell nuclei. No immunofluorescence resembling specific staining pattern was seen.

Appendix 29 Summary values of VEGFR1 and sVEGFR1 levels in HBMEC lysates.

HBMEC		Normoxia	N + $A\beta_{1-40}$	N + $A\beta_{1-42}$	Hypoxia	H + $A\beta_{1-40}$	H + $A\beta_{1-42}$
VEGFR1	Median	100	131.4	118.5	125.7	130.7	155.3
	IQR	0	59.3	92.26	101.6	136.4	85.51
	N	6	6	6	6	6	6
sVEGFR1	Median	100	103.6	98.11	129.9	125.8	111.6
	IQR	0	19.4	37.19	41.1	44.4	43.3
	N	8	6	6	8	6	6

Summary values of VEGFR1 and sVEGFR1 levels in HBMEC lysates.

Appendix 30 Summary values of VEGFR1, sVEGFR1 and VEGFR2 levels in HBVP lysates.

HBVP		Normoxia	N + Aβ$_{1-40}$	N + Aβ$_{1-42}$	Hypoxia	H + Aβ$_{1-40}$	H + Aβ$_{1-42}$
VEGFR1	Median	100	141.3	105.1	119.6	163	148.9
	IQR	0	42.9	105.18	89.9	94.7	105.3
	N	6	6	6	6	6	6
sVEGFR1	Median	100	118.4	134.8	141.4	101.8	154.4
	IQR	0	43.06	85.79	150.9	70.68	104.5
	N	8	5	6	8	6	6
VEGFR2	Median	100	86.74	98.6	33.03	44.08	41.2
	IQR	0	26.33	25.77	22.61	35.15	47.66
	N	7	7	7	7	7	7

Summary values of VEGFR1, sVEGFR1 and VEGFR2 levels in HBVP lysates.